Universität Hamburg
DER FORSCHUNG | DER LEHRE | DER BILDUNG

BNITM
Bernhard Nocht Institute for Tropical Medicine

Funded by
DFG Deutsche Forschungsgemeinschaft
German Research Foundation

RNAi-based adaptive immunity in *Aedes aegypti* against arboviruses

---

CUMULATIVE Dissertation

Submitted in fulfilment of the requirements for the degree of

doctor rerum naturalium (Dr. rer. nat.)

Faculty of Mathematics, Informatics and Natural Sciences

Department of Biology

University of Hamburg

&

Working group Mosquito-Virus-Interactions

Bernhard-Nocht-Institute for Tropical Medicine

Submitted by

Melinda Reuter

Hamburg

2026

This work was performed under the guidance of Prof Dr Esther Schnettler at the Bernhard Nocht Institute for Tropical Medicine (BNITM) Hamburg, Germany

1st reviewer

Prof. Dr. Esther Schnettler

Group leader ‚Mosquito-Virus Interactions' at Bernhard-Nocht-Institute for Tropical Medicine, Hamburg

Universität Hamburg / BNITM

2nd reviewer

Dr. Stephanie Jansen

Postdoctoral researcher Arbovirology at Department of Biology

Universität Hamburg

Oral defence: 04.09.2026

Publications and manuscript

This dissertation is based on three publications and one manuscript in preparation.

Publications:

Chapter 2

Reuter, M.#, Parry, R. H.#, McFarlane, M., Gestuveo, R. J., Arif, R., Khromykh, A. A., Brennan, B., Varjak, M., Castello, A., Redecke, L., Schnettler, E., Kohl, A. "The PAZ domain of *Aedes aegypti* Dicer 2 is critical for accurate and high-fidelity size determination of virus-derived small interfering RNAs". RNA. 2025 Apr 16;31(5):679-691. doi: 10.1261/rna.080149.124. PMID: 39947927; PMCID: PMC12001973.

Chapter 3

Reuter, M.#, Böhmer, P.#, Altinli, M., Schnettler, E., „Detection and characterization of antiviral proteins against bunyaviruses in mosquito-derived cells". In H. Boshra (Ed.), *Bunyaviruses – Methods and Protocols* (pp. 73-84). Springer Protocols. https://doi.org/10.1007/978-1-0716-4338-9.

Chapter 4

Reuter, M.#, Dornbusch, S.#, Parry, R. H., Stern, M., Becker, S. C., Schnettler, E. "Dicer-2 mutations in *Aedes aegypti* cells lead to a diminished antiviral function against Rift Valley fever virus and Bunyamwera virus infection". J Gen Virol. 2024 Nov;105(11):002046. doi: 10.1099/jgv.0.002046. PMID: 39508739; PMCID: PMC11542633.

#These authors contributed equally

Manuscript in preparation:

Chapter 5

Reuter, M., Scherer, C., Parry, R. H., Fuss, J., Schnettler, E. „RNAi-based adaptive immunity in *Aedes aegypti* against arboviruses."

Parts of this thesis have been previously presented at conferences:

Melinda Reuter, Susann Dornbusch, Rhys H. Parry, Melanie McFarlane, Rommel J. Gestuveo, Alexander A. Khromykh, Benjamin Brennan, Lars Redecke, Margus Varjak, Michael Stern, Steffi Becker, Esther Schnettler, Alain Kohl. "Importance of different domains of *Ae. aegypti* Dicer 2 in the antiviral response against arboviruses". GfV 2024 - *33rd annual meeting of the German Society of Virology, Vienna, Austria.* 25.-28.03.2024. **Poster**

Melinda Reuter, Christina Scherer, Esther Schnettler. "RNAi-based immunity in *Aedes aegypti* against arboviruses". GfV 2025 – *34th annual meeting of the German Society of Virology, Hamburg, Germany.* 04.-07.03.2025. **Poster**

Further contributions were made to the following publications:

Gothe, S., Jagtap, S., Böhmer, P., **Reuter, M.**, Frank, S., Sreenu, V. B., Bell-Sakyi, L., Marits, A., Altinli, M., Schnettler, E. „Characterization of *Culex pipiens* cell lines: virus infection and RNAi response." Parasites & Vectors 19, 94 (2026). https://doi.org/10.1186/s13071-026-07248-w.

Funding:

This thesis has been funded by the Deutsche Forschungsgemeinschaft (DFG; German Research Foundation; project number 497659464).

Universität Hamburg
DER FORSCHUNG | DER LEHRE | DER BILDUNG

FACULTY
OF MATHEMATICS, INFORMATICS
AND NATURAL SCIENCES

Declaration about personal contribution to manuscripts/publications in a cumulative thesis (please submit one form per manuscript/publication)
Candidate's name: Melinda Reuter

Manuscript (including all authors, title, and if applicable journal, year; mark all first authors with asterisk):
Reuter, M.*, Parry, R. H.*, McFarlane, M., Gestuveo, R. J., Arif, R., Khromykh, A. A., Brennan, B., Varjak, M., Castello, A., Redecke, L., Schnettler, E., Kohl, A. "The PAZ domain of Aedes aegypti Dicer 2 is critical for accurate and high-fidelity size determination of virus-derived small interfering RNAs". RNA. 2025 Apr 16;31(5):679-691. doi: 10.1261/rna.080149.124. PMID: 39947927; PMCID: PMC12001973

Link to publication (if published): https://pmc.ncbi.nlm.nih.gov/articles/PMC12001973/

Detailed description of own contribution to this manuscript

Conceptualization and planning of project:

I contributed to the conceptualization of the project and planning of the experimental work.

Method development:

I contributed to the implementation of the experimental methodology and optimization/ standardization of experimental procedures.

Data generation and analyses (including contribution to specific figures):

I performed all experiments, generated the complete data set, carried out parts of the data analysis and prepared some of the figures for the manuscript (Fig. 1-3).

Writing and editing of manuscript:

I was involved in the writing of the original draft and editing of the manuscript.

I confirm that the above information is accurate

Candidate

Hamburg, 13.06.26

Place, date | Signature of candidate

Supervisor name: Prof. Dr. Esther Schnettler

Hamburg, 20.06.2026

Place, date | Signature of supervisor

Universität Hamburg
DER FORSCHUNG | DER LEHRE | DER BILDUNG

FACULTY
OF MATHEMATICS, INFORMATICS
AND NATURAL SCIENCES

Declaration about personal contribution to manuscripts/publications in a cumulative thesis (please submit one form per manuscript/publication)
Candidate's name: Melinda Reuter

Manuscript (including all authors, title, and if applicable journal, year; mark all first authors with asterisk): Reuter, M.#, Böhmer, P.#, Altinli, M., Schnettler, E., „Detection and characterization of antiviral proteins against bunyaviruses in mosquito-derived cells". In H. Boshra (Ed.), *Bunyaviruses – Methods and Protocols* (pp. 73-84). Springer Protocols. https://doi.org/10.1007/978-1-0716-4338-9.

Link to publication (if published): https://link.springer.com/protocol/10.1007/978-1-0716-4338-9_7

Detailed description of own contribution to this manuscript

Conceptualization and planning of project:

I contributed to the conceptualization of the project/ described experimental procedures.

Method development:

I contributed to the implementation of the experimental methodology of the described experimental procedures.

Data generation and analyses (including contribution to specific figures):

I was involved in the experiments and experimental set up that were used as examples for this method chapter.

Writing and editing of manuscript:

I contributed to the writing of the original draft and editing of the manuscript.

I confirm that the above information is accurate

Candidate		**Supervisor name: Prof. Dr. Esther Schnettler**	
Hamburg, 13.06.26		Hamburg, 20.06.2026	
Place, date	Signature of candidate	Place, date	Signature of supervisor

Universität Hamburg
DER FORSCHUNG | DER LEHRE | DER BILDUNG

FACULTY
OF MATHEMATICS, INFORMATICS
AND NATURAL SCIENCES

Declaration about personal contribution to manuscripts/publications in a cumulative thesis (please submit one form per manuscript/publication)
Candidate's name: Melinda Reuter

Manuscript (including all authors, title, and if applicable journal, year; mark all first authors with asterisk): Reuter, M.*, Dornbusch, S.*, Parry, R. H., Stern, M., Becker, S. C., Schnettler, E. “Dicer-2 mutations in Aedes aegypti cells lead to a diminished antiviral function against Rift Valley fever virus and Bunyamwera virus infection”. J Gen Virol. 2024 Nov;105(11):002046. doi: 10.1099/jgv.0.002046. PMID: 39508739; PMCID: PMC11542633.

Link to publication (if published): https://pmc.ncbi.nlm.nih.gov/articles/PMC11542633/

Detailed description of own contribution to this manuscript

Conceptualization and planning of project:

I contributed to the conceptualization of the project and planned most of the experimental work.

Method development:

I was involved in the implementation of the experimental methodology, including optimization/ standardization of the experiments.

Data generation and analyses (including contribution to specific figures):

I performed most experiments, thus generated most of the data set, and carried out parts of the data analysis and prepared some of the figures for the manuscript (Fig. 1 and 2). I also contributed to the data sets used for analysis shown in Fig. 3 and 4.

Writing and editing of manuscript:

I contributed to the writing of the original draft and editing of the manuscript.

I confirm that the above information is accurate

Candidate		**Supervisor name: Prof. Dr. Esther Schnettler**	
Hamburg, 13.06.26		Hamburg, 20.06.2026	
Place, date	Signature of candidate	Place, date	Signature of supervisor

Universität Hamburg
DER FORSCHUNG | DER LEHRE | DER BILDUNG

FACULTY
OF MATHEMATICS, INFORMATICS
AND NATURAL SCIENCES

Declaration about personal contribution to manuscripts/publications in a cumulative thesis (please submit one form per manuscript/publication)
Candidate's name: Melinda Reuter

Manuscript (including all authors, title, and if applicable journal, year; mark all first authors with asterisk): Reuter, M.*, Scherer, C., Parry, R. H., Stern, M., Fuss, J., Schnettler, E. “RNAi-based adaptive immunity in *Aedes aegypti* against arboviruses”.

Link to publication (if published):

Detailed description of own contribution to this manuscript

Conceptualization and planning of project:

I contributed to the project conceptualization and experimental plans.

Method development:

I contributed to the implementation of the experimental methodology and optimization/ standardization of experimental procedures.

Data generation and analyses (including contribution to specific figures):

I performed almost all experiments, generated the complete data set, carried out the full data analysis and prepared all of the figures for the manuscript.

Writing and editing of manuscript:

I wrote the original draft of the manuscript and was involved in the editing.

I confirm that the above information is accurate

Candidate		**Supervisor name: Prof. Dr. Esther Schnettler**	
Hamburg, 13.06.26		Hamburg, 20.06.2026	
Place, date	Signature of candidate	Place, date	Signature of supervisor

Eidesstattliche Versicherung:

Hiermit versichere ich an Eides statt, die vorliegende Dissertationsschrift selbst verfasst und keine anderen als die angegebenen Hilfsmittel und Quellen benutzt zu haben.

Sofern im Zuge der Erstellung der vorliegenden Dissertationsschrift generative Künstliche Intelligenz (gKI) basierte elektronische Hilfsmittel verwendet wurden, versichere ich, dass meine eigene Leistung im Vordergrund stand und dass eine vollständige Dokumentation aller verwendeten Hilfsmittel gemäß der Guten wissenschaftlichen Praxis vorliegt. Ich trage die Verantwortung für eventuell durch die gKI generierte fehlerhafte oder verzerrte Inhalte, fehlerhafte Referenzen, Verstöße gegen das Datenschutz- und Urheberrecht oder Plagiate.

Affidavit:

I hereby declare and affirm that this doctoral dissertation is my own work and that I have not used any aids and sources other than those indicated.

If electronic resources based on generative artificial intelligence (gAI) were used in the course of writing this dissertation, I confirm that my own work was the main and value-adding contribution and that complete documentation of all resources used is available in accordance with good scientific practice. I am responsible for any erroneous or distorted content, incorrect references, violations of data protection and copyright law or plagiarism that may have been generated by the gAI.



Hamburg, den 13.06.2026 Unterschrift

Table of contents

Abstract ..... **I**
Zusammenfassung ..... **III**
List of abbreviations ..... **V**

Chapter 1: Introduction **1**
Arboviruses 1
Semliki Forest virus 1
Zika virus 2
Bunyamwera orthobunyavirus 2
Rift Valley Fever virus 3
Arboviral mosquito vectors 5
Insect-specific viruses in mosquitoes 5
Aedes aegypti 5
Aedes aegypti life cycle 5
The arboviral transmission cycle 6
Transmission of *Aedes*-borne arboviruses 7
Mosuito-vector control strategies 8
Antiviral immune pathways in mosquitoes 9
RNA interference in mosquitoes 11
Dicer-type ribonucleases 13
Dicer 2 domain organization 14
Importance of RNAi effector proteins in arboviral defence 14
Production of vsiRNA and vpiRNA in different arboviruses and ISVs 15
Production of viral DNA from RNA arboviruses 16
Non-retroviral integrated RNA virus sequences 17
Objectives 19

Chapter 2: Publication 1: The PAZ domain of *Aedes* aegypti Dicer 2 is critical for accurate and high-fidelity size determination of virus-derived small interfering RNAs **20**
Chapter 3: Publication 2: Detection and characterization of antiviral proteins against bunyaviruses in mosquito-derived cells **41**
Chapter 4: Publication 3: Dicer-2 mutations in *Aedes aegypti* cells lead to a diminished antiviral function against Rift Valley fever virus and Bunyamwera orthobunyavirus infection **51**
Chapter 5: Publication 4: RNAi-based adaptive immunity in *Aedes aegypti* against arboviruses **67**

Chapter 6: General discussion **100**

Dcr2 domain mutants show different effects on the RNAi response after alphavirus and bunyavirus infection 100

Dcr2 domain mutants reveal differing 21 nt sRNA production after alpha- and bunyaviral infection 102

Primed cells exhibit clone- and virus-specific antiviral activity 106

Priming effects exhibit time-sensitive changes 109

Small RNA sequencing of primed cells shows inconsistencies to antiviral activity and again exhibits clone- and virus-specific effects 110

Uninfected primed cells show no clear evidence for base-line NIRVS-specific vpiRNA production except for one SFV primed clone 113

Conclusion 114

Chapter 7: References **116**

Acknowledgements 129

Chapter 8: Supplementary Data **130**

Publication 1 130

Publication 3 130

Publication 4 130

General discussion 149

Abstract

Arthropod-borne (arbo-) viruses belong to the emerging viruses and pose a continued threat to both human and animal health. Mosquitoes like *Aedes aegypti* present the most prevalent vectors, transmitting arboviruses from multiple different viral families, including dengue virus (DENV), Rift Valley Fever virus (RVFV) and chikungunya virus (CHIKV). As arboviruses establish a productive infection within mosquitoes, the vector mounts an antiviral response. Mosquito species differ strongly in their susceptibility to arboviral infection and transmission. These differences are hypothesized to arise, at least in part, from variation in antiviral immune responses that influence vector comptetence, affecting the ability of arboviruses to establish infection, dissemination to secondary tissues, and ultimately be transmitted to vertebrate hosts.

The main antiviral defense within the mosquito is conveyed by the RNA interference (RNAi) pathways, including the exogenous small interfering (exo-si) RNA pathway. While the overall mechanism of the siRNA pathway is well understood today, little is known about the antiviral importance of the individual domains of Dicer 2 (Dcr2), a key protein within the siRNA pathway. To investigate the antiviral activity of the Dcr2 domains, specifically the helicase, PAZ and RNase III domains, conserved amino acids were determined via multiple sequence alignment with subsequent establishment of multiple mutants containing mutations in the respective domains. After previous studies have established the critical role of both the helicase and RNase III domain in antiviral and silencing activity against Semliki Forest virus (SFV), including a reduced SFV-specific small (s)iRNA production, *Ae.* aegypti-derived Dcr2 knockout cells were transfected with PAZ mutant Dcr2. The PAZ mutant Dcr2 exhibited loss of antiviral activity in comparison to WT Dcr2 after SFV infection, however, they retained intermediate silencing activity. Additionally, the typically 21 nt siRNA production was broadened to 20-22 nt lengths, demonstrating the importance of the PAZ domain processing the correct vsiRNA lengths.

As arboviruses can be found in many different viral families, and thus exhibit strong differences in genome organization, we sought to investigate the effect of the mutant Dcr2 on bunyaviral infection, specifically RVFV and Bunyamwera orthobunyavirus (BUNV). As bunyaviruses, both viruses possess a tri-segmented negative-sense ssRNA genome as opposed to the singular positive-sense ssRNA genome of the alphavirus SFV. All three investigated Dcr2 domains were found to be important for antiviral activity against both RVFV and BUNV. However, one helicase mutant showed continued antiviral activity against RVFV comparable to WT Dcr2 despite RVFV-specific sRNA production comparable to the Dcr2-deficient control. Further investigation is needed to determine the mechanism through which this mutant is still able to mount a functional antiviral response.

Arboviruses have been previously shown to establish prersistent infections in mosquitoes, leading to continued survival of the mosquito and successful transmission to the vertebrate host. While the exact mechanism is part of ongoing research, the production of vDNA from the mostly RNA-based arboviruses is implicated to play a crucial role. Furthermore, these vDNAs are hypothesized to be incorporated into the mosquito genome as non-retroviral integrated RNA virus sequences (NIRVS), as has been shown in case of insect-specific viruses (ISVs). Additionally, the PIWI-interacting (pi)RNA pathway, another RNAi pathway, has been linked to antiviral activity through NIRVS-derived piRNAs targeting actively replicating viral RNA. For investigation of vDNA production, possible NIRVS incorporation and resulting NIRVS-specific sRNA response, primed cells were produced by previous exposure to arboviral challenge, including different arboviral families, before clearance of the infection. The now primed cells were subsequently “re-“ infected with either the virus used for priming or a non-priming virus. Upon investigation of antiviral activity of these primed cells, virus- and clone-specific differences were observed. This includes a decrease of SFV replication in BUNV primed cells which gets more pronounced with higher passage number of the cells, indicating a possible

time-depency of the observed priming effect. This clone-specificity was also observed in the sRNA production of the primed cells. However, both the priming process itself as well as other viral and vector-specific factors could influence the observed effect. Further experiments are needed, included Whole Genome Sequencing and transcriptomics.

Taken together, the findings from this thesis highlight the differences in antiviral response against different arboviral families, including strong variations in effects after previous arboviral priming to secondary arboviral challenge. They even lead to the observation of time-dependent changes of priming effects on antiviral activity in some cases. Additionally, the importance of the individual Dcr2 domains within the siRNA-mediated antiviral response against infections of arboviruses from different viral families has been shown, especially underscoring the antiviral involvement of the helicase- and PAZ domains independent of the RNase III domain. These findings provide new insights into the complexity of arbovirus-mosquito-interactions and antiviral immunity, implying future research opportunities into viral priming and ultimately, its influence on antiviral defense and vector competence.

Zusammenfassung

Arthropoden übertragene (Arbo-) Viren gehören zu den „emerging viruses“ und präsentieren eine wachsende Gefahr für sowohl Menschen als auch Tiere. Stechmücken wie *Aedes aegypti* stellen den am weitesten verbreiteten Vektor dar und übertragen Arboviren aus unterschiedlichen viralen Familien, u.a. Dengue-Virus (DENV), Rift Valley Fieber-Virus (RVFV) und Chikungunya-Virus (CHIKV). Da Arboviren eine produktive Infektion in Stechmücken ausbilden, führt dies zu einer antiviralen Antwort innerhalb des Vektors. Stechmückenarten unterscheiden sich stark in ihrer Anfälligkeit für arboviral Infektionen und deren Übertragung. Es wird vermutet, dass diese Unterschiede zumindest teilweise auf Variationen in den antiviralen Immunantworten zurückzuführen sind, welche die Vektorkompetenz beeinflussen und sich somit auf die Fähigkeit von Arboviren auswirken, eine Infektion zu etablieren, sich in sekundäre Gewebe auszubreiten und schließlich auf Wirbeltiere übertragen zu werden.

Die wichtigste antivirale Abwehr innerhalb der Stechmücken wird durch die RNA-Interferenz (RNAi) Signalwege vermittelt, vorallem dem exogenen small interfering (si)RNA-Signalweg. Während der Mechanismus des siRNA-Signalwegs allgemein gut erforscht ist, ist wenig über die antivirale Bedeutung der individuellen Dicer 2 (Dcr2) Domänen bekannt, welches ein Schlüsselprotein innerhalb des siRNA Signalwegs ist. Um die antivirale Aktivität der Dcr2 Domänen zu untersuchen, speziell der Helikase-, PAZ und RNase III-Domänen, wurden konservierte Aminosäuren mittels Multiple Sequence Alignment ermittelt und darauf basierende Mutanten etabliert, welche Mutationen in den jeweiligen Dcr2 Domänen aufweisen. Frühere Studien haben gezeigt, dass die Helikase- and RNase III-Domänen eine kritische Rolle innerhalb der antiviralen und Silencing-Aktivität gegen Semliki Forest Virus (SFV) haben, und eine verminderte SFV-spezifische small (s)RNA-Produktion. Daraufhin wurden *Ae. aegypti*-basierte Dcr2-Knockout-Zellen mit Dcr2 PAZ-Domänen-Mutanten transfiziert. Die PAZ-Mutanten zeigten einen Verlust der antiviralen Aktivität nach SFV-Infektion in Vergleich zu WT Dcr2, hingegen behielten sie eine intermediäre Silencing-Aktivität. Zudem besaßen die PAZ-Mutanten eine veränderte sRNA-Produktion, die eine erhöhte Produktion von sRNAs von 20-22 nt Länge anstatt der typischen 21 nt aufweist. Dies deutet auf die Relevanz der PAZ-Domäne bei der korrekten Prozessierung der viral dsRNA hinsichtlich der Länge der resultierenden sRNAs hin.

Da Arboviren in vielen viralen Familien zu finden sind, und dementsprechend große Differenzen in der Genomorganisation aufweisen, haben wir entschieden den Effekt der Dcr2-Mutanten auf bunyavirale Infektion zu testen; speziell auf RVFV und Bunyamwera orthobunyavirus (BUNV). Bunyaviren besitzen ein tri-segmentiertes, negativ-orientiertes ssRNA-Genom im Gegensatz zu dem einzelnen positiv-orientierten ssRNA-Genom von Alphaviren wie SFV. Alle drei untersuchten Dcr2-Domänen wurden für wichtig für die antivirale Aktivität gegen RVFV und BUNV befunden. Eine Helikase-Mutante zeigte jedoch weiterhin antivirale Aktivität gegen RVFV vergleichbar mit WT Dcr2 trotz RVFV-spezifischer sRNA-Produktion auf dem Niveau der Dcr2-defizienten Kontrolle. Weitere Untersuchungen werden benötigt, um den Mechanismus, durch den die Mutante weiterhin eine funtkionale antivirale Antwort vermitteln kann, zu entschlüsseln.

Frühere Studien haben gezeigt, dass Arboviren persistente Infektionen in Stechmücken ausbilden, was zu andauerndem Überleben der Stechmücken und so einer erfolgreichen Übertragung zum Wirbeltier-Wirt führt. Während der genaue Mechanismus weiter Teil anhaldender Forschung ist, wurde impliziert, dass die Produktion von viDNA von den großteils RNA-basierten Arboviren eine kritische Rolle dabei spielt. Desweiteren wurde die Hypothese aufgestellt, dass diese vDNA in das Stechmücken-Genom in Form von nicht-retroviralen integrierten RNA-Virussequenzen (NIRVS) eingebaut wird, was für insektenspezifische Viren (ISVs) bereits gezeigt wurde. Zusätzlich wurde der PIWI-interacting (pi)RNA-Signalweg, ein

weiterer RNAi-Signalweg, mit antiviraler Aktivität über NIRVS-basierte piRNAs in Verbindung gebracht, die auf aktiv replizierende virale RNA abzielen. Um vDNA-Produktion, mögliche NIRVS-Integration und daraus resultierende NIRVS-spezifische sRNA-Antwort untersuchen zu können, wurden sogenannte „primed“ Zellen etabliert durch vorangegangene Arbovirus-Infektion aus verschiedenen viralen Familien, die im Anschluss geheilt wurde. Die nun vorbereiteten „primed“ Zellen wurden anschließend erneut mit Arboviren infiziert; entweder mit den zum priming genutzten Virus oder einem nicht-priming Virus. Bei der Untersuchung der antiviralen Aktivität dieser primed Zellen wurden virus- und zellklonspezifische Unterschiede festgestellt. Diese inkludieren eine reduzierte SFV-Replikation in Zellen mit vorrangegangener BUNV-Infektion, welche mit voranschreitender Passagenanzahl der Zellen weiter ausgeprägt wird und somit eine Zeitabhängigkeit des beobachteten „Priming“-Effekts präsentieren. Diese Klonspezifität wurde auch bei der sRNA-Produktion der primed Zellen nachgewiesen. Dennoch können sowohl der „Priming“-Prozess selbst als auch andere virale und vektor-spezifische Faktoren einen erheblichen Einfluss auf den beobachteten Effekt haben. Weitere Experimente werden benötigt, inklusive Whole Genome Sequenzing (dt.: „Gesamtgenom-Sequenzierung“) und Transcriptomics.

Insgesamt zeigen die beschriebenen Experimente die Unterschiede in antiviraler Reaktion auf Arboviren aus verschiedenen viralen Familien, einschließlich starker Variationen hinsichtlich der Effekte von vorherigem antiviralen „Priming“ auf erneute arbovirale Infektion. In manchen Fällen führte dies zudem zu beobachteten zeitabhängigen Veränderungen der “Priming”-Effekte auf die antivirale Aktivität. Zusätzlich wurde die Bedeutung der individuellen Dcr2-Domänen innerhalb der siRNA-vermittelten antiviralen Abwehr gegen Arboviren aus unterschiedlichen viralen Familien gezeigt, die vorallem die antivirale Funktion der Helikase- und PAZ-Domänen unabhängig der RNase III-Domäne unterstreicht. Diese Ergebnisse liefern neue Einblicke in die Komplexität von Arbovirus-Stechmücken-Interaktionen und antiviraler Immunität, und deutet auf Ansatzpunkte für zukünftige Furschungsmöglichkeiten im Bereich des viralen „Primings“ und dem damit verbundenen Einfluss auf die antivirale Abwehr und Vektorkompetenz hin.

List of abbreviations

%	percent
α	alpha
β	beta
µ	micro
A	Adenine/ Alanine
aa	amino acid(s)
Aaeg	*Aedes aegypti*
Ae. aegypti	*Aedes aegypti*
Ae. albopictus	*Aedes albopictus*
Ago	Argonaute
A_i	anti-genome coverage proportion
AMP	antimicrobial peptide
arbovirus	arthropod-borne virus
ATP	Adenosine 5'-triphosphate
ATPase	Adenosine 5'-triphosphatase
AZT	azidothymidine
b	base(s)
BHK	Baby Hamster Kidney cells
BUNV	Bunyamwera orthobunyavirus
C	Cytosine
C-terminus	carboxy-terminus
Cas	CRISPR-associated protein
cDNA	complementary DNA
CEV	California encephalitis virus
CFAV	Cell-fusion agent virus
CHIKV	Chikungunya virus
CPE	cytopathic effect
CPM	counts per million
CRISPR	Clustered Regularly Interspaced Short Palindrome Repeats
Cx. pipiens	*Culex pipiens*
Cx. quinquefasciatus	*Culex quinquefasciatus*

d	day(s)
D	Aspartic acid
D. melanogaster	*Drosophila melanogaster*
Da	Dalton
DCL3	Dicer-like 3 protein
Dcr	Dicer
DENV	dengue virus
d_i	differential coverage
dim	dimension
Dm	*Drosophila melanogaster*
Dmel	*Drosophila melanogaster*
DNA	desoxyribonucleic acid
DNase	desoxyribonuclease
dpi	day(s) post infection
Dredd	Death-related ced-3/Nedd2-like protein
ds	double-stranded
dsRBD	dsRNA-binding-domain
DUF	domain of unknown function
DVRF	*dengue virus restriction factor*
E	Glutamic acid
e.g.	exempli gratia (for example)
ECDC	European Centre for Disease Prevention and Control
eGFP	enhanced green fluorescent protein
endo	endogenous
etc.	et cetera
EVE	endogenous viral element
exo	exogenous
Exp	Exportin
FADD	Fas-associated death domain
FBS	fetal bovine serum
FFLuc	firefly luciferase
Fig.	figure
g	gram(s)

G	Guanine/ Glycine
G_i	genome coverage proportion
GMEM	Glasgow Minimum Essential Medium
GMM	genetically modified mosquito(es)
GR	Dcr2 helicase mutant G488R
h	hour(s)
Hel	helicase subdomain
hpi	hour(s) post infection
hpt	hour(s) post transcription
i	genome position i
i.e.	id est (in other words/ that is)
icDNA	infectious cDNA
IGR	intergenomic region
IMD	immune deficiency
INF	interferon
ISV	insect-specific virus
JAK-STAT	Janus kinase-signal transducer and activator of transcription
JEV	Japanese Encephalitis virus
JNK	c-Jun NH 2-terminal kinase
k	kilo
K	Lysine
KN	Dcr2 helicase mutant K39N
KO	knockout
L	litre/ Leucine
LACV	La Crosse virus
log	logarithm
Loq	Loquacious
m	milli/ meter
M1-M4	Dcr2 PAZ domain mutants
MDS	multi-dimensional scaling
MEB	midgut escape barrier
MIB	midgut infection barrier
min	mínimum/ minute(s)

miRISC	miRNA-induced silencing complex
miRNA	microRNA
MOI	mode of infection
mRNA	messenger RNA
mtR3	Dcr2 RNase III A and B mutant
mut	mutant
n	nano
N	Asparagine
N-terminus	amino-terminus
NGS	Next Generation Sequencing
NIRVS	non-retroviral integrated RNA virus sequence(s)
NLuc	nano luciferase
nt	nucleotide(s)
ONNV	O'nyong-yong virus
ORF	open reading frame
PAMP	pathogen-associated molecular pattern
PAZ	PIWI-Argonaute-Zwille
PBS	phosphate buffered saline solution
PBS-T	PBS-Tween 20
PCLV	Phasi-Charoen-like virus
PCR	polymerase chain reaction
PEG	polyethylene glycol
pen-strep	penicillin-streptomycin
PGN	peptidoglycan
PGRP	PGN-recognition protein
PI3K	phosphatadylinositol-3-kinase
piRNA	PIWI-interacting RNA
PIWI	P-element induced wimpy testis
PLB	Passive Lysis Buffer
pLDDT	predicted local distance difference test
pp	ping-pong
pre	precursor/ premature
pri	primary

PRR	pattern-recognition receptor
qPCR	quantitative PCR
qRT-PCR	quantitative real-time PCR
R	Arginine
R^2	coefficient of determination
RdRp/RDRP	RNA-dependent RNA-polymerase
Rel	*Relish*
RISC	RNA-induced silencing complex
RNA	ribonucleic acid
RNAi	RNA interference
RNase	ribonuclease
RNP	ribonucleoprotein
RLuc	*Renilla* luciferase
Rnt1	yeast ribonuclease T1
RT	reverse transcriptase/ real-time
RT-qPCR	reverse transcriptase quantitative PCR
RVFV	Rift Valley Fever virus
SD	standard deviation
SEM	standard error of the mean
SF2	helicase superfamily 2
SFV	Semliki Forest virus
SFV-FFLuc	SFV4(3H)-FFLuc
SGEB	salivary gland escape barrier
SGIB	salivary gland infection barrier
SINV	Sindbis virus
siRISC	siRNA-induced silencing complex
siRNA	small interfering RNA
sRNA	small RNA
ss	single-stranded
T	Thymine
TAB	TAK1-binding protein
TAK	transforming growth factor β-activated kinase
TBEV	tick-borne encephalitis virus

TCID50	tissue culture infectious dose 50
TLR	Toll-like receptor
TotM	*Turandot M*
TPB	tryptose phosphate broth
U	Uridine
UPD	Unpaired
UTR	untranslated region
V	Valin
Vir-1	*virus-induced RNA-1*
vDNA	viral DNA
vRNA	viral RNA
vpiRNA	viral piRNA
vsiRNA	viral siRNA
w/v	weight/volume
WHO	World Health Organization
WNV	West Nile virus
WT	wild-type
Y	Tyrosine
YFV	Yellow Fever virus
ZIKV	Zika virus
Zuc	Zucchini

Chapter 1: Introduction

Arboviruses

Arboviruses are a distinct group of viruses that are characterized by being transmitted to vertebrates by arthropods including mosquitoes, ticks, midges and sandflies. Arboviruses are found in a plethora of different viral orders, families and genera, with most clinically important arboviruses being RNA viruses. The arthropods serve as both the vector and natural reservoir, with arboviruses being able to establish a productive infection, meaning they are actively replicating in both the arthropod vector and the vertebrate host. Many arboviruses are zoonotic and cause millions of infections in humans, leading to clinical symptoms, including fever, headache, rash, haemorrhagic fever or encephalitis (Salimi et al., 2016). The idea of arthropods, namely mosquitoes, being able to transmit diseases was first proposed by Cuban physician Carlos Finlay in 1881 among a Yellow Fever outbreak in Havana, Cuba (Chaves-Carballo, 2005).

Today, mosquitoes are still considered to be main vector of many clinically important arboviruses like Yellow Fever virus (YFV, *Flaviviridae*, *Orthoflavivirus*), Rift Valley Fever virus (RVFV, *Phenuiviridae*, *Phlebovirus*), chikungunya virus (CHIKV, *Togaviridae*, *Alphavirus*) and dengue virus (DENV, *Flaviviridae*, *Orthoflavivirus*), with DENV alone causing around 100-400 million infections in humans annually according to the World Health Organization (WHO).

Semliki Forest virus

Semliki Forest virus (SFV, *Togaviridae*, *Alphavirus*) was discovered in 1944 when it was isolated from mosquitoes in the Semliki Forest in Uganda (Smithburn and Haddow, 1944). SFV is considered a model virus for arboviral research in general as well as for other alphaviruses, due to its close relation to clinically important arboviruses like CHIKV, while it generally does not cause disease in humans (Atkins et al., 1985). *Alphaviruses* like SFV contain a positive single-stranded ((+)ss) RNA genome with a 5'-cap and 3'- polyadenylation (see Fig. 1). It encodes for at least nine proteins as part of either the structural and non-structural polyprotein which are cleaved by separate post-translational cleavage pathways (Strauss and Strauss, 1994). The non-structural proteins nsP1, nsP2, nsP3 and nsP4 are responsible for RNA synthesis and are situated at the 5' end of the viral genome, as part of the non-structural polyprotein (Contu et al., 2021). The subgenomic promotor separates the non-structural from the structural proteins, followed downstream by the structural polyprotein comprised of the Capsid protein (C), Envelope proteins 3 and 2 (E3 and E2) as part of p62, 6K and the Envelope protein 1 (E1). The envelope proteins E1, E2 and E3 make up the viral envelope, while the C protein makes up the isohedral capsid containing the genome and is encased in a lipid bilayer derived from the host cell. The small 6 kDa long protein (6k) is not incorporated into the virion, but facilitates the budding process (Contu et al., 2021; Roussel et al., 2006).

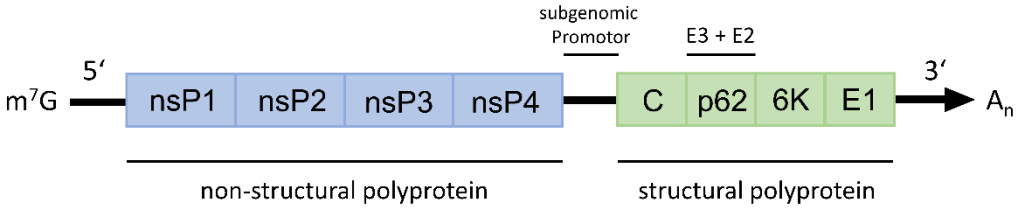


Fig. 1: Alphaviral genome organization. *Alphaviruses* like SFV possess a (+)ssRNA genome that possesses a 5'-cap (m^7G) and 3'-polyadenylation (A_n). The genome is comprised of two open reading frames (ORFs) encoding for the non-structural polyprotein (blue), made up of nsP1, nsP2, nsP3 and nsP4, and the structural polyprotein (green), containing the Capsid (C) protein, p62 (Envelope proteins 3 and 2, E3 and E2) and Envelope protein 1 (E1), separated by the subgenomic promotor.

Zika virus

Zika virus was first identified in rhesus monkeys in 1947 in the Zika Forest in Uganda (Dick et al., 1952). It belongs to the genus *Orthoflavirus* as part of the family *Flaviviridae*, thus possessing a (+)ssRNA genome with a 5'-cap and no 3'-polyadenylation. The genome is flanked by 5' and 3' untranslated regions (UTRs), with especially the 3' UTR containing multiple secondary structures required for viral replication, translation and pathogenesis (Brinton and Basu, 2015; Fernández-Sanlés et al., 2017; Ng et al., 2017; Ramos-Lorente et al., 2021). It encodes for a polyprotein which is post-translationally cleaved into its ten proteins, three structural and seven non-structural (see Fig. 2). The structural proteins include the Capsid (C) protein, the precursor membrane (prM) protein the envelope (E) protein and are situated at the 5' end of the polyprotein. The non-structural proteins include NS1, NS2A, NS2B, NS3, NS4A, 2K, NS4B and NS5, which are responsible for RNA synthesis and other interaction with the cell, for example the immune response (Donaldson et al., 2025; Zhang et al., 2025). ZIKV infections generally cause asymptomatic or only mild symptoms, but it can also lead to severe fetal malformations in pregnant patients. Multiple intermittent outbreaks have been reported in Asia, Africa and the Pacific region, with the biggest outbreak observed in the Americas in 2015-2026 (Rabe et al., 2025).

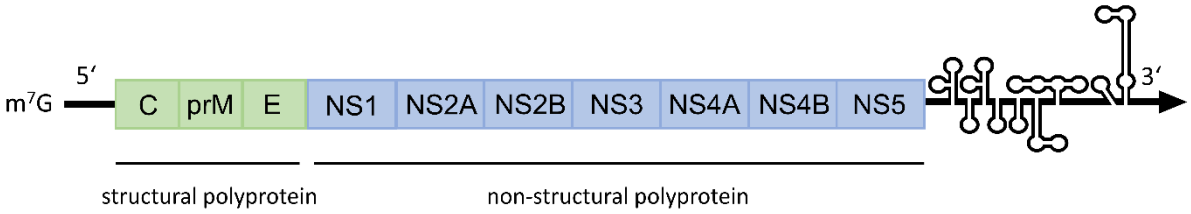


Fig. 2: Genome organization of ZIKV. The (+)ssRNA genome of *Orthoflaviviruses* contains a 5'-cap (m7G) and one ORF encoding for a polyprotein containing both structural (green) and non-structural (blue) proteins. The capsid (C) protein, the precursor membrane (prM) and envelope (E) protein belong to the structural proteins, while NS1, NS2A, NS2B, NS3, NS4A, NS4B and NS5 belong to the non-structural proteins. The 3' UTR contains several functionally important secondary structures.

Bunyamwera orthobunyavirus

Bunyamwera orthobunyavirus (BUNV, *Peribunyaviridae*, *Orthobunyavirus*) belongs to the class *Bunyaviricetes* and thus possesses a tri-segmented negative-sense single-stranded ((-)ss) RNA genome. It was first discovered in the Semliki Forest in Western Uganda in 1943 (Dutuze et al., 2018; Kokernot et al., 1958). Primarily found throughout sub-Saharan Africa,

BUNV is a zoonotic disease, presenting with generally mild symptoms like fever, rash and joint pain in mammals, including humans (Dutuze et al., 2018; Evans et al., 2021). Its genome is tri-segmented, without a 5'-cap or 3'-polyadenylation, and is comprised of a small (S), medium (M) and large (L) segment. The L-segment expresses for the viral polymerase (L protein), while the M-segment encodes for a polyprotein which is co-translationally processed into the non-structural protein NSm and the external glycoproteins Gn and Gc (Blakqori et al., 2012). The nucleocapsid (N) protein as well as the non-structural NSs protein are both translated from the same mRNA of the S-segment, likely from two overlapping ORFs (Blakqori et al., 2012; Bridgen et al., 2001). During replication, "cap snatching" takes place, a mechanism in which the 5' cap of host RNAs is transferred to the viral mRNA to prime for viral transcription (Olschewski et al., 2020).

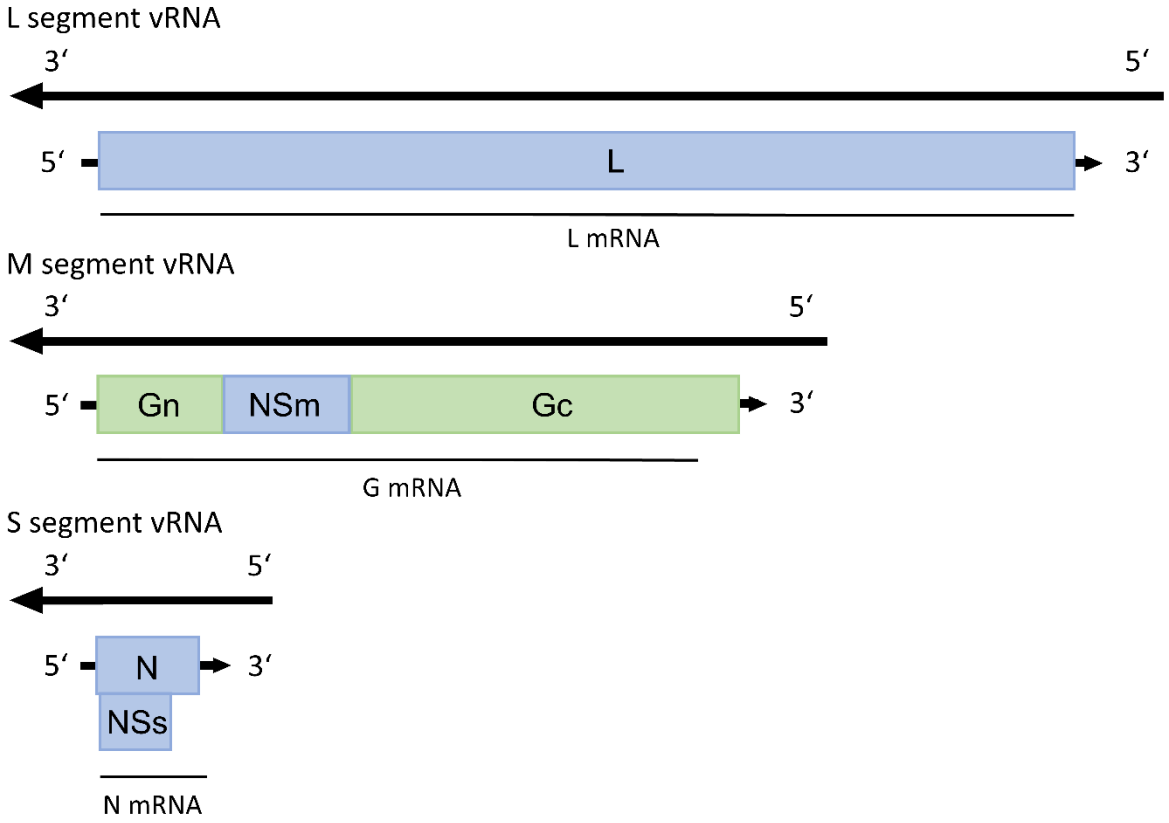


Fig. 3: *Orthobunyavirus* genome organization. *Orthobunyaviruses* possess a tri-segmented (-)ssRNA genome with a large (L, top), medium (M, middle) and small (S, bottom) segment The coloured boxes on the mRNA depict the ORFs that encodes for structural (green) and non-structural (blue) proteins. The L mRNA of the L-segment encodes for the L protein (L), the G mRNA of the M-segment encodes for the external glycoproteins (Gn and Gc) and the non-structural NSm protein, and the N mRNA of the S-segment encodes for the nucleocapsid (N) protein as well as the non-structural NSs protein.

Rift Valley Fever virus

The Rift Valley Fever virus (RVFV, *Phenuiviridae*, *Phlebovirus*) also belong to the class of *Bunyaviricetes*, so just like BUNV, it possesses a tri-segmented (-)ssRNA genome. The first isolation of RVFV goes back to 1930 in the Rift Valley in Kenya (Daubney and Hudson, 1931). RVFV is the causative agent of Rift Valley Fever, a zoonotic disease associated with mild symptoms, including dizziness, fever and weight loss, with rare cases of encephalitis and shock, leading to a lethality of 0.5-2% (Kim et al., 2023; Pepin et al., 2010). Originally a disease

contained to the region of sub-Saharan Africa, cases have since been reported in Yemen, China and Saudi Arabia, among others (Liu et al., 2016; Nanyingi et al., 2015). Like the *Orthobunyaviruses*, genomes of *Phleboviruses* also possess no 3'-polyadenylation nor a 5' cap, thus transcription priming of the viral mRNAs is reliant on a "cap-snatching" mechanism (Olschewski et al., 2020). The genome contains an L-segment encoding for the RNA-dependent RNA polymerase (L protein), and an M-segment encoding for a polyprotein including the external glycoproteins Gn and Gc and the non-structural NSm protein, and a 78 kDa glycoprotein (P78) important for viral dissemination in the mosquito vector from a separate AUG (Kreher et al., 2014; Terasaki et al., 2021). While the S-segment also expresses the nucleocapsid (N) protein and the non-structural NSs protein, here, the S-segment is ambisense, with the N protein in negative-sense at the 3' end and the NSs protein in positive-sense at the 5' end (Bouloy and Weber, 2010; Giorgi et al., 1991; Shalamova et al., 2024). Located between the two opposing ORFs of the S-segment is an intergenic region (IGR) that includes a stem-loop structure and is responsible for the transcription termination (Albariño et al., 2007; Ikegami et al., 2007).

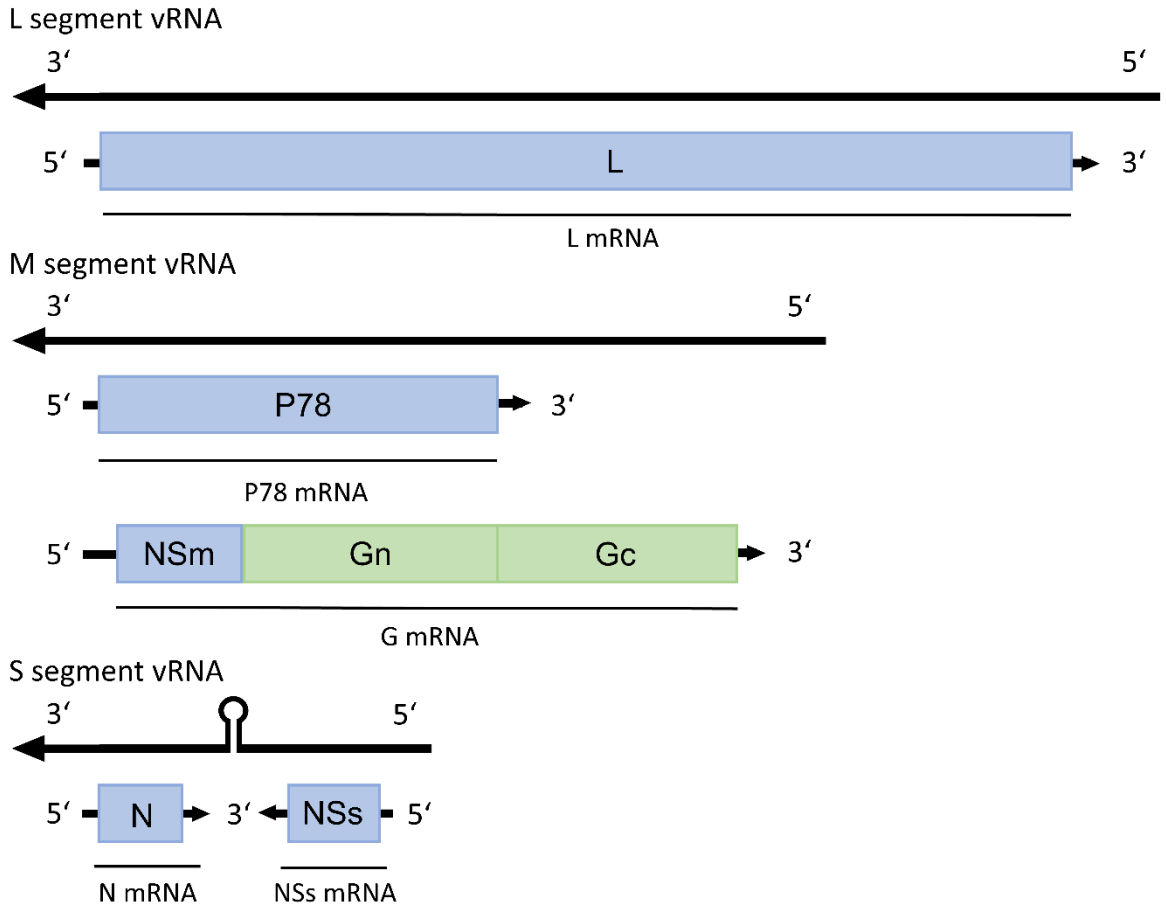


Fig. 4: Genome organization of RVFV. The genome of *Phleboviruses* is a tri-segmented (-)ssRNA genome comprised of an L (top), M (middle) and S (bottom) segment. Beneath the vRNA of the segments, the respective mRNAs are shown, including coloured boxes indicating the encoded structural (blue) and non-structural (green) proteins. The L-segment encodes for the L protein, and the M-segment for the non-structural NSm protein and the external glycoproteins Gn and Gc, as well as a 78 kDa glycoprotein (P78) from a separate AUG. The ambisense S-segment expresses for the nucleocapsid (N) protein in negative sense on the 3' end, and the non-structural NSs protein in positive-sense at the 5' end, with a stem-loop structure in the IGR.

Arboviral mosquito vectors

Arboviruses are considered emerging viruses and pose a significant challenge to public health globally due to the continued spread of their most important vector, the mosquito. The two most important mosquito vectors are *Aedes aegypti* and *Aedes albopictus*, being able to transmit DENV, CHIKV and YFV, among others. Originally contained to sub-Saharan Africa and Southeast Asia, respectively, both vectors have found their way to the Americas and Europe due to climate change and globalisation (Abbasi, 2025; Paupy et al., 2009; Powell and Tabachnick, 2013). Other important mosquito vectors are *Culex* mosquitoes, including *Cx. pipiens* and *Cx. quinquefasciatus*, with *Cx. pipiens* able to transmit RVFV and Sindbis virus (SINV, *Togaviridae*, *Alphavirus*), and both species functioning as a vector for West Nile virus (WNV, *Flaviviridae*, *Orthoflavivirus*) (Shocket et al., 2020).

Insect-specific viruses in mosquitoes

Insect-specific viruses (ISVs), like arboviruses, belong to a variety of different viral families like *Flaviviridae*, *Togaviridae*, *Phenuiviridae* and *Peribunyaviridae*, with many being closely related to arboviruses. These include viruses able to productively infect mosquitoes, but, like all insect-specific viruses, lack the ability to replicate in vertebrates (Bolling et al., 2015; Vasilakis and Tesh, 2015). ISVs are predominantly transmitted vertically and are thus sustained in natural mosquito populations (Cook et al., 2006; Lutomiah et al., 2007). The first ISV identified to be able to infect both *Ae. albopictus* and *Ae. aegypti* cells is Cell-fusing agent virus (CFAV; *Flaviviridae*, *Flavivirus*) (Stollar and Thomas, 1975). The cytopathic effect (CPE) typical for CFAV leads to the eponymous fusion of cells. Previous studies have shown that simultaneous infection with CFAV and DENV or ZIKV resulted in a significant inhibition of arboviral dissemination within mosquitoes both *in vivo* and *in vitro*, leading to a potential reduction in transmission efficiency for DENV and ZIKV (Baidaliuk et al., 2019).

Aedes aegypti

Ae. aegypti originates from the zoophilic forest-dwelling treehole mosquito *Ae. aegypti formosus* in sub-Saharan Africa (Brown et al., 2014). The development and expansion of human settlements lead to the establishment of alternate food sources and breeding grounds for the mosquitoes, resulting in the human-adapted vector species of *Ae. aegypti* with frequent backcrossing with forest-dwelling species [45]. It is likely that these mosquitoes were introduced to the Americas by following along the routes of slave-trade and subsequently spreading to tropical and sub-tropical areas throughout the world, including big parts of the Asian continent (Brown et al., 2014).

Today, *Ae. aegypti* is continually invading new regions globally, aided by e.g. human travel routes like shipping routes, globalization, climate change and the extensive urbanization of rural areas. As of June 2025, the European Centre for Disease Prevention and Control (ECDC) reports established *Ae. aegypti* colonies in Cyprus and the Black Sea coastal regions of Turkey, Georgia and Russia.

Aedes aegypti life cycle

As for all *Aedes* species, there are four distinct life cycle phases: egg, larva, pupa and adult mosquito (see Fig. 5A). After mating, female mosquitoes take up blood meals to supply for the development of their eggs, which they lay in still bodies of water or moist surfaces. The eggs

are black and elliptical with a diameter of ~0.5 mm. Embryogenesis generally takes two to three days (Rogers, 2025), but in absence of water, the eggs can remain viable for up to a year due to high resistance to desiccation (Farnesi et al., 2009; Faull and Williams, 2015).

After the eggs hatch, the emerging larvae undergo multiple developmental stages, which include the only growth stage in the life cycle and the only feeding stage during maturation. The length of the larvae stage depends on multiple environmental factors like temperature, availability of food and larval density, with the average time span being four to five days. As soon as the larvae enter the non-feeding pupa stage, a series of internal transformations take place before the adult mosquito emerges after about two days under optimal conditions (Carvalho and Moreira, 2017), before mating takes place within two days of the emergence from the pupal stage and female mosquitoes consume their first blood meal (Rogers, 2025).

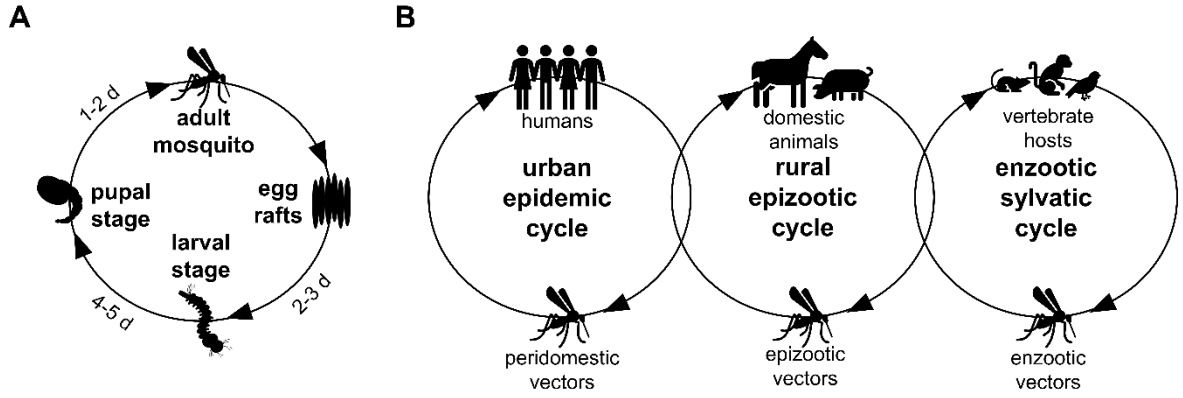


Fig. 5: *Aedes* life cycle and arboviral transmission cycle. Schematic representation of the life cycle of *Aedes* mosquitoes (**A**) and the arboviral transmission cycle (**B**). The *Aedes* life cycle involves female mosquitoes laying black, elliptical eggs in wet environments. These eggs hatch within 2-3 d under optimal conditions, starting the larval stage with an average length of 4-5 d. The larva then develops into a non-feeding pupa, with the adult mosquito emerging after 1-2 d before mating and the subsequent first blood meal of the female mosquito. The arboviral transmission cycle includes three distinct cycles: the enzootic sylvatic cycle involving rodents, non-human primates and birds, the rural epizootic cycle involving domestic animals, and the urban epidemic cycle involving humans. Figure 5B adapted from (Mueller and Cao-Lormeau, 2018).

The arboviral transmission cycle

While the transmission of arboviruses is mainly based on biological transmission which involves active pathogen development and reproduction in the vector, mechanical transmission through contaminated mouthparts of the mosquito, direct transmission through infected material or vertical transmission can occur (Kuno and Chang, 2005).

Most arboviruses are zoonotic, leading to the enzootic sylvatic transmission cycle including birds, rodents and non-human primates as reservoirs (see Fig. 5B). Due to the spread of human settlements, new transmission cycles are established through expansion of the vectors host range, thus leading to the rural epizootic cycle in which the mosquito also targets domestic animals like horses and pigs, bringing them closer to human hosts until a urban epidemic cycle is established involving humans (Mueller and Cao-Lormeau, 2018). Another possible route for human infection is spill-over events from both the enzootic sylvatic and rural epizootic cycle unto humans.

Transmission of *Aedes*-borne arboviruses

Upon ingestion of a blood meal by the female *Aedes* mosquito from a host or reservoir, the arboviral particles are taken up and disseminate throughout the mosquito, starting with the midgut (see Fig. 6). To establish viral replication within the midgut lumen, virions must pass the midgut infection barrier (MIB) which may hinder the viral particles from entrance due to virus-receptor incompatibilities or immune responses in the midgut (Carpenter and Clem, 2023). After crossing the MIB and successful replication establishment, the viral particles need to pass the midgut basal lamina known as the midgut escape barrier (MEB), which likely happens due to changes in permeability or possible damage to the basal lamina (Johnson et al., 2024). From there, the virus disseminates throughout the mosquito, e.g. to fat tissues, haemocytes or nerve and muscle tissue through the haemolymph (Franz et al., 2015; Rückert and Ebel, 2018). To reach the salivary glands for viral transmission from the mosquito to a vertebrate host, the virus is required to pass the salivary gland infection barrier (SGIB). Virus amplification in the haemolymph seems to be a prerequisite for penetration of the basal lamina of the salivary glands (Vega-Rúa et al., 2015). The virus replicates within the salivary glands and the newly produced viral particles are then stored until the next blood meal. For successful transmission, the last hurdle is represented by the salivary gland escape barrier (SGEB), constituted by different genetic or environmental factors that might hinder the virus to be released alongside the saliva (Sanchez-Vargas et al., 2021).

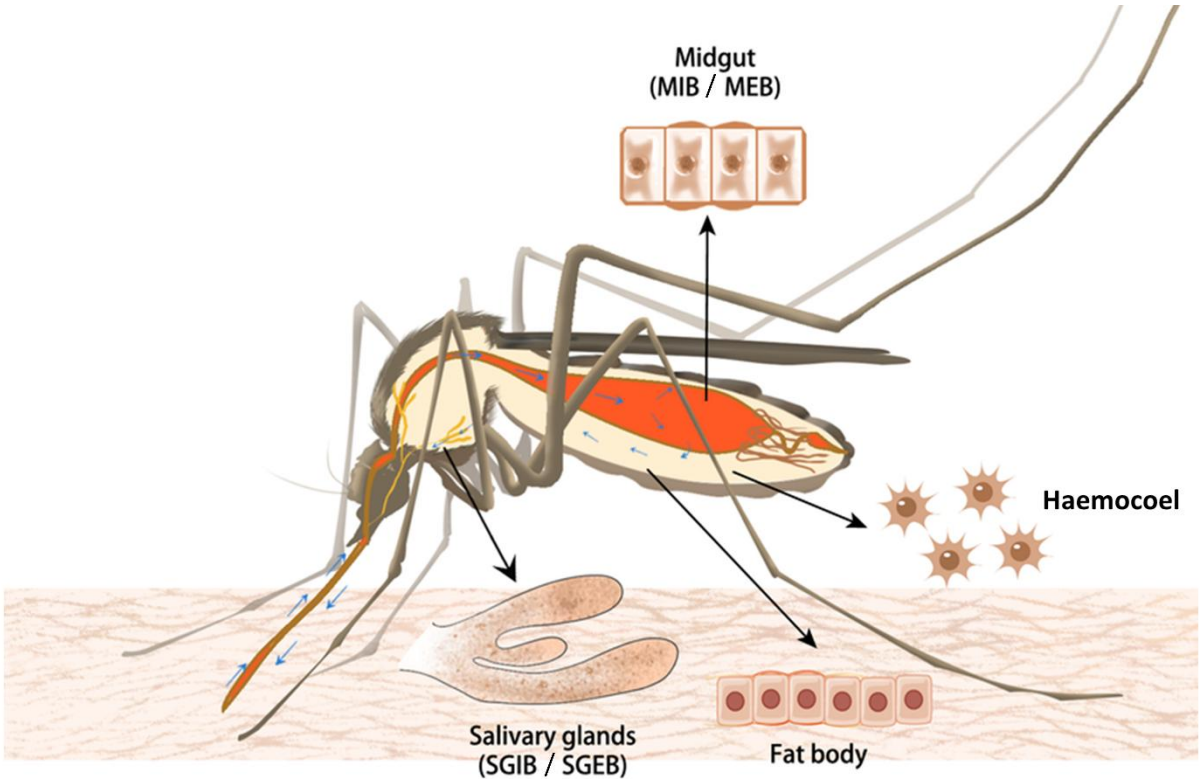


Fig. 6: Arboviral infection and dissemination in the mosquito vector. Upon ingestion of arboviral particles while blood feeding, the virus enters the midgut epithelium to establish viral replication by passing the midgut infection barrier (MIB). As soon as the virus passes the first physical barrier represented by the basal lamina of the midgut, also known as the midgut escape barrier (MEB), it disseminates throughout the mosquito's body, specifically including the fat body and the haemolymph, before reaching and entering the salivary glands by overcoming the salivary gland infection barrier (SGIB). The virus replicates again in the salivary glands before finally being released together with the saliva upon the next blood meal and thus transmitting to the vertebrate host after evading the salivary glands escape barrier (SGEB). Figure adapted from (Li et al., 2024).

Mosquito-vector control strategies

Vector control strategies, in this case aimed at mosquitoes can be grouped into three distinct groups depending on who or what the control measures target within the transmission cycle: the human host, the human-vector interaction or the vector itself (see Fig. 7). Human-vector interaction control includes measures to avoid or reduce contact like mosquito nets, which show limited impact against both *Ae. aegypti* and *Ae. albopictus*, as both are day-biting insects. Preventative measures directly including the human host, mostly vaccination, are often either unavailable or difficult to develop and administer. Only a few effective vaccines are available, including vaccines against YFV, Japanese encephalitis virus (JEV, *Flaviviridae*, *Orthoflavivirus*), DENV, tick-borne encephalitis (TBEV, *Flaviviridae*, *Orthoflavivirus*) and new vaccines against CHIKV, while there is no vaccine for other clinically important arboviruses like WNV or ZIKV.

Control strategies directly aimed at the mosquito vector can also be divided into three different categories based on their mode of operation: environmental, chemical or biological. Chemical control strategies, including indoor residual spraying and insecticide treated materials, are limited by e.g. environmental contamination, toxin accumulation, toxicity to humans and potential resistances to insecticides developing in the targeting vector (Horstick et al., 2017). Environmental methods aim at reducing or destroying breeding sites, including the restriction of access to water reservoirs, the emptying or destroying of residual water sites, and implementing strategic schemes for waste management (Buhler et al., 2019). These measures heavily depend on large-scale compliance of the general public, and get even more complicated when faced with species like *Aedes*, which can lay eggs in very small amounts of water, with their eggs also able to withstand desiccation for up to a year. While environmental vector control mainly focusses on the reduction of vector population, biological strategies also involve modifying the vector population itself to reduce the potential of transmission, e.g. through the use of intracellular endosymbionts like *Wolbachia* (Flores and O'Neill, 2018; Yen and Failloux, 2020). *Wolbachia* is a bacterium belonging to the family of *Anaplasmataceae* and is found in a wide range of invertebrates like nematodes and arthropods, including *Drosophila melanogaster* and *Ae. albopictus* (Werren, 1997). It can be extracted from native hosts and introduced into other mosquitoes like *Ae. aegypti* via microinjection before releasing the mosquitoes, as *Wolbachia* is transmitted vertically from the female mosquito to its eggs. In *Ae. aegypti*, *Wolbachia* halves the lifespan, leading to less offspring, and has been shown to directly inhibit DENV and CHIKV infection in the mosquito (Moreira et al., 2009). Other biological strategies involve the use of genetically modified mosquitoes, aiming to lead to either immunity against arboviruses in female mosquitoes, death of the mosquito upon arboviral infection, rendering the mating of modified males and wild-type females unproductive or produce non-viable offspring (Evans et al., 2019; Flores and O'Neill, 2018). Despite the potential, introducing genetically mosquitoes into wild populations could lead to unforeseen ecological damage, making this approach more complicated and riskier, with a need of close surveillance in case of genetically modified offspring reaching adulthood.

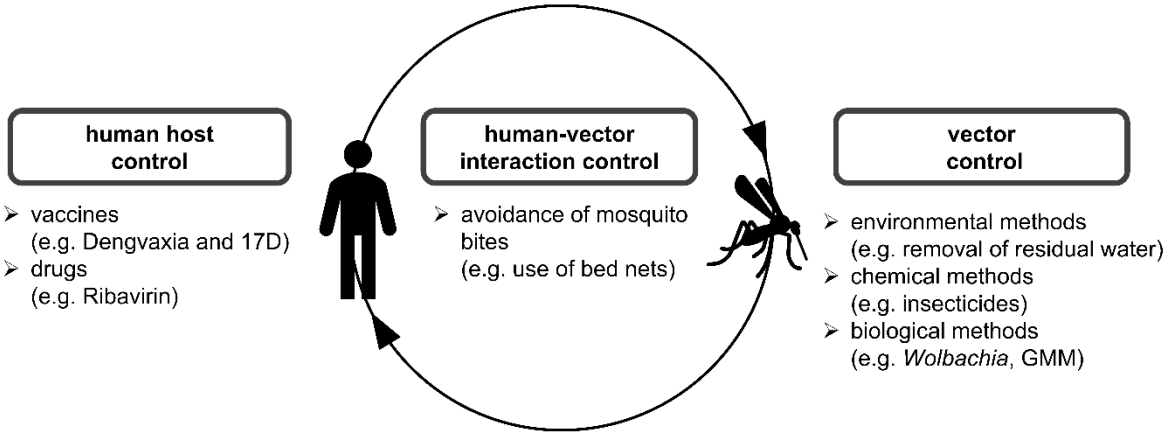


Fig. 7: Vector control strategies for mosquitoes. Depicted are the different methods including examples for mosquito-borne arbovirus control. The strategies can be divided into human-host control (left), human-vector interaction control (middle) and vector control (right). Human-host control includes vaccines, e.g. Dengvaxia, a DENV vaccine and 17D, a YFV vaccine, and anti-viral drugs like Ribavirin. Human-vector-interaction control strategies focus on the avoidance of contact between human and mosquito to reduce the chance of mosquito bites and thus arboviral transmission, including the use of bed nets. Lastly, vector control is divided into environmental methods, e.g. the removal of residual water, chemical methods, e.g. insecticides, and biological methods including injection of *Wolbachia* into new species or introduction of genetically modified mosquitoes (GMM).

Antiviral immune pathways in mosquitoes

It is generally accepted that insects lack a classical, pathogen-specific adaptive immune system, thus lacking an immunological memory, instead relying solely on innate immunity (see Fig. 8). The innate immunity in mosquitoes relies physical barriers like the MIB, MEB, SGIB and SGEB, and upon crossing of those barriers by a pathogen, cellular and humoral responses are activated depending on the pathogen. While the cellular response including phagocytosis, autophagy and apoptosis, are directly engaged upon infection of the haemolymph, the humoral response takes multiple hours before its employed. The resulting pathways either provide general antiviral defence like RNA interference (RNAi), while others, like autophagy, only present antiviral response against specific viruses (Palmer et al., 2018). To induce autophagy, viruses, specifically rhabdoviruses and bunyaviruses, may bind to the transmembrane receptor Toll-7, leading to the virus being enveloped by membrane vesicles before fusing with a lysosome, resulting in a autophagolysosome and subsequent degradation (Brackney et al., 2020).

Both the Toll and the immune deficiency (IMD) pathway involve nuclear factor κB (NF-κB). Generally, these pathways are activated by recognition of a pathogen associated molecular pattern (PAMP) by a pattern recognition receptor (PRR). In case of the Toll pathway, Toll-like receptors (TLRs), like Toll-9, can recognize and bind viral components like viral RNA (Chauhan et al., 2025). Viruses are not able to activate the IMD pathway directly, as they lack the peptidoglycans (PGNs) typically found on the surface of bacteria, but both the blood meal and the virus itself can influence the mosquito's microbiota, leading to the induction of the IMD pathway to regulate the bacterial growth and thus ultimately limiting viral replication as well (Barletta et al., 2017). In both signalling pathways, the inhibitor of κB (IκB) is phosphorylated by the IκB kinase, resulting in the degradation of IκB and subsequently to the release of the *NF-κB* transcription factor, which induce antimicrobial peptides (AMPs) (Palmer et al., 2018).

Another important antiviral defence mechanism is presented by the Janus kinase-signal transducer and activator of transcription (JAK-STAT) pathway. Viral entry of a cell leads to cellular damage and stress, likely triggering cytokines of the unpaired (UPD) family to bind to the Domeless receptor, thus activating the JAK-STAT pathway (Palmer et al., 2018). Another possibility for JAK-STAT activation relays on the antiviral gene *Vago* induced by the siRNA pathway, likely using a yet unidentified receptor (Paradkar et al., 2012), though the possible involvement of *vago* in mosquito antiviral immunity is still debated (Couderc et al., 2025). Upon activation of the pathway, the receptor associated JAK Hopscotch phosphorylates Domeless on the cytoplasmic side, leading to recruitment of Stat92E and the formation of the receptor/JAK/STAT complex using further phosphorylation and dimerization before translocation of dimerized Stat92E to the nucleus where it initiates transcription of antiviral genes (Arbouzova and Zeidler, 2006; Kumar et al., 2018; Xia et al., 2025).

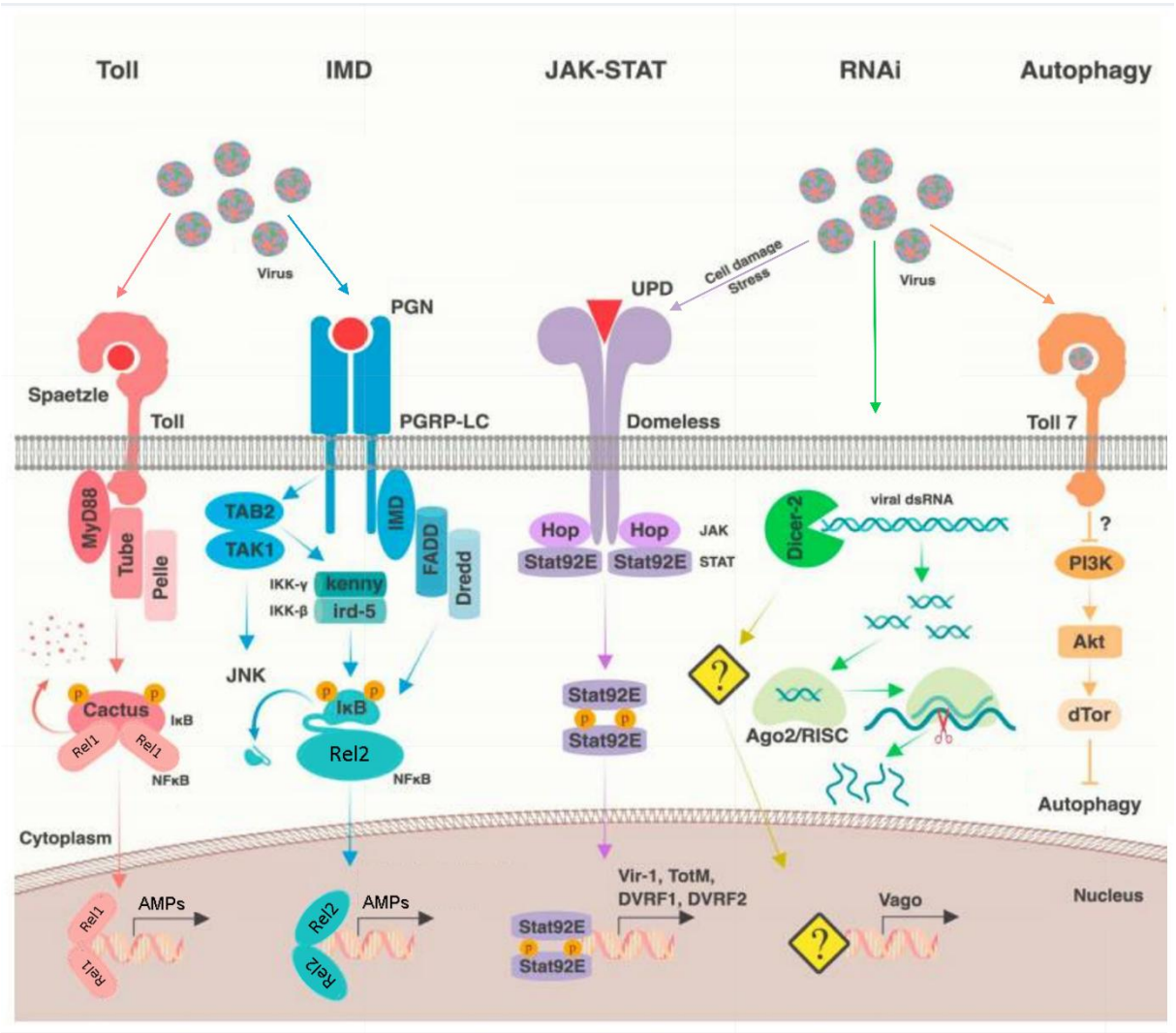


Fig. 8: Antiviral immune pathways in mosquitoes. The antiviral immune defence in mosquitoes includes the **Toll pathway, the immune deficiency (IMD) pathway, the Janus kinase-signal transducer and activator of transcription (JAK-STAT) pathway, the RNA interference (RNAi) pathway** and **autophagy**, among others. In the classical **Toll pathway**, recognition of PAMPs by PRRs leads to the binding of Spaetzle to a Toll receptor, which then recruits the adapter proteins *MyD88*, *Tube* and *Pelle*. These proteins phosphorylate *Cactus* which encodes for the IκB, leading to its degradation and subsequent release of the

transcription factor *Rel1* in mosquitoes, finally resulting in transcription of antimicrobial peptides (AMPs). The **IMD pathway** is classically activated by the recognition and binding of peptidoglycans (PGNs) to the peptidoglycan recognition protein LC (PGRP-LC). These PGNs are found on the surface of gram-positive bacteria, and the binding might result from a change in the microbiota of the mosquito after a blood meal and subsequent viral infection. The activated IMD and Fas-associated death domain (FADD) adapter molecules themselves stimulate the caspase Death-related ced-3/Nedd2-like protein (Dredd), transforming growth factor β- activated kinase 1 (TAK1) and TAK1-binding protein 2 (TAB2), which activate the IκB kinases Kenny and ird-5, and are also associated with the c-Jun NH 2-terminal kinase (JNK) pathway, which plays a major role in inducing cell death via apoptosis. The two IκB kinases phosphorylate the transcription factor *Rel2*, activating it with the help of Dredd via proteolytic cleavage. Upon translocation to the nucleus, *Rel2* facilitates the transcription of AMPs. The **JAK-STAT pathway** is activated through binding of the unpaired (UPD) ligand to the Domeless receptor, likely caused by cellular damage and stress signals after viral infection. The receptor, the JAK-tyrosine kinase hopscotch and Stat92E build a complex, leading to the dimerization and relocation of Stat92E to the nucleus, leading to the transcription of antiviral genes like the *virus-induced RNA-1* (*vir-1*) gene, the *Turandot M* (*TotM*) gene, and the *dengue virus restriction factor 1* and *2* (*DVRF-1* and *DVRF-2*) genes. The **RNAi pathway**, more specifically the exogenous (exo-) small interfering (si)RNA pathway, starts with the recognition and subsequent cleavage of viral dsRNA into typically 21 nt long viral small interfering (vsi)RNAs by the endonuclease Dicer-2. These vsiRNAs are then used as a guide by Argonaute-2 (Ago2) as part of the RNA-induced silencing complex (RISC) to target and terminate complementary viral RNA, thus leading to the inhibition of viral replication. Dicer-2 might also be involved in the activation of the *Vago* gene, itself possibly involved in alternative activation of the JAK-STAT pathway. To initiate **autophagy**, some viruses may bind to Toll-receptor 7 (Toll 7), likely leading to autophagy induction via negative regulation of the phosphatidylinositol-3-kinase (PI3K)-Akt pathway. Figure adapted from (Palmer et al., 2018).

RNA interference in mosquitoes

RNA interference (RNAi) presents as the most vital antiviral immune pathway within mosquitoes. There are three distinct pathways, named after the eponymous source RNA inducer molecules: **the micro (mi)RNA pathway**, **the P-element induced wimpy testis (PIWI)-interacting (pi)RNA pathway** and **the small interfering (si)RNA pathway**, which can be further divided into the endogenous (endo-) and exogenous (exo-) siRNA pathway depending on the siRNA source (see Fig. 9).

The **miRNA pathway** is involved in gene expression regulation, with the eponymous miRNAs being small non-coding RNAs of ~22-23 nt length (Asgari, 2014). Primary (pri-) miRNAs are transcribed from DNA sequences, typically containing hairpin structures, before being processed into precursor (pre-) miRNA duplexes by the ribonuclease Drosha and then finally into mature miRNA/miRNA* duplexes in the cytoplasm by the ribonuclease Dicer 1 (Dcr1) accompanied by its co-factor Loquacious (Breving and Esquela-Kerscher, 2010; O'Brien et al., 2018). The miRNA/miRNA* duplex is then taken up by the miRNA-induced silencing complex (miRISC) including Argonaute 1 (Ago1), where the duplex is unwind and the miRNA strand is used to target partially complementary cellular mRNA leading to degradation of the transcript, translational inhibtion or in some rare cases increased translation (Donald et al., 2012; Liu et al., 2023; Rozen-Gagnon et al., 2021).

The **piRNA pathway** relies on 24-32 nt long piRNAs and is known for transposon repression and gene expression modulation. The piRNAs arise from ssRNA precursors, called premature (pre-) piRNAs, from genomic loci termed piRNA clusters, which are processed into primary

piRNAs (pri-piRNAs) through cleavage by the ss-specific nuclease Zucchini (Zuc), thus generating an initial pool of piRNAs (Lucas et al., 2013). Primary piRNAs are further processed by Argonaute 3 (Ago3), PIWI 5 and 6 into secondary piRNAs, which themselves are used to target and process primary piRNAs, leading to a so called “ping-pong” amplification loop (Chary et al., 2025). The involvement of PIWI 5 and 6 is specific to viral piRNAs, with other e.g. transposon-derived piRNAs being often dependent on different PIWI proteins (Miesen et al., 2015). The Ago3 associated piRNAs are also used to target cognate transposon mRNA sequences, leading to post-transcriptional repression of transposable elements (Duc et al., 2019; Gunawardane et al., 2007). Within the amplification loop, the PIWI or Ago3 associated piRNAs acquire a characteristic pattern presented by a 10 nt overlap, an Uridine at position 1 (U_1, PIWI5/6) in the anti-sense strand and an Adenine at position 10 (A_{10}, Ago3) in the sense strand, with Ago3 associated piRNAs also being methylated at the 3’ prime end, resulting in mature piRNAs. The exact mechanisms and involvements of the different PIWI proteins are still subject to speculation and ongoing research, including a potential antiviral role of PIWI4.

Both the **endo- and the exo-siRNA pathway** start with the recognition and subsequent cleavage of dsRNA by the ribonuclease Dicer 2 (Dcr2). In case of the endogenous pathway, these RNA molecules derive from sense-antisense RNA duplexes from the transposon, stem loop structures or transcript containing overlaps of protein-coding genes and non-coding regions (Donald et al., 2012). Viral dsRNA produced during viral replication present in infected cells is the basis for the exo-siRNA pathway. The dsRNA is processed into siRNA in the endo- or viral si (vsi)RNA in case of the exo-siRNA pathway. The (v)siRNAs are 21 nt long duplexes with 19 nt overlap and 2 nt 3’ overhangs and are loaded onto Argonaute 2 (Ago2) as part of the siRNA-induced silencing complex (siRISC) with the help of the dsRNA-binding protein R2D2. The (v)siRNA duplex is unwound by Ago2 with the “guide” strand being methylated and used as a template to target and subsequently degrade complementary RNA sequences, while the antisense or “passenger” strand is discarded by the endonuclease C3PO (Elbashir et al., 2001; Okamura et al., 2004). For targeting these complementary sequences, Ago2 requires base-pairing of the entire small RNA, setting it apart from the mechanism of Ago1 of the miRNA pathway (Schuster et al., 2019).

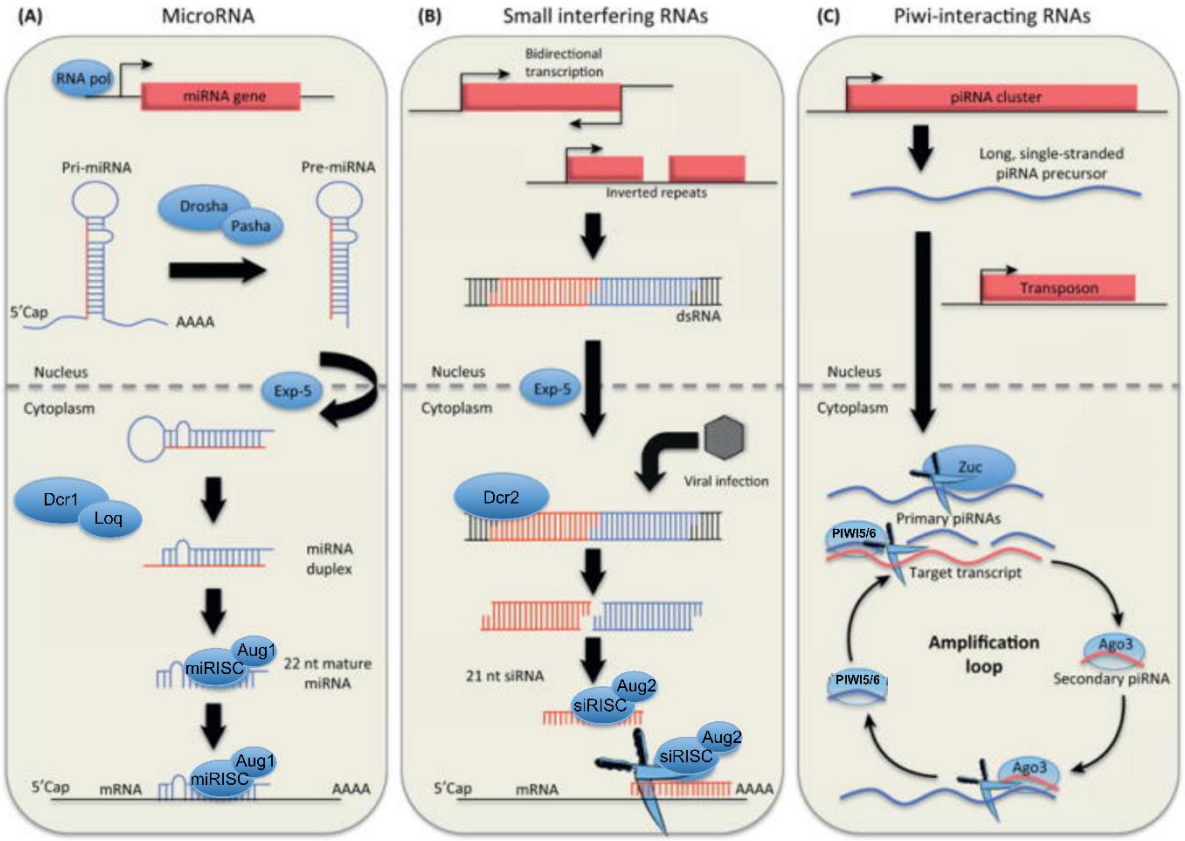


Fig. 9: RNA interference pathways in mosquitoes. There are three distinct RNAi pathways in mosquitoes: the **micro (mi)RNA pathway (A)**, the **small interfering (si)RNA pathway (B)** and the **PIWI-interacting (pi)RNA pathway (C)**. In the **miRNA pathway**, primary (pri)-miRNAs containing stem loops are transcribed from DNA sequences before being processed by Drosha with its co-factor Pasha into precursor (pre-)miRNA before being transported to the cytoplasm by Exportin 5 (Exp-5). There, the pre-miRNA is further processed by Dicer 1 (Dcr1) and Loquacious (Loq) into mature miRNA duplexes. The ~22 nt duplexes are used by Argonaute 1 (Ago1) associated with the miRNA-induced silencing complex (miRISC) to target and degrade mRNA for gene expression modulation. The **siRNA pathway** starts with the recognition of either viral dsRNA (exo-siRNA pathway) or dsRNA derived from the transposon, stem loops or overlapping genes (endo-siRNA). The dsRNA is cleaved by Dicer 2 (Dcr2) into 21 nt long (viral) siRNA which is taken up by Argonaute 2 (Ago2) and the siRNA-induced silencing complex (siRISC) to be used as a template to target and degrade complementary RNA sequences. For the **piRNA pathway**, primary piRNAs are processed from long ssRNA precursors by Zucchini (Zuc) before being further processed into secondary piRNAs in a “ping-pong” amplification cycle including Argonaute 3 (Ago3) and PIWI 5/6, in which secondary piRNAs are used to target transcripts. Figure adapted from (Lucas et al., 2013).

Dicer-type ribonucleases

The Dicer ribonucleases belong to the family of RNase III endoribonucleases capable of hydrolyzation of phosphodiester bonds in dsRNAs, leading to the production of 5’- phosphate, 3’-hydroxyl dsRNAs with a 2 nt 3’ overhang (MacRae et al., 2006). There are three distinct subfamilies, categorized by their domain organization and resulting biological function. The Dicer-type subfamily contains an N-terminal helicase domain, followed by a domain of unknown function (DUF), a PIWI-Argonaute-Zwille (PAZ) domain, two RNase III domains and the C-terminal dsRNA-binding domain (dsRBD) (Ciechanowska et al., 2024) (see Fig. 10). In

comparison to the Dicer-like subfamily, the other two subfamilies either one RNase III and one dsRBD, e.g. bacterial RNase III and yeast ribonuclease T1 (Rnt1), ot two RNase III domains and one C-terminal dsRBD, e.g. ribonuclease Drosha which is part of the miRNA pathway. Even within the subfamily of Dicer-like ribonucleases, there are exceptions to the domain organization, like a missing DUF in the Dicer-like 3 (DCL3) protein from *Arabidopsis thaliana*, among others (Jänkänpää et al., 2013).

Dicer 2 domain organization

Dcr2 is highly conserved between different species, including between *D. melanogaster* and *Ae. aegypti* (see Fig. 10). The highly conserved N-terminal helicase domain possesses a high sequence similarity to the helicase superfamily SF2, comprised of three subdomains Hel1, Hel2i and Hel2, with its main function being the binding of blunt-end dsRNA and unwinding of the dsRNA in an ATP-dependent manner (Aderounmu et al., 2023; Hansen et al., 2019; Sinha et al., 2015a). The DUF of Dcr2 is located C-terminal of the helicase domain, and while its exact function is unknown, as its name suggests, it shows high structural similarities to typical eucaryotic, procaryotic and viral dsRBDs (Gleghorn and Maquat, 2014). The functional core of Dcr2 is made up of the PAZ domain and the two RNase III domains, with PAZ being responsible for binding of 3' overhang dsRNA (Ma et al., 2004), while the RNase III domains facilitate cleavage of dsRNA into ~21 nt long siRNAs and binding to Ago2 (Ji, 2008; Takeshita et al., 2007). Finally, the C-terminal dsRBD is directly responsible for binding the substrate dsRNAs (Wostenberg et al., 2012). Previous studies by Gestuveo et al. have highlighted the importance of the helicase and RNase III domains for *Ae. aegypti* Dcr2 silencing and antiviral activity, including the correct processing of dsRNA into 21 nt long vsiRNAs (Gestuveo et al., 2022).

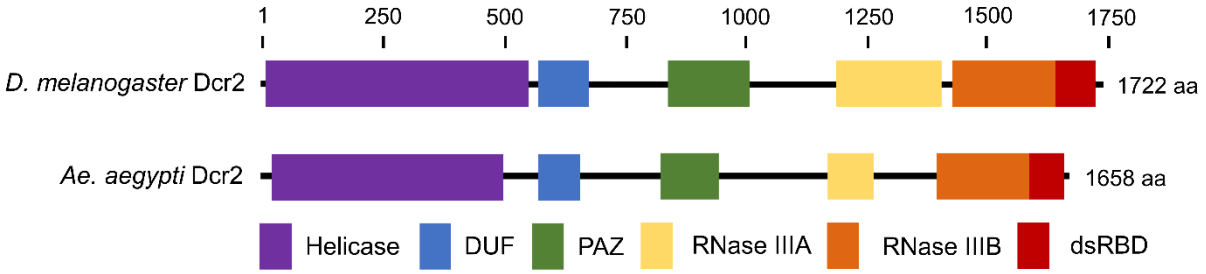


Fig. 10: Dicer 2 domain organization in *D. melanogaster* and *Ae. aegypti*. *D. melanogaster* and *Ae. aegypti* exhibit a closely similar Dcr2 domain structure. Both possess the same general domain organization, including the N-terminal helicase domain (blue), the domain of unknown function (DUF, purple), the PIWI-Argonaute-Zwille (PAZ) domain (yellow), the RNase III A (orange) and III B (red) domains, and the C-terminal dsRNA-binding domain (dsRBD, green). The protein length is indicated at the C-terminus respectively, with 1722 amino acids (aa) for *Dmel* and 1658 aa for *Aaeg* including a scale on top. Adapted from (Gestuveo et al., 2022).

Importance of RNAi effector proteins in arboviral defence

Many studies in recent years have focussed on the differing influence of the RNAi effector proteins on infections from different arboviral families within mosquitoes. Both Dcr2 and Ago2 silencing has been shown to lead to increased viral replication for most tested arboviruses, including ZIKV, SINV, DENV, CHIKV, BUNV, SFV and O'nyong-nyong virus (ONNV, *Togaviridae*, *Alphavirus*). (Campbell et al., 2008; Dietrich et al., 2017b; Keene et al., 2004;

McFarlane et al., 2014; Sánchez-Vargas et al., 2009, p. 2; Schnettler et al., 2013; Varjak et al., 2017a).

Following CRISPR-Cas9-mediated gene editing in *Ae. aegypti* mosquitoes, Dcr2 mutant mosquitoes exhibited loss of siRNA production and impaired Dcr2 silencing activity after ZIKV and DENV infection, yet no immediate impact on arboviral replication after infectious blood meal was detected, based on the fact that Dcr2 antiviral activity was only present during early stages of midgut infection (Merkling et al., 2023). Additionally, the mutant mosquitoes exhibited a significant increase in CHIKV-induced mortality as opposed to DENV infected mosquitoes (Merkling et al., 2023). In Dcr2 deficient mosquitoes, alphavirus infection again lead to a significantly higher mortality in comparison to flaviviruses with high SINV-induced mortality as opposed to low YFV-induced mortality (Samuel et al., 2023).

While the antiviral activity of the exo-siRNA pathway is well defined today, the mechanism and role of the piRNA pathway within the mosquito's defence against arboviral infection is still subject to speculation. Initially only characterized as a germline-specific mechanism conferring protection against transposons, the piRNA pathway has since been investigated for its possible antiviral role outside the germline. Out of 20 tested arthropod species, 16 showed somatic function of piRNAs, with 5 of those, including *Ae. aegypti*, exhibiting production of virus-derived piRNAs (vpiRNAs), also exhibiting the characteristic U_1 bias, yet all but *Ae. aegypti* were missing the typical 10 nt overlap (Lewis et al., 2018). Loss of piRNA effector molecules Ago3, PIWI5 and PIWI6 lead to decreased production of virus-derived piRNAs from both alpha- and flaviviruses including CHIKV, SFV, SINV and DENV (Miesen et al., 2015, 2016a; Schnettler et al., 2013; Varjak et al., 2017a, 2018a).

PIWI4 has previously been reported to be associated with Ago3, PIWI5 and PIWI6, as well as Ago2 and Dcr2, being predominately associated with vsiRNAs despite its antiviral activity seemingly being independent of Dcr2 and thus the exo-siRNA pathway (Varjak et al., 2017b). PIWI4 silencing lead to an increased viral replication after SFV infection, yet no influence on vpiRNA production was detected, which suggests the role of PIWI4 as an effector protein for antiviral defence, but no involvement in SFV-specific vpiRNA production (Schnettler et al., 2013; Varjak et al., 2017a, 2017b, 2018a). Antiviral activity of PIWI4 was also shown for RVFV, CHIKV, BUNV, DENV and SINV and ZIKV after PIWI4 knockdown (Dietrich et al., 2017b, 2017b; Tassetto et al., 2019; Varjak et al., 2017a, 2018a). Additionally, PIWI4 has been shown to bind CFAV-derived antisense piRNAs after incorporation of CFAV vDNA into the mosquito genome; specifically, these piRNAs were explicitly used to inhibit viral replication (Tassetto et al., 2019).

Production of vsiRNA and vpiRNA in different arboviruses and ISVs

Efficient vsiRNA production has been reported for an abundance of arboviruses, yet the genome distribution differs. For alphaviruses including SINV, SFV and CHIKV, and flaviviruses including ZIKV and DENV, produced vsiRNAs map to both the genome and antigenome, covering the whole genome sequence evenly (Goic et al., 2016; Marconcini et al., 2021; Miesen et al., 2016a; Morazzani et al., 2012; Myles et al., 2008; Saldaña et al., 2017; Schnettler et al., 2013; Varjak et al., 2017a). ISV-derived siRNAs also generally map evenly across the genome and antigenome, yet siRNA production from many insect-specific flaviviruses (ISFs) exhibit a bias to the 3' UTR (Besson et al., 2024; Frangeul et al., 2020).

As opposed to the positive sense alpha- and flaviviruses, negative sense arboviruses like BUNV and RVFV exhibited mapping bias to specific genomic regions. In case of BUNV, vsiRNAs were shown to map to all three segments, with both the L- and S-segment exhibiting

vsiRNA mapping to both genome and antigenome, while M-segment specific vsiRNAs mapped predominantly to the anti-genomic regions (Dietrich et al., 2017b). RVFV-specific vsiRNAs again mapped to all the segments for both the genome and anti-genome equally, but a hotspot was identified in the intergenomic region of the ambisense S-segment (Dietrich et al., 2017a).

Virus-specific piRNAs (vpiRNAs) have been reported for both infected mosquitoes and mosquito-derived cell lines for many arboviruses from the major arboviral families, including for DENV, SINV, SFV, CHIKV, BUNV, RVFV and ISVs (Aguiar et al., 2015; Brackney et al., 2010; Dietrich et al., 2017a, 2017b; Goic et al., 2016; Léger et al., 2013; Miesen et al., 2015, 2016b, 2016a; Morazzani et al., 2012; Schnettler et al., 2013; Varjak et al., 2018a; Vodovar et al., 2012).

While vsiRNAs generally originate from both the genome and antigenome, vpiRNAs mostly map to specific hotspots within the arboviral genome, their location and abundance specific to different virus families and genera. In case of *Flaviviridae*, these hotspots were mainly located at the 3' end of the genome (Miesen et al., 2016b, 2016b; Varjak et al., 2017a), while arboviruses of the *Bunyaviricetes* class, including BUNV and RVFV, exhibit a vpiRNA mapping bias towards the antigenomic strand for the S- and M-segment, with a low production of vpiRNAs from the L-segment, which mostly map to the genomic strand (Dietrich et al., 2017a, 2017b; Léger et al., 2013). Alphavirus-specific vpiRNAs mainly map to the region downstream of the sub-genomic promotor which encodes for the structural proteins including the capsid, presenting as a possible target for antiviral defence (Miesen et al., 2016a, 2016b, 2015; Morazzani et al., 2012; Schnettler et al., 2013; Varjak et al., 2018b, 2018a; Vodovar et al., 2012).

Like transposon-derived piRNAs, vpiRNAs also present with a genomic A_{10} bias and an antigenomic U_1 bias (Léger et al., 2013; Miesen et al., 2016b, 2015; Morazzani et al., 2012; Varjak et al., 2018b; Vodovar et al., 2012). In contrast to alphaviruses and bunyaviruses, flavirus-derived piRNA-sized small RNAs in mosquitoes exhibit primarily genomic polarity and frequently lack canonical ping-pong amplification signatures, with DENV only exhibiting A_{10} bias while CFAV only shows U_1 bias; both also missing the characteristic 10 nt overlap. (Miesen et al., 2016b, 2016a; Schnettler et al., 2016; Varjak et al., 2017a). While ISV-specific siRNA production has been reported for all tested ISVs independent of viral family, ISV-specific piRNAs have only been shown for some, with both the biological and antiviral function of those ISV-specific piRNAs remaining largely unknown (Aguiar et al., 2015; Crava et al., 2021; Suzuki et al., 2020).

Production of viral DNA from RNA arboviruses

While the antiviral pathways in mosquitoes help to control infections, they do not eliminate the pathogens, which in turn are able to establish persistent infection (Goic et al., 2016). This is a vital step for the possible transmission of arboviruses to vertebrate hosts, as the mosquitoes, while infected, do not exhibit significant impact on fitness or survivability and are thus able to infect vertebrates upon their next blood meal. An important step in the establishment of persistent infections is the production of viral (v)DNA, which assists in the antiviral RNAi immune response (Goic et al., 2013). Production of vDNA has been observed for WNV, DENV, CHIKV and ZIKV both *in vivo* and in *Aedes*-derived cell lines as early as 24 hours post infection (hpi) (Goic et al., 2016; Marconcini et al., 2021; Nag et al., 2016; Nag and Kramer, 2017), for SFV in *Ae. aegypti* mosquitoes (Rodriguez-Andres et al., 2023), as well as for BUNV and WNV in *Culex*-derived cells (Altinli et al., 2023; Rückert et al., 2019a).

As most arboviruses are RNA viruses and do not possess their own RNA-dependent DNA-polymerase or reverse transcriptase (RT), they need to rely on host RTs. While the exact RTs are unknown, previous studies have investigated the claim of the involvement of host RTs by treating mosquitoes or derived cells with azidothymidine (AZT), an RT-inhibitor. CHIKV-infected and AZT-treated mosquitoes exhibited both a delay and reduction of vDNA production with only 35% presenting vDNA versus 80% in untreated mosquitoes. Additionally, AZT-treated mosquitoes exhibited a rapid decline in survivability, leading to the conclusion that the production of vDNA and thus persistent infection is vital for the continued survival of the infected mosquito and possible transmission to the vertebrate host (Goic et al., 2016).

Non-retroviral integrated RNA virus sequences

In recent years, new molecular technologies have become widely accessible, including Next Generation Sequencing (NGS), leading to the whole genome sequence of both vector species and ISVs to become available. Upon investigation of said sequences, virus-derived sequences have been discovered within the host genome, labelled endogenous viral elements or EVEs.

EVEs are generally believed to be the product of vDNA being incorporated into the host genome by integrase enzymes from retroviruses or retrotransposons. Similarly, virus-derived host genome sequences from non-retroviral viruses have been discovered, thus named non-retroviral integrated RNA virus sequences or NIRVS. The first discovery of RNA virus gene sequences integrated into the host genome involved CFAV fragments found in the genome of *Ae. aegypti* and *Ae. albopictus* mosquitoes (Crochu et al., 2004). While the occurrence of NIRVS in a wide array of insect genomes suggests similar mechanisms of biogenesis and integration, NIRVS in *Aedes* mosquitoes are significantly more abundant and differ in their viral origins in comparison to other insects (Blair et al., 2019). NIRVS can occur from the integration of either complete or interrupted viral ORFs, with similarities to coding regions of RNA-polymerases, nucleo- and glycoproteins of retroviral genomes, while the exact mechanism of integration remains unknown (Blair et al., 2019). Thorough analysis of NIRVS from over 400 different RNA viruses showed the integration of viral sequences only from *Flaviridae*, *Rhabdoviridae*, *Bunyaviridae* and *Reoviridae*, leading to the hypothesis of a species-specific NIRVS production in mosquitoes (Olson and Bonizzoni, 2017; Palatini et al., 2017).

Both EVEs and NIRVS generally lose the ability to produce virions due to either the integration of interrupted ORFs or possible insertions and mutations in the integrated sequences, yet some retain the ability to be transcribed into mRNA and translated into their encoded proteins (Bannert and Kurth, 2004; Stoye, 2012). Like EVEs, NIRVS have been suggested to be vertically inherited and possess biological functions beneficial to the host (Blair et al., 2019; Suzuki et al., 2020; Whitfield et al., 2017). In *Ae. aegypti*, large quantities of NIRVS from vertically transmitted ISVs have been reported, including CFAV (Chen et al., 2015; Miesen et al., 2016b; Palatini et al., 2017; Whitfield et al., 2017).

The location of NIRVS in the mosquito genome is not random but rather focuses on specific loci, including a high likelihood of NIRVS being present in piRNA cluster loci, possibly leading to the production of NIRVS-specific vpiRNAs which present in anti-sense orientation including the typical U_1 bias (Palatini et al., 2020, 2017; Whitfield et al., 2017). Furthermore, while vsiRNA production has only been reported after viral infection, vpiRNAs have been found in both infected and uninfected cells (Arensburger et al., 2011; Blair et al., 2019; Brackney et al., 2010; Palatini et al., 2017). Other studies showed the presence of anti-sense vpiRNAs stemming from CFAV-specific NIRVS, which were shown to associate with PIWI 4, presenting a potential antiviral defence against CFAV (Suzuki et al., 2020; Tassetto et al., 2019). Next to the possible antiviral function of NIRVS-specific vpiRNAs, a regulatory function on the expression of

mosquito transcript has been proposed, based on findings suggesting that while CHIKV infection in *Ae. albopictus* mosquitoes did not lead to the production of new NIRVS, CHIKV-specific piRNAs derived from existing NIRVS were found to map to *Ae. albopictus* transcripts (Marconcini et al., 2021). The exact mechanisms involved in NIRVS production is still part of ongoing research, including exact NIRVS location and the potential antiviral function of NIRVS in similar matter to an adaptive immunity. However, the current evidence points to a pathway beginning with the production of vDNA from RNA viruses using mosquito RTs and incorporation of those vDNAs into the mosquito genome, giving rise to NIRVS which may act antiviral through the piRNA pathway by production of NIRVS-specific vpiRNAs (see Fig. 11). However, despite the involvement of NIRVS-specific piRNAs in an antiviral manner, this pathway may not lead to clearance of the infection but rather to the establishment of a persistent infection, heightening the mosquito's survivability and thus supporting its vector competence.

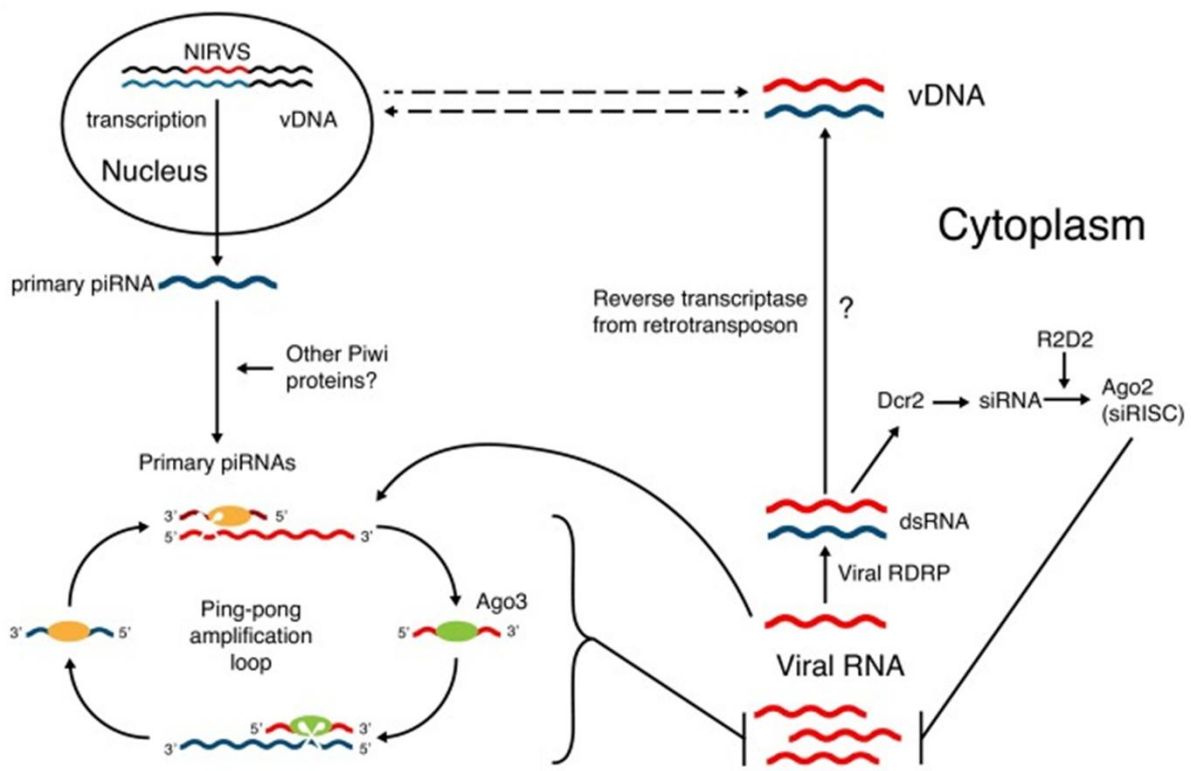


Fig. 11: Proposed mechanism of NIRVS production and RNAi involvement in mosquitoes. Upon infection with a non-retroviral RNA virus, viral dsRNA is produced during viral replication using a viral RNA-dependent RNA-polymerase (viral RDRP). The viral dsRNA is recognized and cleaved by Dicer 2 (Dcr2), producing small interfering RNAs (siRNAs). These virus-derived siRNAs are loaded onto Argonaute 2 (Ago2) as part of the siRNA-induced silencing complex (siRISC) with the help of the dsRNA-binding protein R2D2. The siRISC then targets and degrades complementary viral RNA. The viral dsRNA is also used to produce viral DNA (vDNA) via host reverse transcriptase, before being integrated into the mosquito genome as a non-retroviral integrated RNA virus sequence (NIRVS). Upon translation, these NIRVS give rise to primary NIRVS-specific virus-derived piRNAs, which are integrated into the piRNA pathway, possibly involved in antiviral defence mediated by different PIWI proteins, including PIWI4 (Olson and Bonizzoni, 2017).

Objectives

Due to the globally increasing risk of arboviral infections, the need to understand and assess every part of the arboviral life cycle and transmission arises, including the antiviral response not just in the human host, but also its vectors. As the most important mode of antiviral defence within mosquitoes, the RNAi pathways and their key proteins are the focus of many recent studies, including the influence of these key proteins on the production of vsiRNA and vpiRNA. To assess the importance of Dcr2 as a key component of the siRNA pathway in mosquitoes, this study investigates the functions and antiviral involvement of its domains on both positive and negative strand arboviruses.

Both the production of vDNA and the generation of NIRVS have emerged as key factors in modulating viral replication and controlling viral loads within the mosquito. This research holds promise for the development of new vector control strategies, including genetic modifications to disrupt viral replication or boost antiviral immune responses. Ultimately, gaining a deeper understanding of the piRNA and siRNA pathways in mosquitoes and the potential production and antiviral activity involving arbovirus-specific NIRVS is crucial for developing effective countermeasures against the growing threat of arboviral diseases. To this day, little is known about the potential production of arbovirus-specific NIRVS including their possible role within an adaptive immune response within the mosquito, presenting a main research focus of this thesis.

To investigate the importance of Dcr2 as part of the siRNA pathway and the potential production and influence of vDNA and NIRVS after infection with different arboviruses, the following objectives have been formulated:

i. Assessment of the importance of the different domains of Dcr2 as part of the siRNA pathway within mosquitoes and their influence on antiviral and silencing activity, including vsiRNA production after infection with different arboviruses.

ii. Investigate the production of vDNA in both acute and persistent infection from different arboviruses.

iii. Generation of mosquito cells primed by previous arboviral challenge, analysing the influence of the priming on antiviral activity upon repeated infection.

iv. Investigate the potential production of NIRVS from different arboviral families, including analysis of their influence on transcripts and vsiRNA and vpiRNA production.

Chapter 2: Publication 1

Supplements for Publication 1 can be found in the online version under:
RNA. 2025 Apr 16;31(5):679-691. doi: 10.1261/rna.080149.124. PMID: 39947927; PMCID: PMC12001973.

The PAZ domain of *Aedes aegypti* Dicer 2 is critical for accurate and high-fidelity size determination of virus-derived small interfering RNAs.

Melinda Reuter[1,2,3,4#], Rhys H. Parry[5#], Melanie McFarlane[1], Rommel J. Gestuveo[6], Rozeena Arif[1], Alexander A. Khromykh[5,7], Benjamin Brennan[1], Margus Varjak[8], Alfredo Castello[1], Lars Redecke[9,10], Esther Schnettler[2,3,4], Alain Kohl[1,11]

[1]MRC-University of Glasgow Centre for Virus Research, Glasgow, UK

[2]Bernhard-Nocht-Institute for Tropical Medicine, Hamburg, Germany

[3]German Centre for Infection Research (DZIF), Partner Site Hamburg-Luebeck-Borstel-Riems, Hamburg, Germany

[4]Faculty of Mathematics, Informatics and Natural Sciences, University Hamburg, Hamburg, Germany

[5]School of Chemistry and Molecular Biosciences, The University of Queensland, St. Lucia, Australia

[6]Division of Biological Sciences, University of the Philippines Visayas, Miagao, Iloilo, Philippines

[7]Australian Infectious Diseases Research Centre, Global Virus Network Centre of Excellence, Brisbane, Queensland, Australia

[8]Institute of Technology, University of Tartu, Estonia; [9]University of Lübeck, Institute of Biochemistry, Lübeck, Germany

[10]Deutsches Elektronen Synchrotron (DESY), Photon Science, Hamburg, Germany

[11]Centre for Neglected Tropical Diseases, Departments of Tropical Disease Biology and Vector Biology, Liverpool School of Tropical Medicine, Pembroke Place, Liverpool, UK

[#]These authors contributed equally to this manuscript.

Correspondence: schnettler@bnitm.de and alain.kohl@lstmed.ac.uk

Short title: Analysis of the *Aedes aegypti* Dicer 2 PAZ domain

Keywords: RNA interference; small RNA; Dcr2; arbovirus; mosquito cell; host response.

Data deposition:
Data underlying figures are available under http://dx.doi.org/10.5525/gla.researchdata.1479. Small RNA sequencing data generated for this study have been deposited in the NCBI Sequence Read Archive (SRA), available under accession number PRJNA1014654. Scripts utilized for small RNA analysis are available from the viral_sRNA_tools GitHub repository at: https://github.com/rhparry/viral_sRNA_tools

Abstract

The exogenous siRNA (exo-siRNA) pathway is a critical RNA interference response involved in controlling arbovirus replication in mosquito cells. It is initiated by the detection of viral long double-stranded RNA (dsRNA) by the RNase III enzyme Dicer 2 (Dcr2), which is processed into predominantly 21 nucleotide (nt) virus-derived small interfering RNAs, or vsiRNAs that are taken up by the Argonaute 2 (Ago2) protein to target viral single-stranded RNAs. The detailed understanding of Dicer structure, function and domains owes much to studies outside the context of viral infection and studies in model organisms, and as such how Dcr2 domains contribute to detecting viral dsRNA to mount antiviral responses in infected mosquito cells remains less well understood. Here, we used a Dcr2 reconstitution system in *Aedes aegypti* derived Dcr2 KO cells to assess the contribution of the PAZ domain to induction of the exo-siRNA pathway following infection with Semliki Forest virus (SFV; *Togaviridae*, *Alphavirus*). Amino acids critical for PAZ activity were identified, and loss of PAZ function affected the production of 21 nt vsiRNAs -with enrichment of 22 nt SFV-derived small RNAs observed- and silencing activity. This study establishes PAZ domain's functional contribution to Dcr2 processing of viral dsRNA to 21 nt vsiRNAs.

Introduction

The emergence and re-emergence of arboviruses pose a continuing threat to human and animal health, with mosquito-transmitted pathogens such as dengue virus (DENV; *Flaviviridae, Flavivirus*), Zika virus (ZIKV; *Flaviviridae, Flavivirus*) and chikungunya virus (CHIKV; *Togaviridae, Alphavirus*) as prominent examples of the threats posed (Zaid et al. 2021; Halstead 2019; Weaver et al. 2018; Weaver and Reisen 2010; Huang et al. 2019; Pierson and Diamond 2020). The mosquito *Aedes aegypti* is an important vector for the transmission of many human-infecting arboviruses, including DENV, ZIKV and CHIKV. It is found across many areas of the tropics and subtropics where it is well adapted to the human environment, preferentially taking bloodmeals from human hosts which can result in arbovirus transmission. Prevention of transmission frequently relies on chemical control measures that target vectors, though novel approaches such as *Wolbachia* endosymbionts and gene drive-based approaches are promising (Achee et al. 2019; Facchinelli et al. 2023; Carvalho and Moreira 2017; Brady and Hay 2020; Caragata et al. 2021; Wang et al. 2021, 2022).

Arboviruses actively replicate in their vectors, which results in the induction of immune responses. Understanding these is relevant for a better comprehension of vector processes that impact arbovirus transmission and thus targets for intervention (Alonso-Palomares et al. 2018; Lambrechts and Saleh 2019). Among host responses that control arbovirus replication in vectors, the RNA interference response -specifically the exogenous siRNA (exo-siRNA) pathway- plays a critical role. Much of our current understanding of this pathway comes from studies in *Drosophila melanogaster*, including *in vitro* studies, with critical components and mechanisms also conserved in mosquitoes, thus proving the importance of the exo-siRNA pathway across insects. It is initiated following targeting of viral replication induced long double-stranded RNA (dsRNA) by the RNase III enzyme Dicer 2 (Dcr2), which cleaves the dsRNA into virus-derived small interfering RNAs (vsiRNAs). In mosquitoes and *D. melanogaster*, each vsiRNA strand is predominantly 21 nucleotides (nt) in length, with a 19 nt overlap and 2 nt overhangs at the 3´end. In the next step, 21 nt vsiRNAs are taken up by Argonaute 2 (Ago2). Ago2 is part of the RNA-induced silencing complex (RISC) and retains one strand of the siRNA

to target and degrade complementary viral RNAs (Blair and Olson 2015; Tikhe and Dimopoulos 2021; Olson and Blair 2015; Bronkhorst and van Rij 2014; Swevers et al. 2018; Prince et al. 2023; Leggewie and Schnettler 2018; Samuel et al. 2018). Indeed, absence of Dcr2 in mosquito cell lines resulted in the loss of 21 nt vsiRNAs and impaired antiviral responses (Brackney et al. 2010; Gestuveo et al. 2022; Scott et al. 2010; Varjak et al. 2017), while *Ae. aegypti* mosquitoes without functional Dcr2 develop disease phenotypes, increased replication and dissemination following arbovirus infection (Merkling et al. 2023; Samuel et al. 2023). These data show the importance of Dcr2 as an initiator of the exo-siRNA pathway, but other functional aspects of this effector protein are less understood especially in the context of viral infection and targeting of viral derived dsRNA. The domain structure of *Ae. aegypti* Dcr2 (Aaeg Dcr2) is similar to that of *D. melanogaster* Dcr (Dm Dcr2), with helicase-DUF-PAZ-RNase 3A-RNase 3B-dsRBD from N to C terminus of the protein (Fig. 1), though other functional domains are present in the protein, too (Paturi and Deshmukh 2021). Structural studies have revealed that Dicer proteins generally have an L shape in which these different domains are arranged (Paturi and Deshmukh 2021; Zapletal et al. 2023; Ciechanowska et al. 2021). Analyses of Dm Dcr2 have confirmed this shape (Yamaguchi et al. 2022; Sinha et al. 2018; Su et al. 2022) , which was also predicted for Aaeg Dcr2 using AlphaFold (Gestuveo et al. 2022). The bottom (or base) module of the L-shaped Dcr2 structure contains the helicase domain; the core comprises RNase 3A/B and dsRBD domains, and the cap module the PAZ (Piwi/Ago/Zwille) domain. Biochemical and structural studies have investigated the dsRNA binding properties of Dm Dcr2 domains, with the PAZ domain preferably binding dsRNA termini with 3' overhangs (Sinha et al. 2018). The structural arrangements of the 3' nt overhang binding pocket in the PAZ domain and 5' monophosphate in the adjacent Platform domain have been investigated in detail. Importantly, interactions of dsRNA with PAZ and Platform via 3' 2 nt overhang and 5' monophosphate of the dsRNA allows positioning and spacing of the dsRNA for precise dicing activity and siRNA length (Su et al. 2022; Yamaguchi et al. 2022). These structural data consolidate a previous study on the importance of binding of the 5' monophosphate in dsRNA for length fidelity in 21 nt siRNA production from long dsRNA- though not efficiency of small RNA production *per se*; and mutagenesis analysis of the Dm Dcr2 PAZ domain also demonstrated the critical role of 21 nt siRNAs in silencing an inverted repeat transgene in the fly model (Kandasamy and Fukunaga 2016). Interestingly, the presence of 5' monophosphate and two specific arginine residues in Dm Dcr2 PAZ were found to be critical for cleavage of short dsRNA (Cenik et al. 2011; Fukunaga et al. 2014), though not longer ones where (as stated above) accurate length determination of siRNAs is the critical contribution of 5' monophosphate binding to the dicing process.

A limitation of studies on Dm Dcr2 PAZ domain is their reliance on *in vitro* studies with dsRNA substrates or endogenous small RNAs, while the role of this domain in antiviral responses during infection when targeting viral derived dsRNA in the cell is, to our knowledge, still unclear. The importance of the Dcr2 helicase domain in antiviral responses has been previously shown (Gestuveo et al. 2022; Marques et al. 2013; Donelick et al. 2020), there remains a critical gap because the nature of the viral dsRNA substrate is unknown- does Dcr2 detect long, short, or different types of dsRNA in infected cells, and how does recognition occur? Here we aimed to expand our previous studies on the role of Dcr2 domains in mosquito cell antiviral responses by investigating the role of the Aaeg Dcr2 PAZ domain in mosquito antiviral vsiRNA generation and its requirement for efficient antiviral responses. For this, we used the previously described Aaeg Dcr2 activity reconstitution system in *Ae. aegypti* derived Dcr2 KO cells, with which we demonstrated the importance of the helicase and RNase domains and that 21 nt vsiRNAs are

generally produced by a processive production mechanism from viral dsRNA (Gestuveo et al. 2022). To understand the contribution of the PAZ domain to the antiviral activity of Aaeg Dcr2, we identified conserved amino acids in Aaeg Dcr2 PAZ domain which were mutated to assess their impact on dsRNA processing activity. Mutations abrogated antiviral activity against a positive sense RNA virus, Semliki Forest virus (SFV), a member of the *Togaviridae* family, genus *Alphavirus*. PAZ function inactivating mutations resulted in a loss of 21 nt vsiRNA generation, and enrichment of 22 nt SFV-derived small RNAs. These findings indicate that PAZ domain functionality is critical for determination of the usually predominant vsiRNA length of 21 nt, but mutations did not affect processive cleavage of viral dsRNA as such.

Materials and methods

Cells

The Dcr2 knockout cell line Aag2-AF319 (subsequently abbreviated to AF319) used here is derived from *Ae. aegypti* Aag2-AF5 cells, a clone derived from the Aag2 cell line (provided by Kevin Maringer, The Pirbright Institute, UK) (Fredericks et al. 2019; Varjak et al. 2017). As previously described AF319 cells were cultured in Leibovitz's L-15 medium with GlutaMax (Gibco) with 10% tryptose phosphate broth (TPB; Gibco), 10% fetal bovine serum (FBS; Gibco), and penicillin-streptomycin (pen-strep; 100 U/mL-100 µg/mL; Gibco) at 28 °C (Fredericks et al. 2019; Varjak et al. 2017). Cell lines are available as Aag2-AF319 (ECACC 19022602) and Aag2-AF5 (ECACC 19022601) through Public Health England. Baby hamster kidney (BHK-21) cells are a commonly used cell line available at the MRC-University of Glasgow Centre for Virus Research; these cells were grown in Glasgow Minimum Essential Medium (GMEM; Gibco) supplemented with 10% TPB, 10% newborn calf serum (Gibco), and pen-strep at 37 °C with 5% CO_2.

Viruses

Virus production from icDNA and plaque assay titrations were performed as previously described (Ulper et al. 2008; Varjak et al. 2017) to produce SFV4 (abbreviated to SFV; GenBank ID: KP699763) and SFV4(3H)-*FFLuc* (abbreviated to SFV-FFLuc; reporter virus expressing FFLuc).

Plasmid generation

Mutations in the PAZ domain of Aaeg Dcr2 (GenBank ID: AAW48725) were created by In-Fusion cloning of synthetically generated PAZ domain mutant fragments into the previously generated pPUb-myc-Dcr2 (Varjak et al. 2017) following the manufacturer's guidelines. Briefly, pPUb-myc-Dcr2 was linearised by PCR, removing the WT PAZ domain. Mutant PAZ domain fragments were PCR amplified using primers with extensions that were homologous to the linearised vector. In-Fusion cloning was then performed to create pPUb-myc-Dcr2 constructs containing the various mutants. Mutations were based on multiple sequence alignment and identification of conserved amino acids in *Ae. aegypti*, *D. melanogaster* and *Ae. albopictus*.

Virus infections

For investigations of antiviral activity against SFV, AF319 cells were seeded at 2 x 10^5 cells/well in 24-well plates and transfected with 1 µg pPUb plasmid expressing WT or mutant Dcr2 or eGFP (as control) after 24 h using Dharmafect2 (Horizon Discovery) following the recommended protocol. At 24 hpt, the cells were infected with SFV-FFLuc (MOI=0.1) and lysed at 48 hpi using 1X Passive Lysis Buffer (PLB; Promega). FFLuc levels were measured using a Luciferase Assay System (Promega) according to the manufacturer's protocol in GloMax Multi-Detection System with Dual Injectors (Promega). For the production of samples for small RNA sequencing, 2.5 x 10^5 cells/well AF319 cells were seeded in 8 wells of a 24 well plate, transfected as above after 24 h and infected with SFV (MOI=1) at 24 hpt for 48 h. For RNA extraction and follow up small RNA sequencing, cells from 7 wells were combined and lysed using TRIzol (Thermo Fisher Scientific) according to the manufacturer's guidelines, with glycogen as a carrier. The remaining well was lysed in LDS protein lysis buffer and used for confirmatory western blot analysis.

dsRNA production

FFLuc (dsFFLuc) and eGFP (dseGFP) were amplified using T7 RNA polymerase promoter-flanked primers (Varjak et al. 2017; McFarlane et al. 2020) and dsRNAs produced with MEGAscript RNAi kits (Thermo Fisher Scientific) by *in vitro* transcription as per manufacturer's guidelines. Following *in vitr*o transcription, products were treated with DNaseI, and RNase A. dsRNA was purified by column purification.

RNAi reporter assay

RNAi reporter assays were performed as previously described (Varjak et al. 2017) to assess the silencing activities of mutant Dcr2 compared to WT Dcr2. For this, 2 x 10^5 AF319 cells/well were seeded in 24-well plates. After 24 h cells were co-transfected with 1 µg pPUb-based expression plasmid, 50 ng pGL3-PUb (Anderson et al. 2010) and 20 ng pPUb-RLuc (Alexander et al. 2023) together with either 20 ng dsRNA targeting FFLuc (dsFFLuc) or 20 ng dsRNA control (dseGFP) and lysed at 24 hpt in 1X PLB (Promega). To determine FFLuc/RLuc levels, dual luciferase assays were performed using a Dual-Luciferase Reporter Assay System (Promega) according to the manufacturer's protocol in a GloMax Multi-Dectection System with Dual Injectors (Promega).

Western Blot analysis

Cell lysis was performed in 1X Bolt sample reducing agent and 1X Bolt LDS sample buffer (Invitrogen). The lysate was separated using a 4-12% Bis-Tris Plus gel (Invitrogen). For transfer onto a nitrocellulose membrane, a Trans-Blot SD Semi-Dry Transfer Cell (BioRad) was used. Membranes were blocked for a minimum of 1 h using 5% (w/v) non-fat dry milk powder in PBS-Tween (PBS with 0.05% Tween 20, PBS-T) and then washed three times for 10 min using PBS-T. As primary antibodies, mouse anti-myc tag antibody (1:2000, Abcam) and mouse anti-α tubulin antibody (1:2000; Sigma-Aldrich) in 5% (w/v) non-fat dry milk powder in PBS-T were used. After overnight incubation at 4 °C, membranes were again washed three times in PBS-T. This was followed by incubation of 1 h with goat anti-mouse DyeLight 800 (1:5000; Invitrogen) secondary antibody conjugated with a near fluorescent dye in 5% (w/v)

non-fat dry milk powder in PBS-T. The membranes were again washed three times with PBS-T and a final wash with distilled water and analysed using an Odyssey CLx and Image Studio Lite v.5.2.5 (LI-COR Biosciences).

Small RNA sequencing

To investigate small RNA production, at least 1 µg isolated total RNA per condition were sent for analysis. Small RNA sequencing was performed at BGI-Tech Solutions (DNBSeq, UMI small library, SE50), UMI being unique molecular identifiers. With a minimum of 10 million clean reads, with final libraries resulting between 11-18 million reads (Supplemental Table S2).

Small RNA analysis

Using fastp (v0.23.2) (Chen et al. 2018), adapters and low-quality reads from basecalled fastq files were trimmed, retaining reads between 18-32 nt. The distribution of read sizes and first position bias was calculated using the script '1_fastq_histogram.sh' from the GitHub repository (rhparry/viral_sRNA_tools). Clean, trimmed reads were then mapped to the SFV genome (GenBank ID: KP699763) with Bowtie2 (v2.4.5) (Langmead and Salzberg 2012), using the sensitive mapping flag (—sensitive) as specified in the script '2_mapping_vrnas.sh'. Histograms of mapped read lengths and first base pair bias were generated using samtools (v1.16.1) and '3_bam_sRNA_histogram.sh'. Output BAM files were filtered to include only the 21 nt reads. Coverage statistics across the SFV genome were calculated using '4_viral_srna_coverage.sh', which employs the bedtools genome coverage tool (v.2.27.1) (Quinlan and Hall 2010). For calculating the harmony metric, coverage at the 5' end (-5 flag) of each read was normalized over the whole genome. Normalised coverage files were processed with awk '{f[NR]=$2;r[NR]=$3;sumf+=$2;sumr+=$3} END {for (i=1;i<=NR;i++) {printf "%d %.6e\n", i, (f[i]/sumf)-(r[i]/sumr)}}' to calculate d_i values for each position *i* of the SFV genome. Linear regression analyses for downstream analysis scatter plots of per position d_i values of the SFV genome were analysed in GraphPad Prism (v10.0.2), and R^2 values for all pairwise treatments were computed and presented as a heat map. Overlapping virus-derived small RNA pairs and overlap probabilities (z-score) were calculated iteratively from BAM files using the 'signature.py' small RNA signatures Python script, both single read lengths from 18-30 nt were calculated as per the following conditions (--minquery 18 --maxquery 18 --mintarget 18 --maxtarget 18 --minscope 1 --maxscope 18), collective 18-30 nt read lengths were computed as follows (--minquery 18 --maxquery 30 --mintarget 18 --maxtarget 30 --minscope 1 --maxscope 30) (Antoniewski 2014). To examine the diversity and populations of SFV-derived small RNA species, unique 20-23 nt SFV mapped reads were treated as discrete virus-derived small RNAs. Counts tables for all extracted SFV-derived small RNAs from extracted fasta files from individual libraries were converted, processed, and enumerated in bash (v.3.2). The dimensions of count tables for 20-23 nt virus-derived small RNA species (n = 75710), 20 nt (n = 13430), 21 nt (n = 27592), 22 nt (n = 20536) and 23 nt (n = 14155) species. Differential gene expression analysis was performed using package edgeR (v.3.30.3) (Robinson et al. 2009) in R Studio (v.1.3.1073), with library size normalization using the weighted TMM method in calcNormFactors() and filtered for a minimum count of 10 with filterByExpr(). Relationships between samples were explored using an MDS plot of normalized count tables with plotMDS(top = 500) of all SFV-derived small RNA species.

Protein structure predictions

The WT sequence of Aaeg Dcr2 (GenBank ID: AAW48725) was used as a query for structure prediction. AlphaFold 2 algorithm (Jumper et al. 2021) was run in monomer mode using a local install of version 2.3.2 without any restrictions. The resulting models were examined and, in accordance with overall model quality predictions, summarised in mean pLDDT value with the highest quality model selected for further analysis. Structural analyses were performed in PyMOL Molecular Graphics System (version 4.5.0, Schrödinger, LLC). Domain positions were assigned and labelled by color based on GenBank sequence annotations, and residues mutated were highlighted.
Ae. aegypti Dcr2-dsRNA interactions were assessed using AlphaFold 3. The WT sequence of *Ae. aegypti* Dcr2 (GenBank ID: AAW48725) and derived mutant sequences (M1-M4) were modelled as interacting with dsRNA. The 53 bp dsRNA sequence was obtained from PDB ID: 7W0E for *D. melanogaster* Dcr2 in the active dicing state (Su et al. 2022). Sequences for WT or M1-M4 *Ae. aegypti* Dcr2 and each mutant were fed into AlphaFold 3 webserver (Abramson et al. 2024) along with the dsRNA sequence to predict protein structures and their interaction with dsRNA. Molecular graphics and analysis of structures were performed using UCSF ChimeraX (Pettersen et al. 2021).

Data analyses

Virus-derived small RNA metrics, coverage and overlapping pairs analysis were visualized using GraphPad Prism (v10.0.2).

Results

Identification of amino acids in Aaeg Dcr2 PAZ domain required for antiviral activity

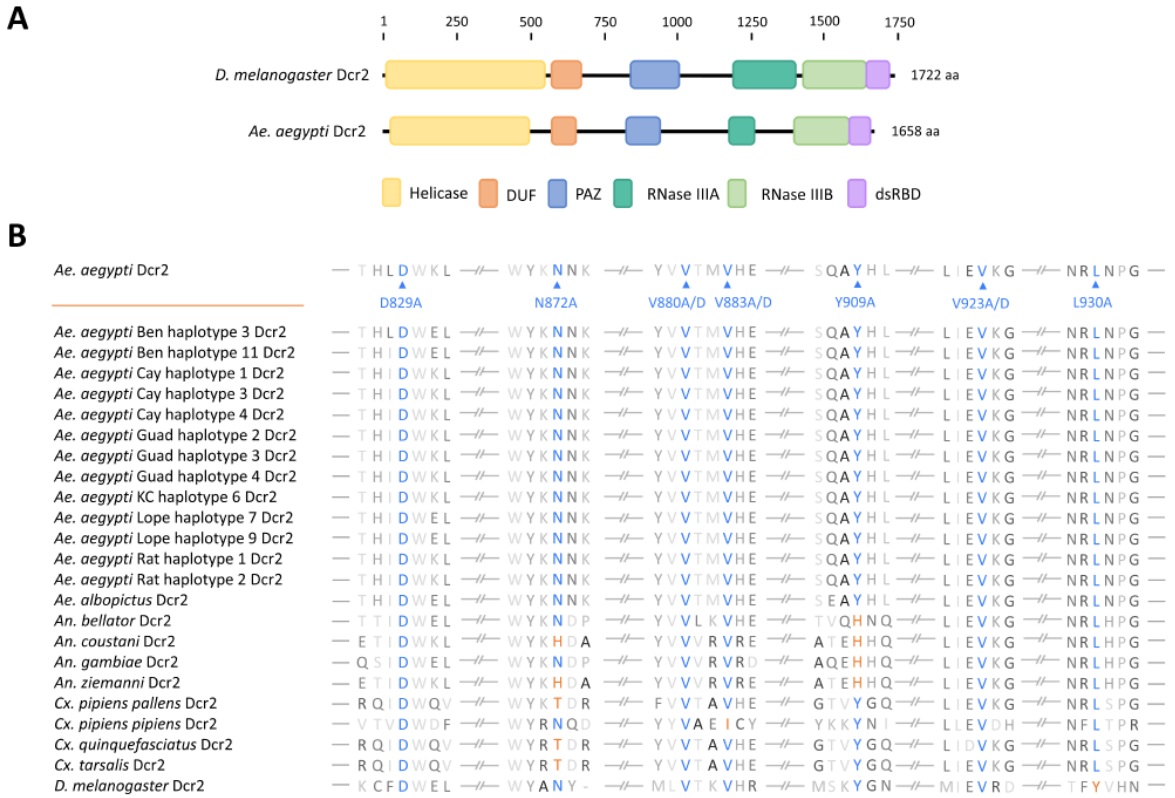


Fig. 1: Domain features of Dcr2. (A) Schematic representation of *D. melanogaster* and *Ae. aegypti* Dcr2, including functional domains: Helicase domain, domain of unknown function (DUF), PIWI-Argonaute-Zwille (PAZ) domain, RNase IIIA and IIIB domains, and dsRNA binding domain (dsRBD); aa, amino acid. **(B)** Multiple sequence alignment of insect Dcr2 referring to Aaeg Dcr2 AAW48725, including the selected mutations of highly conserved amino acids for potential PAZ domain loss of function. Accession numbers for sequences used are indicated in Supplemental Table S1. Alignment was produced using Benchling (https://www.benchling.com/).

Analysis of Aaeg Dcr2 sequence (InterProScan, Geneious) indicated that the PAZ domain was located from positions N824 to G941 (Fig. 1A). This was in line with NCBI domain analysis, which also located the PAZ domain between amino acids 824-941. Next, Dcr2 PAZ domain sequences of *Ae. aegypti* (including recently available sequences, see (Gestuveo et al. 2022), *Ae. albopictus*, *D. melanogaster* as well as *Anopheles* and *Culex* spec. were aligned to identify highly conserved amino acids in the PAZ domain and thus with potential functional activities. Several positions, as shown in Fig. 1B, were either fully conserved between at least *Ae. aegypti, Ae. albopictus*, and *D. melanogaster* Dcr2 PAZ domains (amino acids D829, N872, V880, V883, Y909, V923) OR across mosquitoes (amino acid L930) and chosen for mutagenesis in different combinations, which we assumed would give the best chance of success to disrupt PAZ domain functionality. For completeness, corresponding amino acid positions in Dm Dcr2 are indicated in Fig. 2A. Using NCBI domain analysis, the PAZ domain of Dm Dcr2 (1722 amino acids in length) was shown as located from amino acids 843-1004.

A

Dcr2 mutant	Dcr2 mutations *Ae. aegypti*	Corresponding aa residues *D. melanogaster*
M1	V880A	V895
	V883A	V898
	Y909A	Y925
	V923A	V942
M2	V880D	V895
	V883D	V898
	Y909A	Y925
	V923D	V942
M3	D829A	D845
	N872A	N888
	V880A	V895
	V883A	V898
	Y909A	Y925
	V923A	V942
	L930A	Y949
M4	D829A	D845
	N872A	N888
	V880D	V895
	V883D	V898
	Y909A	Y925
	V923D	V942
	L930A	Y949

B

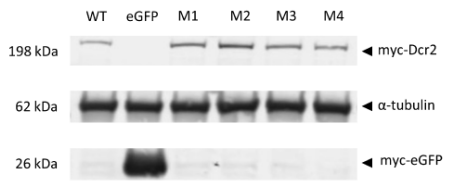


Fig. 2: Mutation and expression of Aaeg Dcr2. (A) Table showing produced Aaeg Dcr2 PAZ domain mutants M1-M4, the respective introduced loss-of-function mutations, as well as corresponding amino acid residues in Dm Dcr2; aa, amino acid. **(B)** Assessment of (myc-tagged) Aaeg Dcr2 expression by western blot analysis. AF319 cells were transfected with either pPUb plasmids expressing WT Dcr2 or Dcr2 PAZ domain mutants M1-M4, using pPUb-myc-eGFP as control. Anti-myc and anti-α tubulin (control) antibodies were used. Representative of three independent repeats (other repeats in Supplemental Fig. S2).

Alphafold was used to determine the location/structure of these conserved amino acids within the structure of the Aaeg Dcr2 PAZ domain, which appeared mainly located (with the exception of L930) around its core (Supplemental Fig. S1) when compared to Dm Dcr2 (Yamaguchi et al. 2022), suggesting structural and/ or functional importance.
Combinatorial mutagenesis was carried out as described for mutants M1-4, with conserved amino acids replaced in the combinations shown as indicated with the aim of achieving disruption PAZ domain function with a high degree of certainty (Fig. 2A). PAZ domain mutant M1-M4 and WT Dcr2 expression in AF319 Dcr2 KO cells transfected with the corresponding expression constructs was assessed by western blot, showing that all proteins were expressed (Fig. 2B, Supplemental Fig. S2).

Next, we assessed the functionality of the Aaeg Dcr2 mutants for their silencing ability and antiviral activity. WT Dcr2 displayed antiviral activity against SFV-FFLuc in this transfection-based assay (Fig. 3), as previously demonstrated (Gestuveo et al. 2022). M1-M4 Dcr2 mutants lost SFV-FFLuc antiviral activity, compared to WT Dcr2. Similarly, the functional silencing

abilities of the mutant Dcr2 were investigated in a reporter plasmid-based assay, where exogenous dsRNA is provided to induce the exo-siRNA pathway against a reporter gene (Gestuveo et al. 2022). Here, M1-M4 Dcr2 mutants only retained residual (although significant compared to control) ability to silence the reporter gene. This indicated that the mutation combinations in M1-M4 all affected Dcr2 PAZ domain functionality, and thus Dcr2's ability as an effector in the exo-siRNA pathway.

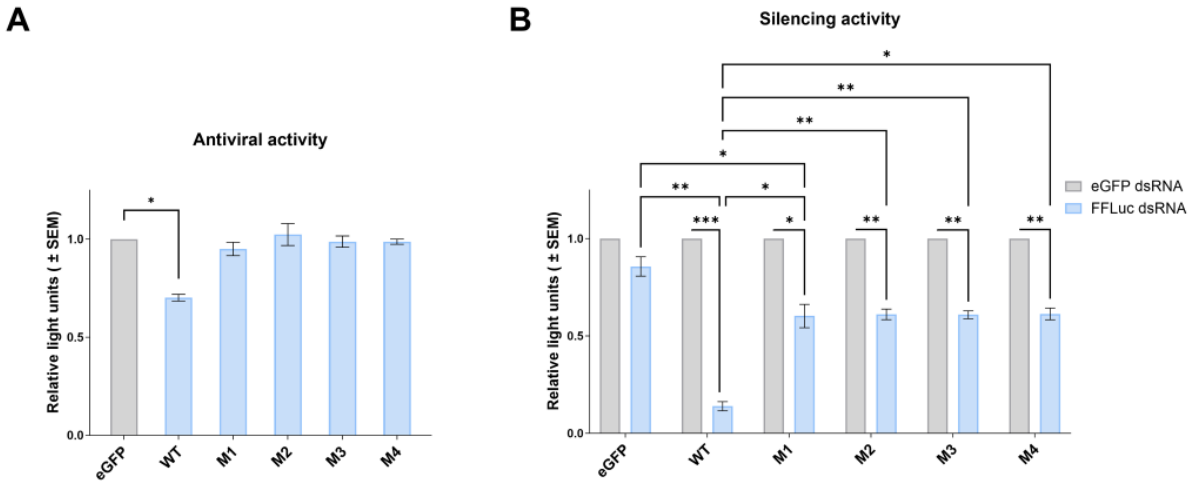


Fig. 3: Functional analysis of Aaeg Dcr2 PAZ domain mutants. (A) Antiviral activity of Aaeg Dcr2. AF319 cells were transfected with expression plasmids encoding myc-tagged WT Dcr2 or Dcr2 PAZ domain mutants M1-M4 or eGFP (negative control). These cells were infected with SFV-FFLuc (MOI = 0.1) 24 hours post-transfection (hpt). FFLuc-levels were measured at 48 hours post-infection (hpi) and are shown as mean ± SEM relative light units compared to eGFP control set to 1 from 3 independent repeats, performed in technical triplicate with * indicating $p<0.05$ according to Student's t-test. **(B)** Silencing activity of mutant Aaeg Dcr2. AF319 cells were co-transfected with (i) myc-tagged pPUb plasmids expressing WT Dcr2 or Dcr2 PAZ domain mutants M1-M4 (with eGFP as control), (ii) FFLuc and RLuc (internal control) reporter plasmids and (iii) dsRNA targeting FFLuc (FFLuc dsRNA, blue) or eGFP (eGFP dsRNA; non-silencing control, grey). At 24 hpt, FFLuc and RLuc levels were measured and are shown as mean ± SEM relative light units (FFLuc/RLuc) normalized to dseGFP from 3 independent repeats, performed in technical triplicate, with * = $p<0.05$, ** = $p<0.01$, *** = $p<0.001$ versus controls according to two-way ANOVA.

Aag Dcr2 PAZ domain los of function mutations: effects on 21 nt vsiRNA production

The impact of Aaeg Dcr2 PAZ domain mutations on vsiRNA production was investigated utilising high throughput small RNA sequencing from AF319 cells transiently expressing Dcr2 PAZ domain mutants or WT Dcr2 and infected with SFV. Raw populations of small RNA read lengths prototypical of miRNAs (22 nt), siRNAs (21 nt) and piRNAs (24-30 nt) (Supplemental Fig. S3) were observed in all cells. Small RNA profiles from Dcr2 PAZ domain mutants M1-4 and the eGFP control demonstrated a bias towards a read length of 22 nt rather than 21 nt observed in the WT Dcr2 expressing cells. Read mapping profiles of SFV-derived small RNAs indicated that WT Dcr2 efficiently mediated the production of SFV-derived 21 vsiRNAs (Fig. 4A), which are (as expected, see (Gestuveo et al. 2022)) the predominant length in the 18-22 nt size range and aligned along the length of the SFV genome and antigenome. Almost no

such vsiRNAs were detected in the eGFP control. Importantly, M1-M4 Dcr2 mutants showed reduced production of 21 nt vsiRNAs (though those remaining align along the length of SFV4 genome and antigenome) and a more even distribution of read numbers across the 20-22 nt small RNA size range, compared to WT Dcr2, was observed. This indicates that Dcr2 PAZ domain mutants M1-M4 have lost the ability to precisely measure siRNA length and consequently do not predominantly produce 21 nt vsiRNAs; but have retained the ability to process viral dsRNA into small RNAs. Crucially we examined absolute magnitudes of SFV-derived small RNAs in the sizes of 20 nt and 22 nt and observed a clear enrichment for 22 nt, ranging from 2.18-fold (Dcr 2 PAZ domain mutant M3) to 3.02-fold (Dcr2 PAZ domain mutant M4) (Fig. 4B). For the 20 nt size, we found modest or no significant change (0.91-1.45fold) consistent with previous results (Kandasamy and Fukunaga 2016). Critically, AlphaFold 3 based modelling of Aaeg Dcr2 PAZ domain interactions with dsRNA suggested that mutations did not abrogate the ability to bind dsRNA (Supplemental Fig. S4). This consolidates the idea that conserved amino acid are required for keeping dsRNA in a precise position for accurate cleavage to occur.

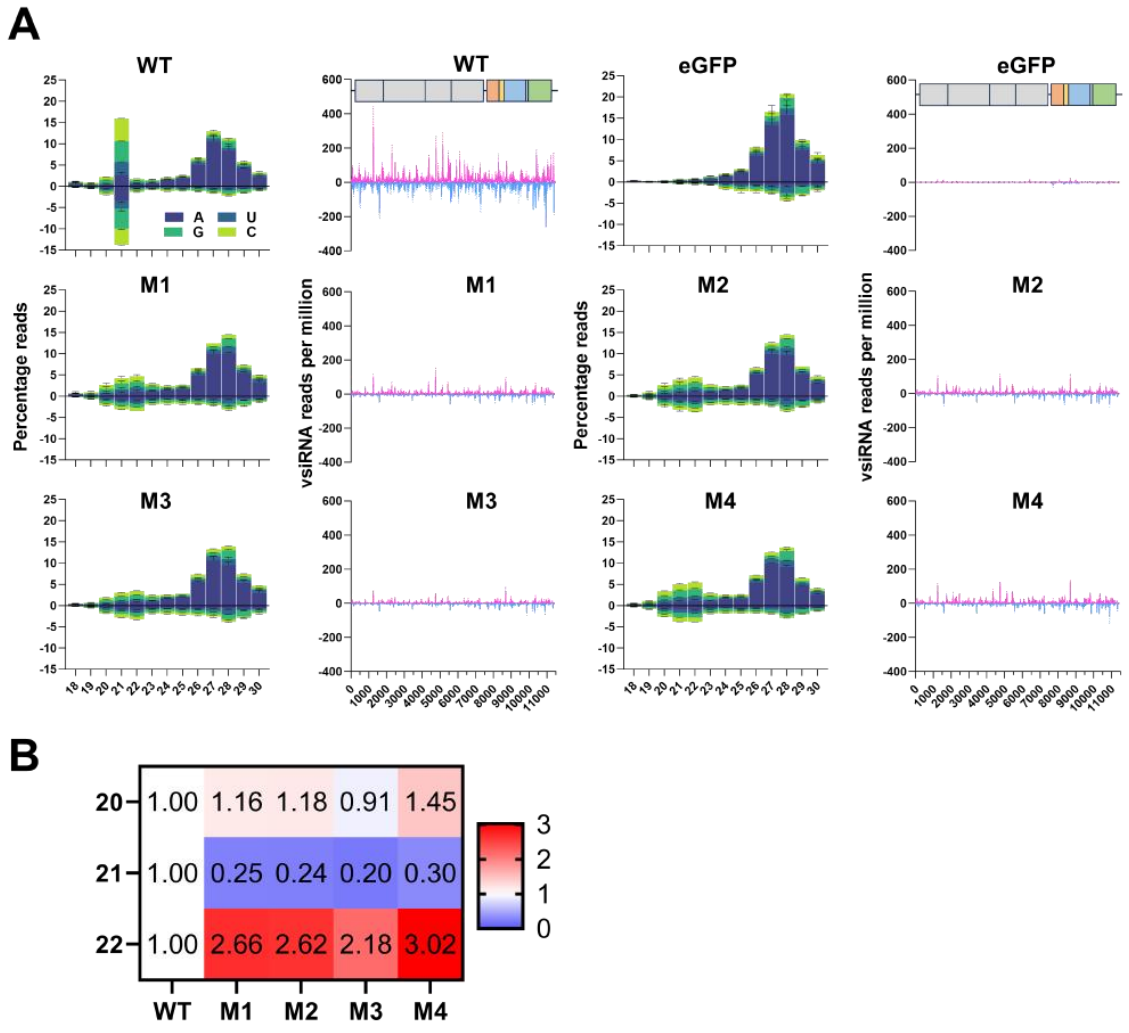


Fig. 4: Aaeg Dcr2 PAZ domain mutations affected 21 nt vsiRNA magnitude and length. (A) Small RNA sequencing of AF319 cells, transiently expressing Dcr2 PAZ domain mutants M1-M4 or WT Dcr2, or eGFP (as negative control), and infected with SFV (MOI=1) at 48 hpi.

Histogram of small RNA reads 18-30 nt in length, mapped to the SFV (SFV4 GenBank ID: KP699763) genome (positive numbers) and antigenome (negative numbers) with colours indicating first base nucleotide prevalence per size, shown as mean % mapped reads (Y axis, percentage reads) from two independent experiments +/- SD. Mapping of SFV-derived 21 nt vsiRNAs, mapped along the SFV genome (magenta) or anti-genome (cyan) (Y axis, vsiRNA reads per million) +/- SD. **(B)** Fold change of magnitude of SFV-derived small RNAs of lengths 20-22 nt of Dcr2 PAZ domain mutants M1-M4 compared to WT Dcr2.

Virus-derived small RNAs retain a 2 nt overhang cleavage pattern independently of Aaeg Dcr2 PAZ domain functionality

The predominant 21 nt vsiRNAs produced by Dcr2 cleavage that are commonly observed following arbovirus infection of mosquito cells are generated as duplexes. Assuming that mechanisms observed for *D. melanogaster* also apply in mosquitoes, they consist of two 21 nt strands that overlap by 19 nt with a 2 nt overhang at each 3´end. To investigate if and how dsRNA cleavage patterns were affected by the PAZ domain for generating virus-derived small RNAs, we analysed strand overlapping small RNA patterns (Fig. 5A, heat maps that show mean overlap probability z-scores of SFV-derived small RNAs 18-30 nt; Fig. 5B, showing number of overlapping pairs per million mapped reads of 19-23 nt SFV-derived small RNAs). For WT Dcr2, but also Dcr2 PAZ domain mutants M1-M4, all virus derived small RNAs in the range of 18-23 nt all showed a clear pattern, with strand complementarity significantly enhanced for overlaps that result in 2 nt overhangs. For example, 21 nt vsiRNAs overlapped with complementary sequences also by 19 nt (thus confirming observations in *D. melanogaster*); virus-derived small RNAs that are 20 nt in length overlapped with sequences that are 18 nt in length etc. This showed that PAZ domain mutations affected Aaeg Dcr2's ability to produce the usually predominant 21 vsiRNA over other lengths but did not affect the cleavage mechanism itself. We did however note a higher frequency of precise 2 nt overhangs for virus-derived small RNAs in AF319 expressing M1-M4 Dcr2 mutants compared to WT Dcr2. Indeed, further analysis noted a marked Z score drop for example for 19 nt overlap (in 21 nt vsiRNA) and +2 nt overhangs for WT Dcr2 compared to Dcr2 PAZ domain mutants M1-M4 (Supplemental Fig. S5, left panel). Interestingly, when we reanalysed 21 nt vsiRNA data previously published from SFV infection of the Ago2 KO cell line AF525, compared to parental AF5 cells (Scherer et al. 2021), we also observed higher frequencies of virus-derived small RNA duplexes with +2 nt overhangs (Supplemental Fig. S5, right panel). This leaves the possibility that failure to efficiently transfer or to Ago2, or fully process small RNA (and failure to degrade passenger strands) contributes to the increased presence of intact virus-derived small RNAs duplexes that are detected in this overlap analysis.

Production of virus-derived PIWI-interacting small RNAs (vpiRNAs), which are generally longer (24-30 nt) with a 10 nt overlap of the sense and antisense piRNAs as a result of the so-called ping-pong amplification mechanism in a Dcr2 independent manner (Varjak et al. 2018), was detected across all conditions.

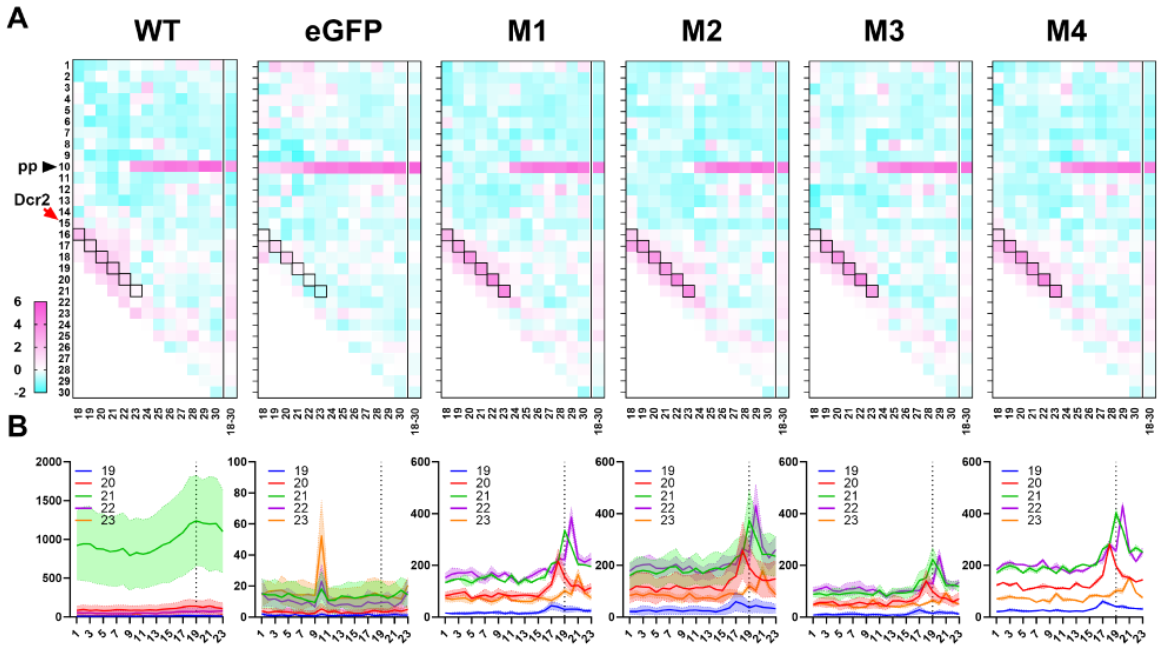


Fig. 5: Aaeg Dcr2 PAZ domain mutations result in dysregulated vsiRNA duplex overlap lengths. (A) Heat maps showing mean overlap probability z-scores of 18-30 nt SFV-derived small RNAs from AF319 transiently expressing Dcr2 PAZ domain mutant M1-M4 or WT Dcr2, or eGFP (control) from 2 independent repeats, as initially characterized in Fig 4. Differing lengths of vsiRNAs, analysed individually, are shown horizontally, and nt overlaps are listed vertically. The red arrow labelled Dcr2 indicates the expected 2 nt overlap from dsRNA cleavage with cells boxed in black. The black arrow labeled pp (ping-pong) shows the expected 10 nt overlap from potential ping-pong amplification in the piRNA pathway. **(B)** Number of overlapping pairs per million mapped reads of 19-23 nt virus-derived small RNAs from AF319 transiently expressing Dcr2 PAZ domain mutants M1-M4 or WT Dcr2, or eGFP (control) infected with SFV. Data are shown as the mean of 2 independent repeats with the range of values.

Loss of Aaeg Dcr2 PAZ domain functionality changes the position and magnitude of vsiRNA cleavage

We have previously shown that Aaeg Dcr2 produces a diverse but largely consistent pool of 21 nt vsiRNAs following SFV infection; a characteristic lost in helicase domain mutants (Gestuveo et al. 2022). To assess the impact of PAZ domain mutations on virus-derived small RNA population, diversity and cleavage bias, we examined these through two different analyses. First, we defined a position-based “harmony” metric which incorporates the strand bias and magnitude of the vsiRNAs and second, using a vsiRNA population approach where each unique siRNA was treated as an individual gene and examined differential vsiRNA expression between treatment groups. While visualization of virus-derived small RNA coverage, as demonstrated in Fig. 4, provides a reasonable indicator of the origin and magnitude of vsiRNAs, a more nuanced analysis of the consistency of Dcr2 cleavage over the SFV-derived dsRNA requires consideration of the position, magnitude and strandedness of 21 nt vsiRNAs. To develop a unified metric that encapsulates these attributes at each genomic position, we calculated the terminal 5’ vsiRNA read depth at each position of the SFV genome and antigenome, and normalized the total depth to one. Subsequently, we computed the normalized differential coverage, d_i, as the difference between the normalised genome

(positive-sense) and anti-genome (negative-sense) coverage proportions at each position. The genome coverage proportion at position *i*, G_i, is defined as the positive-sense coverage at *i* divided by the total positive-sense coverage for all *N* positions. The anti-genome coverage proportion, A_i, is similarly calculated as the negative-sense coverage at *i* normalized by the total negative-sense coverage. The formula for the normalized differential coverage at each position *i* is given by:

$$d_i = \frac{G_i}{\sum_{j=1}^{N} G_j} - \frac{A_i}{\sum_{j=1}^{N} A_j}$$

Through this measure, we obtained a ratio reflecting the balance of genome to antigenome virus-derived small RNA coverage, which provides insight into the strand-specific cleavage patterns of WT Dcr2 across the positions of the SFV genome. Using this metric, we generated a series of scatter plots (Fig. 6A) to compare the d_i values for each position of the SFV genome between WT Dcr2, negative control eGFP and the Dcr2 PAZ domain mutants M1-M4. Importantly, if the d_i value was 0 for a position for the comparison between treatments it was excluded from the analysis, keeping only non-zero d_i values for downstream analysis. We utilized linear regression analysis to assess the relationship between d_i values for all positions on the SFV genome from the WT Dcr2 and each mutant, with the coefficient of determination (R^2) reflecting the extent to which both treatments shared related vsiRNA profile "harmony". The regression analysis revealed varying degrees of correlation, with the lowest correlation between the eGFP control treatments compared to the WT Dcr2 (R^2=0.115). This suggests very little positional cleavage harmony between the WT Dcr2 and eGFP control, which is to be expected. Dcr2 PAZ domain mutants M1-M4 showed a more consistent pattern of Dcr2 cleavage to WT with R^2 values between 0.39-0.41. Finally, we compared d_i values for all 21 nt vsiRNA reads for all treatments and between mutants and summarised the R^2 values as a heat map (Figure 6B). The results indicated that the PAZ domain mutants M1-M4 were more closely related to each other than WT Dcr2 or eGFP control with R^2 between 0.74-0.84, indicating that the introduced mutations resulted in more harmonious cleavage patterns across the SFV genome but different from wild type.

In addition to analyzing positional cleavage patterns of 21 nt vsiRNAs (Fig. 6A-B), we examined population-level patterns and diversity of SFV-derived small RNA populations for individual lengths of 20 nt, 21 nt, 22 nt, and 23 nt, as well as combined lengths of 20-23 nt by conducting a differential transcript abundance analysis using edgeR (Fig. 6C). Through the generation of a non-redundant list of unique small RNAs, we generated count tables and normalized for library size using the weighted trimmed mean of M-values (TMM) method. Through multi-dimensional scaling (MDS), plots we were able to visualize the relationships between the treatments. MDS plots are a form of dimensionality reduction; visually, the distances between points represent the dissimilarities or differences between the treatments. Specifically, these distances correspond to the leading log-fold changes between the treatments, which reflect the relative expression levels of vsiRNAs across conditions. The MDS plots revealed varying degrees of similarity between the WT Dcr2 and Dcr2 PAZ domain mutant treatments across different virus-derived small RNA size classes. Notably, the 21 nt vsiRNAs displayed distinct clustering patterns, indicating that specific mutations in the Dcr2 PAZ domain contribute to the altered distribution and abundance of these vsiRNA species.

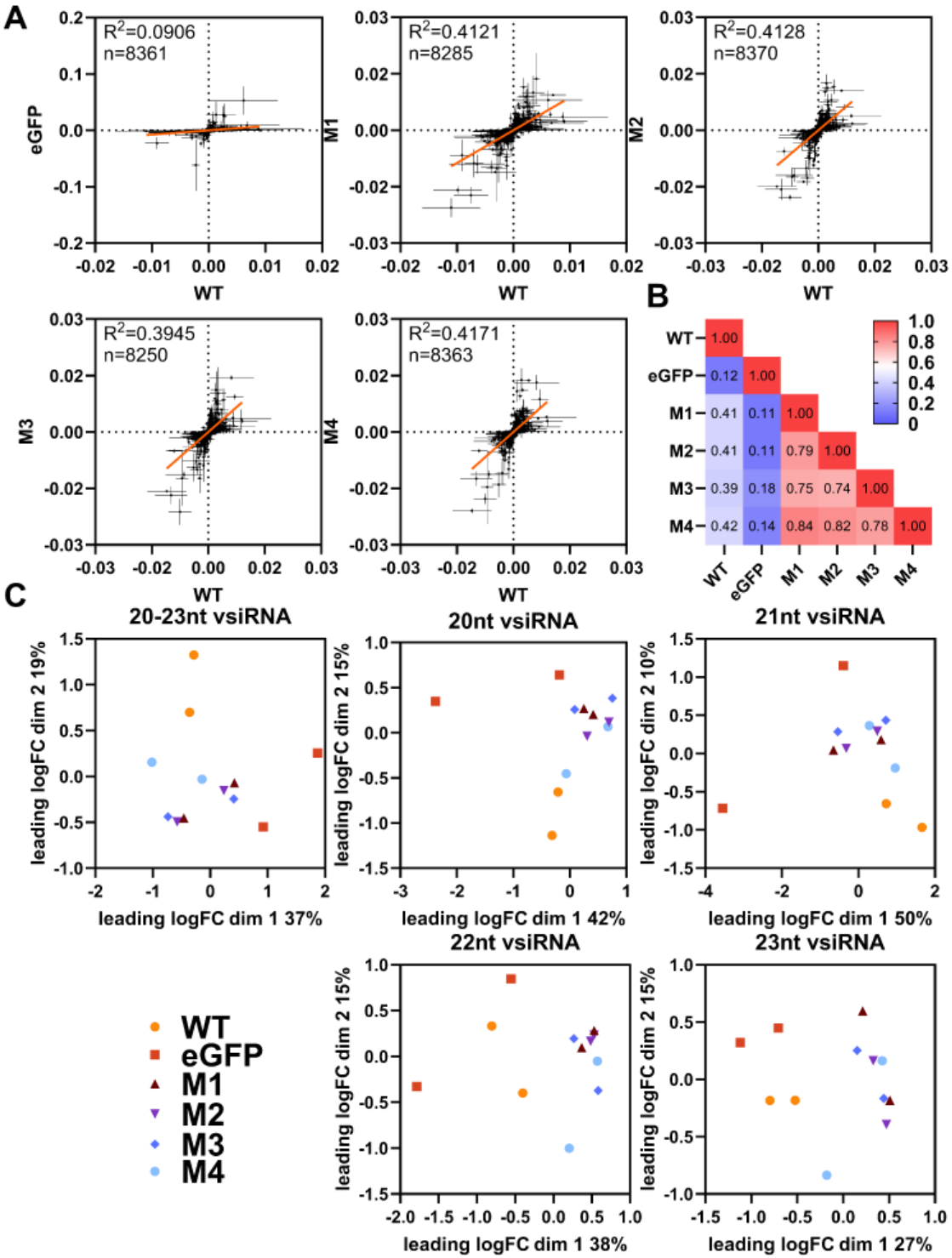


Fig. 6: Mutations in the PAZ domain of Aaeg Dcr2 change the position and magnitude of cleavage over the SFV genome and virus-derived small RNA populations compared to WT Dcr2. Samples from Fig 4 were analysed as follows. **(A)** Scatter plots showing normalized differential coverage (d_i) for each position in the SFV genome. Each panel compares WT Dcr2 with no Dcr2, an eGFP expressing Dcr2 negative treatment, or Dcr2 PAZ domain mutants M1-M4. The linear regression line is depicted within each plot, with the R^2 value indicating the fit of the model. The number of datapoints (n) with d_i >0 over the SFV genome used for the calculation is shown on each graph. **(B)** Heatmap displaying pairwise R^2

values from the linear regressions, comparing the similarity of differential coverage profile between treatments, as indicated. **(C)** Multidimensional scaling (MDS) plots representing the relationships between different size classes of vsiRNA reads from WT Dcr2, eGFP control and Dcr2 PAZ domain mutants M1-M4. Each plot corresponds to a specific size class of SFV-derived small RNA: 20 nt, 21 nt, 22 nt, and 23 nt, as well as a combined plot of 20-23 nt. The axes represent the leading two log-fold change (logFC) dimensions and the percentage of variation indicated.

Discussion

While the importance of the helicase domain has been demonstrated for both Dm and Aaeg Dcr2 antiviral responses (Gestuveo et al. 2022; Marques et al. 2013; Donelick et al. 2020), the relevance of the PAZ domain had not yet been investigated for Aaeg Dcr2 and processing of viral dsRNA in the context of arboviral replication in mosquito cells. Here, we identified conserved amino acids in Aaeg Dcr2 that inactivate PAZ domain function and antiviral activity. Critically, we observed that while inactivation did affect the production of 21 nt vsiRNA, it did not affect Aaeg Dcr2's virus-derived small RNA production in general but broadened the length of the produced SFV-derived small RNAs and led to an enrichment of specifically 22 nt SFV-derived small RNAs, similar to previous mutational analysis of Dm Dcr2 PAZ domain (Kandasamy and Fukunaga 2016). Thus, key observations hold true for viral dsRNAs and Aaeg Dcr2. The specific functions that are affected by the mutations we set in Aaeg Dcr2 PAZ will require further investigation. However, structural modelling (Supplemental Fig. S1) suggests positioning mostly in the core of the PAZ domain and thus a role in the binding mechanism of the dsRNA termini. This is further confirmed by modelling Aaeg PAZ domain interactions with dsRNA (Supplemental Fig. S4). Suggesting that the location of dsRNA is not affected but most likely mutations destabilise binding and thus allow flexibility in the interaction, which in turn leads to variable small RNA lengths following cleavage and in particular enrichment of 22 nt SFV-derived small RNAs. We cannot of course fully exclude effects on dsRNA binding or impaired processing that may not be captured by our analysis. Importantly, the critical PAZ domain amino acids we described here in Aaeg Dcr2 are different from those previously identified in Dm Dcr2 (Kandasamy and Fukunaga 2016). Based on our and previous data that demonstrate the importance of the Dcr2 helicase domain in the exo-siRNA pathway, we propose that the helicase binds usually blunt-ended, long viral dsRNA and cleavage of these termini -which is likely to generate small RNAs of variable length- generates the first dsRNA terminus with 2 nt overhang and 5' monophosphate that will be used by the PAZ domain to anchor the dsRNA strand and allow Dcr2 to produce mostly, though not exclusively, 21 nt vsiRNAs, and phase variation from occasional unprecise binding that allows the production of a diverse pool of vsiRNAs from dsRNA, may therefore start from early cleavage events onwards. Importantly, the size of 21 nt is critical and the most efficient siRNA length for silencing to target RNAs in the fly system (Kandasamy and Fukunaga 2016; Elbashir et al. 2001). It is intriguing to note that U is enriched in first position in libraries (Supplemental Fig. S3) compared to vsiRNAs where a bias towards C or G can be seen. Indeed, this may be due to presence of host derived sequences e.g. miRNAs that frequently have a U in the 5' first base position (Ghildiyal et al. 2010; Mi et al. 2008; Warf et al. 2011). Indeed in *D. melanogaster*, it has been shown that siRNAs derived from siRNA pathway, for example following processing long dsRNA, give rise to siRNAs with frequently C in position 1 which has been suggested to facilitate sorting into Ago2 (Ghildiyal et al. 2010) . A similar mechanism may be at play here in the production of vsiRNAs. Our data also suggest that maturation of vsiRNAs -by cleaving the

passenger strand- is less efficient with Dcr2 PAZ domain mutants M1-M4. While the exact processes would need further investigations, the marked increases in duplexes (with +2 nt overhangs) similar to what is observed in Ago2 KO cells infected SFV where an accumulation of duplexes is seen (Scherer et al. 2021), might be due for example to a failure of vsiRNAs to efficiently transfer into Ago2 via dysfunctional Dcr2 PAZ domain, or a processing issue. This requires further investigation, and there is a degree of “noisiness” in such assays that needs to be taken into account. Indeed, in our previous work (Gestuveo et al. 2022) for WT Dcr2, 19 nt overlaps with 2 nt overhangs for example in 21 nt vsiRNAs were easily observed than in this study. This may be due to technical issues, for example small RNA sequencing, transfection levels of Dcr2 expression plasmids etc. and to some extent production of stable Dcr2 expressing cell lines may remediate small differences for future work.

In summary, this study demonstrates the critical role of the Aaeg Dcr2 PAZ domain in the precise production of 21 nt vsiRNAs. Its critical contribution is in accurate vsiRNA length determination, which in turn is critical for the *Ae. aegypti* exo-siRNA to mount an antiviral response against SFV. Moreover, future work will determine how arboviruses of different families are targeted by Dcr2 and give us further insights into the nature of the viral dsRNA substrate.

Competing interest statement

The authors declare no competing interests. The funder had no role in study design, data collection and analysis, decision to publish, or preparation of the manuscript.

Acknowledgements

For the purpose of open access, the authors have applied a Creative Commons Attribution (CC BY) licence to any Author Accepted Manuscript version arising from this submission.
This study was supported by the UK Medical Research Council (MC_UU_12014/8, MC_UU_00034/4) (A.K.) and (MR/R021562/1, MC_UU_00034/2) (A.C.); European Research Council (ERC) Consolidator Grant ‘vRNP-capture’ N# 101001634 (A.C.); German Centre for Infection Research (DZIF) (TTU 01.708) (E.S.); DFG (project 497659464) (M.R.); Wellcome Trust/Royal Society Sir Henry Dale Fellowship (210462/Z/18/Z) (B.B.); Overseas Scholarship Scheme for PhD by Higher Education Commission of Pakistan (R.A.).

Funding

This study was supported by the UK Medical Research Council (MC_UU_12014/8, MC_UU_00034/4) (A.K.) and (MR/R021562/1, MC_UU_00034/2) (A.C.); European Research Council (ERC) Consolidator Grant ‘vRNP-capture’ N# 101001634 (A.C.); German Centre for Infection Research (DZIF) (TTU 01.708) (E.S.); DFG (project 497659464) (M.R.); Wellcome Trust/Royal Society Sir Henry Dale Fellowship (210462/Z/18/Z) (B.B.); Overseas Scholarship Scheme for PhD by Higher Education Commission of Pakistan (R.A.). The authors declare no conflict of interest. The funders had no role in study design, data collection and analysis, decision to publish, or preparation of the manuscript.

Author contributions are recognised as follows. Conceptualization: M.R., R.P., M.M., R.J.G., A. C., M.V., L.R., E.S., A.K.; Methodology: M.M., M.R., R.P., R.A., R.J.G., L.R.; Formal analysis: M.R., R.P., M.M., R.A., L.R.; Investigation: M.R., R.P., M.M., R. A., L.R.; Validation: M.R., R.P., M.M., R.A., L.R..; Resources: A.A.K., B.B., A.C., L.R., E.S., A.K.; Writing - Original Draft Preparation: M.R., R.P., M.M., R.J.G., R.A., A.C., L.R., E.S., A.K.; Writing - Review and Editing: M.R., R.P., M.M., R.J.G., R.A., A.A.K., B.B., M.V, A.C., L.R., E.S., A.K..; Visualization: M.R., R.P, M.M., R.A., L.R..; Data Curation: M.R., R.P., M.M., E.S., A.K.; Supervision: M.M., A.A.K., B.B., A.C., E.S., A.K.; Project Administration: M.M., E.S, A.K.; Funding Acquisition: R.A., B.B., A.C., E.S., A.K.

References

Abramson J, Adler J, Dunger J, Evans R, Green T, Pritzel A, Ronneberger O, Willmore L, Ballard AJ, Bambrick J, et al. 2024. Accurate structure prediction of biomolecular interactions with AlphaFold 3. *Nature*.

Achee NL, Grieco JP, Vatandoost H, Seixas G, Pinto J, Ching-Ng L, Martins AJ, Juntarajumnong W, Corbel V, Gouagna C, et al. 2019. Alternative strategies for mosquito-borne arbovirus control. *PLoS Negl Trop Dis* **13**: e0006822. https://www.ncbi.nlm.nih.gov/pubmed/30605475.

Alexander AJT, Salvemini M, Sreenu VB, Hughes J, Telleria EL, Ratinier M, Arnaud F, Volf P, Brennan B, Varjak M, et al. 2023. Characterisation of the antiviral RNA interference response to Toscana virus in sand fly cells. *PLoS Pathog* **19**: e1011283. https://www.ncbi.nlm.nih.gov/pubmed/36996243.

Alonso-Palomares LA, Moreno-Garcia M, Lanz-Mendoza H, Salazar MI. 2018. Molecular Basis for Arbovirus Transmission by Aedes aegypti Mosquitoes. *Intervirology* **61**: 255–264. https://www.ncbi.nlm.nih.gov/pubmed/31082816.

Anderson MA, Gross TL, Myles KM, Adelman ZN. 2010. Validation of novel promoter sequences derived from two endogenous ubiquitin genes in transgenic Aedes aegypti. *Insect Mol Biol* **19**: 441–449. https://www.ncbi.nlm.nih.gov/pubmed/20456509.

Antoniewski C. 2014. Computing siRNA and piRNA overlap signatures. *Methods Mol Biol* **1173**: 135–146. https://www.ncbi.nlm.nih.gov/pubmed/24920366.

Blair CD, Olson KE. 2015. The role of RNA interference (RNAi) in arbovirus-vector interactions. *Viruses* **7**: 820–843. https://www.ncbi.nlm.nih.gov/pubmed/25690800.

Brackney DE, Scott JC, Sagawa F, Woodward JE, Miller NA, Schilkey FD, Mudge J, Wilusz J, Olson KE, Blair CD, et al. 2010. C6/36 Aedes albopictus cells have a dysfunctional antiviral RNA interference response. *PLoS Negl Trop Dis* **4**: e856. https://www.ncbi.nlm.nih.gov/pubmed/21049065.

Brady OJ, Hay SI. 2020. The Global Expansion of Dengue: How Aedes aegypti Mosquitoes Enabled the First Pandemic Arbovirus. *Annu Rev Entomol* **65**: 191–208. https://www.ncbi.nlm.nih.gov/pubmed/31594415.

Bronkhorst AW, van Rij RP. 2014. The long and short of antiviral defense: small RNA-based immunity in insects. *Curr Opin Virol* **7**: 19–28. https://www.ncbi.nlm.nih.gov/pubmed/24732439.

Caragata EP, Dutra HLC, Sucupira PHF, Ferreira AGA, Moreira LA. 2021. Wolbachia as translational science: controlling mosquito-borne pathogens. *Trends Parasitol* **37**: 1050–1067. https://www.ncbi.nlm.nih.gov/pubmed/34303627.

Carvalho FD, Moreira LA. 2017. Why is Aedes aegypti Linnaeus so Successful as a Species? *Neotrop Entomol* **46**: 243–255. https://www.ncbi.nlm.nih.gov/pubmed/28401481.

Cenik ES, Fukunaga R, Lu G, Dutcher R, Wang Y, Tanaka Hall TM, Zamore PD. 2011. Phosphate and R2D2 restrict the substrate specificity of Dicer-2, an ATP-driven ribonuclease. *Mol Cell* **42**: 172–184. https://www.ncbi.nlm.nih.gov/pubmed/21419681.

Chen S, Zhou Y, Chen Y, Gu J. 2018. fastp: an ultra-fast all-in-one FASTQ preprocessor. *Bioinformatics* **34**: i884–i890. https://www.ncbi.nlm.nih.gov/pubmed/30423086.
Ciechanowska K, Pokornowska M, Kurzynska-Kokorniak A. 2021. Genetic Insight into the Domain Structure and Functions of Dicer-Type Ribonucleases. *Int J Mol Sci* **22**. https://www.ncbi.nlm.nih.gov/pubmed/33435485.
Donelick HM, Talide L, Bellet M, Aruscavage J, Lauret E, Aguiar E, Marques JT, Meignin C, Bass BL. 2020. In vitro studies provide insight into effects of Dicer-2 helicase mutations in Drosophila melanogaster. *RNA*. https://www.ncbi.nlm.nih.gov/pubmed/32843367.
Elbashir SM, Martinez J, Patkaniowska A, Lendeckel W, Tuschl T. 2001. Functional anatomy of siRNAs for mediating efficient RNAi in Drosophila melanogaster embryo lysate. *EMBO J* **20**: 6877–6888. https://www.ncbi.nlm.nih.gov/pubmed/11726523.
Facchinelli L, Badolo A, McCall PJ. 2023. Biology and Behaviour of Aedes aegypti in the Human Environment: Opportunities for Vector Control of Arbovirus Transmission. *Viruses* **15**. https://www.ncbi.nlm.nih.gov/pubmed/36992346.
Fredericks AC, Russell TA, Wallace LE, Davidson AD, Fernandez-Sesma A, Maringer K. 2019. Aedes aegypti (Aag2)-derived clonal mosquito cell lines reveal the effects of pre-existing persistent infection with the insect-specific bunyavirus Phasi Charoen-like virus on arbovirus replication. *PLoS Negl Trop Dis* **13**: e0007346. https://www.ncbi.nlm.nih.gov/pubmed/31693659.
Fukunaga R, Colpan C, Han BW, Zamore PD. 2014. Inorganic phosphate blocks binding of pre-miRNA to Dicer-2 via its PAZ domain. *EMBO J* **33**: 371–384. https://www.ncbi.nlm.nih.gov/pubmed/24488111.
Gestuveo RJ, Parry R, Dickson LB, Lequime S, Sreenu VB, Arnold MJ, Khromykh AA, Schnettler E, Lambrechts L, Varjak M, et al. 2022. Mutational analysis of Aedes aegypti Dicer 2 provides insights into the biogenesis of antiviral exogenous small interfering RNAs. *PLoS Pathog* **18**: e1010202. https://www.ncbi.nlm.nih.gov/pubmed/34990484.
Ghildiyal M, Xu J, Seitz H, Weng Z, Zamore PD. 2010. Sorting of *Drosophila* small silencing RNAs partitions microRNA* strands into the RNA interference pathway. *RNA* **16**: 43–56.
Halstead SB. 2019. Travelling arboviruses: A historical perspective. *Travel Med Infect Dis* **31**: 101471. https://www.ncbi.nlm.nih.gov/pubmed/31472285.
Huang YS, Higgs S, Vanlandingham DL. 2019. Emergence and re-emergence of mosquito-borne arboviruses. *Curr Opin Virol* **34**: 104–109. https://www.ncbi.nlm.nih.gov/pubmed/30743191.
Jumper J, Evans R, Pritzel A, Green T, Figurnov M, Ronneberger O, Tunyasuvunakool K, Bates R, Zidek A, Potapenko A, et al. 2021. Highly accurate protein structure prediction with AlphaFold. *Nature* **596**: 583–589. https://www.ncbi.nlm.nih.gov/pubmed/34265844.
Kandasamy SK, Fukunaga R. 2016. Phosphate-binding pocket in Dicer-2 PAZ domain for high-fidelity siRNA production. *Proc Natl Acad Sci U S A* **113**: 14031–14036. https://www.ncbi.nlm.nih.gov/pubmed/27872309.
Lambrechts L, Saleh MC. 2019. Manipulating Mosquito Tolerance for Arbovirus Control. *Cell Host Microbe* **26**: 309–313. https://www.ncbi.nlm.nih.gov/pubmed/31513769.
Langmead B, Salzberg SL. 2012. Fast gapped-read alignment with Bowtie 2. *Nat Methods* **9**: 357–359. https://www.ncbi.nlm.nih.gov/pubmed/22388286.
Leggewie M, Schnettler E. 2018. RNAi-mediated antiviral immunity in insects and their possible application. *Curr Opin Virol* **32**: 108–114. https://www.ncbi.nlm.nih.gov/pubmed/30428425.
Marques JT, Wang JP, Wang X, de Oliveira KP, Gao C, Aguiar ER, Jafari N, Carthew RW. 2013. Functional specialization of the small interfering RNA pathway in response to virus infection. *PLoS Pathog* **9**: e1003579. https://www.ncbi.nlm.nih.gov/pubmed/24009507.
McFarlane M, Almire F, Kean J, Donald CL, McDonald A, Wee B, Laureti M, Varjak M, Terry S, Vazeille M, et al. 2020. The Aedes aegypti Domino Ortholog p400 Regulates Antiviral Exogenous Small Interfering RNA Pathway Activity and ago-2 Expression. *mSphere* **5**. https://www.ncbi.nlm.nih.gov/pubmed/32269152.

Merkling SH, Crist AB, Henrion-Lacritick A, Frangeul L, Couderc E, Gausson V, Blanc H, Bergman A, Baidaliuk A, Romoli O, et al. 2023. Multifaceted contributions of Dicer2 to arbovirus transmission by Aedes aegypti. *Cell Rep* **42**: 112977. https://www.ncbi.nlm.nih.gov/pubmed/37573505.

Mi S, Cai T, Hu Y, Chen Y, Hodges E, Ni F, Wu L, Li S, Zhou H, Long C, et al. 2008. Sorting of Small RNAs into Arabidopsis Argonaute Complexes Is Directed by the 5′ Terminal Nucleotide. *Cell* **133**: 116–127.

Olson KE, Blair CD. 2015. Arbovirus-mosquito interactions: RNAi pathway. *Curr Opin Virol* **15**: 119–126. https://www.ncbi.nlm.nih.gov/pubmed/26629932.

Paturi S, Deshmukh M V. 2021. A Glimpse of “Dicer Biology” Through the Structural and Functional Perspective. *Front Mol Biosci* **8**: 643657. https://www.ncbi.nlm.nih.gov/pubmed/34026825.

Pettersen EF, Goddard TD, Huang CC, Meng EC, Couch GS, Croll TI, Morris JH, Ferrin TE. 2021. <scp>UCSF ChimeraX</scp> : Structure visualization for researchers, educators, and developers. *Protein Science* **30**: 70–82.

Pierson TC, Diamond MS. 2020. The continued threat of emerging flaviviruses. *Nat Microbiol* **5**: 796–812. https://www.ncbi.nlm.nih.gov/pubmed/32367055.

Prince BC, Walsh E, Torres TZB, Ruckert C. 2023. Recognition of Arboviruses by the Mosquito Immune System. *Biomolecules* **13**. https://www.ncbi.nlm.nih.gov/pubmed/37509194.

Quinlan AR, Hall IM. 2010. BEDTools: a flexible suite of utilities for comparing genomic features. *Bioinformatics* **26**: 841–842. https://www.ncbi.nlm.nih.gov/pubmed/20110278.

Robinson MD, McCarthy DJ, Smyth GK. 2009. edgeR: a Bioconductor package for differential expression analysis of digital gene expression data. *Bioinformatics* **26**: 139–140. https://doi.org/10.1093/bioinformatics/btp616.

Samuel GH, Adelman ZN, Myles KM. 2018. Antiviral Immunity and Virus-Mediated Antagonism in Disease Vector Mosquitoes. *Trends Microbiol* **26**: 447–461. https://www.ncbi.nlm.nih.gov/pubmed/29395729.

Samuel GH, Pohlenz T, Dong Y, Coskun N, Adelman ZN, Dimopoulos G, Myles KM. 2023. RNA interference is essential to modulating the pathogenesis of mosquito-borne viruses in the yellow fever mosquito Aedes aegypti. *Proc Natl Acad Sci U S A* **120**: e2213701120. https://www.ncbi.nlm.nih.gov/pubmed/36893279.

Scherer C, Knowles J, Sreenu VB, Fredericks AC, Fuss J, Maringer K, Fernandez-Sesma A, Merits A, Varjak M, Kohl A, et al. 2021. An Aedes aegypti-aerived Ago2 knockout cell line to investigate arbovirus infections. *Viruses* **13(6)**: 1066.

Scott JC, Brackney DE, Campbell CL, Bondu-Hawkins V, Hjelle B, Ebel GD, Olson KE, Blair CD. 2010. Comparison of dengue virus type 2-specific small RNAs from RNA interference-competent and -incompetent mosquito cells. *PLoS Negl Trop Dis* **4**: e848. https://www.ncbi.nlm.nih.gov/pubmed/21049014.

Sinha NK, Iwasa J, Shen PS, Bass BL. 2018. Dicer uses distinct modules for recognizing dsRNA termini. *Science (1979)* **359**: 329–334. https://www.ncbi.nlm.nih.gov/pubmed/29269422.

Su S, Wang J, Deng T, Yuan X, He J, Liu N, Li X, Huang Y, Wang HW, Ma J. 2022. Structural insights into dsRNA processing by Drosophila Dicer-2-Loqs-PD. *Nature* **607**: 399–406. https://www.ncbi.nlm.nih.gov/pubmed/35768513.

Swevers L, Liu J, Smagghe G. 2018. Defense Mechanisms against Viral Infection in Drosophila: RNAi and Non-RNAi. *Viruses* **10**. https://www.ncbi.nlm.nih.gov/pubmed/29723993.

Tikhe C V, Dimopoulos G. 2021. Mosquito antiviral immune pathways. *Dev Comp Immunol* **116**: 103964. https://www.ncbi.nlm.nih.gov/pubmed/33301792.

Ulper L, Sarand I, Rausalu K, Merits A. 2008. Construction, properties, and potential application of infectious plasmids containing Semliki Forest virus full-length cDNA with an inserted intron. *J Virol Methods* **148**: 265–270. https://www.ncbi.nlm.nih.gov/pubmed/18054090.

Varjak M, Leggewie M, Schnettler E. 2018. The antiviral piRNA response in mosquitoes? *J Gen Virol* **99**: 1551–1562. https://www.ncbi.nlm.nih.gov/pubmed/30372405.
Varjak M, Maringer K, Watson M, Sreenu VB, Fredericks AC, Pondeville E, Donald CL, Sterk J, Kean J, Vazeille M, et al. 2017. Aedes aegypti Piwi4 Is a Noncanonical PIWI Protein Involved in Antiviral Responses. *mSphere* **2**. https://www.ncbi.nlm.nih.gov/pubmed/28497119.
Wang GH, Du J, Chu CY, Madhav M, Hughes GL, Champer J. 2022. Symbionts and gene drive: two strategies to combat vector-borne disease. *Trends Genet* **38**: 708–723. https://www.ncbi.nlm.nih.gov/pubmed/35314082.
Wang GH, Gamez S, Raban RR, Marshall JM, Alphey L, Li M, Rasgon JL, Akbari OS. 2021. Combating mosquito-borne diseases using genetic control technologies. *Nat Commun* **12**: 4388. https://www.ncbi.nlm.nih.gov/pubmed/34282149.
Warf MB, Johnson WE, Bass BL. 2011. Improved annotation of *C. elegans* microRNAs by deep sequencing reveals structures associated with processing by Drosha and Dicer. *RNA* **17**: 563–577.
Weaver SC, Charlier C, Vasilakis N, Lecuit M. 2018. Zika, Chikungunya, and Other Emerging Vector-Borne Viral Diseases. *Annu Rev Med* **69**: 395–408. https://www.ncbi.nlm.nih.gov/pubmed/28846489.
Weaver SC, Reisen WK. 2010. Present and future arboviral threats. *Antiviral Res* **85**: 328–345. https://www.ncbi.nlm.nih.gov/pubmed/19857523.
Yamaguchi S, Naganuma M, Nishizawa T, Kusakizako T, Tomari Y, Nishimasu H, Nureki O. 2022. Structure of the Dicer-2-R2D2 heterodimer bound to a small RNA duplex. *Nature* **607**: 393–398. https://www.ncbi.nlm.nih.gov/pubmed/35768503.
Zaid A, Burt FJ, Liu X, Poo YS, Zandi K, Suhrbier A, Weaver SC, Texeira MM, Mahalingam S. 2021. Arthritogenic alphaviruses: epidemiological and clinical perspective on emerging arboviruses. *Lancet Infect Dis* **21**: e123–e133. https://www.ncbi.nlm.nih.gov/pubmed/33160445.
Zapletal D, Kubicek K, Svoboda P, Stefl R. 2023. Dicer structure and function: conserved and evolving features. *EMBO Rep* **24**: e57215. https://www.ncbi.nlm.nih.gov/pubmed/37310138.

Chapter 3: Publication 2

Detection and Characterization of Antiviral Proteins Against Bunyaviruses in Mosquito-Derived Cells.

Melinda Reuter[1,2,3#], Phillip Böhmer[1,2,3#], Mine Altinli[1,2,3], Esther Schnettler[1,2,3]

[1]Bernhard-Nocht-Institute for Tropical Medicine, Hamburg, Germany

[2]German Centre for Infection Research (DZIF), Partner Site Hamburg-Luebeck-Borstel-Riems, Hamburg, Germany

[3]Faculty of Mathematics, Informatics and Natural Sciences, University Hamburg, Hamburg, Germany

[#]These authors contributed equally to this manuscript.

Correspondence: schnettler@bnitm.de

Keywords: dsRNA transfection, Mosquito-derived cells, *Bunyaviricetes*, Antiviral, RNAi

Abstract

Viruses of the class *Bunyaviricetes* are often transmitted by arthropods, including mosquitoes. The innate immune response in mosquitoes comprises several pathways, including sequence-specific degradation through RNA interference (RNAi). It is known that bunyavirus infections are targeted by the innate immune response in mosquitoes and derived cells; however, detailed information is often still missing. In this chapter, we describe a detailed protocol to determine if a protein of interest acts antiviral against bunyavirus infection in mosquito-derived cells. In line, we also describe a detailed protocol to investigate the effect of over-expression of a mosquito-encoded protein or analysis of mutant proteins on bunyavirus infection.

1 Introduction

Investigating the antiviral activity of specific mosquito proteins in mosquito-derived cell culture by either dsRNA / siRNA-based silencing approach or overexpression has been a very important method in the past for various mosquito infecting viruses, including viruses of the class *Bunyaviricetes* [1-3]. The dsRNA-based silencing approach involves the production of sequence-specific dsRNA molecules by in vitro transcription with T7 RNA polymerase from PCR products, followed by their transfection to mosquito-derived cells with the help of lipocomplexes. These dsRNA molecules are recognized as foreign in the cell and enter the exogenous siRNA pathway, resulting in the production of 21 nt long small interfering (si)RNAs, which in turn are incorporated into the RNA-induced silencing complex, specifically the Argonaute-2 protein. Following, complementary mRNA is recognized and degraded, resulting in reduced protein production [4]. Due to the lack of antibodies for most mosquito proteins, successful transcript silencing is often determined by quantitative real-time PCR. The effect of

protein silencing on virus infection is investigated following virus infection of dsRNA/siRNA transfected cells (Fig.1), either detecting virus production (TCID50 or plaque assays), viral RNA (qRTPCR) or reporter detection in case of reporter viruses (e.g. luciferase).

On the other hand, overexpression of proteins of interest and their effect or interaction with bunyavirus infection are used to investigate more detailed molecular interactions (Fig. 1). This can either be done in cells already endogenously expressing the protein of interest or resubstituting the protein of interest or mutants in cells not expressing the protein of interest (e.g., knockout cell lines produced by CRISPR/Cas9 or TALENS). Such an investigation is specifically useful to understand the importance of various domains or even specific amino acids of, for example, key antiviral proteins, like the Dicer-2 or Argonaute-2 protein of the siRNA pathway in mosquitoes [5, 6]. Until now, most knowledge about RNAi proteins still comes from the model organism Drosophila. Although this knowledge can often be extrapolated, it has been shown that this is not always the case, for example looking at the encoded Piwi, Argonaute and Aubergine proteins [7]. In addition, overexpression of wild-type target proteins, which were identified to be downregulated upon infection, can be used to determine its effect and possible antiviral activity on virus infection.

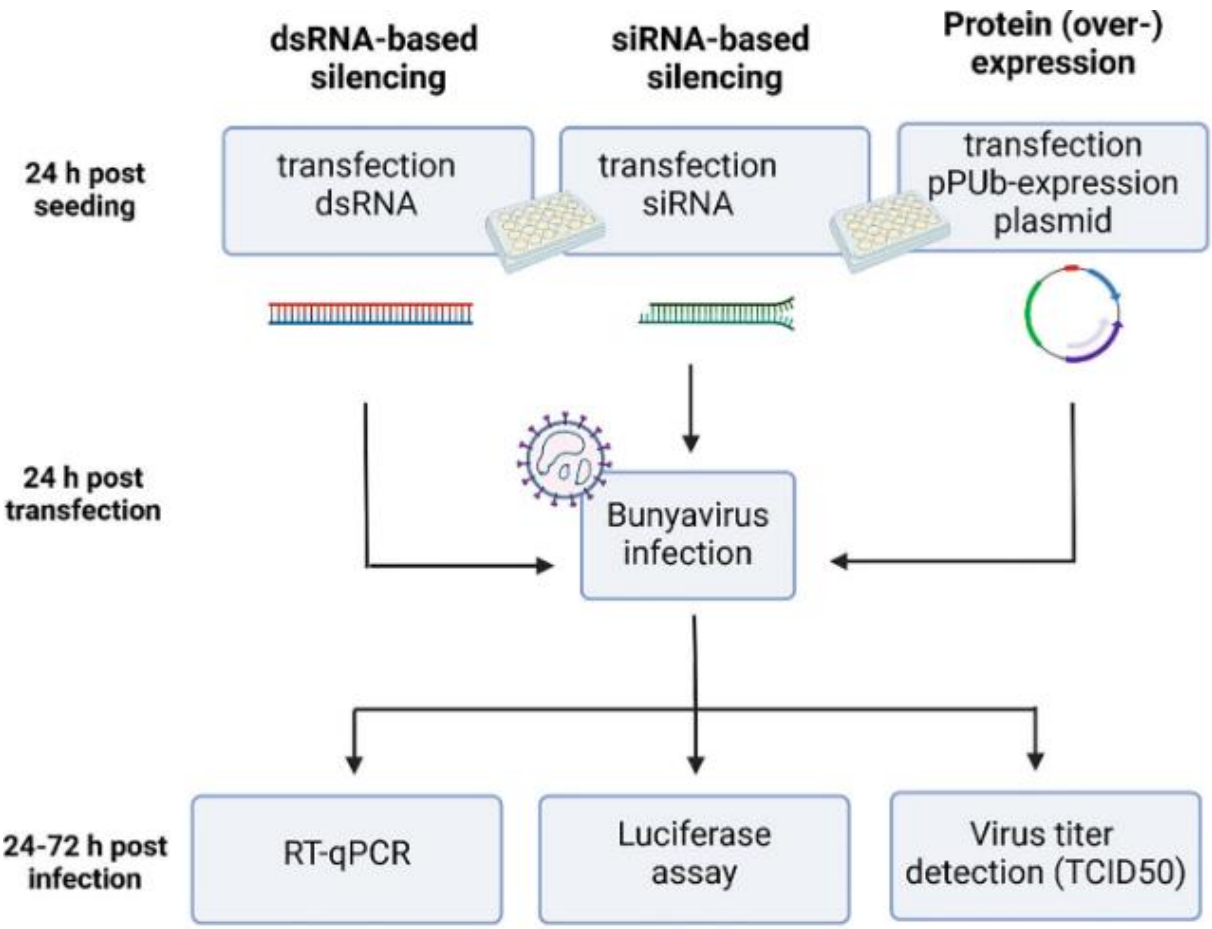


Fig. 1: Schematic outline of experiments to detect and characterize antiviral proteins against bunyaviruses in mosquito-derived cells using silencing and overexpression assays. For details, see the text.

2 Materials

2.1 Cell culture

1. *Aedes aegypti* derived Aag2-AF5 (ECACC 19022601), Aag2-AF319 (CRISPR/Cas9 produced Dicer-2 knock out cells; ECACC 19022602) and BHK-21 (ECACC 85011433) cells
2. Medium*:* Aag2-derived cells: Leibovitz L15 medium supplemented with 10% heat-inactivated Fetal Calf Serum (FCS), 10% Tryptose phosphate broth (TPB) and 1x Penicillin/Streptomycin. BHK-21 cells: GMEM supplemented with 10% heat-inactivated Fetal Calf Serum (FCS) and 1x Penicillin/Streptomycin. DPBS (sterile), Trypsin-EDTA . Store at 4°C.
3. Cell scraper
4. 25 cm^2 culture flask
5. 24-well and 96-well culture plates
6. Neubauer counting chamber
7. Cell incubator 28°C without CO_2 supply
8. Cell incubator 37°C with 5% CO_2

2.2 Design of primers and generation of templates for *in vitro* transcription of dsRNA production

2.2.1 RNA isolation

Any RNA isolation method (either for total RNA or mRNAs) can be used. We report here how it works for total RNA isolation using NucleoZOL®.

1. NucleoZOL® (Machery&Nagel)
2. 70% EtOH
3. Isopropanol
4. RNase free water

2.2.2 cDNA production

1. RNase free water
2. Random hexamer primers
3. Oligo(dT) primers
4. M-MLV 5x Buffer
5. M-MLV (200U/µL)
6. RNase inhibitor
7. dNTPs (10mM)

2.2.3 PCR with T7-primers

1. Kod Hot Start polymerase Kit (Thermofisher, Waltham USA), or any other proof-reading DNA polymerase
2. gene-specific primers with attached T7 sites
3. 2% Agarose Gel
4. Gel and PCR Clean-up kit

2.3 PCR with T7 primers

1. Kod Hot Start polymerase Kit (Thermofisher, Waltham USA), or any other proof-reading DNA polymerase

2.4 Transfection and infection

1. *Aedes aegypti*-derived cells (AF5 or AF319) in a 24-well plate, seeded 1 day prior to transfection (2.8*10*5 cells per well), to have a confluence of 50-70% on the day of transfection
2. DharmaFECT2 (Horizon, Waterbeach, United Kingdom)
3. Reduced Serum medium OptiMEM
4. Double-stranded RNA (specific for the investigated target and a non-targeting control)
5. Commercially bought siRNAs (specific for the investigated target and a non-targeting control)
6. Plasmids pPUb, expressing the protein of interest (e.g. Dicer-2 wt or mutants) and a control plasmid (e.g. expressing eGFP) from the ubiquitous promoter of *Ae. aegypti*
7. Virus stock (with a known sufficient titer of the Bunyavirus to be investigated, either wildtype or expressing a luciferase reporter protein).

2.5 Effect on virus infection

2.5.1 qRT-PCR

1. 96-well plate
2. PCR foil
3. QuantiTect SYBR Green PCR Mastermix (Qiagen, Hilden, Germany), or any other quantitative PCR Mastermix
4. Target-specific primer pair
5. Housekeeping gene-specific primer pair (e.g. ribosomal S7)
6. RNase free H_20

2.5.2 TCID50

1. 96-well plate
2. Formaldehyde
3. Crystal violet

2.5.3 Luciferase measurement

1. Passive Lysis Buffer (Promega)
2. Luciferase kit, according to the reporter luciferase used (Promega)
3. Luminometer and corresponding plates

3 Methods

Carry out all procedures at room temperature unless otherwise specified. dsRNA and siRNA molecules, as well as RNA, should be kept on ice.

3.1 Cell culture

1. AF cells and BHK-21 cells are cultured in a 25 cm^2 flask either at 28°C without CO_2 or 37°C with 5% CO_2, respectively. Cells are subcultured when reaching confluency.
2. For subculturing the AF cells, they are detached using the cell scraper and resuspended in their culture medium by slowly pipetting up and down several times. In the case of BHK-21 cells, the media is removed and the cells are shortly washed with PBS. After removing the PBS, 1 mL Trypsin-EDTA is added to detach the cells. After detaching, 4 mL of

complete culture media is added. Transfer the desired amount to a new 25 cm^2 flask, previously filled with fresh culture media. For routine passaging, use a splitting ratio of 1:5 for AF5 cells and 1:10 for BHK-21 cells.
3. For silencing or overexpression assays, AF cells are counted using a Neubauer counting chamber and $2.8*10^5$ cells are seeded in 1 mL culture medium per well in a 24-well plate. Experiments are performed in technical triplicates, therefore seed three wells for each construct/dsRNA/siRNA to be tested for a specific bunyavirus.
4. For TCID50 assays, BHK-21 cells are counted, and $4*10^4$ cells are seeded in 180 µL per well in a 96-well plate.

3.2 Design of primers and generation of templates for *in vitro* transcription of dsRNA production

After identifying a target mRNA for silencing, a specific target nucleotide sequence should be chosen to produce dsRNA from this sequence.

1. Choose a dsRNA target sequence that is between 150 and 500 bp long and shows no similarity with other host mRNA regions for at least a 19 nt stretch.
2. Design primers for the last 20-22 nt of the ends of the target side. Add to the 5' end of the designed primers the sequence for the T7 RNA polymerase promoter (5´gta ata cga ctc act ata ggg 3´)

3.2.1 RNA isolation

For total RNA isolation (either for dsRNA production or to quantify viral infection, see 3.6.1), seed $2.5*10^5$ cells in 1 mL culture medium per well in a 24-well plate 3 days prior to RNA isolation.

1. Remove cell medium from AF cells
2. Add 500 µL Nucleozol®
3. Ensure complete lysis by pipetting up and down (See **Note 1**)
4. Add 200 µL RNase-free water per 500 µL Nucleozol®
5. Shake the sample vigorously for 15 sec
6. Incubate at room temperature for 5 min
7. Centrifuge for 15 min at 12.000 x g at RT (See **Note 2**)
8. Transfer 500 µL of the supernatant to a new tube
9. Add 500 µL isopropanol per 500 µL supernatant to precipitate RNA
10. Incubate 10 min at RT
11. Centrifuge the sample for 10 min at 12.000 x g
12. Discard supernatant (See **Note 3**)
13. Add 500 µL 70% EtOH for washing
14. Centrifuge for 3 min at 8000 x g
15. Remove Ethanol by pipetting (See **Note 4**)
16. Repeat the washing step (Add 500 µL 70% EtOh, centrifuge 3 min at 800 x g)
17. Remove the supernatant (See **Note 5**)
18. Dissolve the pellet in 25 µL RNAse-free water (See **Note 6**)
19. Measure RNA concentration (e.g. Nanodrop)

3.2.2 cDNA production and T7-based PCR product

1. Mix 1.5 µg total RNA with 1 µL of oligo(dT) primers in a total volume of 15 µL filled up with ddH20
2. Incubate for 5 min at 70°C
3. Place 1 min on ice

4. Add 5 µL 5x M-MLV buffer, 1.25 µL dNTPs (10 mM), 1 µL RNAse inhibitor, 1.75 µL water (molecular grade, RNAse free), 1 µL M-MLV (200 U/µL)
5. Incubate 1 h at 42°C.
6. Run a KOD hot start PCR reaction with the generated cDNA as a template using your designed primers (See **Note 7**)
7. Run the PCR product on a 2% TAE agarose gel and purify the PCR product with a kit according to the manufacturer's instructions (See **Note 8**)

3.3 *In vitro transcription and dsRNA production*

Use the purified PCR products as templates for *In vitro* transcription and dsRNA production

1. Generate dsRNA according to the manufacturer's instruction using the RNAi Megascript kit (Thermofisher) (See **Note 9**)
2. Measure the dsRNA concentration (e.g. Nanodrop), make aliquots and store the dsRNA at -80°C or use it directly for transfection experiments.

3.4 Transfection of cells with dsRNA/ siRNA or pPUb-expression plasmid

dsRNA or siRNA-based silencing or overexpression of a protein of interest is done 24 hours prior to infection (Fig1). The following procedure exemplifies one well of a 24-well plate:

1. On Day 1: 24 h prior to transfection, seed $2.5x10^5$ AF cells/mL in 1 mL in a 24-well plate.
2. Incubate the cells at 28°C without CO_2.
3. On Day 2: Prepare either i) the in vitro transcribed dsRNA, ii) the commercially bought siRNAs (sequence-specific and control) or iii) the pPUb-based expression plasmid
4. Check your seeded cells for confluency under a microscope. They should be evenly distributed at the bottom of the well at about 50-80% confluency.
5. Prepare two 1.5 mL reaction tubes
6. Prepare Tube 1: i) 200 ng dsRNA, ii) 20 nM siRNA or iii) 500 ng PpUb-expression plasmid + reduced serum medium (OptiMEM) in a total volume of 50 µL (see **Note 10**)
7. Prepare Tube 2: 2 µL Dharmafect 2 + 48 µL reduced serum medium (OptiMEM) (See **Note 11**)
8. Incubate for 5-10 minutes.
9. Add the mix of tube 2 to tube 1. The total transfection volume will be 100 µL/well. (See **Note 12, Note 13**)
10. Mix by tapping or vortexing shortly and centrifuge briefly.
11. Incubate the mix for 30 min at RT. The incubation time should be a minimum of 20 min and should not exceed 1 h.
12. After the incubation time, add the mix drop by drop to the cells.
13. Incubate cells at 28°C without CO_2 for 24 h.

3.5 Infection

1. On Day 3: Check your cells under a microscope. (See **Note 14**)
2. Remove the medium from the well and replace it with fresh medium (0.5 mL) (See **Note 15**)
3. For the infection, calculate the amount of virus needed per well according to the desired multiplicity of infection (MOI) in 100 µL growth medium:

$$\frac{cell\ number\ (2.8 * 10^4) * desired\ MOI}{Virustiter} * 1000 = amount\ of\ virus\ added\ per\ well\ (\mu L)$$

4. Add the virus onto the cells drop by drop in a circular manner. Leave the virus on the cells for 2 h at 28°C without CO_2. Afterwards, remove the inoculum from the well and replace it with fresh medium (1 mL)
5. Remove the medium from the well and replace it with fresh medium (1 mL)
6. Incubate the cells at 28°C without CO_2 for 48h.

3.6 Effect on virus infection

Depending on the used virus (wt or expressing a luciferase reporter protein) different assays are performed to quantify virus infection. Generally, effects on the viral RNA in the cells are detected by qRT-PCR and are combined with the detection of infectious virus particles in the cell culture media ($TCID_{50}$). In the case of luciferase reporter expressing viruses, the effect on virus protein production by luciferase assays is performed. Again, it can be combined with the detection of infectious virus particles in the cell culture media ($TCID_{50}$). In addition, successful silencing of the target mosquito mRNA in the case of dsRNA/ siRNA-based silencing needs to be checked by qRT-PCR. In case of (over-)expression, the presence of the protein can be detected by SDS-PAGE and Western blot analysis or immunofluorescent staining.

1. Check your cells under the microscope (See **Note 16**).
2. Take off the supernatant and either proceed with 3.6.1 RNA isolation and RT-qPCR, 3.6.2 $TCID_{50}$ or 3.6.3. Luciferase measurement.

3.6.1 RT-qPCR

1. Isolate total RNA (see 3.2.1)
2. Produce cDNA from your isolated RNA (see 3.2.2) (see **Note 17, Note 18, Note 19, Note 20**)
3. Use your produced cDNA to run two Sybr Green qRT-PCRs (Qiagen) reactions with 1 µL cDNA template each:

   PCR 1 to check the silencing efficiency of your transcript: qRT-PCR1 Reaction 1 with a primer pair targeting your gene of interest (Note 21) and a housekeeper gene (e.g. ribosomal S7 [8])

   PCR 2 to check the effect of your silencing upon viral replication. qRT-PCR 2 with a primer pair targeting your virus and a housekeeper (ribosomal S7)

3.6.2 TCID50

1. Take off the supernatant and either use it directly or freeze it at -80°C until use.
2. Seed 4x10^4 BHK-21 cells in 180 µL per well in a 96-well plate and incubate overnight at 37°C and 5% CO2.
3. Add 20 µL of supernatant in the first row (use 4 columns per sample).
4. Gently mix and take 20 µL of row 1 and add to row 2 (**Note 22**)
5. Repeat this process, creating 10-fold dilutions. Leave 1 row as uninfected control.
6. Incubate the plate at 37°C, 5% CO2, for the appropriate time, depending on the virus (check the plate for CPE every day)
7. After the incubation is complete, fix the plate for 30-60 min in 8% formaldehyde in a fume cupboard.
8. Gently tap off excess formaldehyde before adding 100 µL crystal violet per well.
9. Gently wash off the dye using tap water and let the plate air-dry.

3.6.3 Luciferase measurement

1. Dilute 5x passive lysis buffer (Promega) with water to get 1x passive lysis buffer.
2. Remove cell medium
3. Lyse cells using 100 µl 1x passive lysis buffer (Promega) (**Note 23** and **Note24**).
4. Incubate the cells 15-20min at room temperature on a rocking plate.
5. Measure luminescence according to the manufacturer's protocol.

3.7 Data analysis

3.7.1 Data analysis of qRT-PCR data

1. For analysis of qRT-PCR data the $2^{-\Delta\Delta CT}$ method is used with the ribosomal S7 gene as housekeeping gene.
2. After calculating the relative quantification, each sample is normalized to its control knockdown. To normalize it calculate: *RQ knockdown target/RQ knockdown control.*
3. Present your data in a graph (see example below; Figure 2 and 3).

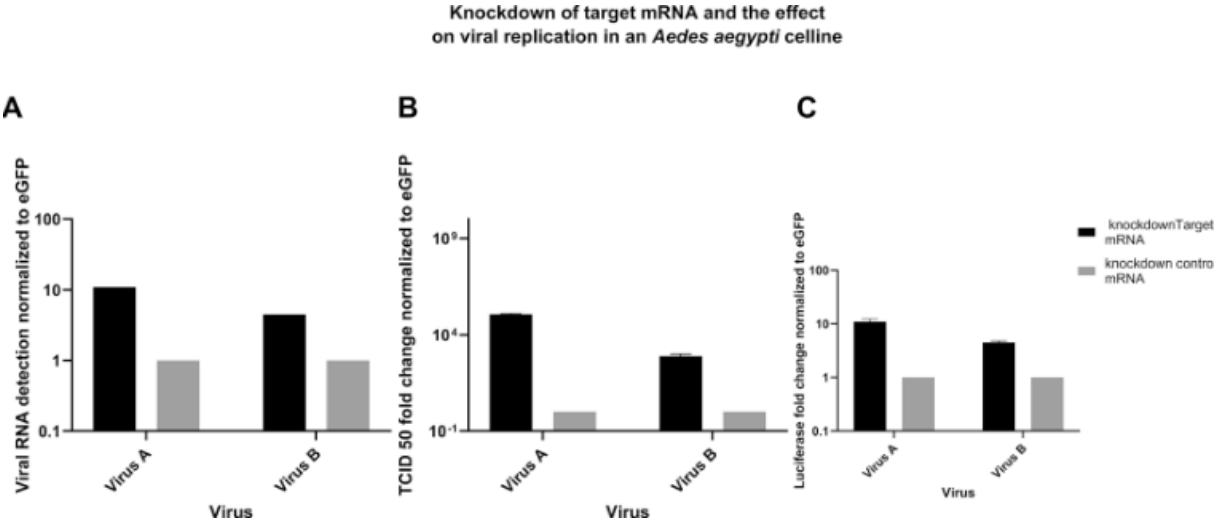


Fig. 2: Exemplary Graph to show the effects on bunyavirus infection upon silencing a target mosquito mRNA. Regarding the method the results should be represented in different graphs. The graph should present the used virus on the x-axis and the fold change of either A: viral RNA detection B: TCID50 fold change or C: Luciferase fold change. The data is normalized to the control treatment (non-targeting dsRNA/ siRNA).

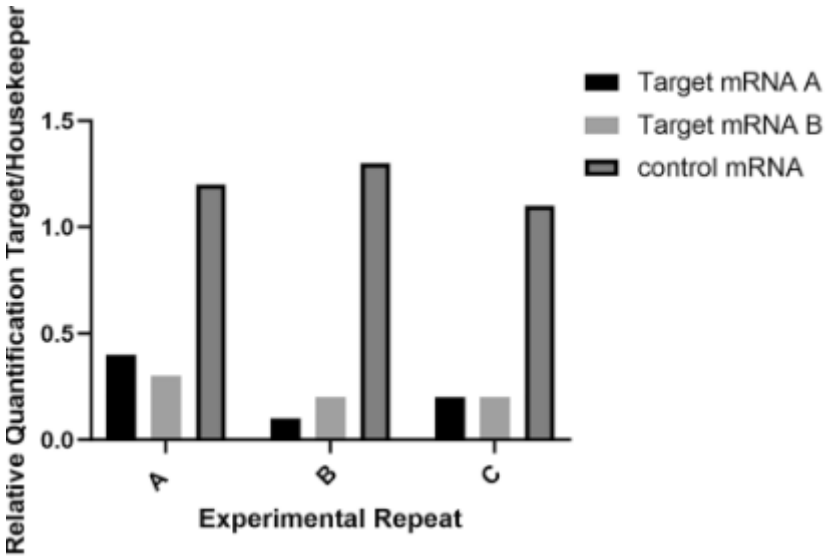


Fig. 3: Exemplary Graph showing the qRT-PCR data to determine the success of silencing the target transcript. The Y axis shows the relative Quantification determined by the $2^{-\Delta\Delta CT}$ method. The x-axis shows the different experimental repeats.

3.7.2 Data analysis of TCID 50 data

1. Determine the number of positive (no staining; no cells due to CPE) and negative wells (blue staining of the well, due to cells).
2. Calculate the 50% Tissue Culture Infectious Dose ($TCID_{50}$) using the Reed-Muench, Spearman-Kärber or Weil method. For example, the Reed-Muench formula is as follows, with I being the interpolated value of the 50% endpoint and h being the dilution factor:

$$I = \frac{(\%\ of\ wells\ infected\ at\ dilution\ above\ 50\% - 50\%)}{(\%\ of\ wells\ infected\ at\ dilution\ above\ 50\% - \%\ of\ wells\ infected\ at\ dilution\ below\ 50\%)}$$

$$50\%\ endpoint\ titer = 10^{\log total\ dilutions\ above\ 50\% - I * \log h}$$

3. Present your data in a graph (see Fig. 2B).

3.7.3 Data analysis of luciferase data

a. Normalize your measured luminescence of your target knockdown to that of your control: RLU target/RLU control
b. Present your data in a graph (see Fig 2C).

4 Notes

1. NucleoZOL® homogenate can be stored at -80 °C for up to a year for later use.
2. A blue pellet should be seen at the bottom. Sometimes, no pellet is visible, and the fluid looks bluish. In both cases, you can continue.
3. The RNA appears as a gel-like pellet at the bottom of the tube. White RNA can be seen as contamination. Sometimes, you don't see a pellet, but continue anyway.
4. Remove the supernatant carefully since the pellet is not as adherent anymore.
5. Drying of the pellet is not necessary and might even reduce solubility.
6. Leave the sample on ice for 20–60 min for efficient solubilization.
7. Calculate the primer annealing temperature according to the binding sequence.
8. To verify the amplified sequence, the PCR product should be sequenced afterwards.
9. To increase the amount of perfect dsRNA molecules, the in vitro transcript is heated up and cools down slowly before adding DNAse I and RNAseA.
10. Check your concentration of dsRNA prior to use! When handling RNA always keep RNA on ice!
11. Tube 2 can be prepared as a mastermix for all wells.
12. Pipette Dharmafect slowly to prevent shearing forces, which might destroy the Dharmafect micelles and reduce transfection efficiency.
13. Make sure to change the tips between each dsRNA-Mix and pipette directly into the liquid as to create as little droplets on the side of the tube as possible.
14. The cell shape and appearance might have changed due to the transfection. Clumped and/or detached cells are normal cell behaviour after transfection.
15. Replace the medium carefully, as you work with semi-adherent and transfected cells, which can be washed off easily. An additional flask with growth medium for infection is advised to prevent cross-contamination with viruses.
16. Depending on which antiviral protein was silenced, cells can show a severe reaction and detach and/or die.
17. You can use less RNA but you have to adjust the total amount of RNA in the other samples accordingly for comparing samples.
18. For viruses with a poly-A tail use oligo(dT) primers for other viruses' random hexamers.

19. For checking silencing efficiency, use oligo(dT) primers since the dsRNA can sometimes be detected in case of cDNA production with random hexamers.
20. When using random Hexamers, incubate 1 h at 37 °C and inactivate the MMLV by 10 min at 70 °C.
21. Primer pairs that are used to check knockdown efficiency should not overlap with the region of the gene that is targeted by the dsRNA.
22. Change tips for each time to ensure accurate dilutions.
23. Passive Lysis Buffer is provided as 5× buffer. Dilute first in ddH20.
24. You can store the lysed cells in Passive Lysis Buffer at -20 °C for 1 month.

Acknowledgements

This work is supported by the German Centre for Infection Research (DZIF; TTU 01.708, MA; ES) and the DFG (project number 497659464; MR and 500072465; PB).

References

1. Walsh E, Torres T Z B Rückert C (2022) Culex Mosquito Piwi4 Is Antiviral against Two Negative-Sense RNA Viruses. Viruses **14**(12).
2. Dietrich I, Shi X, McFarlane M, Watson M, Blomström AL, Skelton J K, Kohl A, Elliott R M, Schnettler E (2017) The Antiviral RNAi Response in Vector and Non-vector Cells against Orthobunyaviruses. PLoS Negl Trop Dis **11**(1): p. e0005272.
3. Blair C D, (2023) A Brief History of the Discovery of RNA-Mediated Antiviral Immune Defenses in Vector Mosquitos. Microbiol Mol Biol Rev **87**(1): p. e0019121.
4. Tikhe C V, Dimopoulos G (2021) Mosquito antiviral immune pathways. Dev Comp Immunol **116**: p. 103964.
5. Gestuveo R J, Parry R, Dickson L B, Lequime S, Sreenu V S, Arnold M J, Khromykh A A, Schnettler E, Lambrechts L, Varjak M, Kohl A (2022) Mutational analysis of Aedes aegypti Dicer 2 provides insights into the biogenesis of antiviral exogenous small interfering RNAs. PLoS Pathog **18**(1): p. e1010202.
6. Varjak M, Maringer K, Watson M, Sreenu V B, Fredericks A C, Pondeville E, Donald C L, Sterk J, Kean J, Vazeille M, Failloux AB, Kohl A, Schnettler E (2017) Aedes aegypti Piwi4 Is a Noncanonical PIWI Protein Involved in Antiviral Responses. mSphere **2**(3).
7. Lewis S H, Salmela H, Obbard D J (2016) Duplication and Diversification of Dipteran Argonaute Genes, and the Evolutionary Divergence of Piwi and Aubergine. Genome Biol Evol **8**(3): p. 507-18.
8. Leggewie M, Cherer C, Altinli A, Gestuveo R J, Sreenu V B, Fuss J, Vazeille M, Mousson L, Badusche M, Kohl A, Failloux AB, Schnettler E (2023) The Aedes aegypti RNA interference response against Zika virus in the context of co-infection with dengue and chikungunya viruses. PLoS Negl Trop Dis **17**(7): p. e0011456.

Chapter 4: Publication 3

Supplements for Publication 1 can be found in the online version under:
J Gen Virol. 2024 Nov;105(11):002046. doi: 10.1099/jgv.0.002046. PMID: 39508739; PMCID: PMC11542633.

Dicer 2 mutations in *Aedes aegypti* cells lead to a diminished antiviral function against Rift Valley Fever virus and Bunyamwera virus infection

Susann Dornbusch[1,4#], **Melinda Reuter**[2#], Rhys H. Parry[3], Michael Stern[4], Stefanie C. Becker[1], Esther Schnettler[2,5,6]

[1]Institute for Parasitology and Research Center for Emerging Infections and Zoonoses, University of Veterinary Medicine Hannover, Hannover, Germany
[2]Bernhard-Nocht-Institute for Tropical Medicine, Hamburg, Germany
[3]School of Chemistry and Molecular Biosciences, The University of Queensland, St. Lucia, Australia
[4]Institute for Physiology and Cell Biology, University of Veterinary Medicine Hannover, Hannover, Germany
[5]Faculty of Mathematics, Informatics and Natural Sciences, University Hamburg, Hamburg, Germany
[6]German Center for Infection Research (DZIF), partner side HH-HL-Bo-Ri, Hamburg, Germany

[#]These authors contributed equally to this manuscript.
Correspondence: schnettler@bnitm.de and stefanie.becker@tiho-hannover.de

Keywords: RNA interference; Dicer-2; BUNV; RVFV; mosquito

Repositories: The RNA sequencing data generated for this study are available at the NCBI Sequence Read Archive under BioProject ID: PRJNA1120211. Bash scripts utilized for the small RNA analysis can be found in the viral_sRNA_tools GitHub repository at the following URL: https://github.com/rhparry/viral_sRNA_toolsAbstract

Abstract

Mosquitoes are known to transmit different arthropod-borne (arbo-) viruses belonging to various virus families. The exogenous small-interfering RNA (exo-siRNA) pathway plays an important role in the mosquito defence against such virus infections, with Dicer-2 (Dcr2) as one of the key proteins that initiates the cleavage of viral double-stranded (ds)RNAs into 21 nucleotide (nt) long virus-derived small interfering RNAs (vsiRNAs). Previous data identified the importance of various motifs in Dcr2 for its siRNA-mediated antiviral activity. However, all this data focuses on positive-strand RNA viruses, although negative-strand RNA viruses, like *Bunyaviricetes*, include several important mosquito-borne viruses. Although the antiviral activity of the siRNA pathway and its key proteins (Dcr2 and Argonaute-2) have previously been reported, a lot of information is still lacking. Here, we used the *Ae. aegypti*-derived Dcr2 knock-out (KO) cell line Aag2-AF319 to study the importance of the helicase, RNase III, and PIWI-Argonaute-Zwille (PAZ) domains of Dcr2 on the antiviral activity of two viruses belonging to different families of the *Bunyaviricetes*: the Rift Valley Fever virus vaccine strain MP12 (RVFV; *Phenuiviridae*, *Phlebovirus,*) and the Bunyamwera orthobunyavirus (BUNV; *Peribunyaviridae*, *Orthobunyavirus*). All three domains were determined to be critical for the antiviral activity against both RVFV and BUNV. Interestingly, one specific mutation in the helicase domain (KN) did not result in a loss of antiviral activity for RVFV, but for BUNV, despite losing the ability to produce 21 nt siRNAs.

Introduction

As the world currently faces an emerging threat of arthropod-borne (arbo-) virus infections, it becomes increasingly important to understand and assess every part of the arboviral life cycle, transmission, and antiviral responses in the vertebrate host and invertebrate vector. Mosquitoes transmit various arboviruses belonging to different virus families, with dengue virus (DENV; *Flaviviridae, Orthoflavivirus*), Chikungunya virus (CHIKV; *Togaviridae, Alphavirus*) and Rift valley fever virus (RVFV; *Phenuiviridae, Phlebovirus)*, only naming a few [1], [2], [3], [4], [5], [6], [7], [8].

Mosquitoes actively fight arbovirus infection using various immune responses. These include the RNA interference (RNAi) response with the exogenous small interfering RNA (exo-siRNA) pathway known as a major antiviral response in mosquitoes. This pathway is initiated by recognition of long viral double-stranded (ds)RNA molecules as a pathogen-associated molecular pattern [9], [10]. Subsequently, these dsRNAs are cleaved into 21 nucleotide (nt) long viral small interfering RNAs (vsiRNAs), facilitated by the RNase III endoribonuclease: Dicer-2 (Dcr2) [11]. The vsiRNAs are loaded onto Argonaute-2 (Ago2), which is part of the siRNA-induced silencing complex (siRISC). Ago2 unwinds the vsiRNAs and retains one strand for recognition and subsequent degradation and silencing of complementary viral RNAs [12].
The importance of Dcr2 has been illustrated by Dcr2 knock-out (KO) *Aedes aegypti* (*Ae. aegypti*) mosquitoes and Dcr2 KO *Ae. aegypti*-derived cell lines. In Dcr2 KO mosquitoes, some arbovirus infections (DENV, CHIKV, Zika virus, Mayaro virus) resulted in exacerbated viral replication in the early stages of infection and heightened systemic viral dissemination while the vector competence of the mutant mosquitoes was found to be comparable to wild-type (WT) mosquitoes [13]. In other studies, Dcr2 KO *Ae. aegypti* mosquitoes showed a higher pathogenesis/mortality to Sindbis virus (SINV) and Yellow fever virus infection (YFV) [14]. Along these lines, increased virus infection/replication was observed for various arboviruses of different families in *Ae. aegypti*-derived Dcr2 KO cells, including members of the

Bunyaviricetes [15], [16], [17], [18]. These results highlight the importance of the Dcr2 protein in the antiviral response in mosquitoes as well as its effect on vector competence and capacity. However, most knowledge about the interaction of the RNAi response and arboviruses has been investigated for positive-strand RNA viruses; whereas relatively little is known about RNAi in the context of infections caused by negative single-stranded ((-ss))RNA viruses [19], [20]. Sequence analysis of Dcr2 in *Ae. aegypti* identified several domains, which are mostly conserved between Dcr2 of different organisms; supporting their importance. The N-terminal helicase domain is highly conserved among all Dicer proteins with a high sequence similarity to the helicase superfamily SF2, with its main function being the binding of blunt-end dsRNA [21], [22], [23], [24]. Following the helicase domain is a domain of unknown function (DUF283). While the role of DUF283 in the (exo-) siRNA pathway remains unknown, it shows high structural similarity to typical dsRNA binding domains (dsRBDs) found in eukaryotic, prokaryotic, and viral proteins [25]. C-terminal of the DUF are the PIWI-Argonaute-Zwille (PAZ) and the two RNase III domains, RNase IIIA and RNase IIIB, which together are considered to be the functional core of Dcr2. The PAZ domain is responsible for binding of 3ˈ overhanging dsRNA [26], while the RNase III domains are required to process the dsRNA into typically 21 nt siRNA and binding to Ago2 [27], [28]. The C-terminus of Dcr2 contains a dsRBD that directly contributes to binding the substrate dsRNAs, facilitating efficient siRNA production, and enabling their loading into Ago2 [29], [30].

Until now, only a handful of experiments have been performed to investigate the hypothesized function of the different domains of *Ae. aegypti* Dcr2 or determine their importance for the antiviral activity of Dcr2. Mutational analysis, followed by infection with Semliki Forest alphavirus (SFV), has shown that the helicase, RNase III and PAZ domains are important for the siRNA-based antiviral activity of Dcr2 in *Ae. aegypti*-derived cells as well as the vsiRNA production. For this, multiple sequence alignment was used to identify highly conserved amino acids within these domains, leading to the production of multiple different Dcr2 mutants, some of which were used within this study, namely K39N (abbreviated to KN), G488R (abbreviated to GR), mtR3, M1 and M3. While the helicase mutants KN and GR only possess one eponymous mutation each, the RNase III mutant mtR3 (D1198A, E1341A, D1444A, E1548A) and the two PAZ mutants M1 (V880A, V883A, Y909A, V923A) and M3 (D829A, N872A, V880A, V883A, Y909A, V923A, L930A) have multiple different mutations. All mentioned mutants exhibited a significant decrease in antiviral and reporter-based silencing activity, as well as an impaired 21 nt vsiRNA production after SFV infection [31], [32].

Arboviruses of the order *Elliovirales* and *Hareavirales* account for a high proportion of medically and livestock-important mosquito-borne viruses. However, in comparison to orthoflaviviruses and alphaviruses, little is known about their interaction with the antiviral RNAi response in mosquitoes. Orthobunya- and phlebovirus-specific small RNAs have been reported in infected mosquitoes and derived cell lines. In addition, the antiviral activity of some key RNAi proteins, e.g. Dcr2, for a small selection of *Bunyaviricetes* were shown. However, nothing is known about the importance of the different Dcr2 domains regarding their antiviral activity against representative viruses of the *Bunyaviricetes*, like RVFV and Bunyamwera orthobunyavirus (BUNV; *Peribunyaviridae*, *Orthobunyavirus*) [18], [33], [34], [35]. This might also be attributed to the fact that negative-strand RNA viruses and especially members of the *Elliovirales* and *Phleboviruses* produce much less dsRNA during replication than positive-strand RNA viruses, thus dsRNA-triggered RNAi might play a lesser role in antiviral defence [20].

RVFV and BUNV both share a similar genomic organisation, consisting of a tri-segmented (-ss)RNA genome with different segment sizes. The L segment (RVFV: 6,4 kb; BUNV: 6,9 kb) encodes for the RNA-dependent-RNA-polymerase (RdRp) needed for replication and transcription of the virus genome [36], [37]. The M segment (RVFV: 3,8 kb; BUNV: 4,4 kb) contains sequences for the structural glycoproteins Gn and Gc, enabling virus particle entry into host cells and, in case of RVFV, sequences for a non-structural NSm-protein and a 78 kDa accessory protein. The coding strategy of the S segment (RVFV: 1,7 kb, BUNV: 0,9 kb) differs between BUNV and RVFV, with the latter using an ambisense coding strategy via a hairpin structure instead of a negative-strand coding strategy as in BUNV. For both viruses, the S segment encodes for a non-structural NSs-protein (known to counteract the host immune responses) [38], [39] and a nucleocapsid protein (N). The latter is responsible for the encapsidation of viral RNA genome into ribonucleoprotein complexes (RNPs) [40], [41], [42], [43], [44], [45], [46], [47].

In this study, we investigated the antiviral activity against RVFV MP12 (abbreviated to RVFV) and BUNV in a Dcr2 deficient *Ae. aegypti*-derived cell background for previously identified non-functional Dcr2 mutants: PAZ (M1, M3), helicase (KN, GR) or RNase III (mtR3) domain (Fig. 1A). Except for the helicase mutant, KN, with RVFV all mutants showed an antiviral activity similar to the negative control. Surprisingly, small RNA sequencing supported the inability of KN to produce 21 nt RVFV specific small RNAs, similar to GR.

Materials and methods

Cells

In this study, we used the Aag2-AF319 (ECACC 19022602; Public Health England) cells, which contain a Dcr2 KO mutation and were derived from Aag2-AF5 (ECACC 19022601, Public Health England) embryonic cells [48]. For Aag2-AF319 cell maintenance, Leibovitz's L-15 medium (Gibco ThermoFisher Scientific Inc., Waltham, MA, USA) was supplemented with 10% fetal bovine serum (FBS; Gibco Capricorn Scientific GmbH, Ebsdorfergrund, Germany), 10% tryptose phosphate broth (TBP; Gibco Thermo Fisher Scientific Inc., Waltham, MA, USA) and penicillin-streptomycin (pen-strep; 100 U/mL-100 µg/mL; PAN BIOTECH, Aidenbach, Germany). The cells were grown at 28°C without $_{CO2}$, and passaged twice a week.

Viruses

BUNV (accession numbers: NC_001927.1; NC_001926.1; NC_001925.1) was produced in BHK-21 cells and the titer was determined by plaque assays as previously described for Schmallenberg virus (SBV) (Varela et al. 2013; https://pubmed.ncbi.nlm.nih.gov/23326235/). RVFV MP12 (abbreviated to RVFV; provided by Prof. Elliot, CVR, UK) was amplified in BHK-21 cells with an MOI of 0.01. On day three, virus was harvested via PEG precipitation and the titer (2.9 x 10^8 PFU/mL) was determined via the TCID50 method. The viruses were stored at -80°C.

Plasmids

For Aag2-AF319 KO cell line transfection experiments, previously described expression plasmids pPUb-myc-Dcr2 WT and pPUb-myc-eGFP or pPUb-plasmids expressing mutant Dcr2 (KN, GR, M1, M3, mtR3) were used [31], [32].

Assessment of antiviral activity of mutant Dcr2 via qPCR and statistical analysis

For determination of the antiviral activity of the mutant Dcr2 against BUNV and RVFV, 2 x 10^5 Aag2-AF319 cells/well were seeded in 24-well plates. After the cells were allowed to settle for at least 4 h, cells were transfected with 500 ng expression plasmids: WT Dcr2, mutant Dcr2s, or eGFP (as control) and 1 µL DharmaFECT2 (Horizon Discovery LtD, Cambridge, UK). At 24 hours post transfection (hpt), the cells were infected with either BUNV or RVFV (MOI 0.1) for 2 h at 28°C, followed by replacement with fresh complete media. For total RNA extraction, the cells were lysed using TRIzol (ThermoFisher Scientific Inc., Waltham, MA, USA; BUNV) or QIAzol (Qiagen, Hilden, Germany; RVFV) at 72 hours post infection (hpi), according to the manufacturer's protocol. 1 µL RVFV-specific RNA of the L segment or S7 ribosomal RNA (as housekeeper) was detected via Luna Universal Probe One-Step RT-qPCR Kit from New England Biolabs GmbH (Frankfurt am Main, Germany) according to the manufacturer`s instructions via the AriaMx Real-time PCR system (Agilent Technologies, Santa Clara, CA, USA). Previously described primers [33] were used. For BUNV detection, 1.5 µg total RNA was first reverse-transcribed with MML-V (Promega Corporation, Madison, WI, USA) and random hexamers, according to the manufacturer's protocol. To quantify BUNV and S7 ribosomal RNA (as housekeeper), 1 µL cDNA was used together with the QuantiTect SYBR Green PCR Kit (Qiagen, Hilden, Germany) and the LightCycler480 System (Roche Diagnostics, Mannheim, Germany). For primers see Table S1. To ensure effective control of Dcr2 protein expression, western blot analysis was conducted with the results presented in Figure S1. For statistical analysis of the RT-qPCR RVFV results, the Agilent Aria Software v1.71 was used, while LightCycler480 was used for two-step qPCR results of BUNV and RVFV. The fold gene expression (2^-(ΔΔCt); RQ) was calculated using S7 ribosomal RNA as housekeeper and eGFP transfected cells as control. The results were plotted and statistically tested using GraphPad Prism 10 (GraphPad Software, Boston, MA, USA).

Small RNA sequencing and analysis

For small RNA sequencing, 2.5 x 10^5 Aag2-AF319 cells/well were seeded in four wells of a 24-well plate and transfected with either 500 ng pPUb-myc-Dcr2 WT, pPUb-myc-Dcr2 KN, pPUb-myc-Dcr2 GR, or pPUb-myc-eGFP (control) together with 1 µL DharmaFECT 2 (Horizon Discovery LtD, Cambridge, UK), followed by infection with RVFV MOI 1, 24 hpt. For total RNA isolation, four wells per construct were combined using 1 mL TRIzol (ThermoFisher Scientific Inc., Waltham, MA, USA) and glycogen as carrier; following the manufacturer's protocol. Small RNA sequencing was performed at BMKGene (Münster, Germany) on an Illumina Novaseq SP (Illumina, San Diego, CA, USA) with SE50 and 10 M clean reads/sample. A minimum of 1.5 µg total RNA was sent per sample to BMKGene for the library preparation with the VAHTS Small RNA Library Prep Kit for Illumina (Vazymebiotech, Nanjing, China) according to the manufacturer's protocol. Small RNA sequencing data can be accessed at the NCBI Sequence Read Archive under BioProject ID: PRJNA1120211. Basecalled fastq files were quality and

adapter trimmed using the fastp tool (v0.23.2) [49] retaining 16-30 nt reads under default conditions. The clean, trimmed reads were then mapped to the RVFV genome (GenBank ID: L segment DQ375404.1, M segment DQ380208.1, S segment DQ380154.1) using Bowtie2 (v2.4.5) [50] with the sensitive mapping flag (—sensitive). Trimming and mapping statistics summary is available in S2 Table. The histogram of mapped read lengths and first base pair bias was generated using viral_sRNA_tools/3_bam_sRNA_histogram.sh script, which utilises samtools (v1.16.1). Overlapping pairs probabilities (z-score) for of 25-30 nt reads were calculated using the small RNA signatures Python script signature.py [51], with the following conditions (--minquery 25 --maxquery 31 --mintarget 25 --maxtarget 30 --minscope 1 --maxscope 20). Biases in extracted piRNAs for both the genome and antigenome strand were visualised using WebLogo3 [52]. Output BAM files from Bowtie2 were filtered to include only the 21 nt reads for the vsiRNA mapping. Coverage statistics for each position of the RVFV genome were extracted using bedtools genome coverage tool (v.2.27.1) [53] and visualized using GraphPad Prism (v10.0.2).

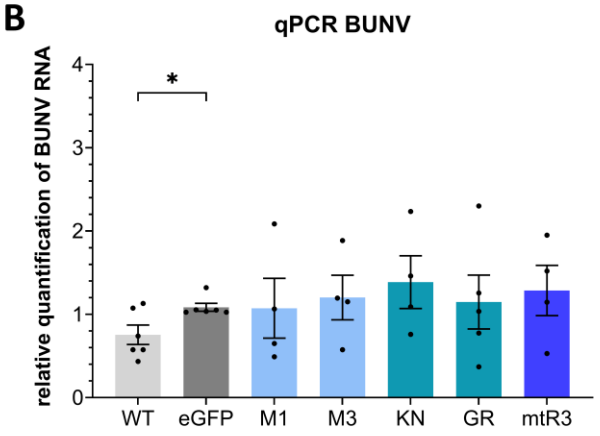
Results

Analysis of the antiviral activity of mutant Dcr2 against RVFV and BUNV

A

Dcr2 mutant (domain)	**Dcr2 mutations** *Ae. aegypti*
M1 (PAZ)	V880A V883A Y909A V923A
M3 (PAZ)	D829A N872A V880A V883A Y909A V923A L930A
KN (Helicase)	K39N
GR (Helicase)	G488R
mtR3 (RNase III)	D1198A E1341A D1444A E1548A

B



C

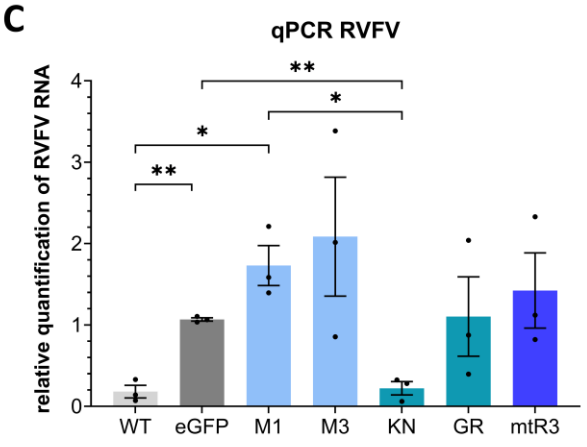


Fig. 1. Antiviral activity of different mutant *Ae. aegypti* Dcr2 against RVFV and BUNV. (A) Table of Dcr2 mutants with corresponding mutations and their domain location. **(B)** Effect of mutant Dcr2 on BUNV and **(C)** RVFV viral RNA. Aag2-AF319 cells were transfected with pPUb-plasmids expressing WT or mutant Dcr2s, with pPUb-myc-eGFP as control. Cells were infected at 24 hpt with BUNV or RVFV (both MOI 0.1), respectively. At 72 hpi, total RNA was isolated and analysed using qRT-PCR. Relative quantification (RQ) was calculated using S7 ribosomal RNA as a housekeeper gene for qRT-PCR and eGFP as control. The results are shown in as standard error of the mean of at least 3 independent biological replicates. The dots represent different biological replicates, consisting of two technical replicates each with * = $p<0.05$, ** = $p<0.01$ as according to Student's t test.

Cells transfected with WT Dcr2 showed reduced viral RNA for both BUNV ($p=0.0266$) and RVFV ($p=0.0051$) (p-values see Table S3), compared to control cells (eGFP). In contrast, transfection of most of the Dcr2 mutants (KN, GR, M1, M3, and mtR3) did not result in a statistically significant difference from the eGFP control. Surprisingly, RVFV RNA was significantly reduced in cells transfected with the KN helicase mutant, compared to the eGFP transfected negative controls ($p=0.0066$). KN exhibited a ~79% decrease in viral RNA, whereas GR, the second helicase mutant, showed similar levels of RVFV RNA than the eGFP control. Besides, for BUNV, no viral RNA reduction was observed in cells transfected with the KN mutant. With the exception of KN for RVFV, all other mutants, show RVFV RNA levels comparable to the eGFP-transfected control. Quantification of infectious virus particles in the supernatant of the transfected and infected cells, showed comparable results than observed for the viral RNA (Fig. S2).

Production of RVFV specific 21 nt vsiRNAs in KN transfected Dcr2 knock-out cells

It has been previously reported that in case of SFV (*Togaviridae, Alphavirus*) infection, the mutants lost their ability to either produce vsiRNAs at all (for helicase and RNase III mutants) or the size of vsiRNAs were broadened from 21 nt to 18-23 nt in case of the PAZ domain mutants. This depletion or broadening in length of produced vsiRNAs by the different mutants (KN, GR, M1, M3, mtR3) lead to a loss or at least significant decrease in their antiviral activity against SFV as well as in dsRNA-based reporter assays. As the KN helicase mutant is still able to significantly reduce the RVFV infection, it was hypothesized that KN might be able to generate RVFV specific 21 nt siRNAs in contrast to the "non-functional" GR mutant. Therefore, small RNA sequencing was performed from Aag2-AF319 cells transfected with Dcr2 (KN and GR) expression constructs, followed by RVFV infection (MOI 1). As positive or negative control, WT Dcr2 or eGFP expression constructs were included. Total RNA was isolated at 48 hpi and small RNA sequencing was performed. Size distribution of all sequenced small RNA reads indicated a similar distribution of small RNA reads corresponding to siRNAs or micro (mi) RNAs (21-22 nt) and PIWI-interacting (pi) RNAs (24-30 nt) for all treatments (Fig. S3).

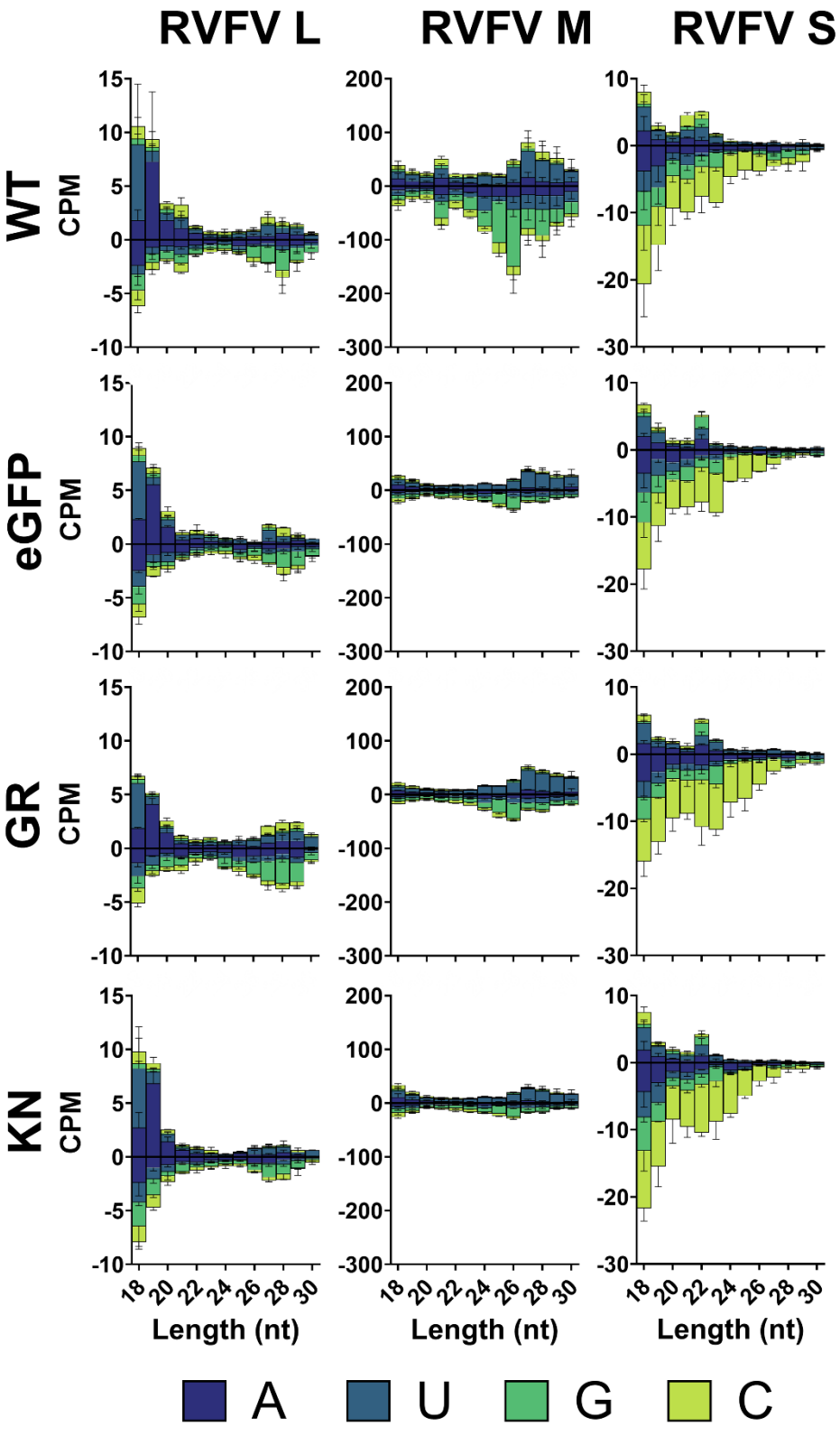


Fig. 2. Mutations in Dcr2 in Aaeg-AF319 cells reduce the vsiRNA production against RVFV M segment. Small RNA sequencing of Aag2-AF319 cells transiently expressing WT Dcr2, eGFP, Dcr2 KN and Dcr2 GR mutations and infected with RVFV (MOI 1) at 48 hpi. Histogram of small RNA reads 18-30 nt in length, mapped to the RVFV antigenome (positive) and genome (negative) with colours indicating first base nucleotide prevalence for each read length, shown as counts per million (CPM) from two independent experiments +/- SD.

Bioinformatic analysis of small RNA libraries revealed the presence of viral derived small RNAs mapping to all three segments of the RVFV genome and antigenome for all treatments (Fig. 2). Overall, a greater number of small RNAs mapping to the M segment than the S and L segment were detected (Table S2) for all conditions. Only the WT Dcr2 treatment showed an induction of vsiRNAs of 21 nt, again with amounts changing from M>S>L segment with the eGFP, KN and GR mutants lacking a 21 nt peak for any genome segment of RVFV associated with vsiRNAs. For the cells expressing WT Dcr2, the 21 nt vsiRNAs map along the whole M and the L segments from the genome and antigenome. Interestingly, in case of the S segment, most 21 nt vsiRNAs map to one region (~900 nt) at the genome, corresponding with the stem loop sequence in the S segment of RVFV (Fig. 3).

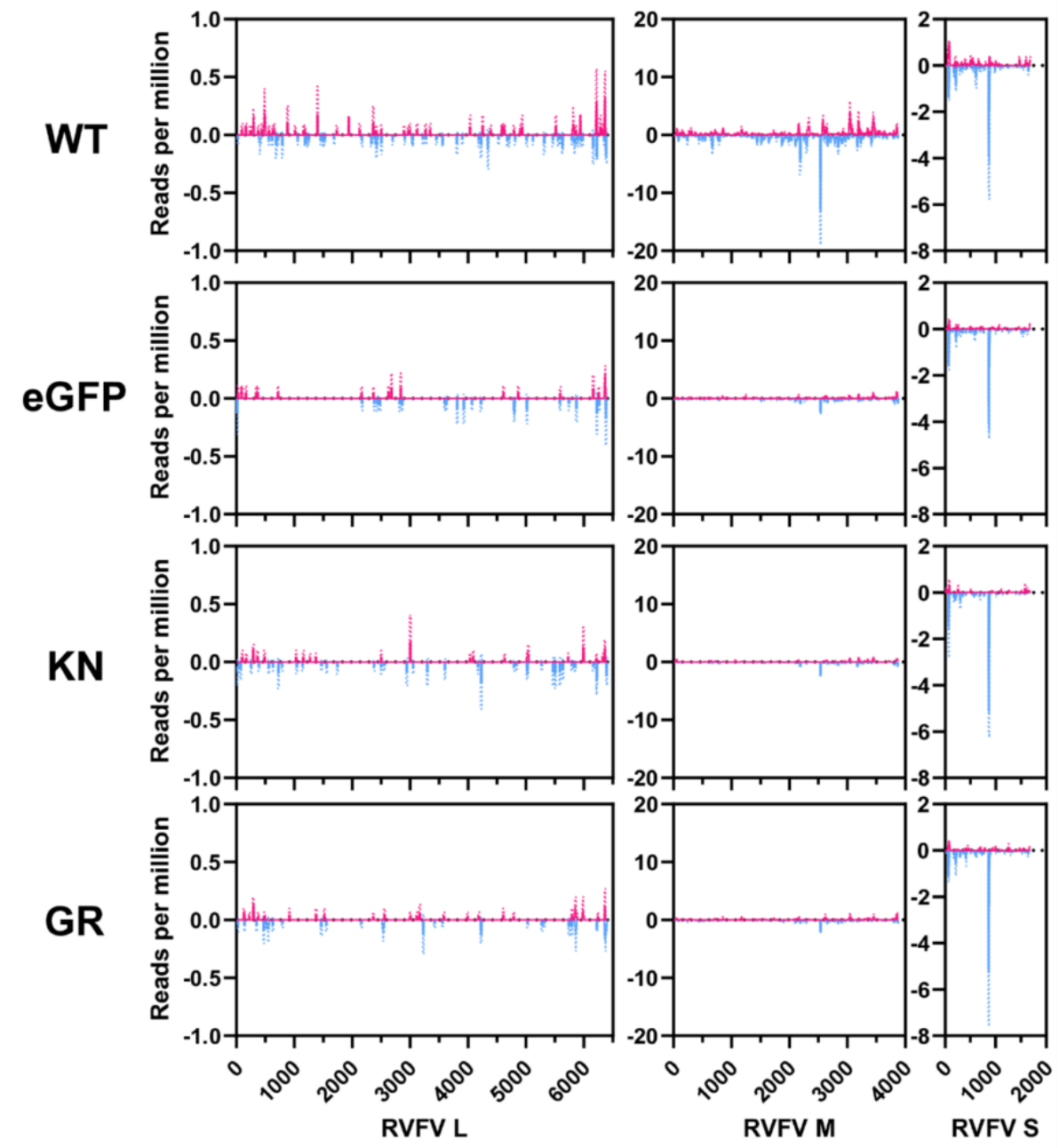


Fig. 3. Differences in the mapping of 21 nt vsiRNAs in KN and GR Dcr2 mutants in RVFV infection. Coverage of RVFV-derived 21 nt vsiRNAs over the antigenome (magenta) or genome (cyan) (Y axis, vsiRNA reads per million) for the L, M and S segments of RVFV from two independent experiments +/- SD.

For cells expressing the eGFP or the helicase mutants, a high amount of RNAs with a length of 22 nt were found for the S segment (Fig. 2). Such vsRNAs were also observed in the cells with WT Dcr2; however, to a lower amount. None of the RNAs between 20-23 nt showed a bias in their first base. In WT transfected cells, in addition to the 21 nt vsiRNAs, longer small RNAs were detected in the length of 24-30 nt, especially for the M segment. Interestingly, a reduction of these RNAs can be observed in eGFP, KN and GR mutants. Small RNAs with a length of 25 and 26 nt mapping to the M segment in the WT Dcr2 expressing cells mostly are derived from the genomic strand (Fig. 2, S4). In cells expressing WT Dcr2, the 25-30 nts sRNAs mapping to the L and M segment, show the ping-pong-produced viral piRNA (vpiRNAs) characteristics: overlap of 10 nts between sense and antisense small RNAs and U_1 and A_{10} bias. For all other treatments an enriched z-score in overlapping sense and antisense small RNAs of 10 nt (Fig. 4) for the M segment as well as a U_1 bias for the genomic sRNAs for the L and M segments are present (Fig. S5). However, in all treatments there was insufficient vpiRNAs generated against the S segment, to observe these biases.

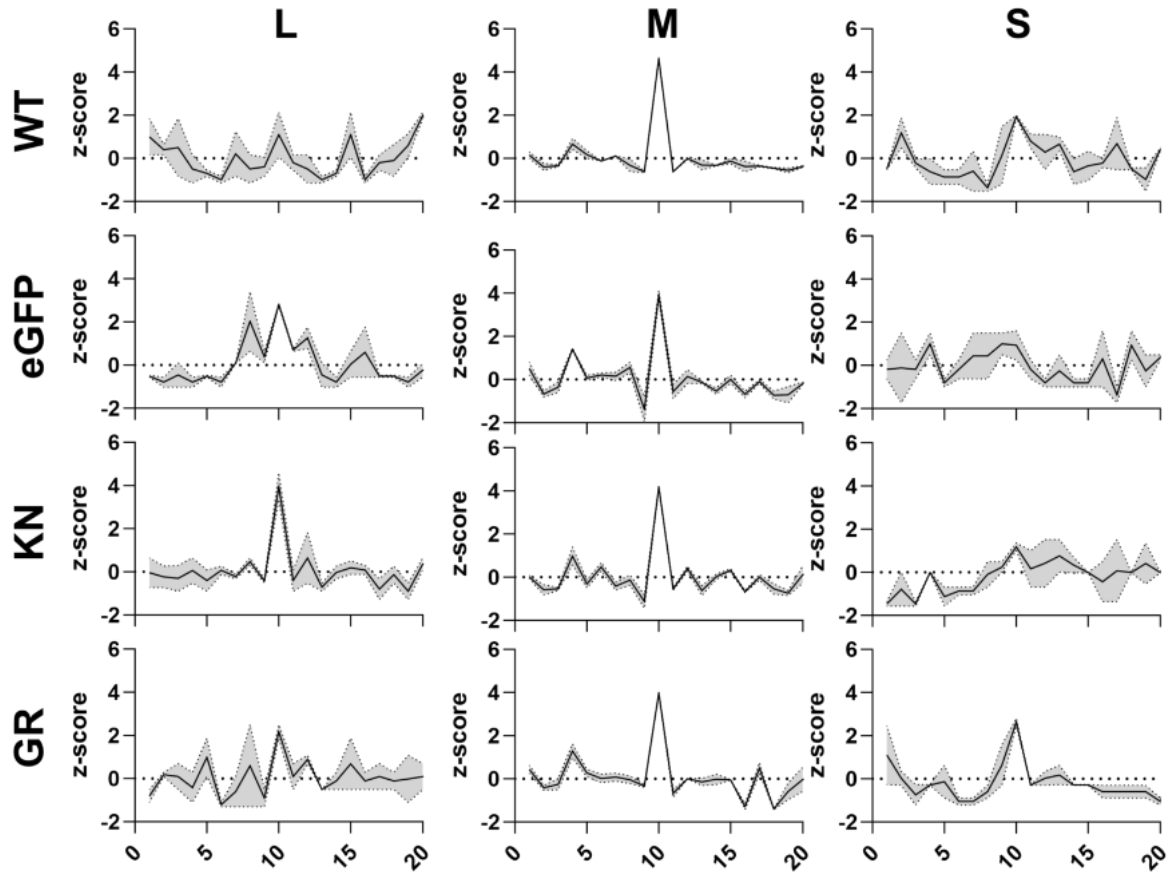


Fig. 4. Limited differences in viral piRNA generation of Aag2-AF319 cells with Dcr2 WT, KN and GR mutants and eGFP control during RVFV infection. Probability of overlapping pairs z-scores of 25-30 nt virus-derived small RNAs. Mean of *n*=2 independent repeats is presented with the grey region indicating the range.

Mapping of these 25-30 nt “vpiRNAs” along the genome and antigenome revealed no difference between the treatments, with the L segment targeted mostly at the 5’ and 3’ ends and the S segment derived 25-30 nt mapping mostly to one region (~900 nt) at the genome, as already observed for the 21 nt vsiRNAs (Fig. S4).

Discussion

Dcr2 is known as key protein in the antiviral exo-siRNA pathway in *Ae. aegypti* for various viruses. It binds long dsRNA, cleaves it into 21 nt long siRNAs and loads them onto another key protein: Ago2. To perform these different tasks, Dcr2 has various domains, including the helicase, PAZ and RNase III domains. Previous experiments have shown the importance of these domains for the antiviral activity against SFV (a positive strand RNA virus) and linked it to the ability of Dcr2 to produce specifically 21 nt long vsiRNA molecules [28], [29]. As positive strand RNA-viruses produce higher levels of dsRNA during replication than negative-strand RNA viruses like BUNV and RVFV, dsRNA-triggered RNAi might play a lesser role in their antiviral defence [20].

Aag2-AF319 (Dcr2 KO) cells transfected with Dcr2 helicase (GR, KN), PAZ (M1, M3) and RNase III (mtR3) mutants were unable to decrease the BUNV infection in contrast to WT Dcr2; supporting a loss in antiviral activity of these mutants. Although similar results were observed for RVFV for most tested mutants, the helicase KN mutant still significantly reduced RVFV infection, comparable to WT Dcr2. The used RVFV MP12 vaccine strain is known to be attenuated in mammals; however, no attenuation has been reported in mosquitoes so far [57]. Therefore, it is expected that the observed results, especially for the KN mutant, would be the same with other RVFV strains, but additional experiments are needed to verify this. With the exception of the helicase KN mutant in combination with RVFV, these results are in line with previously published data of SFV [28]. This leads to the conclusion that all three domains are critical for the overall antiviral defense against positive and negative strand RNA arboviruses. The lower effect of WT Dcr2 on BUNV RNA and infectious virus particles, compared to RVFV, suggests a lower sensitivity of BUNV to the antiviral activity of Dcr2. However, this could also be due to differences in the experimental set up of RVFV versus BUNV.

Based on the strong differences in RVFV infection in KN and GR transfected cells, we hypothesized that the KN mutant is still able to produce 21 nt vsiRNAs after RVFV infection. However, small RNA analysis of KN expressing cells infected with RVFV showed no 21 nt vsiRNA peak for any segment (Fig. 2). In contrast, the positive control expressing WT Dcr2 resulted in 21 nt vsiRNAs production for all three segments, with the highest amount mapping to the M segment which is consistent with previous observation of RVFV infected Aag2 cells [30] and in line with the observed antiviral activity of WT Dcr2 against RVFV. The K39N (KN) mutation in *Ae. aegypti* Dcr2 is the homologous mutation of K34N in *Drosophila melanogaster* Dcr2 and is located in the helicase domain. More specifically, it has been shown that this amino acid is essential for the ATP binding in *D. melanogaster* Dcr2 and the K34N mutant is known as ATPase defective. The main function of the Dcr2 helicase domain is binding of blunt-end dsRNA, which is ATP dependent. In the absence of ATP or in case of the ATPase defective mutant, blunt end dsRNA cannot efficiently be bound but instead 3ˈend overhang dsRNA is bound and cut into 22 nt instead of 21 nt siRNAs [23], [24]. Interestingly, a peak of 22 nt RVFV specific small RNAs for the S segment were detected in cells expressing the KN mutant. However, the same peak of 22 nt viral (v) RNAs was also present in the other helicase mutant,

GR, as well as the negative control lacking Dcr2 expression at all. Even cells expressing WT Dcr2 showed the production of RVFV specific 22 nt vRNAs for the S segment, although the amount was similar to the 21 nt vsiRNA peak. Such production of 22 nt vRNAs for the helicase mutants or the negative control lacking Dcr2 have not been observed for SFV infected cells [28], supporting a RVFV specific observation (independent of Dcr2) although other viruses would need to be tested for a final conclusion.

The two open reading frames of the RVFV S segment are separated by a stem loop structure, which was previously shown to be a main producer of 21 nt vsiRNAs [30]. Similar targeting of the stem loop structure (especially from the genome) and production of 21 vsiRNAs have been observed in *Ae. aegypti* Dcr2 KO cells, independent of expressed Dcr2 proteins (none, WT or helicase mutants) (Fig. 3). As opposed to the exo-siRNA pathway, which relies on viral RNA as the source dsRNA, the endogenous (endo-)siRNA pathway uses either sense-antisense dsRNA formed by transposon sequences or stem loop RNA transcripts [53]. The miRNA pathway utilizes primary (pri-)miRNAs, which are mostly transcribed as ssRNAs possessing hairpin structures and processed into precursor (pre-)miRNA duplexes before being taken up and cut by Dicer-1 (Dcr1) into 22-23 nt mature miRNAs [54], [55]. In both the endo-siRNA pathway and the miRNA pathway, hairpin RNA is efficiently recognized and cleaved by either Dcr2 or Dcr1; resulting in the production of 21 nt siRNAs and 22-23 nt miRNAs; respectively [53], [54], [55]. Therefore, the presence of 22 nt RVFV specific RNAs in all treatments regardless of the presence of Dcr2 might suggest the involvement of Dcr1. It is unknown whether these 22 nt vRNAs are biologically functional, nor why the KN mutant retains antiviral activity in contrast to GR despite showing no significant differences in vRNA production. Further studies are needed to understand this in detail.

Ping-pong produced sense and antisense vpiRNAs, typically exhibit a 10 nt overlap with a U1 bias in the antisense and a A10 bias in the sense strand [15], [28], [50], [56]. A notable increase in vRNA production of 25-30 nt length, with ping-pong produced vpiRNA characteristics, (Fig. 4) predominantly for the M segment, is observed in the presence of functional Dcr2; suggesting that Dcr2 and/or the vsiRNAs produced by Dcr2 are somehow linked to vpiRNA production. However, more research is needed to fully understand the extent of this involvement.

In summary, these results support the previous observations reported for the positive strand RNA virus, SFV, and extend the importance of the different domains in Dcr2 to both positive and negative strand RNA viruses of the *Bunyaviricetes*. Furthermore, it highlights important characteristics in the interaction of the antiviral exo-siRNA pathway and RVFV. Nonetheless, more research is needed to understand the exo-siRNA pathway and the specific functions of the Dcr2 domains in detail. This study focuses on the effects of mutant Dcr2 on RVFV and BUNV in mosquito-derived cells. Although previous research has shown that results observed in *Ae. aegypti*-derived cells are the same or at least similar in mosquitoes, further research is needed to determine this for the Dcr2 mutants.

Conflict of interest

The authors declare no conflict of interest.

Acknowledgements

We thank Dr. Kevin Maringer (Pirbright Institute, UK) for the Aag2-AF5 and Aag2-AF319 cells and Prof. Alain Kohl (Liverpool School of Tropical Medicine, UK) for providing us with the Dcr2 WT, mutants and eGFP expression constructs. We also want to thank Stella Bergmann for constructive feedback on practical procedures and Prof. Elliot (University of Glasgow, Centre for Virus Research, UK) for providing RVFV MP12.

Funding

This research was supported by the Deutsche Forschungsgemeinschaft (DFG; project number 497659464; MR) and (DFG; project number BE 5748/1-2 in collaboration with STE 1428/5-2; SD). S.D. was also supported by the DFG -398066876/GRK 2485/1.

Author contributions

Conceptualization: Esther Schnettler and Stefanie C. Becker; methodology: Susann Dornbusch and Melinda Reuter; experimental work: Susann Dornbusch and Melinda Reuter; visualization: Susann Dornbusch, Melinda Reuter, Rhys H. Parry; original draft preparation: Susann Dornbusch and Melinda Reuter; resources, review and editing: Esther Schnettler, Stefanie C. Becker and Michael Stern; supervision and project administration: Esther Schnettler, Stefanie C. Becker and Michael Stern; funding acquisition: Esther Schnettler and Stefanie C. Becker. All authors have read and agreed to the published version of the manuscript.

References

[1] O. J. Brady and S. I. Hay, 'The Global Expansion of Dengue: How Aedes aegypti Mosquitoes Enabled the First Pandemic Arbovirus', *Annual Review of Entomology*, vol. 65, no. 1, pp. 191–208, 2020, doi: 10.1146/annurev-ento-011019-024918.

[2] F. D. Carvalho and L. A. Moreira, 'Why is Aedes aegypti Linnaeus so Successful as a Species?', *Neotrop Entomol*, vol. 46, no. 3, pp. 243–255, Jun. 2017, doi: 10.1007/s13744-017-0520-4.

[3] S. B. Halstead, 'Travelling arboviruses: A historical perspective', *Travel Medicine and Infectious Disease*, vol. 31, p. 101471, Sep. 2019, doi: 10.1016/j.tmaid.2019.101471.

[4] S. C. Weaver, C. Charlier, N. Vasilakis, and M. Lecuit, 'Zika, Chikungunya, and Other Emerging Vector-Borne Viral Diseases', *Annual Review of Medicine*, vol. 69, no. 1, pp. 395–408, 2018, doi: 10.1146/annurev-med-050715-105122.

[5] S. C. Weaver and W. K. Reisen, 'Present and future arboviral threats', *Antiviral Research*, vol. 85, no. 2, pp. 328–345, Feb. 2010, doi: 10.1016/j.antiviral.2009.10.008.

[6] T. C. Pierson and M. S. Diamond, 'The continued threat of emerging flaviviruses', *Nat Microbiol*, vol. 5, no. 6, Art. no. 6, Jun. 2020, doi: 10.1038/s41564-020-0714-0.

[7] Y.-J. S. Huang, S. Higgs, and D. L. Vanlandingham, 'Emergence and re-emergence of mosquito-borne arboviruses', *Current Opinion in Virology*, vol. 34, pp. 104–109, Feb. 2019, doi: 10.1016/j.coviro.2019.01.001.

[8] A. Zaid *et al.*, 'Arthritogenic alphaviruses: epidemiological and clinical perspective on emerging arboviruses', *Lancet Infect Dis*, vol. 21, no. 5, pp. e123–e133, May 2021, doi: 10.1016/S1473-3099(20)30491-6.
[9] C. Kemp and J.-L. Imler, 'Antiviral immunity in drosophila', *Curr Opin Immunol*, vol. 21, no. 1, pp. 3–9, Feb. 2009, doi: 10.1016/j.coi.2009.01.007.
[10] R. Aliyari and S.-W. Ding, 'RNA-based viral immunity initiated by the Dicer family of host immune receptors', *Immunol Rev*, vol. 227, no. 1, pp. 176–188, Jan. 2009, doi: 10.1111/j.1600-065X.2008.00722.x.
[11] S. M. Elbashir, J. Harborth, W. Lendeckel, A. Yalcin, K. Weber, and T. Tuschl, 'Duplexes of 21-nucleotide RNAs mediate RNA interference in cultured mammalian cells', *Nature*, vol. 411, no. 6836, pp. 494–498, May 2001, doi: 10.1038/35078107.
[12] K. Okamura, A. Ishizuka, H. Siomi, and M. C. Siomi, 'Distinct roles for Argonaute proteins in small RNA-directed RNA cleavage pathways', *Genes Dev*, vol. 18, no. 14, pp. 1655–1666, Jul. 2004, doi: 10.1101/gad.1210204.
[13] S. H. Merkling *et al.*, 'Multifaceted contributions of Dicer2 to arbovirus transmission by Aedes aegypti', Nov. 15, 2022, *bioRxiv*. doi: 10.1101/2022.11.14.516413.
[14] G. H. Samuel *et al.*, 'RNA interference is essential to modulating the pathogenesis of mosquito-borne viruses in the yellow fever mosquito Aedes aegypti', *Proc Natl Acad Sci U S A*, vol. 120, no. 11, p. e2213701120, Mar. 2023, doi: 10.1073/pnas.2213701120.
[15] M. Varjak *et al.*, 'Aedes aegypti Piwi4 Is a Noncanonical PIWI Protein Involved in Antiviral Responses', *mSphere*, vol. 2, no. 3, p. 10.1128/msphere.00144-17, May 2017, doi: 10.1128/msphere.00144-17.
[16] M. Leggewie *et al.*, 'The Aedes aegypti RNA interference response against Zika virus in the context of co-infection with dengue and chikungunya viruses', *PLoS Negl Trop Dis*, vol. 17, no. 7, p. e0011456, Jul. 2023, doi: 10.1371/journal.pntd.0011456.
[17] M. Varjak *et al.*, 'Characterization of the Zika virus induced small RNA response in Aedes aegypti cells', *PLOS Neglected Tropical Diseases*, vol. 11, no. 10, p. e0006010, Oct. 2017, doi: 10.1371/journal.pntd.0006010.
[18] C. Scherer *et al.*, 'An Aedes aegypti-Derived Ago2 Knockout Cell Line to Investigate Arbovirus Infections', *Viruses*, vol. 13, no. 6, Art. no. 6, Jun. 2021, doi: 10.3390/v13061066.
[19] S. Mueller *et al.*, 'RNAi-mediated immunity provides strong protection against the negative-strand RNA vesicular stomatitis virus in Drosophila', *Proceedings of the National Academy of Sciences*, vol. 107, no. 45, pp. 19390–19395, Nov. 2010, doi: 10.1073/pnas.1014378107.
[20] F. Weber, V. Wagner, S. B. Rasmussen, R. Hartmann, and S. R. Paludan, 'Double-stranded RNA is produced by positive-strand RNA viruses and DNA viruses but not in detectable amounts by negative-strand RNA viruses', *J Virol*, vol. 80, no. 10, pp. 5059–5064, May 2006, doi: 10.1128/JVI.80.10.5059-5064.2006.
[21] M. A. Kidwell, J. M. Chan, and J. A. Doudna, 'Evolutionarily Conserved Roles of the Dicer Helicase Domain in Regulating RNA Interference Processing', *J Biol Chem*, vol. 289, no. 41, pp. 28352–28362, Oct. 2014, doi: 10.1074/jbc.M114.589051.
[22] S. A. Shabalina and E. V. Koonin, 'Origins and evolution of eukaryotic RNA interference', *Trends Ecol Evol*, vol. 23, no. 10, pp. 578–587, Oct. 2008, doi: 10.1016/j.tree.2008.06.005.
[23] N. K. Sinha, K. D. Trettin, P. J. Aruscavage, and B. L. Bass, 'Drosophila dicer-2 cleavage is mediated by helicase- and dsRNA termini-dependent states that are modulated by Loquacious-PD', *Mol Cell*, vol. 58, no. 3, pp. 406–417, May 2015, doi: 10.1016/j.molcel.2015.03.012.
[24] N. K. Sinha, J. Iwasa, P. S. Shen, and B. L. Bass, 'Dicer uses distinct modules for recognizing dsRNA termini', *Science*, vol. 359, no. 6373, pp. 329–334, Jan. 2018, doi: 10.1126/science.aaq0921.
[25] J.-B. Ma, K. Ye, and D. J. Patel, 'Structural basis for overhang-specific small interfering RNA recognition by the PAZ domain', *Nature*, vol. 429, no. 6989, pp. 318–322, May 2004, doi: 10.1038/nature02519.
[26] X. Ji, 'The mechanism of RNase III action: how dicer dices', *Curr Top Microbiol Immunol*, vol. 320, pp. 99–116, 2008, doi: 10.1007/978-3-540-75157-1_5.

[27] T. Sasaki and N. Shimizu, 'Evolutionary conservation of a unique amino acid sequence in human DICER protein essential for binding to Argonaute family proteins', *Gene*, vol. 396, no. 2, pp. 312–320, Jul. 2007, doi: 10.1016/j.gene.2007.04.001.
[28] R. J. Gestuveo *et al.*, 'Mutational analysis of Aedes aegypti Dicer 2 provides insights into the biogenesis of antiviral exogenous small interfering RNAs', *PLoS Pathog*, vol. 18, no. 1, p. e1010202, Jan. 2022, doi: 10.1371/journal.ppat.1010202.
[29] M. Reuter *et al.*, 'The PAZ domain of Aedes aegypti Dicer 2 is critical for accurate and high-fidelity size determination of virus-derived small interfering RNAs', Jun. 20, 2024, *bioRxiv*. doi: 10.1101/2024.06.20.599909.
[30] I. Dietrich *et al.*, 'RNA Interference Restricts Rift Valley Fever Virus in Multiple Insect Systems', *mSphere*, vol. 2, no. 3, pp. e00090-17, May 2017, doi: 10.1128/mSphere.00090-17.
[31] I. Dietrich *et al.*, 'The Antiviral RNAi Response in Vector and Non-vector Cells against Orthobunyaviruses', *PLOS Neglected Tropical Diseases*, vol. 11, no. 1, p. e0005272, Jan. 2017, doi: 10.1371/journal.pntd.0005272.
[32] M. Altinli *et al.*, 'Antiviral RNAi Response in Culex quinquefasciatus-Derived HSU Cells', *Viruses*, vol. 15, no. 2, p. 436, Feb. 2023, doi: 10.3390/v15020436.
[33] S. R. Gerrard and S. T. Nichol, 'Synthesis, proteolytic processing and complex formation of N-terminally nested precursor proteins of the Rift Valley fever virus glycoproteins', *Virology*, vol. 357, no. 2, pp. 124–133, Jan. 2007, doi: 10.1016/j.virol.2006.08.002.
[34] T. J. Mottram *et al.*, 'Mutational analysis of Rift Valley fever phlebovirus nucleocapsid protein indicates novel conserved, functional amino acids', *PLOS Neglected Tropical Diseases*, vol. 11, no. 12, p. e0006155, Dec. 2017, doi: 10.1371/journal.pntd.0006155.
[35] R. C. Kading *et al.*, 'Deletion of the NSm Virulence Gene of Rift Valley Fever Virus Inhibits Virus Replication in and Dissemination from the Midgut of Aedes aegypti Mosquitoes', *PLOS Neglected Tropical Diseases*, vol. 8, no. 2, p. e2670, Feb. 2014, doi: 10.1371/journal.pntd.0002670.
[36] A. Billecocq *et al.*, 'NSs Protein of Rift Valley Fever Virus Blocks Interferon Production by Inhibiting Host Gene Transcription', *Journal of Virology*, vol. 78, no. 18, pp. 9798–9806, Sep. 2004, doi: 10.1128/jvi.78.18.9798-9806.2004.
[37] K. Terasaki, S. I. Ramirez, and S. Makino, 'Mechanistic Insight into the Host Transcription Inhibition Function of Rift Valley Fever Virus NSs and Its Importance in Virulence', *PLOS Neglected Tropical Diseases*, vol. 10, no. 10, p. e0005047, Oct. 2016, doi: 10.1371/journal.pntd.0005047.
[38] S. Lerolle, N. Freitas, F.-L. Cosset, and V. Legros, 'Host Cell Restriction Factors of Bunyaviruses and Viral Countermeasures', *Viruses*, vol. 13, no. 5, p. 784, Apr. 2021, doi: 10.3390/v13050784.
[39] H. J. Ly and T. Ikegami, 'Rift Valley fever virus NSs protein functions and the similarity to other bunyavirus NSs proteins', *Virol J*, vol. 13, p. 118, Jul. 2016, doi: 10.1186/s12985-016-0573-8.
[40] A. Balkema-Buschmann, M. Rissmann, N. Kley, R. Ulrich, M. Eiden, and M. H. Groschup, 'Productive Propagation of Rift Valley Fever Phlebovirus Vaccine Strain MP-12 in Rousettus aegyptiacus Fruit Bats', *Viruses*, vol. 10, no. 12, p. 681, Nov. 2018, doi: 10.3390/v10120681.
[41] B. Tercero, K. Terasaki, K. Narayanan, and S. Makino, 'Mechanistic insight into the efficient packaging of antigenomic S RNA into Rift Valley fever virus particles', *Frontiers in Cellular and Infection Microbiology*, vol. 13, 2023, Accessed: Aug. 17, 2023. [Online]. Available: https://www.frontiersin.org/articles/10.3389/fcimb.2023.1132757
[42] A. M. Szemiel, A.-B. Failloux, and R. M. Elliott, 'Role of Bunyamwera Orthobunyavirus NSs protein in infection of mosquito cells', *PLoS Negl Trop Dis*, vol. 6, no. 9, p. e1823, 2012, doi: 10.1371/journal.pntd.0001823.
[43] F. W. Charlton *et al.*, 'Cellular cholesterol abundance regulates potassium accumulation within endosomes and is an important determinant in bunyavirus entry', *J Biol Chem*, vol. 294, no. 18, pp. 7335–7347, May 2019, doi: 10.1074/jbc.RA119.007618.
[44] X. Shi and R. M. Elliott, 'Generation and analysis of recombinant Bunyamwera orthobunyaviruses expressing V5 epitope-tagged L proteins', *J Gen Virol*, vol. 90, no. Pt 2, pp. 297–306, Feb. 2009, doi: 10.1099/vir.0.007567-0.

[45] J. N. Barr, R. M. Elliott, E. F. Dunn, and G. W. Wertz, 'Segment-specific terminal sequences of Bunyamwera bunyavirus regulate genome replication', *Virology*, vol. 311, no. 2, pp. 326–338, Jul. 2003, doi: 10.1016/s0042-6822(03)00130-2.
[46] A. C. Fredericks, T. A. Russell, L. E. Wallace, A. D. Davidson, A. Fernandez-Sesma, and K. Maringer, 'Aedes aegypti (Aag2)-derived clonal mosquito cell lines reveal the effects of pre-existing persistent infection with the insect-specific bunyavirus Phasi Charoen-like virus on arbovirus replication', *PLOS Neglected Tropical Diseases*, vol. 13, no. 11, p. e0007346, Nov. 2019, doi: 10.1371/journal.pntd.0007346.
[47] M. Varela *et al.*, 'Schmallenberg virus pathogenesis, tropism and interaction with the innate immune system of the host', *PLoS Pathog*, vol. 9, no. 1, p. e1003133, Jan. 2013, doi: 10.1371/journal.ppat.1003133.
[48] S. Chen, Y. Zhou, Y. Chen, and J. Gu, 'fastp: an ultra-fast all-in-one FASTQ preprocessor', *Bioinformatics*, vol. 34, no. 17, pp. i884–i890, Sep. 2018, doi: 10.1093/bioinformatics/bty560.
[49] B. Langmead and S. L. Salzberg, 'Fast gapped-read alignment with Bowtie 2', *Nat Methods*, vol. 9, no. 4, pp. 357–359, Mar. 2012, doi: 10.1038/nmeth.1923.
[50] C. Antoniewski, 'Computing siRNA and piRNA overlap signatures', *Methods Mol Biol*, vol. 1173, pp. 135–146, 2014, doi: 10.1007/978-1-4939-0931-5_12.
[51] G. E. Crooks, G. Hon, J.-M. Chandonia, and S. E. Brenner, 'WebLogo: a sequence logo generator', *Genome Res*, vol. 14, no. 6, pp. 1188–1190, Jun. 2004, doi: 10.1101/gr.849004.
[52] A. R. Quinlan and I. M. Hall, 'BEDTools: a flexible suite of utilities for comparing genomic features', *Bioinformatics*, vol. 26, no. 6, pp. 841–842, Mar. 2010, doi: 10.1093/bioinformatics/btq033.
[53] C. L. Donald, A. Kohl, and E. Schnettler, 'New Insights into Control of Arbovirus Replication and Spread by Insect RNA Interference Pathways', *Insects*, vol. 3, no. 2, pp. 511–531, May 2012, doi: 10.3390/insects3020511.
[54] K. Breving and A. Esquela-Kerscher, 'The complexities of microRNA regulation: Mirandering around the rules', *The international journal of biochemistry & cell biology*, vol. 42, pp. 1316–29, Sep. 2009, doi: 10.1016/j.biocel.2009.09.016.
[55] J. O'Brien, H. Hayder, Y. Zayed, and C. Peng, 'Overview of MicroRNA Biogenesis, Mechanisms of Actions, and Circulation', *Front Endocrinol (Lausanne)*, vol. 9, p. 402, Aug. 2018, doi: 10.3389/fendo.2018.00402.
[56] M. Varjak, M. Leggewie, and E. Schnettler, 'The antiviral piRNA response in mosquitoes?', *J Gen Virol*, vol. 99, no. 12, pp. 1551–1562, Dec. 2018, doi: 10.1099/jgv.0.001157.
[57] Turell MJ, Rossi CA. Potential for mosquito transmission of attenuated strains of Rift Valley fever virus. *Am J Trop Med Hyg*. 1991 Mar;44(3):278-82. doi: 10.4269/ajtmh.1991.44.278. PMID: 2035749.

Chapter 5: Publication 4

RNAi-based adaptive immunity in *Aedes aegypti* against arboviruses

Melinda Reuter[1], Christina Scherer[1], Rhys H. Parry[2], Janina Fuss[3], Esther Schnettler[1,4,5]

[1]Bernhard-Nocht-Institute for Tropical Medicine, Hamburg, Germany
[2]School of Chemistry and Molecular Biosciences, The University of Queensland, St. Lucia, Australia
[3]Institute of Clinical Molecular Biology (IKMB), Kiel University, Kiel, Germany
[4]Faculty of Mathematics, Informatics and Natural Sciences, University Hamburg, Hamburg, Germany
[5]German Center for Infection Research (DZIF), partner side HH-HL-Bo-Ri, Hamburg, Germany

Correspondence: schnettler@bnitm.de

Keywords: RNA interference, arbovirus, small RNA, viral DNA, mosquito

Abstract

Arboviruses are transmitted by arthropods, e.g., mosquitoes like *Aedes aegypti* and *Aedes albopictus*. Clinically important arboviruses include, Zika virus (ZIKV), dengue virus (DENV) and chikungunya (CHIKV) virus, among others. A major part of the mosquito's antiviral response are the RNAi pathways with the exogenous small interfering RNA (exo-siRNA) and PIWI-interacting RNA (piRNA) pathway being of importance for this study. Production of viral DNA (vDNA) has been proposed to be essential for the establishment of a persistent infection, a hallmark of successful transmission of arboviruses. Besides, possible interaction of incorporated vDNA in the form of NIRVS, vDNA derived piRNA production and corresponding virus infection have been suggested; but detailed information is missing. Therefore, to analyse the effects of previous arbovirus infection of mosquito cells on vDNA production and possible incorporation, piRNA production and the effect on a sequential infection, cell culture experiments with representative viruses of the three main arbovirus families were performed. *Aedes aegypti*-derived AF5 cells were persistently infected with either BUNV, SFV or ZIKV and subsequently cleared of the infection, leading to the establishment of primed cells. These cells were then subjected to infection of either the same arbovirus used for priming or one of a different viral family. These primed cells were used to investigate small RNA production and possible changes in susceptibility of the cells to the either the same virus used for priming or an unrelated one. The effects of viral priming were both virus- and clone-specific, with no consistent results between antiviral activity and small RNA (sRNA) production and even observed changes in replication inhibition and sRNA production upon secondary infection with a non-priming virus. Interestingly, the effects on antiviral activity were shown to be time sensitive, mainly leading to an exacerbated effect over time. Especially BUNV primed cells exhibited a decreased SFV replication and clone-specific differences in sRNA production. Additionally, vDNA was shown both in total and genomic DNA of *Aedes*-derived cells after acute RVFV-infection, and acute and persistent SFV and BUNV infection.

Introduction

As the world currently faces an emerging arboviral threat, it becomes critically important to understand not just the antiviral initial immune response in the mammalian host, but also within the mosquito vector. *Aedes aegypti* is known as the most important arboviral vector, transmitting viruses from multiple different viral families, including dengue virus (DENV; *Flaviviridae*; *Orthoflavivirus*), chikungunya virus (CHIKV; *Togaviridae*; *Alphavirus*), Rift valley fever virus (RVFV; *Phenuiviridae*; *Phlebovirus*) and Zika virus (ZIKV; *Flavivirdae*; *Orthoflavivirus*), among many others (Brady and Hay, 2020; Huang et al., 2019; Pierson and Diamond, 2020; Weaver et al., 2018; Weaver and Reisen, 2010; Zaid et al., 2021).

Arboviruses establish productive infections in their arthropod vectors, triggering antiviral immune responses. In mosquitoes, a central component of this defense is the RNA interference (RNAi) system, which includes the small interfering RNA (siRNA) pathway and the PIWI-interacting RNA (piRNA) pathway. The exogenous siRNA pathway is activated when the endoribonuclease Dicer-2 (Dcr2) recognizes viral double-stranded RNA (dsRNA). Dcr2 then cleaves the viral dsRNA into viral siRNAs (vsiRNAs), typically 21 nt in length. These vsiRNAs are subsequently loaded onto Argonaute-2 (Ago2) to form the RNA-induced silencing complex (RISC), which identifies and degrades complementary viral RNA sequences (Elbashir et al., 2001; Okamura et al., 2004).

The piRNA pathway is primarily associated with regulation of gene expression and repression of transposable elements. It begins with precursor piRNAs (pre-piRNAs), which are single-stranded RNA molecules derived from genomic regions known as piRNA clusters. These precursors are processed by the single-strand-specific nuclease Zucchini (Zuc) into primary piRNAs (pri-piRNAs) (Lucas et al., 2013). Primary piRNAs can then enter an amplification cycle known as the ping-pong cycle, involving Argonaute-3 (Ago3) and PIWI proteins, with PIWI5 and PIWI6 being involved in amplification of virus-derived piRNAs (vpiRNAs). During this process, mature piRNAs guide the cleavage and processing of additional precursor transcripts, thereby amplifying piRNA production (Chary et al., 2025). piRNAs generated through the ping-pong cycle display characteristic sequence signatures, including a 10 nt overlap between sense and antisense strands, a uridine at position 1 (U1) in PIWI5/6-associated antisense piRNAs, and an adenine at position 10 (A10) in Ago3-associated sense piRNAs. Ago3-bound piRNAs are also methylated at their 3′ ends, producing mature piRNA. Despite substantial progress in understanding this pathway, the precise functions and interactions of the different PIWI proteins remain unresolved. This includes a proposed antiviral role of PIWI4, which is still under active investigation.

To successfully establish themselves within the vector for possible transmission to the vertebrate host, arboviruses produce persistent infections. The exact mechanism for the establishment of persistence is still unknown, yet previous studies have shown a link to the production of viral DNA (vDNA) (Goic et al., 2016, 2013; Poirier et al., 2018). Arboviruses, which predominantly present as RNA viruses, do not express their own reverse transcriptase (RT), thus relying on mosquito transposon-derived RT for the production of vDNA. This link between transposon-derived RT, vDNA production and establishment of a persistent infection has been investigated previously, leading to the discovery that CHIKV-infected mosquitoes treated with azidothymidine (AZT), an RT-inhibitor, lead to a 45% decline in vDNA production and a rapid decline in survivability in comparison to untreated CHIKV-infected mosquitoes

(Goic et al., 2016). Another study showed that Aedes-derived cells treated with AZT lead to an overall increase in SINV-derived sRNAs, however, while this increase was consistent for SINV-derived vsiRNAs, a decrease in vpiRNA production after SINV infection was observed (Tassetto et al., 2019). vDNA production upon arbovirus infection has also been reported for various other viruses, including for CHIKV in *Culex*- and *Aedes*-derived cells (Goic et al., 2016), for SFV in *Aedes* mosquitoes (Rodriguez-Andres et al., 2023), for West Nile virus (WNV; *Flaviviridae*; *Orthoflavivirus*), DENV, and ZIKV both *in vivo* and in *Aedes*-derived cells, and for Bunyamwera orthobunyavirus (BUNV; *Peribunyaviridae*; *Orthobunyavirus*) and WNV also in *Culex*-derived cells (Altinli et al., 2023; Goic et al., 2016; Marconcini et al., 2021; Nag et al., 2016; Nag and Kramer, 2017; Rückert et al., 2019b).

In addition to the production of vDNA, it has been shown that different mosquito species possess non-retroviral integrated RNA virus sequences (NIRVS) from insect specific viruses (ISVs) like Cell fusion agent virus (CFAV) and Phasi-Charoen-like virus (PCLV) in their genome (Chen et al., 2015; Crochu et al., 2004; Miesen et al., 2016b; Palatini et al., 2017; Whitfield et al., 2017). Although NIRVS are found in many insect genomes, they are especially abundant in *Aedes* mosquitoes and differ in their viral origins compared to other insects (Blair et al., 2019). Comparative analyses of more than 400 RNA viruses detected integrations from multiple different viral families, suggesting species-specific patterns of NIRVS formation in mosquitoes (Olson and Bonizzoni, 2017; Palatini et al., 2017).

NIRVS are thought to be vertically inherited and may provide fitness benefits to the host (Blair et al., 2019; Suzuki et al., 2020; Whitfield et al., 2017). Their genomic distribution is non-random, with many integrations enriched in piRNA clusters. This localization may enable production of NIRVS-specific virus-derived piRNAs (vpiRNAs), typically antisense and showing the characteristic U1 bias (Palatini et al., 2017; Whitfield et al., 2017). Unlike vsiRNAs, which are mainly produced during active infection, vpiRNAs have been detected in both infected and uninfected cells (Arensburger et al., 2011; Blair et al., 2019; Brackney et al., 2010; Palatini et al., 2017). CFAV-derived antisense piRNAs have also been shown to associate with PIWI4, supporting a possible antiviral role (Suzuki et al., 2020; Tassetto et al., 2019). Overall, current evidence supports a pathway in which viral RNA (vRNA) is reverse-transcribed by host reverse transcriptases into vDNA, integrated into the mosquito genome as NIRVS, and later used to generate antiviral piRNAs. Rather than clearing infection completely, this mechanism may promote persistent infections that enhance mosquito survival and vector competence.

In this study, we first showed proof of vDNA production, including genomic vDNA, in *Aedes aegypti*-derived AF5 cells after infection with either the Semliki Forest virus (SFV; *Togaviridae*; *Alphavirus*), BUNV and Rift valley fever virus (RVFV; *Phenuiviridae*; *Phlebovirus*), with the two latter possessing a negative sense ssRNA genome as opposed to the positive orientation of the SFV genome. After production of primed AF5 cells, which have previously seen arboviral challenge (SFV, BUNV or ZIKV) and have since been cleared from their respective infection, the primed cells were either left uninfected to check for possible base-line NIRVS-specific sRNA production or re-infected with their respective arbovirus or an unrelated arbovirus to investigate their small RNA production in comparison to naïve cells. Upon small RNA sequencing, it became clear that we could not see consistent priming results between different clones of the same priming group. The priming effect was also investigated at different time points, again showing clone-specificity, and additionally, some groups exhibited a time-

dependent exacerbation of the detectable effects, yet it is unclear if the effects we observe are a by-product of single cell cloning or true priming effects.

Methods and material

Cells

In this study, a cell clone of the Aag2 cells: Aag2-AF5 (ECACC 19022601, Public Health England), embryonic *Ae. aegypti* cells were used, as well as Aag2-AF5-derived Aag2-AF319 (ECACC 19022602, Public Health England) cells, which contain a Dcr2 KO mutation through CRISPR/ cas9 technology (Fredericks et al., 2019; Varjak et al., 2017b). Both cell lines, as well as *Aedes albopictus*-derived C6/36 (ECACC 89051705, Public Health England) were cultured in Leibovitz's L-15 medium (Gibco ThermoFisher Scientific Inc., Waltham, MA, USA) supplemented with penicillin-streptomycin (pen-strep; 100 U/mL-100 µg/mL; PAN BIOTECH, Aidenbach, Germany), 10% fetal bovine serum (FBS, Gibco Capricorn Scientific GmbH, Ebsdorfergrund, Germany) and 10% fetal tryptose phosphate broth (TBP; Gibco ThermoFisher Scientific Inc.) at 28°C without CO_2. For mammalian cells, Baby hamster kidney (BHK-21) cells (ECACC 85011433, Public Health England) and BSRT7 cells (BHK-21 cells stably expressing the T7 RNA polymerase) (Buchholz et al., 1999), were cultured in Glasgow minimum essential medium (GMEM, Gibco ThermoFisher Scientific Inc.), while Vero cells (ECACC 84113001, Public Health England; African green monkey kidney cells) (Ammerman et al., 2008) and A549Npro cells (human adenocarcinoma alveolar basal epithelial cells expressing the N-terminal protease (Npro) from bovine viral diarrhea virus (BVDV)) (Hilton et al., 2006) were cultured in Dulbecco's modified Eagle's medium (DMEM, Gibco ThermoFisher Scientific Inc.), both media supplemented with 10% FBS (Gibco Capricorn Scientific GmbH), 10% TBP (Gibco ThermoFisher Scientific Inc.), pen-strep (PAN BIOTECH) at 37°C and 5% CO_2 and G418 (1:1000; Sigma-Aldrich, St. Louis, MO, USA) as selection antibiotic.

Viruses

SFV4 (abbreviated to SFV; GenBank ID: KP699763) and BUNV (GenBank ID: NC_001927.1, NC_001926.1 and NC_001925.1) were grown in BHK-21 with a multiplicity of infection (MOI) below 1. After 72h, virus was harvested and the titre was determined using plaque assays with Avicel as overlay, as previously described for Schmallenberg virus (Varela et al., 2013). RVFV MP12 (abbreviated to RVFV, provided by Professor Elliot, CVR, UK) was produced in BHK-21 cells with an MOI below 1. The virus was harvested via polyethylene glycol precipitation at 72hpi and the titre was determined via $TCID_{50}$ as previously described (Hierholzer and Killington, 1996; Kärber, 1931) on BHK-21 cells. SFV6 (GenBank ID: KT009012.1) expressing Nano luciferase from a duplicated subgenomic promoter was produced by transfection of the corresponding plasmid (pCMV-2SG-SFV6-Nluc, abbreviated to SFV-Nluc) harbouring a CMV promoter followed by the viral genome) into BHK-21 cells. BUNV-Nluc expressing Nano luciferase was produced in BSRT7 cells by co-transfection of three plasmids: pTVT7RBUNM-NL (a part of the BUNV NSm cytoplasmic domain was replaced by the Nluc sequence resulting in chimeric NSm-Nluc fusion protein), pT7riboBUNL(+) and pT7riboBUNS(+) encoding the BUNV antigenome. After observation of CPE (for SFV or BUNV), supernatant was transferred to fresh BHK-21 cells and harvested at 48hpi or 96hpi, respectively. Titers were determined via plaque assay (Dietrich et al., 2017b; Scherer et al., 2021). ZIKV expressing Nano luciferase (pCCI-SP6-ZIKV-Nluc, abbreviated to ZIKV-Nluc) was produced by plasmid linearalization,

SP6-based *in vitro* transcription in the presence of a cap analogue and transfection of the *in vitro* transcribed RNA into Vero cells (Mutso et al., 2017). Following CPE observation, the supernatant was transferred to A549-Npro cells. Supernatant containing ZIKV-Nluc was collected at 96hpi with the titre measured via $TCID_{50}$. Recovery of Sindbis virus (SINV) TOTO01101 from infectious cDNA clones has been previously described (Gothe et al., 2026). BHK-21 cells were transfected with the recovered SINV RNA, and supernatant was collected after visible CPE before being used to infect fresh BHK-21 cells. The supernatant was once again collected after visible CPE and subsequently titred via $TCID_{50}$ (Rice et al., 1987). O'nyong Nyong virus (ONNV) SG650 (abbreviated to ONNV; GenBank ID: NC_075006.1) and Tahyna virus (TAHV) Bardos92 strain (abbreviated to TAHV; GenBank ID: HM036213.1, HM036212.1 and HM036211.1) were grown on BHK-21 cells until CPE was observed, at which point supernatant was collected and titred via $TCID_{50}$ or Focus Forming Assay (FFA), respectively. CFAV was produced in *Ae. albopictus*-derived C6/36 cells through transfection with total RNA isolated from AF5 cells. At 5 days post infection (dpi), supernatant containing CFAV was harvested after freezing and thawing the cells to release the virus into the supernatant. CFAV titre was determined via $TCID_{50}$ on C6/36 cells.

Detection of vDNA

AF5 and AF319 cells were seeded at $2x10^5$ cells/well in a 24-well plate and infected after 24h with either BUNV, RVFV or SFV at MOI 1. At 48 hours post infection (hpi), the cells were taken up into phosphate-buffered saline (PBS). For DNA and gDNA extraction, the QIAmp DNA Mini Kit (Qiagen, Hilden, Germany) or the PureLink genomic DNA Kit (Invitrogen ThermoFisher Scientific Inc., Waltham, MA, USA) were used according to the manufacturer's protocol, respectively. The DNA samples were additionally incubated with RNase A for 1h at 37°C. PCR was performed using GoTaq Green Master Mix (Promega Corporation, Madison, WI, USA) with the corresponding primers (see Table S1), as described in the manufacturer's protocol. A 1% agarose gel electrophoresis was performed. The gels were analysed using BioRad ChemiDoc (BioRad, Hercules, CA, USA). The bands were extracted from the gel and purified using Gel and PCR Clean-up Kit (Macherey-Nagel, Düren, Germany) before being sequenced via Eurofins Genomics (Hamburg, Germany).

dsRNA production

BUNV, SFV and ZIKV were amplified using T7 RNA polymerase promotor-flanked primers (see Table S1). The dsRNA synthesis and column purification were done via T7 RNA based in vitro transcription, using the MEGAscript RNAi-Kit (Invitrogen ThermoFisher Scientific Inc.) according to the manufacturer's protocol.

Generation of primed cells

BUNV-Nluc and SFV-Nluc primed cells were produced and provided by Christina Scherer, Bernhard-Nocht-Institut, Hamburg (Scherer, 2021). Following the same protocol for the ZIKV-Nluc primed cells, AF5 cells were seeded at $2x10^5$ cells/well in a 24-well plate and infected after 24h with ZIKV-Nluc at MOI 0.5. At 4 dpi, the infected cells were taken up and seeded in a 6-well plate. After another 3 days, the cells were checked for successful infection via PCR before being transferred to a T25-flask. For clearing of the persistent infection via dsRNA-mediated silencing, the persistently ZIKV-Nluc infected AF5 cells were seeded at $2x10^5$ cells/well in 24-well plates. After 24h, the cells were transfected with 200ng dsRNA targeting

the ZIKV genome sequences using 1µL DharmaFECT2 (Horizon Discovery Ltd., Cambridge, UK). The cells were passaged twice a week, and transfected every second passage, with total RNA isolation via TRIzol, cDNA synthesis and PCR once a week to check for loss of the infection. After 6-10 weeks, the cells were cleared from infection and subsequently seeded by dilution as single cell clones in a 96-well plate. Once the cells reached confluency, they were first taken up into 24-well plates before being transferred to T25 flasks, resulting in AF5 cells primed with ZIKV-Nluc, which were again checked for loss of ZIKV infection, and additionally for CFAV infection.

Small RNA sequencing and analysis

To assess possible changes in small RNA production in primed cells, SFV-Nluc, BUNV-Nluc and ZIKV-Nluc primed AF5 cells were seeded alongside naïve AF5 cells as controls in 24-well plates at $2x10^5$ cells/well before infection at MOI 1. SFV-Nluc primed cells were infected with either SFV-Nluc or BUNV-Nluc, BUNV-Nluc primed cells were infected with BUNV-Nluc or SFV-Nluc, and ZIKV-Nluc primed cells were infected with ZIKV-Nluc, SFV-Nluc or BUNV-Nluc, with naïve AF5 cells infected as controls. Additionally, 1mL of cell suspension of uninfected primed and naïve AF5 cells were used for RNA isolation, too. The cells were lysed using TRIzol at either 48hpi (BUNV-Nluc and SFV-Nluc infection) or 96hpi (ZIKV-Nluc infection) and total RNA was isolated with glycogen as carrier, according to the manufacturer's manual. Small RNA sequencing was performed at the Institute of Clinical Molecular Biology (IKMB), Kiel University, Kiel, Germany on NovaSeq6000 SP v1.0 platform (Illumina Inc., San Diego, CA, USA) using Nextflex Small RNA-Seq Kit v3 (PerkinElmer Inc., Waltham, MA, USA).

Base called fastq files were quality an adapter trimmed using TrimGalore (v0.6.10) (Krueger et al., 2023), including trimming 4 random basepairs both 3' and 5' after adapter trimming, retaining 18-28 nt reads under default conditions. All following scripts were sourced from the Github repository rhparry/viral_sRNA_tools. Read size distribution including first base bias was calculated using "1_fastq_histogram.sh" using Bowtie2 (v2.5.5) (Langmead and Salzberg, 2012). Clean, trimmed reads were then mapped to either the BUNV (GenBank ID: L-segment NC_001927.1, M-segment NC_001926.1 and S-segment NC_001925.1), SFV6 (GenBank ID: KT009012.1) or ZIKV strain BeH819015 (GenBank: KU365778.1) genome using the "2_mapping_vrnas.sh" script including the sensitive mapping flag (--sensitive). Mapping statistics are available in Tables S2-S7. Mapped read size distribution and first base bias was then calculated using "3_bam_sRNA_histogram.sh" utilizing SAMtools (v1.19.2). Overlap probabilities (z-scores) for 25-28 nt mapped reads were generated via small RNA signatures Python script "signature.py" (Antoniewski, 2014) with the following conditions: --minquery 25 --maxquery 28 --mintarget 25 --maxtarget 28 --minscope 1 --maxscope 20. For base position bias of 25-28 nt piRNAs, bam files of independent repeats were merged, filtered to only include 25-28 nt reads and the reads were then trimmed to the first 15 nt using TrimGalore before Sequence Logos were visualized using WebLogo3 (Crooks et al., 2004). Coverage statistics for both 21 nt siRNAs and 25-28 nt piRNAs were calculated using "4_viral_srna_coverage.sh" utilizing bedtools genome coverage tool (v2.31.2) (Quinlan and Hall, 2010). Size distribution histograms, coverage plots and overlap probabilities were visualized using GraphPad Prism (v10.6.1).

Assessment of priming effects on antiviral activity

To assess a possible change in antiviral activity in primed cells versus naïve cells, BUNV-Nluc, SFV-Nluc or ZIKV-Nluc primed and naïve AF5 cells were seeded at $2x10^5$ cells/well in a 24-well plate. Additionally, primed cell clones exhibiting a loss of CFAV infection after single cell selection as confirmed via PCR were previously re-infected with CFAV at an MOI below 1 to check for a possible influence of the loss of CFAV on the results. After 24h, BUNV-Nluc primed cells were re-infected with either BUNV-Nluc or SFV-Nluc, SFV-Nluc primed cells were re-infected with either SFV-Nluc or BUNV-Nluc, and ZIKV-Nluc primed cells were re-infected with either ZIKV-Nluc or BUNV-Nluc as mutual controls. As negative control, naïve AF5 cells were infected with either SFV-Nluc, BUNV-Nluc or ZIKV-Nluc, all at MOI 0.1. Cells were lysed using Passive Lysis Buffer (PLB, Promega Corp., Fitchburg, WI, USA) at 48hpi for SFV-Nluc and BUNV-Nluc infected cells, and at 96hpi after ZIKV-Nluc infection. The cells were analysed via Nano-Glo Luciferase Assay System (Promega Corp.) and Glo-Max Microplate Luminometer (Promega Corp.). For additional experiments, BUNV-Nluc primed cells were again seeded at $2x10^5$ cells/well in 24-well plates before being infected with either BUNV-Nluc, SFV-Nluc, ONNV, SINV or TAHV at MOI 0.1. As ONNV, SINV and TAHV lack reporter-constructs, all cells including the ones infected with BUNV-Nluc and SFV-Nluc were lysed in TRIzol and total RNA was isolated before cDNA synthesis using 1.5 µg RNA, M-MLV (Promega Corporation, Madison, WI, USA) and random hexamers as according to the manufacturer's protocol. Additionally, RNA originally isolated for small RNA sequencing was also used for cDNA synthesis and subsequent qRT-PCR. In both cases, 1 µL cDNA each was used to quantify both virus-specific RNA and S7 ribosomal RNA (as housekeeper) using QuantiTect SYBR Green PCR Kit (Qiagen) and LightCycler 480 System (Roche Diagnostics, Mannheim, Germany). For primers, see Table S1. For statistical analysis, the results of the primed cells were normalized against naïve cells receiving the same arboviral challenge set to 1. Statistical tests were done using Student's t test via GraphPad Prims 10 (GraphPad Software, Boston, MA, USA).

Results

vDNA is produced by arboviruses from multiple different viral families in infected *Ae. aegypti*-derived cells

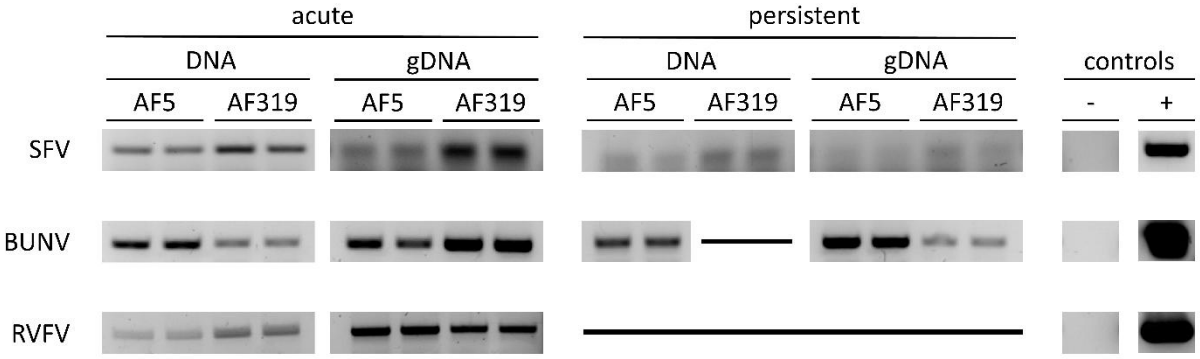


Fig. 1: Arboviral DNA detection in acutely and persistently infected *Ae. aegypti*-derived AF5 and AF319 cells. AF5 and AF319 (Dcr2 knock out) cells were infected with either SFV, BUNV or RVFV at MOI 1. For persistent infection, the cells were passaged for multiple weeks before harvesting, while for acute infection the cells were harvested at 48hpi. In both cases, the cells were taken up into PBS and either total DNA or genomic DNA (gDNA) was extracted, and all samples were additionally treated with RNase A. PCR with virus-specific primers was performed followed by agarose-gel electrophoresis. Results are shown above, with the left side presenting the acute infection results, and on the right side the results of the persistently infected cells. On the right, positive (SFV, BUNV or RVFV infected AF5 cDNA) and negative (uninfected AF5 cDNA) are shown.

While vDNA has been shown to be involved in the establishment of both persistent infection and NIRVS, many clinically important arboviruses have not yet been tested for vDNA production. Additionally, little is known about a possible involvement of the siRNA pathway, specifically Dcr2, in the production of vDNA. Based on this, we set out to check for vDNA production in both presence and absence of Dcr2 from RNA viruses belonging to different arbovirus families: SFV (*Togaviridae*), BUNV (*Peribunyaviridae*) and RVFV (*Phenuiviridae*). *Aedes aegypti*-derived AF5 and AF5-derived Dcr2 KO (AF319) cells were infected with either of the three viruses at MOI 1 for acute and MOI 0.1 for persistent infection. Sample collection at 48hpi for acute infection and >20 passage for persistent infection, followed by DNA or gDNA isolation, and finally PCR (for primers see Table S1) was performed. For all conditions and viruses, the AF319 bands corresponding to the expected length were excised from the gel and send for sequencing, verifying the correct viral sequence.

Arboviral DNA was observed after acute SFV, BUNV and RVFV infection for AF5 and AF319 both after total DNA and gDNA extraction. For the persistently SFV and BUNV infected cells, vDNA was again shown in AF5 and AF319 cells for total DNA and gDNA, with the exception of persistently BUNV-infected AF319 cells after total DNA extraction due to low volume of the sample. RVFV vDNA was not tested for persistent infection.

Primed cells exhibit clone-specific changes in viral replication upon arboviral "re-" infection

To investigate possible changes in viral replication after renewed arboviral infection, primed cells were produced. For this, AF5 cells were persistently infected with either BUNV-Nluc, SFV-Nluc or ZIKV-Nluc as representatives of the different arbovirus families. After verification of the successful persistent infection through PCR, the cells were cleared via continuous transfection with virus-specific dsRNA every second passage, making use of the antiviral activity of the siRNA pathway. Once the cells were confirmed to have lost their respective infection as determined via PCR, which took 13-20 passages depending on virus (SFV-Nluc and BUNV-Nluc: 13 passages, ZIKV-Nluc: 20 passages), they were seeded by dilution as single cell clones and proliferated; which then led to multiple clones per condition (BUNV primed: BUNV-2, BUNV-3, BUNV-9; SFV primed: SFV-1, SFV-2). For ZIKV primed cells only one cell clone survived (ZIKV).

AF5 cells are known to be persistently infected with CFAV and PCLV; however, it can be expected that not all cells are infected in the cell culture. This is supported by previous work that showed loss of at least one of these ISVs after single cell sorting in the corresponding single cell clones (Frederikson et al). Similarly, some of the primed cell clones have lost their CFAV infection along the process of single cell seeding via RT-PCR (BUNV-3, BUNV-9 and SFV-2) (Fig. 2A). Interestingly, CFAV has been shown previously to affect simultaneous arboviral infection for DENV and ZIKV (Baidaliuk et al., 2019). To exclude possible effects of CFAV presence or absence on the re-infected virus in these different cell clones, the CFAV negative clones (BUNV-3, BUNV-9 and SFV-2) were re-infected with CFAV at an MOI below 1.

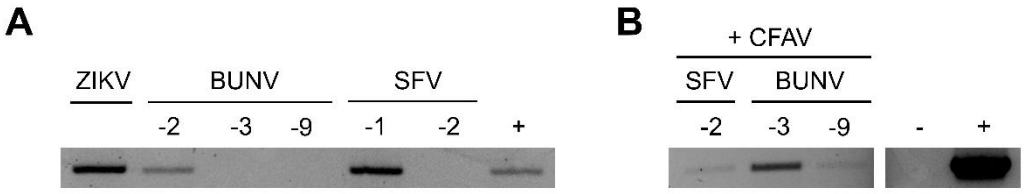


Fig. 2: Check for persistent CFAV infection in primed cells. (A) All clones of ZIKV, BUNV and SFV primed cells were tested for presence of a persistent CFAV infection using RT-PCR with AF5 cells as positive control (+). Total RNA was extracted and synthesized into cDNA before RT-PCR and agarose gel-electrophoresis. **(B)** Previously CFAV negative primed cells were re-infected with CFAV at an MOI below 1 and checked for successful persistent infection after ~5 passages with AF5 cells for positive (+) and AF319 cells for negative controls (-). Total RNA was extracted and synthesized into cDNA before RT-PCR and agarose gel-electrophoresis.

Once persistent CFAV infection has been re-established and confirmed via RT-PCR (Fig. 2B), all primed cells were then infected with a) the same arbovirus used for priming or b) one of the other two arboviruses belonging to a different virus family, as control. Based on this set-up, both SFV-Nluc and BUNV-Nluc primed cells were infected with either BUNV-Nluc or SFV-Nluc, and ZIKV-Nluc primed cells were infected with either ZIKV-Nluc or BUNV-Nluc with naïve AF5 cells as control and MOI 0.1 for each virus. At 48 hpi for BUNV-Nluc or SFV-Nluc infection and 96 hpi after ZIKV-Nluc infection, cells were lysed and Nluc-activity was measured (for p-values according to Student's t-test see Tables S2-S7).

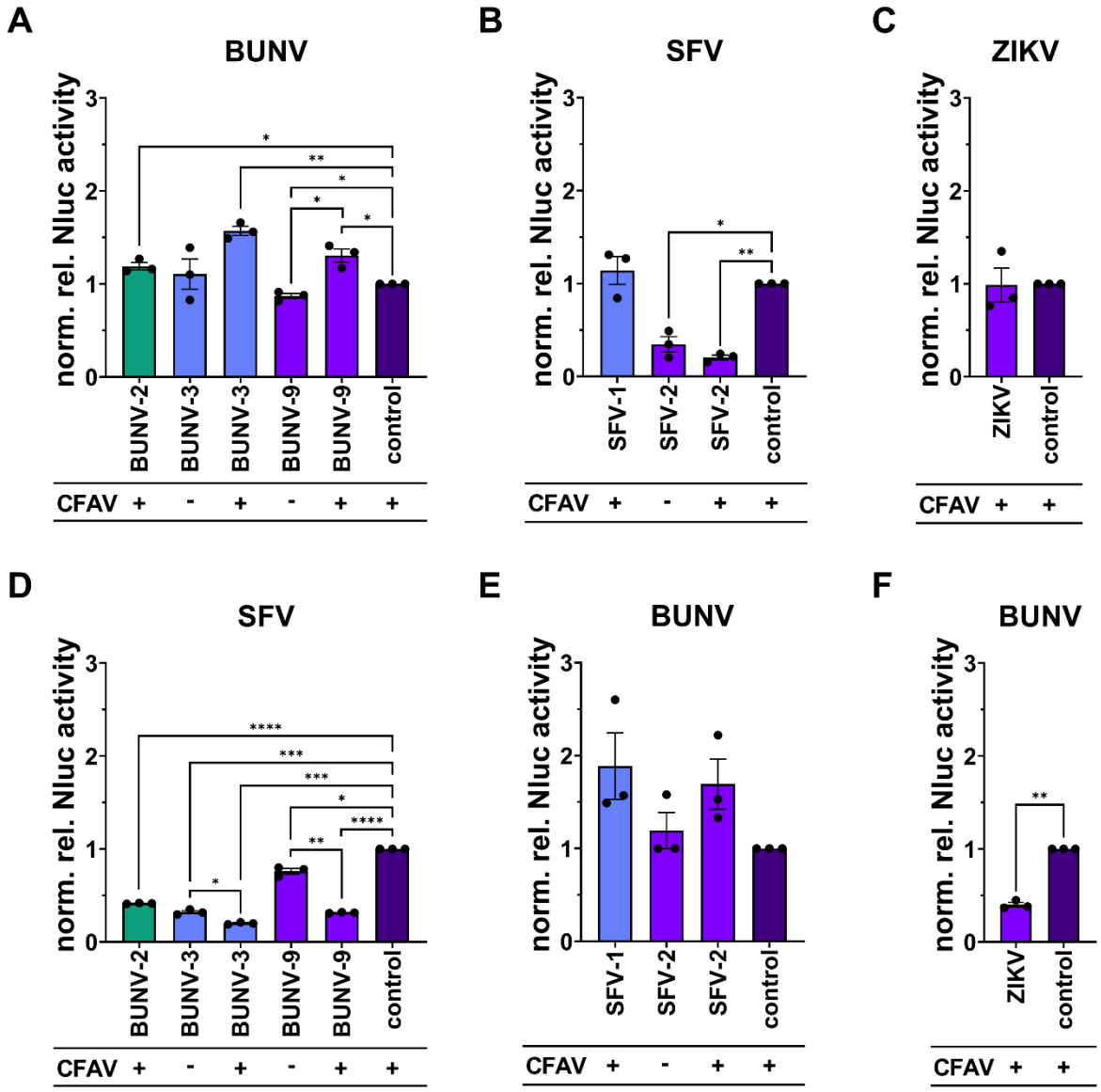


Fig. 3: Effect of BUNV, SFV and ZIKV primed cell clones upon re-infection. BUNV, SFV and ZIKV primed cells, alongside naïve AF5 cells as control, were either re-infected with the same arbovirus used for priming **(A)** – BUNV primed, BUNV-Nluc infected, **(B)** – SFV primed, SFV-Nluc infected, **(C)** – ZIKV primed, ZIKV-Nluc infected or infected with a different arbovirus **(D)** – BUNV primed, SFV-Nluc infected, **(E)** – SFV primed, BUNV-Nluc infected, **(F)** – ZIKV primed, BUNV-Nluc infected as indicated above each graph. Additionally, primed clones that had lost their CFAV infection during single cell clone selection were re-infected with CFAV, namely BUNV-3, BUNV-9 and SFV-2 for the re-infection experiments to exclude possible CFAV-based influences on antiviral activity. All infections were performed at MOI 0.1 and at 48hpi (BUNV-Nluc and SFV-Nluc infections) or 96hpi (ZIKV-Nluc infections) Nano luciferase (Nluc)-levels were measured and are shown as mean ± SEM normalized relative Nluc activity compared to naïve control. These results were produced approximately 40 cell passages before the small RNA sequencing took place. Experiments were performed in three biological repeats, each in technical triplicates with * = $p<0.05$, ** = $p<0.01$, *** = $p<0.001$ and **** = $p<0.0001$ according to Student's t-test. Status of CFAV infection shown on the bottom.

Upon re-infection of BUNV primed cells with BUNV-Nluc, no consistent changes between the three different clones can be observed (Fig. 3A). While some significances are present, the changes seem low and are still close to the luciferase expression seen in the naïve AF5 control. For the SFV-Nluc infected SFV primed cells, we again see significant differences between the two clones with SFV-1 showing Nluc activity levels comparable to the control cells while SFV-2 Nluc activity levels are decreased by ~70% (Fig. 3B). Re-infected ZIKV primed cells do not exhibit any observable change in luciferase activity in comparison to the control cells (Fig. 3C). Interestingly, BUNV primed cells infected with SFV-Nluc all show a significant reduction of Nluc-activity levels as compared to the naïve AF5 cells (Fig. 3D). While SFV primed cells infected with BUNV-Nluc do not display any significant differences (Fig. 3E), a ~60% decline in Nluc activity levels can be observed in ZIKV primed cells infected with BUNV-Nluc as opposed to control (Fig. 3F).

Some significant changes can be observed in the CFAV re-infected versus CFAV negative clones, most notably it seems that upon BUNV-Nluc infection, the CFAV re-infected clones exhibit an increase in Nluc activity in comparison to the CFAV negative clone (Fig. 3A and E) while for SFV-Nluc infection this effect is inverted (Fig. 3B and D). In most cases however, the changes, while significant, are not responsible for the overall observable effects, thus for the following experiments the CFAV negative samples were used.

Clone-specificity is also observable for small RNA production in infected primed cells.

Next, we investigated possible changes in small RNA production in primed cells after a second arboviral infection. For this, the primed cells alongside naïve AF5 cells, as control, were “re-“ infected with either BUNV-Nluc, SFV-Nluc or ZIKV-Nluc at MOI 1 and sent for small RNA sequencing after total RNA isolation at 48 hpi (BUNV, SFV) or 96 hpi (ZIKV). All samples exhibited small RNA read lengths in the raw population corresponding to micro (mi)RNAs (22-23 nt), siRNAs (21 nt) and piRNAs (25-28 nt) (Fig. S1-S3).

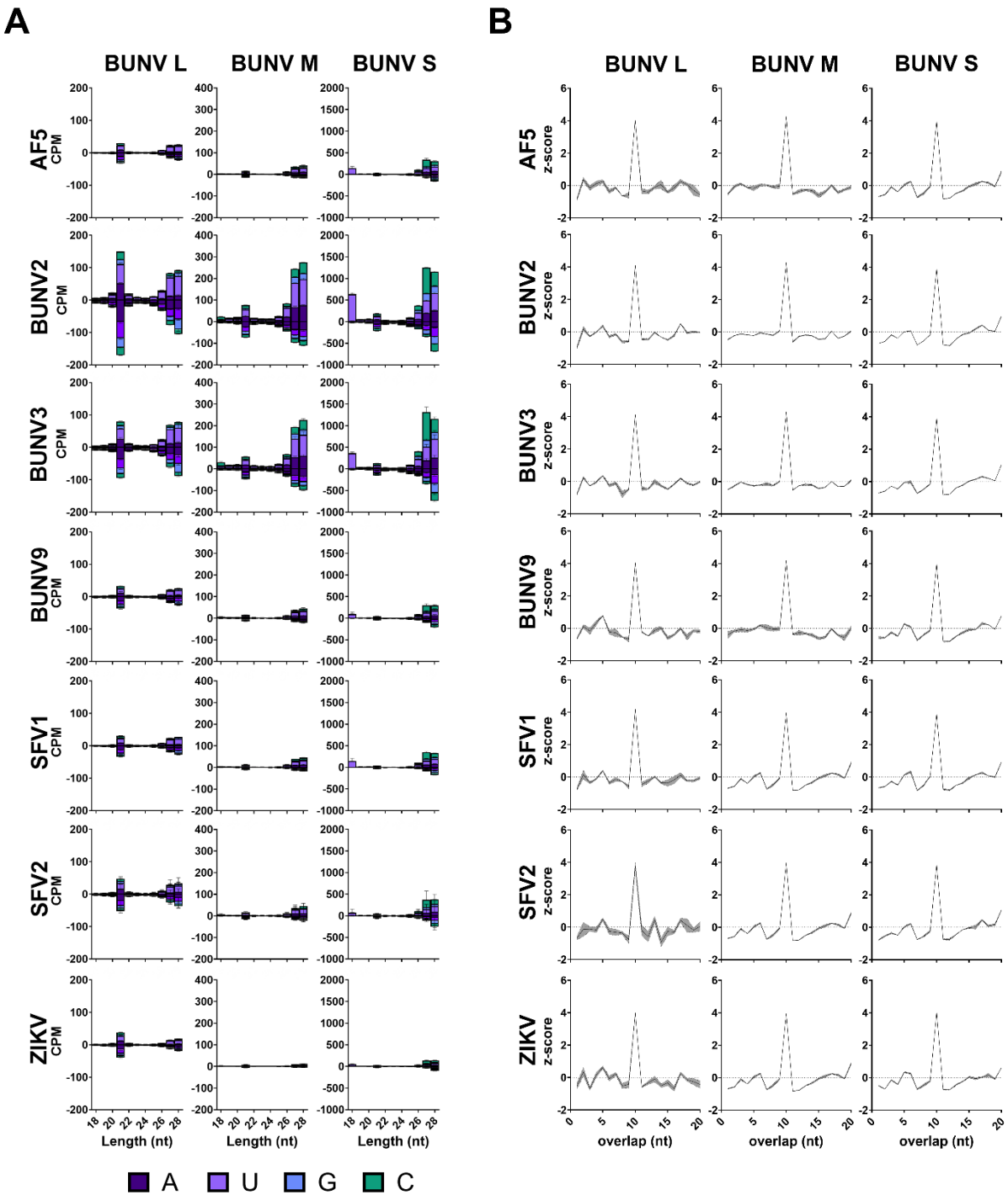


Fig. 4: Small RNA sequencing results of primed cells infected with BUNV-Nluc exhibited clone-specific differences. After production of BUNV, SFV and ZIKV primed AF5 cells, the cells were infected with BUNV-Nluc alongside naïve AF5 cells, as control, before total RNA extraction and small RNA sequencing. **(A)** Size distribution histogram of small RNA reads of 18-28 nt length after BUNV-Nluc infection. sRNA reads were mapped to BUNV (GenBank ID: NC_001927.1 [BUNV L-Segment], NC_001926.1 [BUNV M-Segment] and NC_001925.1 [BUNV S-Segment]) antigenome (positive numbers) and genome (negative numbers) with results shown in counts per million (CPM) ± SD from three independent experiments. The colours indicate first nucleotide prevalence (Adenine – dark purple, Uracil – light purple, Guanine – blue, Cytosine – green). **(B)** Overlapping pairs probability z-scores of 25-28 nt virus-derived sRNAs. Grey region indicates range of the three independent experiments.

In case of the BUNV-Nluc infected primed cells, virus-derived sRNAs mapped to all three segments of the BUNV genome and antigenome for all treatments (Fig. 4A). Across all samples, most reads mapped to the BUNV S-segment while the number of reads mapping to the M- and L-segments was generally comparable to each other (Table S8). Reviewing the small RNA size distribution results of the BUNV-Nluc infected samples (Fig. 4A), both clones of SFV primed cells (SFV-1 and SFV-2) and ZIKV primed cells showed small RNA production comparable to the naïve cells experiencing arboviral challenge for the first time, while the BUNV primed cells did not behave uniformly. The BUNV-9 clone also showed small RNA production at naïve cell level, however, the two other clones, BUNV-2 and BUNV-3 exhibited heightened production of BUNV specific small RNAs across all three segments with ~0.80% and ~0.71% of total sRNA reads versus ~0.18% in case of the naïve AF5 cells.

Both, vsiRNA- (21 nt) and vpiRNA-sized (25-28 nt) factions can be observed across all BUNV-Nluc infected samples and segments, with the larger vpiRNA-sized sRNA fraction showing the typical characteristics of ping-pong amplified piRNAs. These include the A_{10}/U_1 bias (Fig. S5) and the 10 nt overlap (Fig. 4B). Both vsiRNAs and vpiRNAs map along the whole genome and antigenome of BUNV (Fig. 5A and B), with the S-segment presenting as the main producer in both cases. In contrast to the vsiRNAs however, which map evenly in both directions of the genome, the vpiRNAs show a bias of increased mapping to the antigenome (Fig. S4).

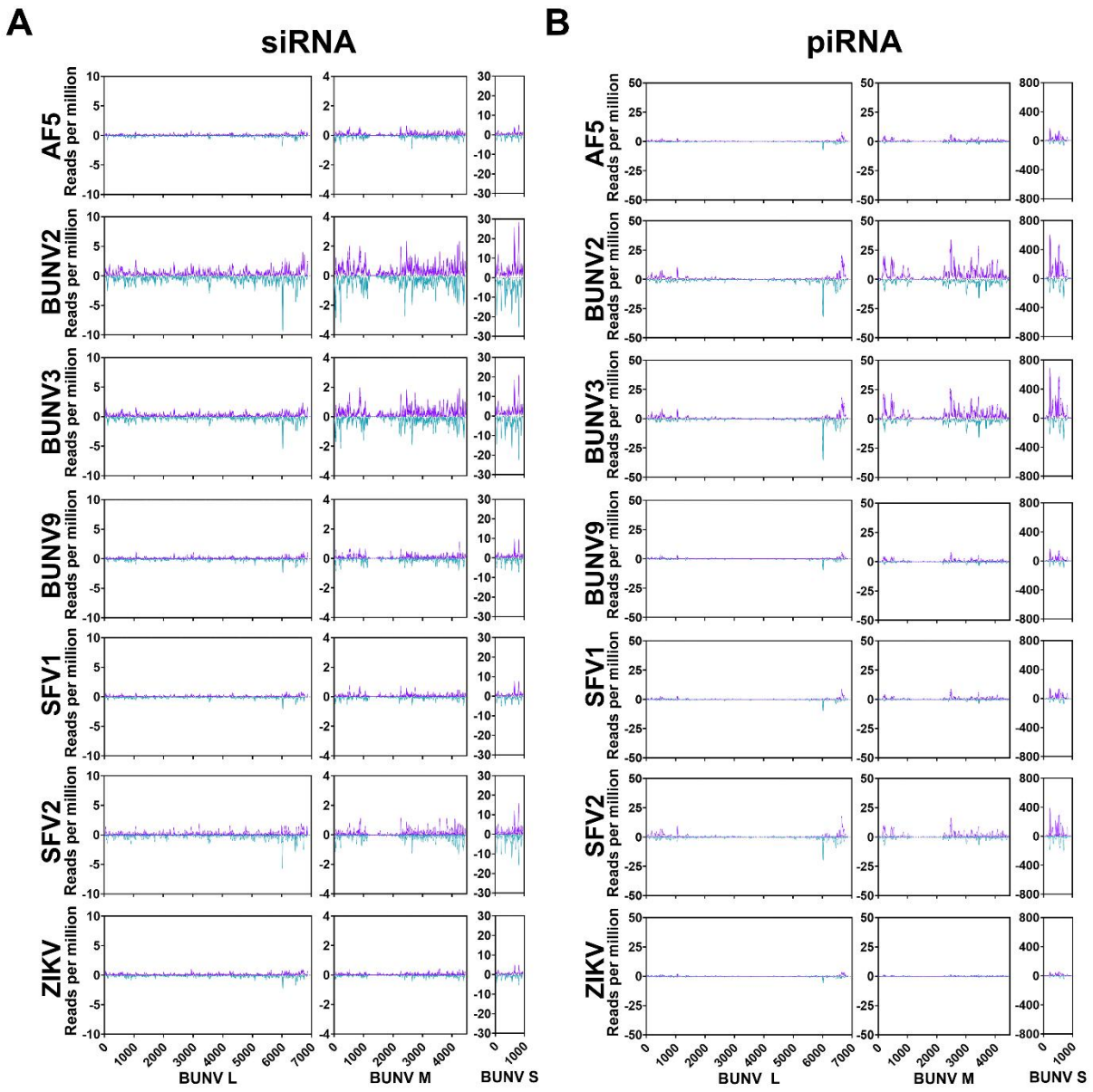


Fig. 5: siRNA and piRNA coverage plots of primed cells after BUNV infection. After production of BUNV, SFV and ZIKV primed AF5 cells, the cells were infected with BUNV-Nluc alongside naïve AF5 cells, as control, before total RNA extraction and small RNA sequencing. BUNV mapped **(A)** 21 nt siRNAs and **(B)** 25-28 nt piRNAs of BUNV, SFV and ZIKV primed cells together with naïve AF5 cells as control, were infected with BUNV-Nluc with purple indicating antigenome mapping and blue indicating genomic mapping. Results are presented in reads per million for the BUNV L (left), BUNV M (middle) and BUNV S-Segment (right) from three independent experiments.

After SFV-Nluc infection, all conditions exhibited virus-derived sRNAs mapping to the SFV genome and antigenome (Fig. 6A). Again, the BUNV-Nluc primed cells show inconsistent small RNA production between different clones. BUNV-9 produces less SFV-specific sRNAs (~0.12% of total reads mapped to the SFV genome; Table S9) than the naïve AF5 control (~0.27%), BUNV-3 exhibiting sRNA levels comparable to the control (~0.31%), and BUNV-2 showing a steep increase in SFV-specific sRNA production (~0.84%). In contrast, both SFV-Nluc primed clones showed percentages of mapped sRNAs comparable to the control, with

SFV-1 displaying a slightly higher percentage (~0.38%) than the SFV-2 clone (~0.32%). Lastly, the ZIKV-Nluc primed cells demonstrated a slight decrease in SFV-specific sRNA production (~0.19%) in comparison to naïve AF5 cells.

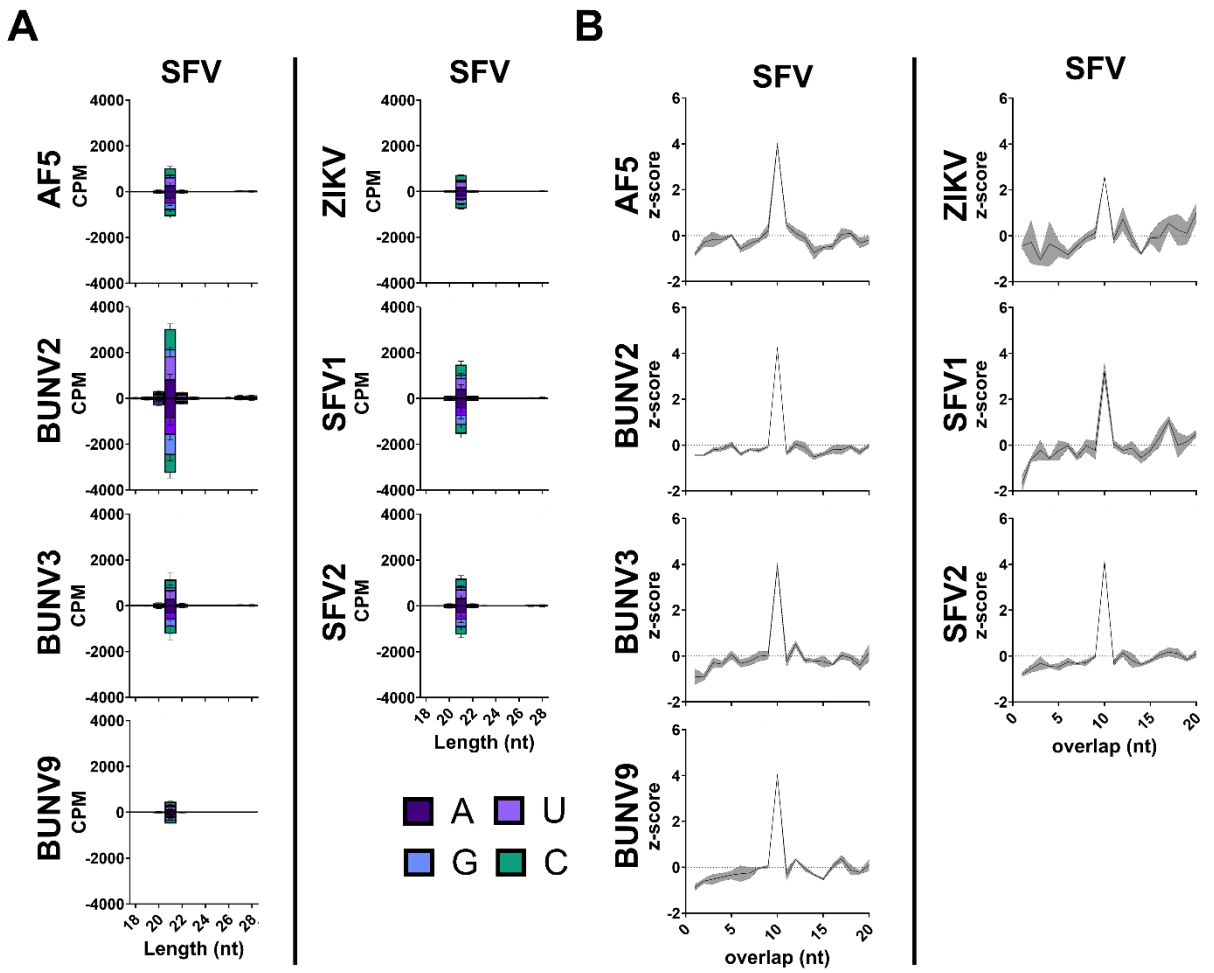


Fig. 6: Small RNA sequencing results of primed cells infected with SFV-Nluc exhibited clone- and virus-specific differences. BUNV, SFV and ZIKV primed AF5 cells were infected with SFV-Nluc alongside naïve AF5 cells, as control, before total RNA extraction and small RNA sequencing. **(A)** Size distribution histogram of small RNA reads of 18-28 nt length after SFV-Nluc infection. sRNA reads were mapped to the SFV (SFV6; GenBank ID: KT009012.1) genome (positive numbers) and anti-genome (negative numbers) with results shown in counts per million (CPM) ± SD from three independent experiments. The colours indicate first nucleotide prevalence (Adenine – dark purple, Uracil – light purple, Guanine – blue, Cytosine – green). **(B)** Probability of overlapping pairs z-score of 25-28 nt virus-derived sRNAs. Grey region indicates range of the three independent experiments.

Noticeably, all samples display a strong bias towards 21 nt vsiRNA-sized sRNAs with very little vpiRNA-sized sRNAs (25-28 nt). Despite the small number, the vpiRNA-sized fraction exhibits the 10 nt overlap (Fig. 6B) typical for ping-pong amplified piRNAs. However, the U_1/A_{10} bias is not observed asa clear U_1 frequency (Fig. S5) is mostly missing. While the vsiRNAs map relatively evenly across the whole SFV genome and antigenome (Fig. 7A), the smaller fraction of vpiRNAs show a bias towards genome mapping, as well as a clear hotspot around genome

position 8,000. Both the siRNA and piRNA mappings are consistent with previous studies (Schnettler et al., 2013; Varjak et al., 2018a).

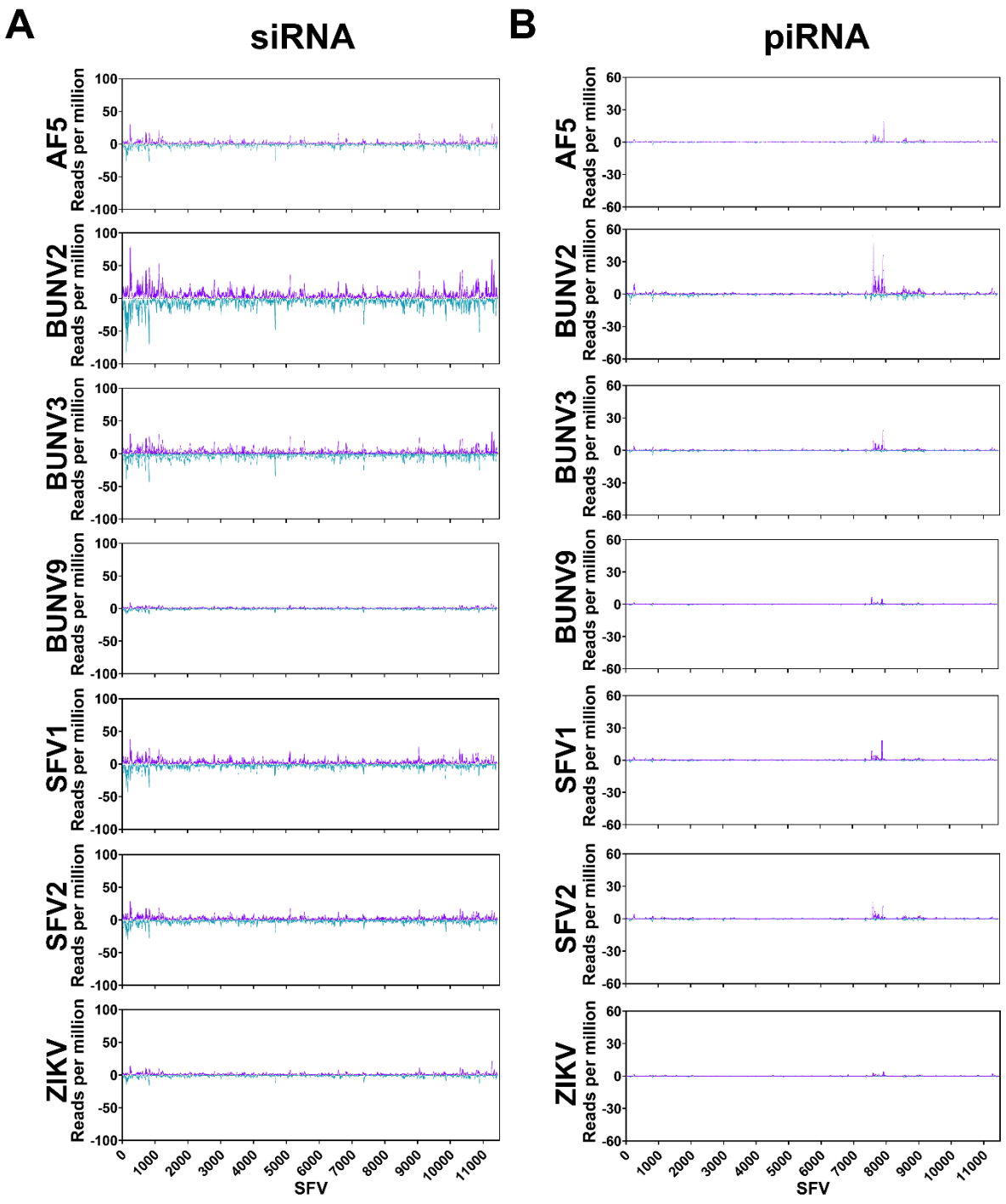


Fig. 7: siRNA and piRNA coverage plots of primed cells after SFV infection. BUNV, SFV and ZIKV primed AF5 cells were infected with SFV-Nluc alongside naïve AF5 cells, as control, before total RNA extraction and small RNA sequencing. SFV mapped **(A)** 21 nt siRNAs and **(B)** 25-28 nt piRNAs of BUNV, SFV and ZIKV primed cells infected with SFV-Nluc with naïve AF5 cells as control. Purple indicates genome mapping and blue indicates antigenomic mapping. Results are presented in reads per million from three independent experiments.

After ZIKV-Nluc infection of both ZIKV-Nluc primed cells and naïve AF5 cells, as control, total RNA was isolated, sequenced and mapped to the ZIKV genome and antigenome (Fig. 8A). While only a small percentage of the total sRNA reads mapped to ZIKV, the ZIKV primed cells still mapped to a lesser degree (~0.01%) than the naïve AF5 cells (~0.06%) (Table S10). As expected for ZIKV infection, the resulting vpiRNA-sized fraction (25-28 nt) does not exhibit ping-pong amplified characteristics, missing both the 10 nt overlap (Fig. 8B) and the U_1/A_{10} bias (Fig. S6). The vsiRNAs (21 nt) map evenly across the whole ZIKV genome and antigenome (Fig. 8C), while the few “vpiRNAs” (25-28 nt) map almost exclusively to the genome, specifically to two hotspots, one being at genome position ~9,200 and the other at ~10,000 (Fig. 8D).

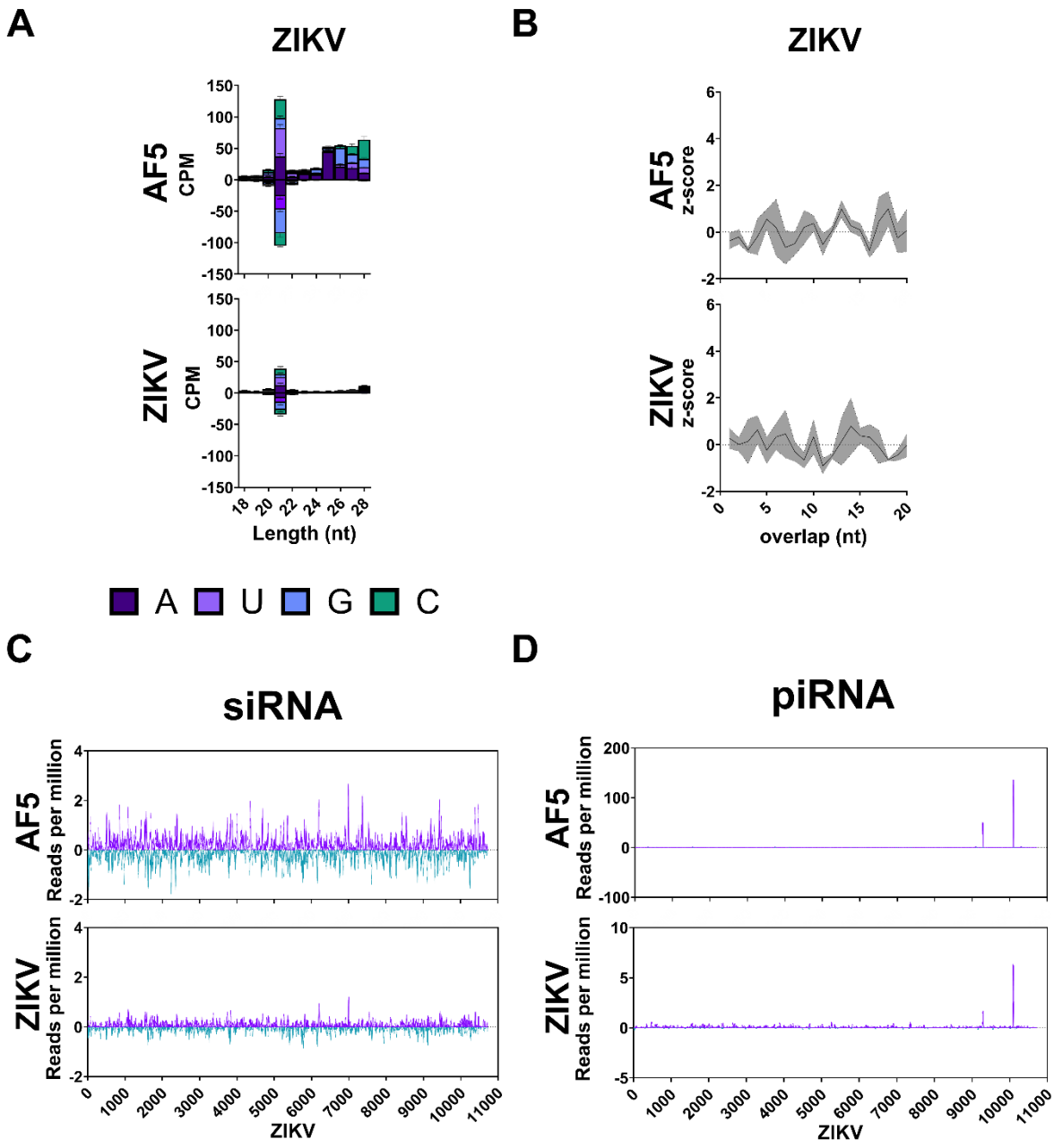


Fig. 8: Small RNA sequencing results of primed cells infected with ZIKV-Nluc. ZIKV primed AF5 cells were infected with ZIKV-Nluc alongside naïve AF5 cells, as control, before total RNA extraction and small RNA sequencing. **(A)** Size distribution histogram of small RNA reads of 18-28 nt length after ZIKV-Nluc infection. sRNA reads were mapped to the ZIKV (ZIKV strain BeH819015; GenBank: KU365778.1) genome (positive numbers) and anti-genome (negative numbers) with results shown in counts per million (CPM) ± SD from three independent experiments. The colours indicate first nucleotide prevalence (Adenine – dark purple, Uracil – light purple, Guanine – blue, Cytosine – green). **(B)** Probability of overlapping pairs z-score of 25-28 nt virus-derived sRNAs. Grey region indicates range of the three independent experiments. **(C)** 21 nt siRNAs and **(D)** 25-28 nt piRNAs of ZIKV primed cells infected with ZIKV-Nluc with naïve AF5 cells as control. Purple indicates genome mapping and blue indicates antigenomic mapping. Results are presented in reads per million from three independent experiments.

Uninfected primed cells do not exhibit clear small RNA production with the exception of the SFV-1 clone

After the small RNA sequencing of BUNV-Nluc, SFV-Nluc and ZIKV-Nluc exhibited inconsistent results across treatments and clones, the next step was to consider possible small RNA production after priming even in the absence of active arboviral infection. For this, RNA was directly isolated from uninfected BUNV, SFV and ZIKV primed cells together with naïve AF5 cells, as control, for additional small RNA sequencing. The control sample is the same for Figures 7-9, mapped to the respective virus genome. The size distribution of the raw libraries, again, shows sRNA lengths corresponding to siRNA (21 nt), miRNA (22-23 nt) and piRNA (25-28 nt) across all conditions (Fig. S7).

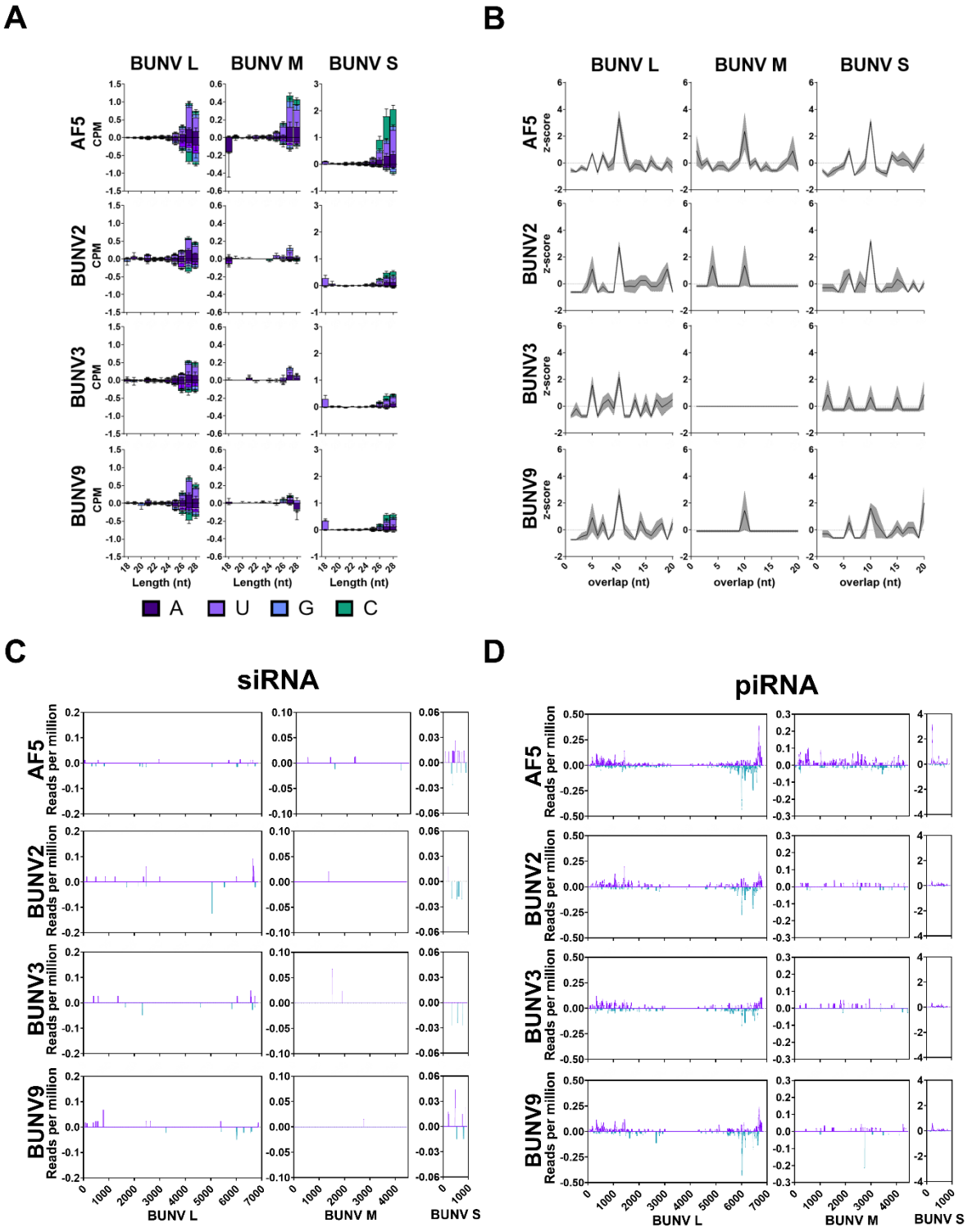


Fig. 9: Small RNA sequencing results of uninfected BUNV primed cells. BUNV primed AF5 cells and naïve AF5 cells for control were used for total RNA extraction and small RNA sequencing. **(A)** Size distribution histogram of small RNA reads of 18-28 nt length. sRNA reads were mapped to the BUNV (GenBank ID: NC_001927.1 [BUNV L-Segment], NC_001926.1 [BUNV M-Segment] and NC_001925.1 [BUNV S-Segment]) antigenome (positive numbers) and genome (negative numbers) with results shown in counts per million (CPM) ± SD from three independent experiments. The colours indicate first nucleotide prevalence (Adenine – dark purple, Uracil – light purple, Guanine – blue, Cytosine – green). **(B)** Probability of overlapping pairs z-score of 25-28 nt virus-derived sRNAs. Grey region indicates range of the three independent experiments. **(C)** 21 nt siRNAs and **(D)** 25-28 nt piRNAs with purple

indicating antigenome mapping and blue indicating genomic mapping. Results are presented in reads per million from three independent experiments.

While sRNAs mapping to both the genome and antigenome of all three BUNV segments can be observed in all BUNV primed cells, the same can also be observed for the naïve AF5 cells (Fig. 9A). Additionally, the CPM are very low in all four cases, meaning the sRNAs in question are likely a result of common contamination during library preperation and sequencing. Due to the low numbers of mapped reads (Table S11), the vpiRNA-sized fraction of reads (25-28 nt), which clearly outnumbers the vsiRNAs (21 nt), shows inconclusive results for both the 10 nt overlap (Fig. 9B) and the U_1/A_{10} bias (Fig. S8) typical for ping-pong amplified piRNAs. As the number of vsiRNAs is even lower than the vpiRNAs, no even mapping across the BUNV antigenome and genome can be observed (Fig. 9C), while for the vpiRNAs a clear mapping bias towards the antigenome can be noted (Fig. 9D, Fig. S8), consistent with the vpiRNA mapping from the BUNV-Nluc infected primed cells (Fig. 5B).

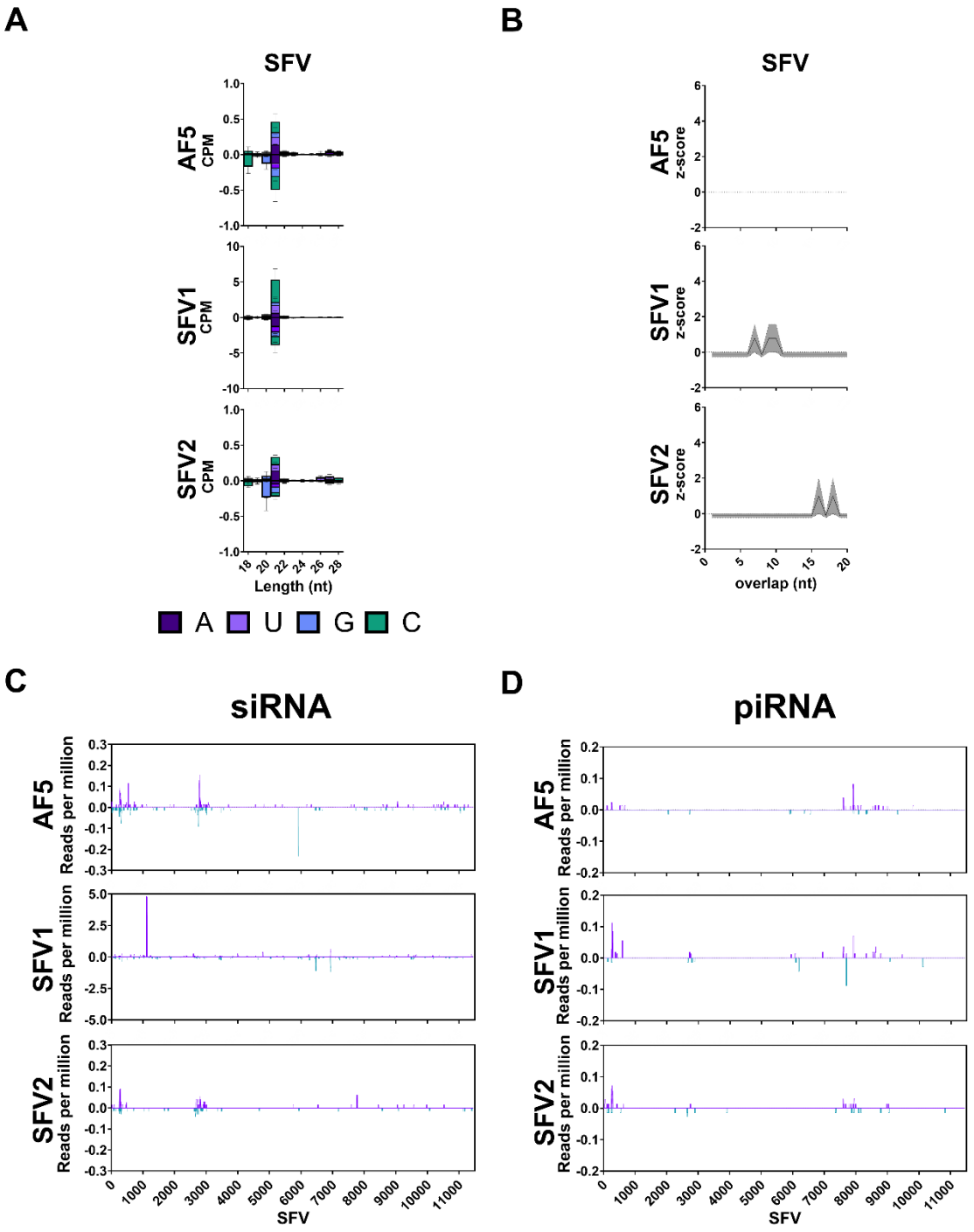


Fig. 10: Small RNA sequencing results of uninfected SFV primed cells. SFV primed AF5 cells and naïve AF5 cells, as control, were used for total RNA extraction and small RNA sequencing. **(A)** Size distribution histogram of small RNA reads of 18-28 nt length. sRNA reads were mapped to the SFV (SFV6; GenBank ID: KT009012.1) genome (positive numbers) and anti-genome (negative numbers) with results shown in counts per million (CPM) ± SD from three independent experiments. The colours indicate first nucleotide prevalence (Adenine – dark purple, Uracil – light purple, Guanine – blue, Cytosine – green). **(B)** Probability of overlapping pairs z-score of 25-28 nt virus-derived sRNAs. Grey region indicates range of the three independent experiments. **(C)** 21 nt siRNAs and **(D)** 25-28 nt piRNAs with purple

indicating genome mapping and blue indicating antigenomic mapping. Results are presented in reads per million from three independent experiments.

The uninfected SFV primed cells also exhibit sRNAs mapping to both the SFV genome and antigenome (Fig. 10A), with naïve AF5 cells and the SFV-2 clone again exhibiting very low amounts of sRNAs mapping to the SFV genome (Table S12) indicating possible contamination. However, the SFV-1 primed cells show an approximately ten-fold higher number of mapped sRNA reads, mostly with a length of 21 nt. Due to the low number of mapped sRNA, no characteristic 10 nt overlap (Fig. 10B) or U_1/A_{10} bias (Fig. S9) can be observed. Additionally, the vsiRNA-sized (21 nt) and vpiRNA-sized (25-28 nt) fractions map only sparsely over the genome and antigenome (Fig. 10C and D), yet there is a slight display of the typical vpiRNA genome hotspot at genome position 8,000, which is consistent with the mapping of SFV-derived vpiRNAs in SFV-Nluc infected primed cells (Fig. 7B).

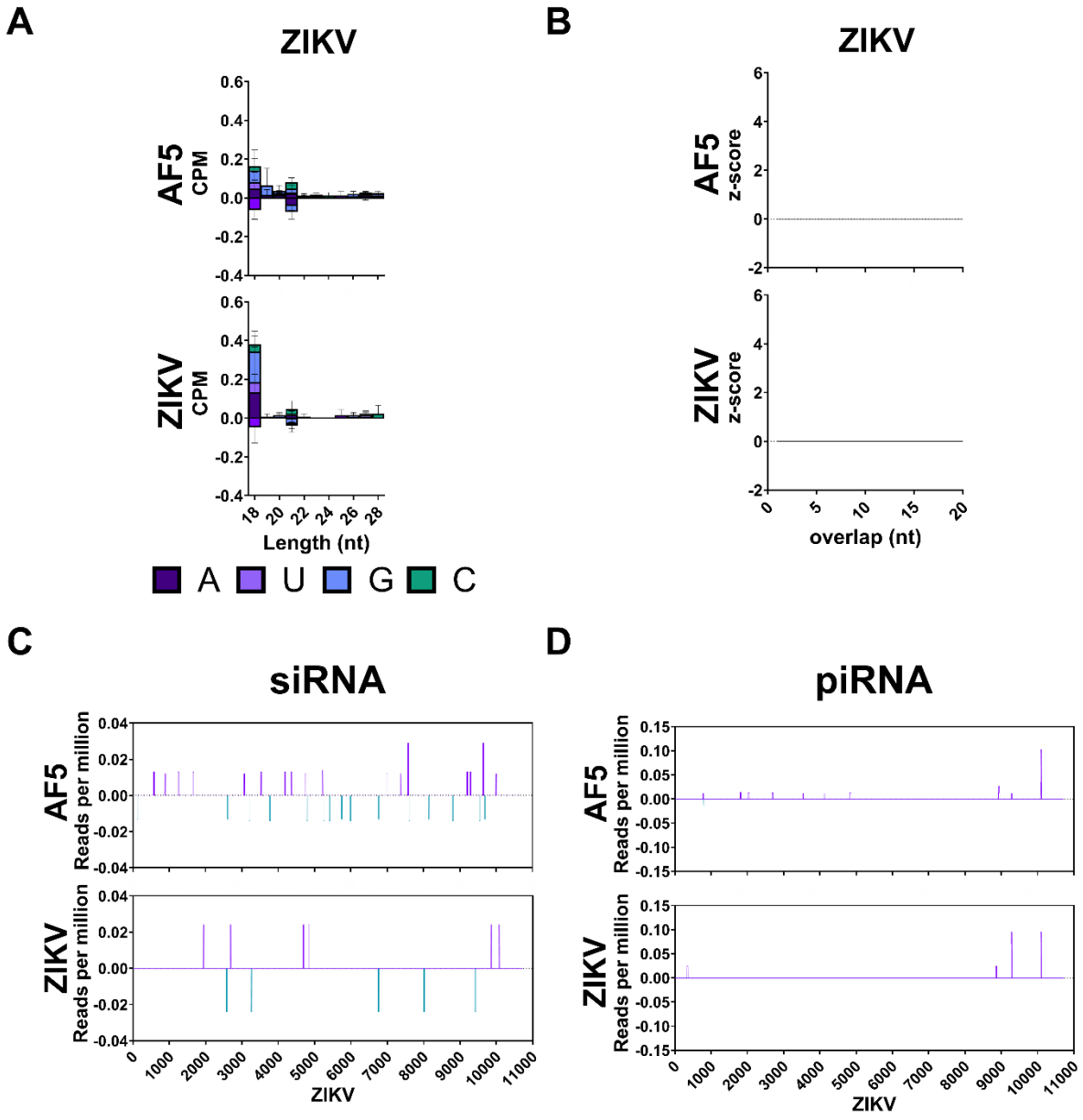


Fig. 11: Small RNA sequencing results of uninfected ZIKV primed cells. ZIKV primed AF5 cells and naïve AF5 cells, as control were used for total RNA extraction and small RNA sequencing. **(A)** Size distribution histogram of small RNA reads of 18-28 nt length. sRNA reads were mapped to the ZIKV (ZIKV strain BeH819015; GenBank: KU365778.1) genome (positive numbers) and anti-genome (negative numbers) with results shown in counts per million (CPM) ± SD from three independent experiments. The colours indicate first nucleotide prevalence (Adenine – dark purple, Uracil – light purple, Guanine – blue, Cytosine – green). **(B)** Probability of overlapping pairs z-score of 25-28 nt virus-derived sRNAs. Grey region indicates range of the three independent experiments. **(C)** 21 nt siRNAs and **(D)** 25-28 nt piRNAs with purple indicating genome mapping and blue indicating antigenomic mapping. Results are presented in reads per million from three independent experiments.

As with the previously mentioned primed cells, the ZIKV-Nluc primed cells also exhibit signs of contamination rather than true small RNA production with only a very low number of sRNAs mapping to the ZIKV genome and antigenome (Fig. 11A). While a lack of 10 nt overlap (Fig. 11B) and U_1/A_{10} bias (Fig. S10) of vpiRNA-sized sRNAs is characteristic for ZIKV infection, no conclusive statement can be made, again due to the low number of mappings (Table S13). This also continues with the sRNAs of vsiRNA (21 nt) length showing patchy genome and antigenome mapping (Fig. 11C), yet the vpiRNA-sized (25-28 nt) fraction does again almost exclusively map to the ZIKV genome, also exhibiting the hotspots at ~9,200 and ~10,000 (Fig. 11D).

Effect of priming on the viral RNA in “re-“ infected cells

The observed reduction in virus infection as determined by reduced luciferase activity in some of the primed, “re-“ infected cells, including clone-specific differences as observed for the SFV primed clones upon SFV-Nluc re-infection, was hypothesized to lead to a corresponding change in vRNA production. However, primed clones exhibiting decreased viral replication upon secondary infection did not consistently show a corresponding sRNA response. A reason for this could be the difference in detection methods or the different passage numbers of the cells used for both experiments with the cells used for luciferase reporter assays ~40 passages younger than those used for small RNA sequencing. Therefore, we decided to determine the effect of priming on virus infection directly in the same sample used for sRNA sequencing. Therefore, cDNA synthesis with random hexamers and subsequent qRT-PCR with the corresponding virus-specific primers and S7 ribosomal RNA as housekeeper was performed (for primers see Table S1). All respective p-values according to Student’s t-test can be found in Tables S14-S19.

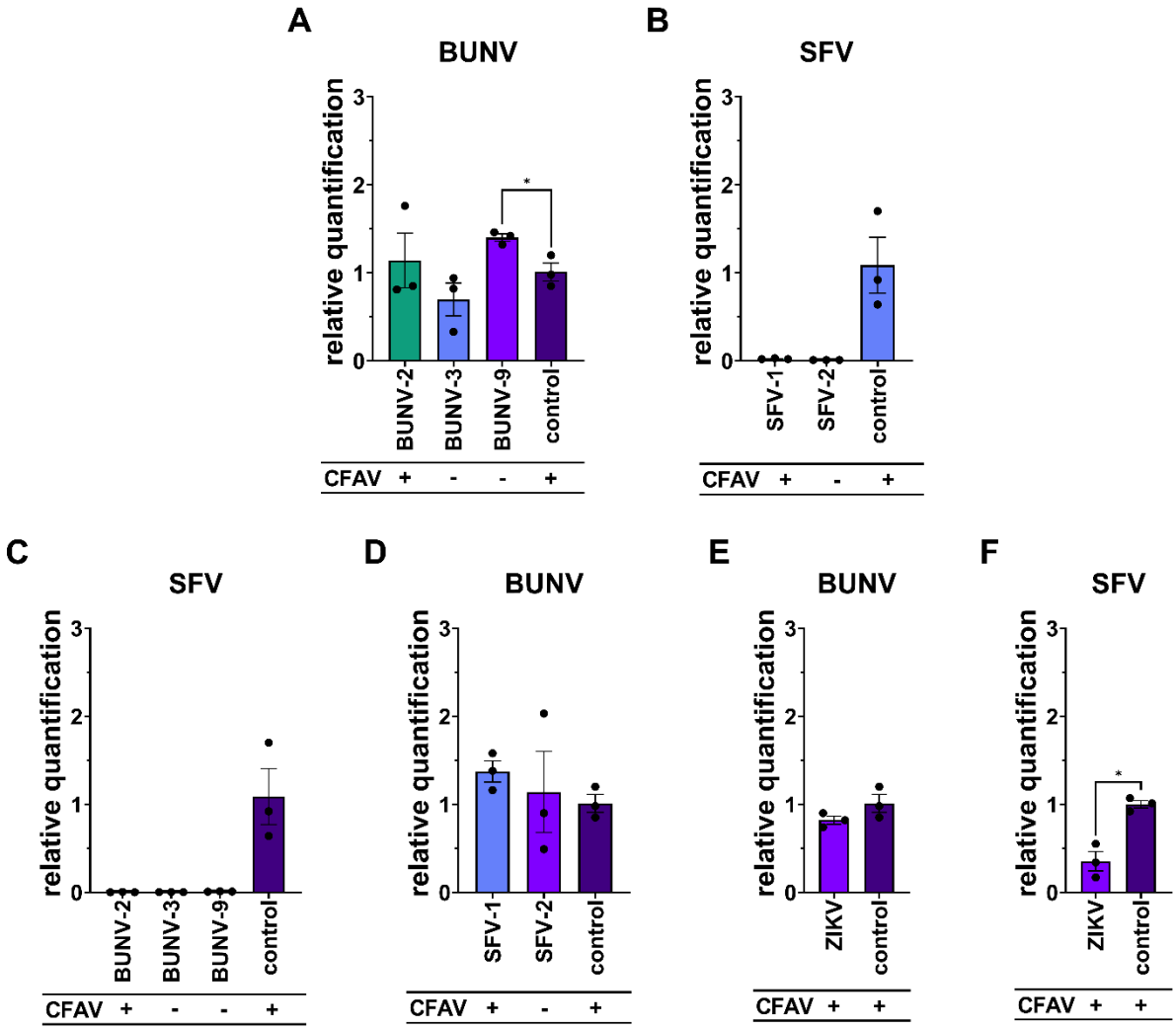


Fig. 12: Effect on viral RNA of BUNV, SFV and ZIKV primed cells upon re-infection. RNA isolated for the small RNA sequencings (Fig. 2-6) was used for cDNA synthesis using random hexamers and subsequent qRT-PCR. Results are shown for BUNV primed cells infected with BUNV-Nluc **(A)** or SFV-Nluc **(C)**, SFV primed cells infected with SFV-Nluc **(B)** or BUNV-Nluc **(D)**, and ZIKV primed cells infected with BUNV-Nluc **(E)** or SFV-Nluc **(F)**. Relative quantification ± SEM was calculated using the housekeeper gene S7 ribosomal RNA and naïve AF5 cells as control set to 1. qRT-PCR was performed with three independent biological replicates and technical triplicates, with * = $p<0.05$ as according to Student's t-test. CFAV presence or absence shown on the bottom.

Again, the BUNV primed cells do not exhibit drastic changes after BUNV-Nluc re-infection (Fig. 12A). Both clones of the SFV primed SFV-Nluc re-infected cells now behave the same with both exhibiting a strong decrease in vRNA levels in comparison to the naïve control; yet no significances could be detected, likely due to scattered control results (Fig. 12B). Similarly, all three BUNV primed clones also have highly decreased SFV-specific vRNA levels, with again no detectable significances (Fig. 12C). Both clones of SFV primed cells re-infected with BUNV-Nluc behave similarly to the BUNV primed cells in that they display reduced vRNA comparable to the naïve control (Fig. 12D). Lastly, the ZIKV primed cells showed no significant changes in comparison to the control after BUNV-Nluc infection (Fig. 12E), but do also exhibit a significant decrease in SFV-specific vRNA levels after SFV-Nluc infection (Fig. 12F). Unfortunately, too little RNA of ZIKV primed cells re-infected with ZIKV-Nluc was left after small RNA sequencing, therefore no cDNA could be synthesized and thus no qRT-PCR was performed.

BUNV primed cells show inconsistent vRNA levels for different bunya- and alphaviruses

After BUNV primed cells exhibited decreased luciferase expression and vRNA levels upon SFV-Nluc infection, we set out to investigate further if we can see similar results using different viruses. Therefore, we used Tahyna virus (TAHV), another bunyavirus closely related to BUNV, and two other alphaviruses, Sindbis virus (SINV) and O'nyong Nyong virus (ONNV). For this, BUNV primed cells, this time having ~60 passages less than the cells used for small RNA sequencing, were seeded alongside naïve AF5 cells as control and infected with either of the viruses at MOI 0.1 (BUNV, TAHV, SFV, SINV and ONNV). At 48 hpi, total RNA was isolated and synthesized into cDNA using random hexamers, before being used for qRT-PCR with virus specific primers and S7 ribosomal RNA specific primer as housekeeper (for primers see Table S1). The p-values according to Student's t-test can be found in Tables S20-S24.

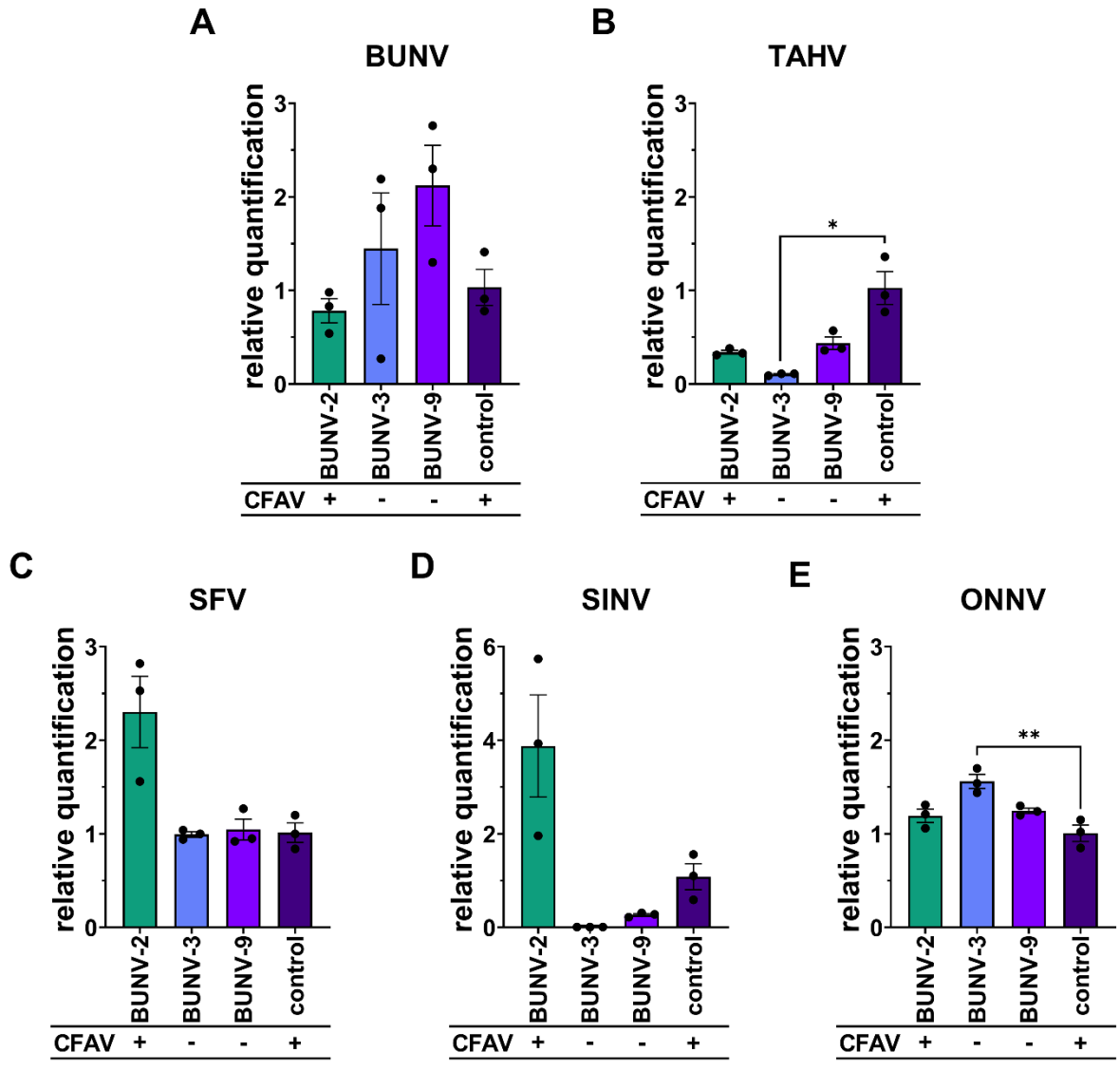


Fig. 13: vRNA levels in BUNV primed cells after infection with different bunya- and alphaviruses. BUNV primed cells or naïve AF5 cells (as control) were infected with either **(A)** BUNV-Nluc, **(B)** TAHV, **(C)** SFV-Nluc, **(D)** SINV or **(E)** ONNV at MOI 0.1. Total RNA was isolated at 48hpi before cDNA synthesis using random hexamers and subsequent qRT-PCR using virus-specific primers and primers for S7 ribosomal RNA as a housekeeper gene. The

cells used for these experiments were approximately 60 passages lower than those used for the small RNA sequencing. Relative quantification was calculated against naïve AF5 cells as control set to 1. qRT-PCR was performed with three independent biological replicates and technical triplicates, with * = $p<0.05$ as according to Student's t-test. CFAV presence or absence shown on the bottom.

While again no significant changes can be observed after BUNV-Nluc re-infection in comparison to the naïve AF5 cells (Fig. 13A), all three clones exhibit a strong decrease in TAHV-specific vRNA levels, with BUNV-3 even showing a significant decrease of ~90% (Fig. 13B). Despite previously exhibiting strong decrease of vRNA of SFV-Nluc, all three BUNV-Nluc clones now show no significant changes in SFV-specific vRNA levels when compared to the control. Interestingly, viral SFV RNA even shows a non-significant, yet clear, increase for BUNV-2 primed cells (Fig. 13C). While no significances between the three clones and the control can be detected after SINV infection, BUNV-2 shows a steep increase in SINV-specific vRNAs (as observed for SFV), while both BUNV-3 and BUNV-9 show a strong decrease (Fig. 13D). Lastly, both BUNV-2 and BUNV-9 display ONNV-specific vRNA detection comparable to the control cells, while BUNV-3 shows a significant increase of ~60% (Fig. 13E).

Discussion

To this day, little is known about the incorporation of ISV-specific NIRVS in the mosquito genome, and even less about possible arboviral NIRVS. It is likely that the process begins with the production of vDNA from the predominantly RNA genome viruses that are part of the different arboviral families as vDNA production has been proven to take place after infection with different arboviruses, including members of the *Flaviviridae* (WNV, DENV, ZIKV), *Togaviridae* (CHIKV, SFV) and *Peribunyaviridae* (BUNV) (Altinli et al., 2023; Goic et al., 2016; Marconcini et al., 2021; Nag et al., 2016; Nag and Kramer, 2017; Rodriguez-Andres et al., 2023; Rückert et al., 2019b). While WNV, DENV and ZIKV vDNA has been studied after persistent infection, CHIKV and BUNV vDNA has only been studied after acute infection, with BUNV and WNV specifically in *Culex*-derived HSU and/ or CT cells, while the others have been tested in *Aedes*-derived cells, and *Aedes*-mosquitoes (in case of ZIKV and CHIKV). In most cases, the vDNA was shown after total DNA extraction, however, for WNV, DENV and SFV, vDNA was shown within genomic DNA, with SFV-specific DNA found in both genomic DNA and episomes (Nag et al., 2016; Rodriguez-Andres et al., 2023). Here, we showed vDNA production after SFV and BUNV infection in *Aedes*-derived cells, both after acute and persistent infection. Additionally, we also showed the production of RVFV-specific vDNA after acute infection. In each case, vDNA production has been demonstrated in both total DNA isolated and genomic DNA, supporting the hypothesis of incorporation of the vDNA into the mosquito genome. vDNA was detected both in AF5 but also AF319 cells, which lack Dcr2, leading to the observation that Dcr2, and thus the siRNA pathway in general, seem to not be involved in vDNA production.

Multiple different studies have previously shown vpiRNAs produced from NIRVS, illustrating their importance for an "adaptive" antiviral defense (Palatini et al., 2017; Suzuki et al., 2020, 2017; Tassetto et al., 2019; ter Horst et al., 2019; Whitfield et al., 2017). To investigate the effect of viral priming on small RNA production, the sRNAs mapping to BUNV, SFV and ZIKV from BUNV-Nluc, SFV-Nluc and ZIKV-Nluc primed cells were analysed both during acute infection and in the uninfected state. BUNV-specific sRNAs predominantly mapped to the S-segment (Fig. 4 and 5), with vpiRNAs exhibiting ping-pong amplified characteristics (Fig. 4 and

S5), aligning with previous reports (Altinli et al., 2023; Dietrich et al., 2017b). SFV-specific vsiRNAs mapped across the whole genome and antigenome, while vpiRNAs almost exclusively mapped a hotspot region around genome position 8,000 (Fig. 7), which also aligns with previous studies for SFV but also other alphaviruses like CHIKV and SINV (Goic et al., 2016; Morazzani et al., 2012; Schnettler et al., 2013; Varjak et al., 2018a; Vodovar et al., 2012). This includes a predominantly siRNA-based sRNA production, with the few vpiRNAs produced mainly mapping to the genome. This is also visible in the fact that despite exhibiting a 10 nt overlap (Fig. 6), no clear U_1 bias is observable despite a strong A_{10} presence (Fig. S6), hinting at a heightened production of sense versus antisense vpiRNAs. This inconsistency to previous publications regarding alphaviral and SFV-specific vpiRNA signatures could be due to differences in protocol or small RNA sequencing reactions. Lastly, ZIKV-specific sRNA production included vsiRNAs mapping across the whole genome and antigenome, while a characteristic absence of ping-pong amplified markers in the piRNA-sized fraction was observed (Fig. 8 and S7), with almost the entire 25-28 nt long sRNAs mapping to hotspots in the genomic direction, consistent with prior research (Varjak et al., 2017a).

Across all small RNA sequencing results of acutely infected primed cells, the BUNV-Nluc and SFV-Nluc primed cells do not exhibit consistent behaviour, exhibiting clone-specific effects. This inconsistency also includes apparent effects on small RNA production in cells primed with a virus that differs from the current infection, e.g. the BUNV-2 clone exhibiting an exacerbated RNAi response upon SFV-Nluc infection as compared to the naïve cell control (Fig. 4). However, in case of the BUNV primed cells, we see a consistency in sRNA production between clones independent of infecting virus: BUNV-2 produces the most sRNAs for both SFV-Nluc and BUNV-Nluc, while BUNV-9 shows the lowest sRNA production in both cases. This possibly shows that the effects we are seeing might not solely be due to the priming itself, but rather might include changes in the cells triggered by clearing of the infection using dsRNA and subsequent single cell seeding, possibly changing the general behaviour of the antiviral response upon subsequent arboviral challenge. Possible clone-specific differences for ZIKV-Nluc can not be discussed, as only one surviving clone could be used. Nevertheless, while the effects in the SFV and BUNV primed cells led to heightened sRNA production in comparison to the naïve AF5 cells, the ZIKV primed cells exhibited a reduction in ZIKV-specific sRNAs upon re-infection with ZIKV-Nluc (Fig. 8), presenting an opposing effect.

As for the uninfected primed cells, only the SFV-1 clone showed clear SFV-specific sRNA production, while all other primed cells showed only low levels of sRNAs, which could be due to incorporated arboviral vDNA generally producing very few sRNAs in absence of an active infection (Fig. 9-11). However, we also see comparable low levels of sRNAs in the naïve cells which did not undergo any priming and thus lack incorporated arboviral vDNA, meaning these few detected sRNAs could possibly be due to contamination during sample and library preparation (Fig. 9-11). Based on previous studies, we expected a production of NIRVS-derived vpiRNAs even in currently uninfected cells (Rodriguez-Andres et al., 2023; Tassetto et al., 2019), yet little to no piRNA-sized sRNAs were observed, instead mostly vsiRNAs were produced, consistent with the results for the acutely SFV-Nluc infected cells (Fig. 6). For better understanding the differences between incorporated vDNA from different arboviral families, and clone-specific differences within the same priming viruses, future experiments should include vDNA detection via PCR and Whole Genome Sequencing to locate arboviral vDNA incorporation in the primed cells.

The antiviral activity of SFV, BUNV and ZIKV primed cells was investigated at different time points, once via luciferase reporter assay approximately 40 cell passages before the small RNA sequencing samples were prepared (t2), and once via qRT-PCR using cDNA synthesized from the small RNA sequencing samples (t3) (Fig. 3 and 12). Additionally, BUNV primed cells were again studied, this time using different bunya- and alphaviruses, at a time point 60 passages before preparation of the small RNA sequencing samples (t1) (Fig. 13).

Focussing on t2 and t3, BUNV primed cells showed antiviral activity comparable to the naïve control cells after BUNV-Nluc infection at both time points (Fig. 7-9). In contrast, BUNV primed cells exhibited reduced viral replication after SFV-Nluc infection, yet no significance was detected at the later time point despite all three clones exhibiting a higher reduction than the earlier time point. This is likely due to relatively high error in the control results. SFV primed cells also showed no changes in comparison to the control after BUNV-Nluc infection at both time points, yet while only one clone (SFV-2) exhibited a significant decrease in viral replication of SFV-Nluc, both clones had severely decreased SFV-specific RNA levels in comparison to the naïve cells at the later time point (again no significance due to scattered control). Lastly, ZIKV primed cells showed no visible difference when compared to the control after ZIKV-Nluc infection at the earlier time point, but a significant decrease in BUNV-Nluc replication. This effect was lost at the second time point with BUNV-specific vRNA levels comparable to the naive control cells. While too little ZIKV-Nluc infected ZIKV primed small RNA sequencing sample was left to evaluate the antiviral activity at the second time point, SFV-Nluc infected ZIKV-Nluc primed cell RNA was available, showing a significant reduction of vRNA levels. Across both experiments, with only one exception (SFV-1 clone at the earlier time point), all primed samples exhibit heightened antiviral activity after SFV-Nluc infection, regardless of the virus used for priming. This again might indicate that clearing of the previous infection and single cell seeding might have influenced the cells in a way that inhibits SFV infection, leading to reduced viral replication.

To investigate if these effects are exclusive to SFV or can be replicated with other alphaviruses, BUNV primed cells were infected with either SFV-Nluc, ONNV or SINV before RNA isolation and qRT-PCR (Fig. 13). Additionally, as no effects of the BUNV-Nluc priming were observed on repeated BUNV-Nluc infection, a close relative of BUNV, TAHV, was also used to investigate possible effects on the viral replication of other bunyaviruses. For this experiment, the cells had an even lower passage number than those of the previous luciferase assay as they were freshly revived from liquid nitrogen. Again, no significant effects were observed after BUNV-Nluc infection. Interestingly, THAV infection in all BUNV primed cell clones exhibited reduced TAHV-specific vRNA levels; yet only BUNV-3 showed significant reduction, likely due to the control showing relatively high SD. Surprisingly, the SFV-Nluc infected BUNV primed cells showed no reduced SFV RNA levels, although previously observed by luciferase and qRTPCR. One clone even exhibits heightened vRNA levels, even if no significance can be detected. The ONNV and SINV results show no significant changes between primed cells and control, yet BUNV-3 and BUNV-9 vRNA levels are reduced after SINV infection, and BUNV-3 vRNA levels are heightened after ONNV infection. Yet while we see no significant results for any of the alphaviruses at this time point, we have shown that at higher passage numbers (t2 and t3), SFV-Nluc infection in BUNV primed cells did lead to partially significant reductions. A similar results could also happen at higher passage numbers for the SINV and ONNV infected BUNV primed cells, but further experiments are needed to verify this. Generally, over all three “re-“ infection experiments, the results after SFV-Nluc infection seem to intensify at higher

passage numbers, supporting the idea of a time-dependent effect of priming, including production of NIRVS-specific sRNAs. Yet as we see the decrease in SFV replication over time in non-SFV primed cells, the effect we see might be due to single cell seeding. Another reason for the time-dependent changes might be a multitude of both mosquito and viral factors, including cell cycle stage, influence of different ISVs present in the cells like PCLV and their changing abundance, changes in methylation or chromatin interactions.

Further experiments have to be conducted to investigate this influence of single cell seeding on the cells, including experiments using control cells that were also seeded as single cell clones to remove these effects from the results, allowing for observation of the full priming effect as opposed to the mix of effects we are currently seeing. Additionally, while small RNA production after priming was thoroughly investigated in this paper, future research should include Whole Genome Sequencing of primed cells to directly locate arbovirus-derived NIRVS within the cell's genome, as well as transcriptomics to analyse a possible influence of NIRVS on transcripts.

In this study, we showed altered antiviral activity upon arboviral "re-" infection of primed cells, particularly reduced SFV replication across multiple independently primed clones and time points, suggesting a potential long-term priming effects associated with prior arboviral exposure, or both. However, the strong clone-specific variability observed both for antiviral activity and small RNA production for different priming conditions indicates that infection clearance and single-cell seeding may substantially influence the results and must be controlled in the future.

References

Altinli, M., Leggewie, M., Schulze, J., Gyanwali, R., Badusche, M., Sreenu, V.B., Fuss, J., Schnettler, E., 2023. Antiviral RNAi Response in Culex quinquefasciatus-Derived HSU Cells. Viruses 15, 436. https://doi.org/10.3390/v15020436

Ammerman, N.C., Beier-Sexton, M., Azad, A.F., 2008. Growth and Maintenance of Vero Cell Lines. Curr Protoc Microbiol APPENDIX, Appendix-4E. https://doi.org/10.1002/9780471729259.mca04es11

Antoniewski, C., 2014. Computing siRNA and piRNA Overlap Signatures, in: Werner, A. (Ed.), Animal Endo-SiRNAs: Methods and Protocols. Springer, New York, NY, pp. 135–146. https://doi.org/10.1007/978-1-4939-0931-5_12

Arensburger, P., Hice, R.H., Wright, J.A., Craig, N.L., Atkinson, P.W., 2011. The mosquito Aedes aegypti has a large genome size and high transposable element load but contains a low proportion of transposon-specific piRNAs. BMC Genomics 12, 606. https://doi.org/10.1186/1471-2164-12-606

Baidaliuk, A., Miot, E.F., Lequime, S., Moltini-Conclois, I., Delaigue, F., Dabo, S., Dickson, L.B., Aubry, F., Merkling, S.H., Cao-Lormeau, V.-M., Lambrechts, L., 2019. Cell-Fusing Agent Virus Reduces Arbovirus Dissemination in Aedes aegypti Mosquitoes In Vivo. Journal of Virology 93, 10.1128/jvi.00705-19. https://doi.org/10.1128/jvi.00705-19

Blair, C.D., Olson, K.E., Bonizzoni, M., 2019. The Widespread Occurrence and Potential Biological Roles of Endogenous Viral Elements in Insect Genomes. Current Issues in Molecular Biology 34, 13–30. https://doi.org/10.21775/cimb.034.013

Brackney, D.E., Scott, J.C., Sagawa, F., Woodward, J.E., Miller, N.A., Schilkey, F.D., Mudge, J., Wilusz, J., Olson, K.E., Blair, C.D., Ebel, G.D., 2010. C6/36 Aedes albopictus cells have a dysfunctional antiviral RNA interference response. PLoS Negl Trop Dis 4, e856. https://doi.org/10.1371/journal.pntd.0000856

Brady, O.J., Hay, S.I., 2020. The Global Expansion of Dengue: How Aedes aegypti Mosquitoes Enabled the First Pandemic Arbovirus. Annual Review of Entomology 65, 191–208. https://doi.org/10.1146/annurev-ento-011019-024918

Buchholz, U.J., Finke, S., Conzelmann, K.K., 1999. Generation of bovine respiratory syncytial virus (BRSV) from cDNA: BRSV NS2 is not essential for virus replication in tissue culture, and the human RSV leader region acts as a functional BRSV genome promoter. J Virol 73, 251–259. https://doi.org/10.1128/JVI.73.1.251-259.1999

Chary, S., Carreira, P.E., Nicholas, S., McNamara, K.B., Cockburn, I.A., Nordström, K., Jones, T.M., Gloag, R., Ashe, A., Hugo, L.E., Hayashi, R., 2025. Conserved but mechanistically diverse piRNA defence against gypsy LTR retrotransposons in insect ovaries. https://doi.org/10.1101/2025.09.05.674496

Chen, X.-G., Jiang, Xuanting, Gu, J., Xu, M., Wu, Y., Deng, Y., Zhang, C., Bonizzoni, M., Dermauw, W., Vontas, J., Armbruster, P., Huang, X., Yang, Y., Zhang, H., He, W., Peng, H., Liu, Y., Wu, K., Chen, J., Lirakis, M., Topalis, P., Van Leeuwen, T., Hall, A.B., Jiang, Xiaofang, Thorpe, C., Mueller, R.L., Sun, C., Waterhouse, R.M., Yan, G., Tu, Z.J., Fang, X., James, A.A., 2015. Genome sequence of the Asian Tiger mosquito, Aedes albopictus, reveals insights into its biology, genetics, and evolution. Proc Natl Acad Sci U S A 112, E5907-5915. https://doi.org/10.1073/pnas.1516410112

Crochu, S., Cook, S., Attoui, H., Charrel, R.N., De Chesse, R., Belhouchet, M., Lemasson, J.-J., de Micco, P., de Lamballerie, X., 2004. Sequences of flavivirus-related RNA viruses persist in DNA form integrated in the genome of Aedes spp. mosquitoes. J Gen Virol 85, 1971–1980. https://doi.org/10.1099/vir.0.79850-0

Crooks, G.E., Hon, G., Chandonia, J.-M., Brenner, S.E., 2004. WebLogo: A Sequence Logo Generator. Genome Research 14, 1188–1190. https://doi.org/10.1101/gr.849004

Dietrich, I., Shi, X., McFarlane, M., Watson, M., Blomström, A.-L., Skelton, J.K., Kohl, A., Elliott, R.M., Schnettler, E., 2017. The Antiviral RNAi Response in Vector and Non-vector Cells against

Orthobunyaviruses. PLOS Neglected Tropical Diseases 11, e0005272. https://doi.org/10.1371/journal.pntd.0005272
Elbashir, S.M., Lendeckel, W., Tuschl, T., 2001. RNA interference is mediated by 21- and 22-nucleotide RNAs. Genes Dev 15, 188–200. https://doi.org/10.1101/gad.862301
Fredericks, A.C., Russell, T.A., Wallace, L.E., Davidson, A.D., Fernandez-Sesma, A., Maringer, K., 2019. Aedes aegypti (Aag2)-derived clonal mosquito cell lines reveal the effects of pre-existing persistent infection with the insect-specific bunyavirus Phasi Charoen-like virus on arbovirus replication. PLoS Negl Trop Dis 13, e0007346. https://doi.org/10.1371/journal.pntd.0007346
Goic, B., Stapleford, K.A., Frangeul, L., Doucet, A.J., Gausson, V., Blanc, H., Schemmel-Jofre, N., Cristofari, G., Lambrechts, L., Vignuzzi, M., Saleh, M.-C., 2016. Virus-derived DNA drives mosquito vector tolerance to arboviral infection. Nat Commun 7, 12410. https://doi.org/10.1038/ncomms12410
Goic, B., Vodovar, N., Mondotte, J.A., Monot, C., Frangeul, L., Blanc, H., Gausson, V., Vera-Otarola, J., Cristofari, G., Saleh, M.-C., 2013. RNA-mediated interference and reverse transcription control the persistence of RNA viruses in the insect model Drosophila. Nat Immunol 14, 396–403. https://doi.org/10.1038/ni.2542
Gothe, S., Jagtap, S., Böhmer, P., Reuter, M., Frank, S., Sreenu, V.B., Bell-Sakyi, L., Merits, A., Altinli, M., Schnettler, E., 2026. Characterization of Culex pipiens cell lines: virus infection and RNAi response. Parasites Vectors 19, 94. https://doi.org/10.1186/s13071-026-07248-w
Hierholzer, J.C., Killington, R.A., 1996. Virus isolation and quantitation. Virology Methods Manual 25–46. https://doi.org/10.1016/B978-012465330-6/50003-8
Hilton, L., Moganeradj, K., Zhang, G., Chen, Y.-H., Randall, R.E., McCauley, J.W., Goodbourn, S., 2006. The NPro Product of Bovine Viral Diarrhea Virus Inhibits DNA Binding by Interferon Regulatory Factor 3 and Targets It for Proteasomal Degradation. Journal of Virology 80, 11723–11732. https://doi.org/10.1128/jvi.01145-06
Huang, Y.-J.S., Higgs, S., Vanlandingham, D.L., 2019. Emergence and re-emergence of mosquito-borne arboviruses. Current Opinion in Virology, Emerging viruses: intraspecies transmission • Viral Immunology 34, 104–109. https://doi.org/10.1016/j.coviro.2019.01.001
Kärber, G., 1931. Beitrag zur kollektiven Behandlung pharmakologischer Reihenversuche. Archiv f. experiment. Pathol. u. Pharmakol 162, 480–483. https://doi.org/10.1007/BF01863914
Krueger, F., James, F., Ewels, P., Afyounian, E., Weinstein, M., Schuster-Boeckler, B., Hulselmans, G., sclamons, 2023. FelixKrueger/TrimGalore: v0.6.10 - add default decompression path. https://doi.org/10.5281/zenodo.7598955
Langmead, B., Salzberg, S.L., 2012. Fast gapped-read alignment with Bowtie 2. Nat Methods 9, 357–359. https://doi.org/10.1038/nmeth.1923
Lucas, K.J., Myles, K.M., Raikhel, A.S., 2013. Small RNAs: a new frontier in mosquito biology. Trends Parasitol 29, 295–303. https://doi.org/10.1016/j.pt.2013.04.003
Marconcini, M., Pischedda, E., Houé, V., Palatini, U., Lozada-Chávez, N., Sogliani, D., Failloux, A.-B., Bonizzoni, M., 2021. Profile of Small RNAs, vDNA Forms and Viral Integrations in Late Chikungunya Virus Infection of Aedes albopictus Mosquitoes. Viruses 13, 553. https://doi.org/10.3390/v13040553
Miesen, P., Joosten, J., Rij, R.P. van, 2016. PIWIs Go Viral: Arbovirus-Derived piRNAs in Vector Mosquitoes. PLOS Pathogens 12, e1006017. https://doi.org/10.1371/journal.ppat.1006017
Morazzani, E.M., Wiley, M.R., Murreddu, M.G., Adelman, Z.N., Myles, K.M., 2012. Production of Virus-Derived Ping-Pong-Dependent piRNA-like Small RNAs in the Mosquito Soma. PLOS Pathogens 8, e1002470. https://doi.org/10.1371/journal.ppat.1002470
Mutso, M., Saul, S., Rausalu, K., Susova, O., Žusinaite, E., Mahalingam, S., Merits, A., 2017. Reverse genetic system, genetically stable reporter viruses and packaged subgenomic replicon based on a Brazilian Zika virus isolate. J Gen Virol 98, 2712–2724. https://doi.org/10.1099/jgv.0.000938

Nag, D.K., Brecher, M., Kramer, L.D., 2016. DNA forms of arboviral RNA genomes are generated following infection in mosquito cell cultures. Virology 498, 164–171. https://doi.org/10.1016/j.virol.2016.08.022

Nag, D.K., Kramer, L.D., 2017. Patchy DNA forms of the Zika virus RNA genome are generated following infection in mosquito cell cultures and in mosquitoes. J Gen Virol 98, 2731–2737. https://doi.org/10.1099/jgv.0.000945

Okamura, K., Ishizuka, A., Siomi, H., Siomi, M.C., 2004. Distinct roles for Argonaute proteins in small RNA-directed RNA cleavage pathways. Genes Dev 18, 1655–1666. https://doi.org/10.1101/gad.1210204

Olson, K.E., Bonizzoni, M., 2017. Nonretroviral integrated RNA viruses in arthropod vectors: an occasional event or something more? Current Opinion in Insect Science 22, 45–53. https://doi.org/10.1016/j.cois.2017.05.010

Palatini, U., Miesen, P., Carballar-Lejarazu, R., Ometto, L., Rizzo, E., Tu, Z., van Rij, R.P., Bonizzoni, M., 2017. Comparative genomics shows that viral integrations are abundant and express piRNAs in the arboviral vectors Aedes aegypti and Aedes albopictus. BMC Genomics 18, 512. https://doi.org/10.1186/s12864-017-3903-3

Pierson, T.C., Diamond, M.S., 2020. The continued threat of emerging flaviviruses. Nat Microbiol 5, 796–812. https://doi.org/10.1038/s41564-020-0714-0

Poirier, E.Z., Goic, B., Tomé-Poderti, L., Frangeul, L., Boussier, J., Gausson, V., Blanc, H., Vallet, T., Loyd, H., Levi, L.I., Lanciano, S., Baron, C., Merkling, S.H., Lambrechts, L., Mirouze, M., Carpenter, S., Vignuzzi, M., Saleh, M.-C., 2018. Dicer-2-Dependent Generation of Viral DNA from Defective Genomes of RNA Viruses Modulates Antiviral Immunity in Insects. Cell Host & Microbe 23, 353-365.e8. https://doi.org/10.1016/j.chom.2018.02.001

Quinlan, A.R., Hall, I.M., 2010. BEDTools: a flexible suite of utilities for comparing genomic features. Bioinformatics 26, 841–842. https://doi.org/10.1093/bioinformatics/btq033

Rice, C.M., Levis, R., Strauss, J.H., Huang, H.V., 1987. Production of infectious RNA transcripts from Sindbis virus cDNA clones: mapping of lethal mutations, rescue of a temperature-sensitive marker, and in vitro mutagenesis to generate defined mutants. Journal of Virology 61, 3809–3819. https://doi.org/10.1128/jvi.61.12.3809-3819.1987

Rodriguez-Andres, J., Axford, J., Hoffmann, A., Fazakerley, J., 2023. Mosquito transgenerational antiviral immunity is mediated by vertical transfer of virus DNA sequences and RNAi. iScience 27, 108598. https://doi.org/10.1016/j.isci.2023.108598

Rückert, C., Prasad, A.N., Garcia-Luna, S.M., Robison, A., Grubaugh, N.D., Weger-Lucarelli, J., Ebel, G.D., 2019. Small RNA responses of CuIex mosquitoes and cell lines during acute and persistent virus infection. Insect Biochem Mol Biol 109, 13–23. https://doi.org/10.1016/j.ibmb.2019.04.008

Scherer, C., 2021. Identifying the diverse functionalities and characteristics of the RNAi response against arthropod-borne viruses in mosquitoes. University Hamburg.

Scherer, C., Knowles, J., Sreenu, V.B., Fredericks, A.C., Fuss, J., Maringer, K., Fernandez-Sesma, A., Merits, A., Varjak, M., Kohl, A., Schnettler, E., 2021. An Aedes aegypti-Derived Ago2 Knockout Cell Line to Investigate Arbovirus Infections. Viruses 13, 1066. https://doi.org/10.3390/v13061066

Schnettler, E., Donald, C.L., Human, S., Watson, M., Siu, R.W.C., McFarlane, M., Fazakerley, J.K., Kohl, A., Fragkoudis, R., 2013. Knockdown of piRNA pathway proteins results in enhanced Semliki Forest virus production in mosquito cells. J Gen Virol 94, 1680–1689. https://doi.org/10.1099/vir.0.053850-0

Suzuki, Y., Baidaliuk, A., Miesen, P., Frangeul, L., Crist, A.B., Merkling, S.H., Fontaine, A., Lequime, S., Moltini-Conclois, I., Blanc, H., van Rij, R.P., Lambrechts, L., Saleh, M.-C., 2020. Non-retroviral Endogenous Viral Element Limits Cognate Virus Replication in Aedes aegypti Ovaries. Curr Biol 30, 3495-3506.e6. https://doi.org/10.1016/j.cub.2020.06.057

Suzuki, Y., Frangeul, L., Dickson, L.B., Blanc, H., Verdier, Y., Vinh, J., Lambrechts, L., Saleh, M.-C., 2017. Uncovering the Repertoire of Endogenous Flaviviral Elements in Aedes Mosquito Genomes. Journal of Virology 91, 10.1128/jvi.00571-17. https://doi.org/10.1128/jvi.00571-17

Tassetto, M., Kunitomi, M., Whitfield, Z.J., Dolan, P.T., Sánchez-Vargas, I., Garcia-Knight, M., Ribiero, I., Chen, T., Olson, K.E., Andino, R., 2019. Control of RNA viruses in mosquito cells through the acquisition of vDNA and endogenous viral elements. eLife 8, e41244. https://doi.org/10.7554/eLife.41244

ter Horst, A.M., Nigg, J.C., Dekker, F.M., Falk, B.W., 2019. Endogenous Viral Elements Are Widespread in Arthropod Genomes and Commonly Give Rise to PIWI-Interacting RNAs. Journal of Virology 93, 10.1128/jvi.02124-18. https://doi.org/10.1128/jvi.02124-18

Varela, M., Schnettler, E., Caporale, M., Murgia, C., Barry, G., McFarlane, M., McGregor, E., Piras, I.M., Shaw, A., Lamm, C., Janowicz, A., Beer, M., Glass, M., Herder, V., Hahn, K., Baumgärtner, W., Kohl, A., Palmarini, M., 2013. Schmallenberg Virus Pathogenesis, Tropism and Interaction with the Innate Immune System of the Host. PLOS Pathogens 9, e1003133. https://doi.org/10.1371/journal.ppat.1003133

Varjak, M., Dietrich, I., Sreenu, V.B., Till, B.E., Merits, A., Kohl, A., Schnettler, E., 2018. Spindle-E Acts Antivirally Against Alphaviruses in Mosquito Cells. Viruses 10, 88. https://doi.org/10.3390/v10020088

Varjak, M., Donald, C.L., Mottram, T.J., Sreenu, V.B., Merits, A., Maringer, K., Schnettler, E., Kohl, A., 2017a. Characterization of the Zika virus induced small RNA response in Aedes aegypti cells. PLOS Neglected Tropical Diseases 11, e0006010. https://doi.org/10.1371/journal.pntd.0006010

Varjak, M., Maringer, K., Watson, M., Sreenu, V.B., Fredericks, A.C., Pondeville, E., Donald, C.L., Sterk, J., Kean, J., Vazeille, M., Failloux, A.-B., Kohl, A., Schnettler, E., 2017b. Aedes aegypti Piwi4 Is a Noncanonical PIWI Protein Involved in Antiviral Responses. mSphere 2, e00144-17. https://doi.org/10.1128/mSphere.00144-17

Vodovar, N., Bronkhorst, A.W., van Cleef, K.W.R., Miesen, P., Blanc, H., van Rij, R.P., Saleh, M.-C., 2012. Arbovirus-derived piRNAs exhibit a ping-pong signature in mosquito cells. PLoS One 7, e30861. https://doi.org/10.1371/journal.pone.0030861

Weaver, S.C., Charlier, C., Vasilakis, N., Lecuit, M., 2018. Zika, Chikungunya, and Other Emerging Vector-Borne Viral Diseases. Annual Review of Medicine 69, 395–408. https://doi.org/10.1146/annurev-med-050715-105122

Weaver, S.C., Reisen, W.K., 2010. Present and future arboviral threats. Antiviral Research 85, 328–345. https://doi.org/10.1016/j.antiviral.2009.10.008

Whitfield, Z.J., Dolan, P.T., Kunitomi, M., Tassetto, M., Seetin, M.G., Oh, S., Heiner, C., Paxinos, E., Andino, R., 2017. The Diversity, Structure, and Function of Heritable Adaptive Immunity Sequences in the Aedes aegypti Genome. Curr Biol 27, 3511-3519.e7. https://doi.org/10.1016/j.cub.2017.09.067

Zaid, A., Burt, F.J., Liu, X., Poo, Y.S., Zandi, K., Suhrbier, A., Weaver, S.C., Texeira, M.M., Mahalingam, S., 2021. Arthritogenic alphaviruses: epidemiological and clinical perspective on emerging arboviruses. The Lancet Infectious Diseases 21, e123–e133. https://doi.org/10.1016/S1473-3099(20)30491-6

Chapter 6: General discussion

Within mosquito antiviral defence, the exo-siRNA pathway presents as the main defensive pathway, with Dcr2 and Ago2 holding the key positions for recognition and targeting of viral RNA for degradation (Donald et al., 2012; Elbashir et al., 2001; MacRae et al., 2006; Okamura et al., 2004; Schuster et al., 2019). Despite the siRNA pathway itself being well understood today, many questions relating the different domains of Dcr2 and their functions remain. The piRNA pathway, mainly known for gene expression modulation and transposon repression, has also been shown to be involved in antiviral activity, explicitly through PIWI4 (Schnettler et al., 2013; Tassetto et al., 2019; Varjak et al., 2018b, 2017b, 2017a). This antiviral function of the piRNA pathway has been directly linked to NIRVS-derived vpiRNAs, with CFAV-derived NIRVS established in the mosquito genome through vDNA production (Tassetto et al., 2019).

Additionally, vsiRNA and vpiRNA production has been shown to differ between viral families, i.e. flaviviral infection does not lead to the production of piRNAs exhibiting ping-pong amplified characteristics as opposed to alpha- and bunyaviruses (Léger et al., 2013; Miesen et al., 2016b, 2016a, 2015; Morazzani et al., 2012; Schnettler et al., 2016; Varjak et al., 2018b, 2017a; Vodovar et al., 2012). As *Ae. aegypti* presents as the most prevalent vector of many arboviruses, including DENV, ZIKV and CHIKV, it is crucial to understand its RNAi-mediated antiviral defence, including vDNA production and NIRVS, in regards to the differences between arboviral families.

Dcr2 domain mutants show different effects on the RNAi response after alphavirus and bunyavirus infection

While the exo-siRNA pathway itself and the overall function of Dcr2 in mosquito antiviral defence is well understood, many questions remain; as to each domain's involvement in antiviral activity, especially considering different arboviral families. Previously, Gestuveo et al. produced *Ae. aegypti* Dcr2 helicase and RNase III domain mutants to investigate their antiviral importance and function within the exo-siRNA pathway in defence against SFV.

For this, conserved amino acids were identified via multiple sequence alignment. Multiple different mutants containing mutations in those conserved amino acids were created, namely the three helicase mutants Y232G, KN (K39N) and GR (G488R), and the RNase III mutant mtR3 (D1198A, E1341A, D1444A, E1548A). Both domains were found to be critical for antiviral and silencing activity, yet Y232G showed to retain silencing activity comparable to WT Dcr2 as opposed to the other mutants which all showed loss of silencing activity comparable to the Dcr2 deficient control (Gestuveo et al., 2022). Additionally, the RNase III domain and thus cleavage of viral dsRNA was shown to not be sufficient for antiviral activity on its own, as SFV replication already increased to control levels as opposed to WT Dcr2 in the helicase mutants with functional RNase III domain.

In the same manner, we used multiple sequence alignment to determine conserved amino acids in the PAZ domain of *Ae. aegypti* Dcr2 to investigate its importance in the antiviral defence and sRNA production after SFV infection, resulting in the *Ae. aegypti* Dcr2 PAZ mutants M1-M4 (see Publication 1, Fig. 1 and 2). All four PAZ mutants possess mutations at the same positions (V880, V883, Y909, V923), with M3 and M4 possessing two additional N-terminal mutations at D829 and N872, and one C-terminal at L930. The only difference between M1/M2 and M3/M4 is, that M1 and M3 have all their mutations sites exchanged to alanine, while M2 and M4 have valine (V880, V883, V923) specifically changed to aspartic acid, as valine and alanine are very similar in structure.

As with KN, GR and mtR3, all four Dcr2 PAZ mutant transfected into Dcr2 KO cells (AF319) lost antiviral activity against SFV, showing SFV replication levels comparable to the eGFP transfected controls (Publication 1, Fig. 3). Interestingly, despite the heightened SFV replication comparable to the controls, the PAZ mutants retained intermediate silencing activity between WT Dcr2 and eGFP control levels. This shows that while residual processing of dsRNA is still present in the PAZ mutants, that alone is not enough to reduce SFV replication.

Antiviral defense within mosquitoes is highly virus-dependent, leading to the question how the antiviral activity of the Dcr2 mutants would fare after bunyaviral infection in comparison to alphaviral infection. Bunyaviruses differ significantly from alphaviruses in their genome organisation, with their genome presenting as a tri-segmented (-)ssRNA genome, as opposed to the single (+)ssRNA genome of alphaviruses. These differences are likely to influence how viral RNA is recognized by mosquito antiviral pathways, particularly the siRNA response. During replication, positive-sense RNA viruses such as alphaviruses generate abundant dsRNA that serve as substrates for Dcr2 (Siu et al., 2011), whereas negative-sense RNA viruses generally produce lower levels of exposed dsRNA due to the encapsidation of genomic and antigenomic RNAs within ribonucleoprotein complexes (Osborne and Elliott, 2000). Consequently, bunyaviruses and alphaviruses differ in both the extent and nature of their interactions with mosquito antiviral defenses, contributing to differences in RNAi activation, viral persistence, and vector competence. Bunyaviruses belong to multiple different viral families, including the *Peribunyaviridae* and *Phenuiviridae*, of which we chose to test BUNV and RVFV as representatives (Publication 3).

For the helicase mutants, KN and GR were chosen, as these two helicase mutants showed the highest deviation in RNAi response from WT Dcr2 in case of SFV infection. As for the PAZ mutants, M1 and M3 were chosen, as there were no discernible differences between the mutants where valine was exchanged with alanine (M1, M3) versus aspartic acid (M2, M4). While there was also no observable difference between M1 and M3 after SFV infection in regards to the RNAi response; M3 does contain 3 additional mutations and might behave differently after bunyaviral infection. Lastly, the mtR3 RNase III mutant was also used as the only available RNase III mutant. All Dcr2 mutants alongside WT Dcr2 and eGFP as control were again transfected into *Ae. aegypti* Dcr2 KO cells, AF319, before infection with either RVFV or BUNV.

Notably, the WT Dcr2 transfected cells showed a substantial difference in viral replication after BUNV and RVFV infection, with only a small yet still significant decrease of ~25% as compared to the eGFP control after BUNV infection, and a ~80% decrease in RVFV replication. While this could be due to the difference in experimental setup of the two experiments, BUNV has also previously been shown to seemingly being less sensitive to Dcr2, instead defence against

BUNV relies more heavily on the piRNA pathway in comparison to other arboviruses (Altinli et al., 2023; Dietrich et al., 2017b). As for mutant Dcr2, after BUNV infection, no significant differences were observed in antiviral activity of any of the Dcr2 mutants as compared to the eGFP transfected control. However, while that was also true for most mutants after RVFV infection, one of the helicase mutants, KN, retained antiviral activity comparable to WT Dcr2.

To conclude the role of the different domains for anti-bunyaviral activity, the helicase, PAZ and RNase III domains are all of crucial importance in the defence of *Ae. aegypti*-cells against BUNV, with the helicase and PAZ domain mutants being sufficient for loss of antiviral function despite functional RNase III domain, which is consistent with the results after SFV infection. The same is true for RVFV infection, as even if the KN helicase mutant still showed decreased RVFV replication comparable to WT Dcr2, the GR helicase mutant exhibited viral replication comparable to the eGFP transfected control.

Dcr2 domain mutants reveal differing 21 nt sRNA production after alpha- and bunyaviral infection

Focusing on the effect of the Dcr2 mutants on vsiRNA production after transfection of *Ae. aegypti* Dcr2 KO cells, AF319, and subsequent SFV infection, all four PAZ mutants, the helicase mutants KN and GR and the RNase III mutant mtR3 showed depletion of the 21 nt sRNA production (Publication 1, Fig. 4; Gestuveo et al., 2022). Only Y232G exhibited higher sRNA production than the other mutants, yet less than WT Dcr2, which could explain the retained silencing ability. In case of M1-M4, while the number of 21 nt sRNAs decreased in comparison to WT Dcr2, a more even distribution of 20-22 nt sRNAs can be observed. This led to the conclusion that while the Dcr2 PAZ mutants lost the ability to precisely measure and cleave viral dsRNA into 21 nt vsiRNAs, they did retain the general ability to process viral dsRNA into sRNAs. This observed change in length of Dcr2-derived sRNAs is in line with previous reports of PAZ mutants in *D. melanogaster* (Kandasamy and Fukunaga, 2016). Interestingly, in the study from Gestuveo et al., 24-30 nt vpiRNAs are produced at a substantially higher rate in comparison to 21 nt vsiRNAs, while in Publication 1, the number of 21 nt vsiRNAs vs 24-30 nt vpiRNAs is more even. Upon transfection with either WT or mutant Dcr2, dependent on transfection efficiency, most AF319 cells present do not express Dcr2, thus their RNAi response is highly reliant on the piRNA pathway instead. In combination with the infection efficiency and different kits and devices used for sequencing, this likely explains the differences we are seeing in size distribution of the SFV-specific sRNAs.

This behaviour of imprecise Dcr2-derived sRNA processing was not seen for KN, GR or mtR3, yet a different peculiarity was observed: a portion of the 21 nt sRNAs produced by these mutants exhibited a strong bias towards 10 nt overlap and the U_1/A_{10} bias, both markers of piRNA ping-pong amplification (Gestuveo et al., 2022). So, while the Dcr2 PAZ mutants retained their processing ability, even if faulty, in case of the dysfunctional KN, GR and mtR3 mutants, the major loss of vsiRNA production lead to a ping-pong biogenesis of 21 nt “vsi-piRNAs”. These “vsi-piRNAs” were not observed for the PAZ mutants which instead exhibited the typical 2 nt overhang for 18-23 nt long sRNAs (Publication 1, Fig. 5). However, in comparison to WT Dcr2, the PAZ mutants exhibited an increase in duplexes with 2 nt overhang. This is likely due to an impaired vsiRNA maturation, which is achieved by loading of the vsiRNAs onto Ago2/siRISC and subsequent cleaving of the passenger strand.

While WT Dcr2 and Y232G produced 21 nt vsiRNAs mapping evenly across the SFV genome and antigenome, in line with previous publications of SFV sRNA production (Schnettler et al., 2013; Varjak et al., 2018a), KN, GR and mtR3 exhibited a bias of mapping in positive sense, mainly towards the 3' end with a hotspot around genome position 9,000. The PAZ mutants on the other hand retained an even mapping of 21 nt sRNAs across both the genome and antigenome of SFV (Publication 1, Fig. 4). As for the produced vpiRNA-sized sRNAs (24-30 nt), in all cases they mapped predominantly to the genome versus the antigenome with two hotspot regions around genome position ~7,500 and ~9,000, respectively (helicase/RNase: Gestuveo et al., PAZ: Fig. S11), concordant with previous studies (Schnettler et al., 2013; Varjak et al., 2018a). The peak at position ~7,500 coincides with the subgenomic promotor region, which is hypothesized to be the main inducer of SFV-specific vpiRNAs. All mutants across Publication 1 and Gestuveo et al. exhibit the characteristic 10 nt overlap and a clear U_1/A_{10} bias, confirming the produced ping-pong amplified vpiRNAs (Publication 1, Fig. S11).

Another notable observation can be made between the WT or PAZ mutant Dcr2 transfected cells and the eGFP control (Fig. S11). The vpiRNAs of the Dcr2 transfected cells, no matter if WT or mutant Dcr2, show a large mapping peak at genome position ~8,000. This peak however is roughly halved for the fully Dcr2 deficient eGFP transfected control, leading to the assumption that the presence of Dcr2 could lead to a higher piRNA production specifically derived from that genomic region. While the PAZ mutant Dcr2 does lose its antiviral activity, it was shown to still retain the ability to process viral dsRNA, even if the resulting "siRNA" lengths are broadened from 21 nt to ~20-22 nt. It has been shown before that Dcr2 and PIWI4 interact in an antiviral manner (Schnettler et al., 2013; Tassetto et al., 2019; Varjak et al., 2018b, 2017b, 2017a), even if the exact mechanisms and functions are still unknown. Potentially, the PAZ domains could retain some manner of antiviral activity, however, at a rate too low to measure effectively, possibly involving vpiRNAs. Further investigation into this is needed, e.g. small RNA sequencing also involving the helicase mutants KN and GR, and the RNase III mutant mtR3. As all three of those mutants were shown to lose functional sRNA production after both alphaviral and bunyaviral infection, a peak similar to that of the fully Dcr2-deficient eGFP control is expected and would hint at an involvement of functional Dcr2 and piRNA production at that genomic locus.

As the PAZ mutants are still able to produce Dcr2-derived sRNAs and retain intermediate silencing activity, future experiments should investigate if these sRNAs are still taken up by Ago2 and thus the siRISC, or if the change in processing hinders the uptake of the differently sized "siRNAs" by Ago2 and thus explaining the loss of antiviral activity and increase in 2 nt overhang duplexes; despite intermediate silencing activity. In *D. melanogaster*, siRNAs are methylated by introducing a methyl group onto the 2' OH of the 3' terminal nucleotide on each strand of the Ago2-associated duplex through the methyltransferase Pimet/DmHen1 (Horwich et al., 2007; Ji and Chen, 2012; Saito et al., 2007; Yang et al., 2007). For *Ae. aegypti*, the exact methyltransferase has not yet been identified, however, through pan-arthropod analysis of RNAi-related genes, *Hen1* was found to be widespread throughout the arthropods (Lewis et al., 2018). Despite the lack of knowledge concerning the exact methyltransferase in *Ae. aegypti*, previous studies have shown that siRNAs in *Ae. aegypti* are methylated only in the presence of Ago2 (Scherer et al., 2021). To assess their association with Ago2 and thus their methylation status, a β-elimination assay can be performed to only retain methylated sRNAs for sequencing. For this, the extracted RNA is treated with sodium periodate to oxidate the 3' ends before β-elimination, which leads to removal of the last nucleotide of the unmethylated

sRNAs; prohibiting linkers to ligate during library prep and thus making them undetectable during small RNA sequencing (Alefelder et al., 1998; Elmer et al., 2014). Another possible explanation for the lack of antiviral activity despite intermediate silencing activity is that the silencing is not efficient enough to keep up with the continued replication of the virus, or the difference of uniform dsRNA used in the silencing assay in comparison to the naturally varied dsRNA during viral replication, potentially leading to the observed differences.

To further investigate the difference in antiviral activity we see between the two helicase mutants after RVFV infection, small RNA sequencing was done to focus on the sRNA production between WT Dcr2, eGFP and KN or GR helicase mutant. Therefore, corresponding expression plasmids were transfected into AF319 cells. RVFV-derived sRNAs mapped similarly to both the RVFV genome and antigenome for all three segments in all samples (Publication 3, Fig. 3).

Consistent with previous publications, 21 nt vsiRNAs predominantly mapped to the M-segment with a genomic peak at genome position ~2,500, and a clear peak in the S-segment coinciding with the location of the stem-loop structure separating the two ORFs of the RVFV S-segment (genome position ~800) (Dietrich et al., 2017a; Léger et al., 2013). Interestingly, Dietrich et al. showed the stem-loop-derived peak for Aag2 cells in both the genome and antigenome, while in case of Publication 3, this peak is only observable for the genomic side. This difference is likely due to either the different cell lines used, with AF319 being derived from Aag2, yet lacking a fully functional siRNA pathway, as well as differences in protocol both regarding sample and library preparation, and small RNA sequencing reactions and devices. While Dietrich et al. and Publication 3 both used the RVFV MP12 strain, Léger et al. used the parental strain, RVFV ZH548. Yet while MP12 is the live-attenuated vaccine strain of ZH548, there is no evidence of attenuation in mosquitoes (Turell and Rossi, 1991). In live *Ae. aegypti* mosquitoes, this S-segment peak derived from the stem-loop region is still observable, again mapping both genomic and antigenomic, yet less distinct in comparison to the *Aedes*-derived cells, with the RVFV-derived siRNAs mapping more evenly across the segments, including the L-segment (Dietrich et al., 2017a).

Despite the Dcr2 KN helicase mutant showing decreased RVFV replication, both helicase mutants (GR and KN) exhibited 21 nt sRNA production comparable to the eGFP transfected control cells, with only Dcr2 WT presenting with clear siRNA production. WT Dcr2 exhibits a size distribution of RVFV-specific sRNAs consistent with previous publications, with most 21 nt vsiRNAs mapping to the M-segment, and least to the L-segment ; as well as most vpiRNA-sized sRNAs being derived from the M-segment (Léger et al., 2013). Multiple other theories as to how KN is able to retain antiviral activity despite showing sRNA production comparable to fully Dcr2 deficient cells were proposed, including possible involvement in helicase ATP-binding. The homologous amino acid in *Dmel* Dcr2 is K34, which is essential for ATP binding. Binding of blunt-ended dsRNA by the helicase domain is ATP-dependent, and in case of an ATPase defective helicase domain, 3’ overhang dsRNA is bound and processed into 22 nt siRNAs (Sinha et al., 2018, 2015b). Yet despite an uncharacteristic enrichment of 22 nt sRNAs observable for the S-segment in the KN transfected cells, the same is also true for GR, eGFP and even Dcr2 (Publication 3, Fig. 2). However, the heightened amount of 22 nt sRNAs mapping to the RVFV S-segment is a novel observation and merits further investigation, possibly also hinting at an involvement of Dcr1 of the miRNA pathway.

As KN and GR transfected cells showed 21 nt sRNAs exhibiting ping-pong amplified characteristics after SFV infection, additional analysis was done to determine if “vsi-piRNAs” can also be observed after RVFV infection. Surprisingly, a U_1 bias can be observed for KN and GR in the RVFV M-segment, yet also in the WT Dcr2 and eGFP transfected control (Fig. S12 and S13). However, the bias is strongest for KN. Additionally, a clear U_1 bias can also be observed for RVFV L. This could hint at a stronger involvement of the piRNA pathway in case of the Dcr2 KN mutant, leading to the production of what resembles “vsi-piRNAs” described by Gestuveo et al. after SFV infection, however, in no case was an A_{10} bias or 10 nt overlap detected after RVFV infection; as opposed to SFV infection. Notably, no clear peak for a typical 19 nt overlap can be observed for WT Dcr2. A possible explanation for this would be that the 21 nt vsiRNAs produced by WT Dcr2 are very efficiently taken up by Ago2 and thus cleaved, resulting in no clear 19 nt overlap peak despite strong vsiRNA production. To investigate this uncharacteristic loss of clear z-score pattern, a β-elimination assay could also be performed to asses the amount of vsiRNAs being taken up and thus methylated, possibly leaving little unmethylated duplex vsiRNA. Additionally, no prior publications have investigated the overlaps of bunya-specific siRNAs. To remedy this and check if a similar pattern can be observed without the issue of a generally low transfection efficiency, we analyzed the BUNV-Nluc infected AF5 samples from Publication 4 for their 21 nt siRNA overlap pattern (Fig. S14A). Again, no clear peak can be observed for 19 nt overlap for any of the segments, presenting a novel observation for bunyavirus specific siRNA duplexes. Furthermore, ZIKV-Nluc infected AF5 cells (Publication 4) exhibited a peak at 18 nt, again differing from the previously accepted 19 nt overlap of vsiRNAs that now presents as being specific to alphaviruses.

No conclusive theory as to why KN is still able to significantly reduce RVFV replication while not retaining functional sRNA production is currently at hand and needs further investigation, e.g. by doing silencing assays to get a better look at functional differences between the two used helicase mutants. Additional experiments could also include silencing proteins involved in the RNAi response, e.g. focusing on fully inactivating the siRNA pathway through additional Ago2 silencing in the already Dcr2-deficient AF319 cells to determine if KN would still be able to retain antiviral activity (experimental setup outlined in Publication 2). Other theories might include the activation of other antiviral pathways, e.g. the Vago-like cytokine (VGL) (Couderc et al., 2025), as there has been no investigation into a possible VGL activation through RVFV, nor that it could act in an antiviral manner.

As for the vpiRNA-sized sRNAs (25-30 nt), these also map to both the antigenome and genome across all three segments for all conditions (Publication 3, S4). The M- and S-segment mappings are consistent with the vsiRNAs, showing genomic peaks at genome positions ~2,500 and ~900, respectively, which does not match previous studies (Dietrich et al., 2017a). Again, this is likely due to differences in protocols and sequencing bias. However, consistent with Léger et al., U_1/A_{10} bias and 10 nt overlap can be observed for all conditions for the L- and M-segment, even if the A_{10} bias is less clear for the M-segment in eGFP or Dcr2 helicase mutant transfected cells (Publication 3, Fig. 4 and S5). The only exception is the S-segment, as too little vpiRNA-sized sRNAs map to the S-segment for conclusive analysis of these ping-pong amplified characteristics.

Going forward, to get a full overview over the effects of the different Dcr2 domain mutants and thus the importance of the respective domains after bunyaviral infection, small RNA sequencing should be done for both BUNV and RVFV, including all mutants, not just the

helicase mutants. While all used mutants showed the same loss of antiviral function after SFV and BUNV infection, the production of sRNAs could still differ, as the two viruses are very dissimilar in genome organisation and also differ in how heavily the antiviral response against them relies on different RNAi pathways, with BUNV seeming to be less sensitive to the siRNA pathway. Additionally, BUNV-derived sRNA production from mutant Dcr2 could also give us another possible glance at “vsi-piRNA” production, specifically from the helicase and RNase III mutants.

Primed cells exhibit clone- and virus-specific antiviral activity

While it is widely accepted that insects do not possess an adaptive immune response, the discovery of vDNA being produced from RNA viruses and associated establishment of NIRVS in the genome have led to speculation of a NIRVS-mediated, heritable immunity acting like an adaptive immune response (Crochu et al., 2004; Goic et al., 2016; Marconcini et al., 2021; Tassetto et al., 2019; ter Horst et al., 2019). The integration of vDNA into the genome as NIRVS has mostly been described for ISVs, including NIRVS-derived vpiRNA production and thus a direct link to an adaptive antiviral immunity (Goic et al., 2016; Mondotte et al., 2020; Suzuki et al., 2020; Tassetto et al., 2019; ter Horst et al., 2019). As ISVs have mostly been described to be transmitted vertically, and the piRNA pathway being primarily involved in protection of the genome from transposable elements, it begs the question whether a NIRVS-derived piRNA-mediated antiviral defence would be sensible for the mainly horizontally transmitted arboviruses (Öhlund et al., 2019). However, vertical transmission has also been shown for multiple important arboviruses, including DENV, ZIKV, RVFV and CHIKV (da Costa et al., 2018, 2017; Ferreira-de-Lima et al., 2020; Ferreira-de-Lima and Lima-Camara, 2018; Gardela et al., 2024; Kwaśnik et al., 2021; Lequime et al., 2016; Mbaoma et al., 2025).

To investigate the incorporation of arboviral DNA and the effect of the resulting NIRVS on subsequent infections, *Ae. aegypti*-derived AF5 cells were subjected to arboviral infection before clearance of said infection, leaving the cells “primed” for subsequent infections (Publication 4). These primed cells were produced using either SFV-Nluc, BUNV-Nluc (Scherer, 2021) or ZIKV-Nluc, to model the results for a representative of each major arboviral group (alphaviruses, bunyaviruses and flaviviruses). Additionally, all three viruses have previously demonstrated to elicit an effective RNAi-mediated antiviral response (Dietrich et al., 2017b; Schnettler et al., 2013; Varjak et al., 2018a, 2017a), also shown in this study in Publication 1 for SFV. Specifically, for both SFV and BUNV a piRNA-mediated antiviral role has been shown in preceding studies (Dietrich et al., 2017b; Varjak et al., 2018a, 2017b). The clearance of infection was done using virus-specific dsRNA, making use of the siRNA pathway to assist the cells in fighting the infection. After clearing the respective arboviral infection, cells were seeded as single cell clones, leading to the establishment of multiple clones for BUNV and SFV primed cells, yet only one surviving clone for ZIKV primed cells.

Upon re-infection of the primed cells with their respective priming viruses (Publication 4, Fig. 2A-C), some BUNV primed clones re-infected with BUNV-Nluc exhibited significant differences in viral replication in comparison to the naïve control cells, yet all clones are overall still comparable to control levels. ZIKV-Nluc infected ZIKV primed cells also showed antiviral activity comparable to the control, however, SFV primed cells re-infected with SFV-Nluc exhibited clone-specific differences, with SFV-1 showing no significant difference to the naïve

control, yet SFV-Nluc replication in SFV-2 was significantly decreased. Unfortunately, no statements can be made about possible clone-specific changes for ZIKV primed cells due to the single surviving clone.

These virus-specific differences were generally expected, as all three viruses belong to different arboviral families with distinct genome organization. However, we expected to see priming effects for BUNV and ZIKV priming like we did for SFV. In Publication 4, we also showed proof for vDNA production in *Aedes*-derived cells after SFV, BUNV and RVFV infection, supporting the idea that BUNV and SFV are likely to incorporate NIRVS (Publication 4, Fig. 1). For SFV and BUNV, this was shown for both acute and persistent infection, while for RVFV, vDNA was only shown for acute infection. Previously, vDNA production has been shown for multiple different arboviruses, including SFV, BUNV and ZIKV. SFV vDNA was detected in *Aedes* mosquitoes (Rodriguez-Andres et al., 2023), ZIKV vDNA in both *Aedes*-mosquitoes and *Aedes*-derived cells (Nag and Kramer, 2017), and BUNV vDNA in *Culex*-derived cells (Altinli et al., 2023). In all cases, the vDNA was detected within total extracted DNA – the only previous publication investigating vDNA within genomic DNA focused on DENV in *Aedes*-derived cells, WNV in *Culex*-derived cells and SFV in *Aedes* mosquitoes (Nag et al., 2016; Rodriguez-Andres et al., 2023). Here, we showed the production of SFV-, BUNV- and RVFV-derived vDNA in both total extracted DNA and gDNA, supporting the idea of incorporation of NIRVS into the genomic versus episomal DNA. Additionally, we detected vDNA in both AF5 and AF319 cells. As AF319 cells are Dcr2 KO cells, this demonstrates that Dcr2, and thus the siRNA pathway, is not essential for vDNA production. This is in line with previous studies in *D. melanogaster*, in which the inheritance of vDNA and the subsequent adaptive immunity within the offspring was shown to be Dcr2-independent (Mondotte et al., 2020). While the PCR was not a quantitative experiment, the bands for vDNA in AF319 cells were consistently more intense than those of AF5, with very little exceptions. This is likely due to the lack of a functional siRNA pathway in the Dcr2-deficient AF319 cells, leaving the viruses to replicate at higher rates than in the immunocompetent AF5 cells, leading to more viral RNA available to be transcribed into vDNA.

Following the re-infection experiments with the priming viruses, the primed cells were also infected with one of the other viruses. Initially, this was done as an internal control, yet as we examined the results, surprisingly, strong effects could be observed (Publication 4, Fig. 2D-F). While SFV primed cells did not show any antiviral activity significantly deviating from the naïve cells, all BUNV primed clones showed highly significant decreases in SFV-Nluc replication in comparison to the naïve cells experiencing any arboviral challenge for the first time. ZIKV primed cells were also able to significantly decrease BUNV-Nluc replication. These re-infections with non-priming viruses were initially done to account for possible side effects of the priming process, but as they showed strong effects themselves in comparison to the re-infection experiments using the priming viruses, we present them separately. Conversely, this means the effects we now see could be a direct result of the priming process. If only one of the BUNV clones would exhibit this behaviour, it could be argued that during single cell seeding a cell was chosen in which SFV struggles to replicate efficiently. However, as we see this behaviour for all clones, it seems that the priming process seems to fundamentally change the cells in a way that affects replication of some viruses, but not others. Yet even in that case the effect is not consistent, as ZIKV primed cells show decreased BUNV-Nluc levels, while BUNV primed cells do not. Additionally, all used viruses are reporter viruses encoding for nanoluciferase. It is possible that the luciferase sequence is also transcribed into DNA before

being incorporated into the genome, however, in that case we again should not just see an effect of SFV-Nluc infection on BUNV primed cells, but BUNV-Nluc replication should be affected as well.

Akin to ISVs continuously circling in wild populations, many mosquito cell lines contain persistent ISV infections; with persistent CFAV and PCLV infections in AF5 cells specifically (Fredericks et al., 2019). CFAV has been previously shown to inhibit arboviral dissemination and replication for DENV and ZIKV (Bolling et al., 2015; Schultz et al., 2018; Vasilakis and Tesh, 2015), yet this effect has not been shown for *Ae. aegypti*-derived cell lines as of now. However, the opposite effect has been shown in *Ae. aegypti*-derived cells, with DENV infection leading to heightened CFAV replication and vise-versa (Zhang et al., 2017). Still, the primed cell clones that have lost their persistent CFAV infection over the course of the priming (BUNV-3, BUNV-9, SFV-2), likely due to single cell seeding, were re-infected with CFAV to ascertain the observed effects are not due to the loss of CFAV in comparison to the CFAV positive, naïve control cells. The CFAV positive versus negative clones did exhibit differences, most notably after BUNV-Nluc infection (Publication 4, Fig. 2A and E), however, these changes were not deemed strong enough to interfere with the investigation of the priming effects. However, possible loss of PCLV infection was not tested and should be taken into future consideration. While PCLV itself was not shown to consistently affect flaviviral (DENV, ZIKV) or alphaviral (SINV) infection (Fredericks et al., 2019), the presence of both PCLV and CFAV in *Ae. aelbopictus*-derived cells lead to replication inhibition of the ZIKV, DENV and the orthobunyavirus LACV in comparison to CFAV presence alone (Schultz et al., 2018).

The effects after priming cells with different arboviruses we are observing so far are heavily virus- and even clone-specific. While it is reasonable to assume that vDNA and NIRVS confer a type of antiviral activity via the piRNA pathway, allowing the cells, and furthermore the mosquitoes, to fight or control a recurrent infection effienctly, many other factors that currently still elude us might be at play. Unidentified cell or viral factors involved in general antiviral defence, including for example the JAK-STAT pathway, may contribute to the defence upon re-infection or might even act in a proviral manner in some cases, as hinted at by e.g. slightly heightened BUNV-Nluc replication in BUNV primed cells. Additonally, the clone-specificity we are observing could be due to the accidental selection of cells during single cell seeding that are less susceptible to specific viruses. Future studies into viral priming could include experiments excluding the siRNA or piRNA pathways, using either Dcr2-deficient AF319 cells, or the Ago2-deficient AF525 cells, which demonstrate impaired antiviral functionality against alpha- and bunyaviruses, which are sensitive to Ago2, while ZIKV replication was not affected by Ago2 silencing (Fredericks et al., 2019; Scherer et al., 2021). To have an even closer look at the influence of specifically the siRNA pathway key proteins, the Dcr2 mutants used in Publication 1 and 3, or Ago2 mutants, like the previously established Ago2mut (Dummunee et al., 2025), could be transfected into AF319 or AF525, respectively, ideally generating stable cell lines expressing the mutant proteins, before priming and re-infection experiments. For the Dcr2 helicase mutants KN and GR, and the Dcr2 PAZ mutants V5-tagged pPUb-expression plasmids for stable cell line production have already been established, with a Zeocin-resistance for selection. In case of the Ago2 mutant, AF525 cells with stable Ago2mut expression already exist (Dummunee et al., 2025).

Priming effects exhibit time-sensitive changes

As the results of the primed cells luciferase assays were inconsistent with the following sRNA sequencing that was done ~40 passages later, with clone-specific differences especially for the BUNV primed cells which were not observed while investigating their antiviral activity, additional experiments were done to determine if these changes were due to the later time point of the sRNA sequencing samples. For this, the RNA that was used for sRNA sequencing was used for cDNA synthesis and subsequent qRT-PCR, making this not just the same time point as the sRNA sequencing, but also the same samples.

For the primed cells re-infected with the same virus used for priming (Publication 4, Fig. 11A and B), we again saw no strong effects on BUNV-Nluc replication in BUNV primed cells – only BUNV-9 exhibits a slight yet significant increase in BUNV-Nluc replication. In contrast, the SFV-Nluc infected SFV primed cells exhibit a strong decrease in SFV-Nluc replication in comparison to the naïve control cells, losing their clone-specific differences. However, while the decrease is substantial for both clones, no significances could be detected due to scattered data points of the naïve control. ZIKV-Nluc infected ZIKV primed cells could not be re-examined at this time point as too little RNA was left for cDNA synthesis.

The primed cells had once more been subjected to infection of a non-priming virus (Publication 4, Fig. 11C-F), and again, all clones of the BUNV primed cells Nluc exhibited a strong antiviral activity against SFV-Nluc, a seemingly even stronger effect than at the first time point ~40 passages earlier, however, as the SFV-Nluc infected naïve control is the same as for the SFV primed cells, no significances could be detected. As for the ZIKV primed cells, at this later time point they have lost the ability to reduce BUNV-Nluc replication, but in contrast show a significant decrease in SFV-Nluc replication in comparison to the naïve controls. This time, all primed cells infected with SFV-Nluc, regardless of used priming virus, showed strong antiviral activity against SFV-Nluc, and seemingly even stronger than the earlier time point.

To investigate if this effect is only reserved for SFV-Nluc or if it can also be observed for other alphaviruses, the BUNV primed cells were subjected to SINV and O'nyong Nyong (ONNV; *Togaviridae*; *Alphavirus*) infection (Publication 4, Fig. 11). Additionally, Tahyna virus (TAHV; *Peribunyaviridae*; *Orthobunyavirus*), a close relative of BUNV, was also used to infect the BUNV primed cells to see if other bunyaviruses will elicit an effect on antiviral activity. To add another timepoint for checking the time sensitivity, the passage of the BUNV primed cells for this experiment was roughly ~60 passages before the sRNA sequencing, presenting as the earliest used time point; thus BUNV-Nluc and SFV-Nluc infection was also tested once more. Looking at the results for the bunyaviruses (Publication 4, Fig. 11A and B), again, no significant changes can be observed for the BUNV-Nluc infected cells. However, all BUNV primed clones exhibit a strong decrease in TAHV replication, with one clone even showing significant results in comparison to the control cells. Surprisingly, at this earliest of the used timepoints, no decrease in SFV-Nluc replication can be detected. The same is true for ONNV replication, however, for SINV, two of the three BUNV primed clones observe a strong antiviral response, yet due to the relatively scattered data points of the control cells, no significance was observed. Interestingly, one clone, specifically BUNV-2, exihibited a strong increase for both SFV-Nluc

and SINV replication, even if in neither case significance was detected, again due to scattered data points.

Again, these results support a timedependency of the priming effects, with all BUNV primed clones showing exacerbation of SFV-Nluc replication inhibition over time – no decrease in SFV-Nluc replication was observed for the earliest timepoint (~60 passages before sRNA sequencing), a significant decrease for the intermediate timepoint (~40 passages before sRNA sequencing), and the strongest decrease at the time of sRNA sequencing. Another notable observation is presented by ZIKV primed cells exhibiting a heightened antiviral response against BUNV-Nluc in comparison to the naïve cells at the intermediate time point. This effect was however lost ~40 passages later at the time of small RNA sequencing, presenting a directly opposite effect than we see with SFV-Nluc in BUNV primed cells. The cause of this timedependency is unclear at this point. It can be hypothesized that NIRVS-derived piRNA production is reduced or even lost over time, however, this would lead to a lessened priming effect over time, not an exacerbation like we observe with SFV-Nluc infection. Should the effects we observe be caused by the process of priming itself, specifically single cell seeding possibly leading to only more resilient cells surviving which display a lessened sensitivity to specific viruses, the question of how this would translate into decreasing viral replication over time still remains. Previous studies have suggested differences in single cell susceptibility to different viruses being linked to variable instrinsic cell states and subpopulations within the parental cell colonie, however, these finding were observed for human cells (Reffsin et al., 2026), with no current studies in insect cells. While multiple studies have investigated NIRVS-mediated antiviral activity and even priming in mosquitoes and mosquito cell lines, no previous publications have done similar priming experiments involving multiple time points or cross-infections with other viruses. Furthermore, the fact that BUNV-primed cells are also able to decrease TAHV and SINV replication, neither of which are reporter viruses, supports the fact that the priming viruses all possessing nanoluciferase is not causal for the effects we observe. While no change in antiviral activity against BUNV-Nluc or SFV-Nluc was observed at the earliest time point, replication inhibition of SINV and TAHV was detected, proving that these effects are not limited to SFV or even alphaviruses.

Small RNA sequencing of primed cells shows inconsistencies to antiviral activity and again exhibits clone- and virus-specific effects

Following the priming experiments focusing on antiviral activity, the focus next shifted to priming effects on sRNA production. SFV, BUNV and ZIKV have all show previously described RNAi-mediated antiviral responses, including a reported antiviral role of the piRNA pathway for SFV and BUNV specifically (Dietrich et al., 2017b; Schnettler et al., 2013; Varjak et al., 2018a, 2017a). Due to the previous viral priming of these cells, and based on the antiviral activity especially demonstrated against SFV-Nluc, it is reasonable to assume detectable effects on the sRNA production within the primed cells.

As with the experiments for antiviral activity of the primed cells against both the priming and the non-priming viruses, all primed cells were subjected to different arboviral challenges regardless of original virus used for priming. For all primed cells independent of virus used for second arboviral exposal, raw libraries show sRNA lengths suggesting the presence of siRNAs (21 nt), miRNAs (22 nt) and piRNAs (25-28 nt) (Publication 4, Fig. S1). sRNAs being presented

for lengths 18-28 nt instead of the more common 18-30 nt is due to the kit used for library preparation and combination with the bioinformatical analysis, leaving reads with a max read length of 28 nt.

BUNV-specific sRNAs were observed for both the antigenome and genome for all samples (Publication 4, Fig. 3). In line with previous publications, most BUNV-specific sRNAs map to the S-segment and least to the L-segment (Altinli et al., 2023; Dietrich et al., 2017b). The percentage of 21 nt sRNAs in comparison to all sRNAs mapping per segment in highest for the L-segment, followed by the M- and then S-segment, also consistent with previous studies (Dietrich et al., 2017b). As for the size distribution of BUNV-specific sRNAs, heightened sRNA production is detectable in two out of the three BUNV primed clones in comparison to the naïve cells; all other primed cells show levels comparable to the control (Publication 4, Fig. 3). SFV and ZIKV primed cells not showing any strong sRNA-mediated reaction to BUNV-Nluc infection is expected and consistent with the observed lack of effect on antiviral activity at the time point of small RNA sequencing (Publication 4, Fig. 11). However, not just do we see effects on sRNA production for the BUNV primed cells that do not match up with the lack of effect on antiviral activity upon BUNV-Nluc re-infection, we also now observed strong clone-specific differences that we did not observe previously. A strong sRNA response could be explained for both a low and high viral replication, with the cells either mounting a defence in the form of increased sRNAs to either fight the now heightened viral load in case of a high replication, or showing an increased sRNA production due to successfully reducing viral replication. Yet, while we see the most BUNV-specific sRNAs, both of vsiRNA- and vpiRNA-sized sRNAs, for the BUNV-2 clone, it did not show any changes in antiviral activity against BUNV-Nluc, regardless of timepoint. Additionally, BUNV-3 also exhibits heightened sRNA production yet no difference in antiviral activity in comparison to the naïve cells, and BUNV-9 even shows a slight increase in BUNV-Nluc replication yet sRNA production comparable to the control. In no case does the antiviral activity match the observed antiviral activity.

For all samples, the 21 nt vsiRNAs map evenly across the genome and antigenome, while vpiRNAs (25-28 nt), all exhibiting a typical 10 nt overlap and U_1/A_{10} bias, show a mapping bias towards the antigenome for the M- and S-segment, and a genomic bias in the L-segment (Publication 4, Fig. 3 and 4, S4). The mapping of BUNV-specific sRNAs, including a mapping bias towards both the 3’ and 5’ ends for the L-segment, is consistent with previous studies (Altinli et al., 2023; Dietrich et al., 2017b). Interestingly, the sense vpiRNAs mapping to the L-segment do exhibit a U_1 bias which is also consistent with the study of Dietrich et al.

SFV infection has previously been shown to lead to a predominantly siRNA-based response as opposed to piRNA (Schnettler et al., 2013; Varjak et al., 2018a), which lines up with the pattern observable for the SFV-specific sRNAs of the primed cells after SFV-Nluc infection (Publication 4, Fig. 5). Despite the antiviral activity at the time of small RNA sequencing showing no clone-specific differences, the SFV-1 clone produces visibly more sRNAs in comparison to both SFV-2 and the naïve control cells. Similarly, the ZIKV primed cells exhibited significantly reduced SFV-Nluc replication, yet the SFV-specific sRNA production is comparable to the naïve cells.

The BUNV primed cells again exhibit clone-specific sRNA production after SFV-Nluc infection. While the sRNA levels do not correlate with the fact that all three clones exhibit roughly the same intensity of increases in antiviral activity against SFV-Nluc in comparison to naïve cells, the sRNA production levels differ greatly with BUNV-2 producing significantely more sRNAs

that the naïve control, BUNV-3 showing sRNA levels comparable to the naïve cells, and BUNV-9 producing even less sRNAs than the control. However, it does match with the sRNA production after BUNV-Nluc infection, suggesting we do indeed see a correlation in spite of different viruses.

While we observed no visible changes in antiviral activity against BUNV-Nluc with the BUNV primed cells, the same pattern of sRNA production between the different clones could be observed for both SFV-Nluc and BUNV-Nluc infection. While the involvement of the Nluc was previously doubtful, looking at these current results, it might be that different clones, especially in case of BUNV primed cells, may incorporate parts of the Nluc sequence into their genomes via vDNA, leading to the same intensity in sRNA production upon secondary infection regardless of infecting virus, as long as they possess Nluc. There have been no previous reports of vDNA or NIRVS interactions with the siRNA pathway, yet SFV-Nluc infection leads to mostly 21 nt siRNAs produced and only few vpiRNAs also in primed cells. Nevertheless, previous publications have made a connection between Dcr2 and PIWI4, so while we understand little about both arboviral DNA and NIRVS incorporation, especially their role in antiviral activity, and the cross-play of si- and piRNA pathway, there is chance that arboviral NIRVS could also function via the siRNA pathway. To investigate this possibility, SFV6 wt could be used for infection of the BUNV primed cells. If the effects we see are at least partially based on incorporation of Nluc-based NIRVS into the genome of the BUNV primed cells, some of the effect we see for SFV-Nluc infection should be lost in case of SFV6 wt infection.

To get a clearer picture about this, especially if and if so, in what capacity and location, arbovirus-derived NIRVS are incorporated into the genome, whole genome sequencing (WGS) of the primed cells needs to be a priority going forward. At the current state of research, little is known about exactly where NIRVS are incorporated into the genome, especially if this incorporation is located in the episomal or genomic DNA. Furthermore, WGS can provide answers as to what parts of the used viruses are actually incorporated and where, or if the incorporation is random both in what viral sequence is transcribed into vDNA before incorporation, and at which location within the mosquito/ cell genome these NIRVS are actually located. Based on the strong differences we see between clones, and the discrepancy between antiviral activity and sRNA production, it is likely that other cellular and/ or viral factors are at play which we do not yet know of. To get closer to the answers, transcriptomics also presents a viable option for future experiments to assess if there are effects of the priming or priming process itself that are visible within the transcriptome of the cells, possibly leading to the discovery of up- or downregulation of genes involved in antiviral defence.

Another logical next step includes the previously discussed establishment of stable cell lines expressing the mutant Dcr2 used in Publications 1 and 2, especially after the effects we saw after SFV infection. Even after priming, the siRNA pathway remains the main RNAi-mediated defence against SFV. With or without using the Dcr2 mutants, future studies should investigate possible priming effects in Dcr2-deficient AF319 cells, as we saw strong differences in sRNA production between AF5 and AF319 cells after SFV infection with a shift towards piRNA production in the absence of the siRNA pathway, possibly allowing a closer look at a NIRVS-specific piRNA production after SFV infection.

Consistent with Publication 1 and other previous publications (Schnettler et al., 2013; Varjak et al., 2018a), SFV-specific vsiRNAs map evenly across both the genome and antigenome, while the vpiRNAs map at a genomic hotspot at genome position ~7,500 which belongs to the

subgenomic promotor (Publication 4, Fig. 6). As SFV-Nluc possesses two subgenomic promotors, with the second located directly downstream of the structural reading frame before the added Nluc sequence (Scherer et al., 2021), the mapping was redone for SFV-Nluc (Publication 4, Fig. S15). This mapping to SFV-Nluc exhibited vpiRNAs mapping to the second subgenomic promotor, even if less than two the original promotor, yet still supporting the idea that the subgenomic promotor is the main inducer of SFV-specific piRNAs. Again, consistent with Publication 1 and other previous studies, all SFV infected samples exhibit the ping-pong amplification characteristics of 10 nt overlap and U_1/A_{10} bias for the vpiRNAs (Publication 4, Fig. 5, S5).

Unfortunately, the viral replication of ZIKV-Nluc in ZIKV primed cells could not be redone for the small RNA sequencing timepoint, but at the ~40 passages earlier timepoint, no difference in replication was observed in comparison to the naïve cell control (Publication 4, Fig. 2). As for the sRNA produced by the ZIKV primed cells, a substantial decrease in ZIKV-derived sRNA production was observed in the ZIKV primed cells in comparison to the naïve cells (Publication 4, Fig. 7). This again is inconsistent with the previous antiviral activity experiment, however, as we have observed timedependent chances in viral replication for SFV-Nluc, yet there is only one time point shown for ZIKV replication, it stands to reason that possible changes could have occurred over time. As there is only one ZIKV primed clone that could be used for the experiments, the general investigating into ZIKV priming effects should be redone, including establishment of multiple ZIKV primed clones and investigation of antiviral activity at different timepoints.

Consistent with preceding studies, ZIKV-specific 21 nt vsiRNAs map to both the genome and antigenome evenly, while the vpiRNA-sized sRNAs (25-28 nt) only map to the genomic side (Varjak et al., 2017a). This mapping includes 3'-located hotspots at genome positions ~9,000 and 10,000. As expected, the ZIKV vpiRNA-sized sRNAs do not exhibit 10 nt overlap or U_1/A_{10} bias, showing no ping-pong amplification.

Uninfected primed cells show no clear evidence for base-line NIRVS-specific vpiRNA-production except for one SFV primed clone

The piRNA pathway's main function lies in transposon repression and gene expression modulation as opposed to antiviral activity, thus its general activity is not dependent on a current infection. While it is still part of ongoing research as to where exactly NIRVS are incorporated into the genome, we theorize that it coincides with the so-called "piRNA clusters" from which pre-piRNAs originate. If true, we expect to observe NIRVS-derived vpiRNA production even in absence of an active arboviral infection. To investigate this, small RNA sequencing was also done for currently uninfected primed cells.

Small RNAs were detected for all samples regardless of previous priming, however, due to the fact of how little sRNAs are present in the samples, it is likely that the "sRNA production" we are observing here is due to contamination during sample or library preparation and sequencing, rather than true sRNAs. Hypothetically, this could also hint at a NIRVS-specific sRNA production that is present yet only residual in absence of arboviral infection, especially as the uninfected BUNV primed samples exhibit a strong shift towards vpiRNA-sized sRNAs rather than vsiRNAs, while the BUNV-Nluc infected BUNV primed cells exhibited a clear 21 nt

vsiRNA peak. However, sRNAs specific to all three tested viruses can also be found in the naïve cell samples used for all three mappings. Nevertheless, there is one clear exception in one SFV primed clone – SFV-1 exhibits sRNA, specifically again vsiRNA, production ~10 times higher than all other samples. Again, further investigation in the form of WGS is needed to truly assess if arboviral NIRVS are present. To account for the potential contamination, small RNA sequencing should be done of only the uninfected primed cells, eliminating the chance of cross-contamination with the “re-“ infected primed cells.

Conclusion

The current state of research includes expansive knowledge about the antiviral defense in mosquitoes mediated by the siRNA pathway; however, information about the individual components and their domains still remains poor. In contrast, little is known about the involvement of the piRNA pathway within antiviral activity, and even less about NIRVS-specific piRNAs. This includes general vDNA production from arboviruses, NIRVS-incorporation and location within the mosquito genome, and a possible function akin to an adaptive immune response involving piRNAs. The combined publications presented here reveal new insights into the roles of different Dcr2 domains within antiviral defense against both alpha- and bunyaviral infection, as well as proof of vDNA production from different arboviral families.

Dcr2 PAZ mutants were established and used to demonstrate the importance of the *Ae. aegypti* PAZ domains in the antiviral and silencing activity, and precise 21 nt vsiRNA production after SFV-infection. The PAZ mutants were also used after bunyaviral infection alongside previously established helicase- and RNase III mutants (Gestuveo et al., 2022). All three domains were shown to be critical for the antiviral defense against both BUNV and RVFV. However, one helicase mutant, KN, continues to show antiviral activity despite lack of detectable RVFV-specific siRNA production, necessitating further investigation.

vDNA production has been shown for both total and genomic DNA for acute and persistent BUNV and SFV infection, and for acute RVFV infection. This is the first proof of vDNA production in genomic loci for representatives of all three major arboviral families, including further evidence that Dcr2 and thus the siRNA pathway is not essential for vDNA production.

The production of primed cells, which had undergone previous arboviral challenge (SFV, BUNV, ZIKV) before clearance of the respective infection, lead to the discovery of virus- and clone-specific effects upon secondary arboviral infection. These effects include time-sensitive changes in antiviral activity upon “re-“ infection and substantial differences in sRNA production between clones primed with the same virus. Despite many new observations involving the effects of viral priming, future experiments are needed to understand the exact cause of the effects, including the apparent timedepency. Possible explanations for these interesting findings include possible mosquito and viral factors, interactions with other antiviral pathways, changes within virus susceptibility of the cells due to the priming process, and virus- and clone-dependent differences in how and where NIRVS are incorporated into the genome.

Overall, the findings of this thesis contribute to a growing understanding of the difference of mosquito antiviral immunity based on its interactions with diverse arboviruses. The observed variation in responses to different arboviral families, as well as the influence of previous

arboviral exposure, highlight the complexity of mosquito-virus interactions and their potential influence on infection outcomes. Furthermore, this work provides new insights into the functional diversity of Dcr2, indicating that multiple domains contribute to antiviral defense against different arboviruses, emphasizing important antiviral functions of the helicase and PAZ domains beyond the canonical RNA-cleavage activity of the RNase III domain. Collectively, these findings supply new perspectives on the intricacies of RNAi-mediated immunity and provide the groundwork for future studies investigating the determinants of vector competence and possible RNAi-mediated adaptive immunity against arboviruses in mosquitoes.

Chapter 7: References

Abbasi, E., 2025. Global expansion of *Aedes* mosquitoes and their role in the transboundary spread of emerging arboviral diseases: A comprehensive review. IJID One Health 6, 100058. https://doi.org/10.1016/j.ijidoh.2025.100058

Aderounmu, A.M., Aruscavage, P.J., Kolaczkowski, B., Bass, B.L., 2023. Ancestral protein reconstruction reveals evolutionary events governing variation in Dicer helicase function. eLife 12, e85120. https://doi.org/10.7554/eLife.85120

Aguiar, E.R.G.R., Olmo, R.P., Paro, S., Ferreira, F.V., de Faria, I.J. da S., Todjro, Y.M.H., Lobo, F.P., Kroon, E.G., Meignin, C., Gatherer, D., Imler, J.-L., Marques, J.T., 2015. Sequence-independent characterization of viruses based on the pattern of viral small RNAs produced by the host. Nucleic Acids Res 43, 6191–6206. https://doi.org/10.1093/nar/gkv587

Albariño, C.G., Bird, B.H., Nichol, S.T., 2007. A Shared Transcription Termination Signal on Negative and Ambisense RNA Genome Segments of Rift Valley Fever, Sandfly Fever Sicilian, and Toscana Viruses. Journal of Virology 81, 5246–5256. https://doi.org/10.1128/jvi.02778-06

Alefelder, S., Patel, B.K., Eckstein, F., 1998. Incorporation of terminal phosphorothioates into oligonucleotides. Nucleic Acids Res 26, 4983–4988. https://doi.org/10.1093/nar/26.21.4983

Altinli, M., Leggewie, M., Schulze, J., Gyanwali, R., Badusche, M., Sreenu, V.B., Fuss, J., Schnettler, E., 2023. Antiviral RNAi Response in Culex quinquefasciatus-Derived HSU Cells. Viruses 15, 436. https://doi.org/10.3390/v15020436

Ammerman, N.C., Beier-Sexton, M., Azad, A.F., 2008. Growth and Maintenance of Vero Cell Lines. Curr Protoc Microbiol APPENDIX, Appendix-4E. https://doi.org/10.1002/9780471729259.mca04es11

Antoniewski, C., 2014. Computing siRNA and piRNA Overlap Signatures, in: Werner, A. (Ed.), Animal Endo-SiRNAs: Methods and Protocols. Springer, New York, NY, pp. 135–146. https://doi.org/10.1007/978-1-4939-0931-5_12

Arbouzova, N.I., Zeidler, M.P., 2006. JAK/STAT signalling in Drosophila: insights into conserved regulatory and cellular functions. Development 133, 2605–2616. https://doi.org/10.1242/dev.02411

Arensburger, P., Hice, R.H., Wright, J.A., Craig, N.L., Atkinson, P.W., 2011. The mosquito Aedes aegypti has a large genome size and high transposable element load but contains a low proportion of transposon-specific piRNAs. BMC Genomics 12, 606. https://doi.org/10.1186/1471-2164-12-606

Asgari, S., 2014. Role of microRNAs in Arbovirus/Vector Interactions. Viruses 6, 3514–3534. https://doi.org/10.3390/v6093514

Atkins, G.J., Sheahan, B.J., Dimmock, N.J., 1985. Semliki Forest Virus Infection of Mice: A Model for Genetic and Molecular Analysis of Viral Pathogenicity. Journal of General Virology 66, 395–408. https://doi.org/10.1099/0022-1317-66-3-395

Baidaliuk, A., Miot, E.F., Lequime, S., Moltini-Conclois, I., Delaigue, F., Dabo, S., Dickson, L.B., Aubry, F., Merkling, S.H., Cao-Lormeau, V.-M., Lambrechts, L., 2019. Cell-Fusing Agent Virus Reduces Arbovirus Dissemination in Aedes aegypti Mosquitoes In Vivo. Journal of Virology 93, 10.1128/jvi.00705-19. https://doi.org/10.1128/jvi.00705-19

Bannert, N., Kurth, R., 2004. Retroelements and the human genome: New perspectives on an old relation. Proceedings of the National Academy of Sciences of the United States of America 14572–14579.

Barletta, A.B.F., Nascimento-Silva, M.C.L., Talyuli, O.A.C., Oliveira, J.H.M., Pereira, L.O.R., Oliveira, P.L., Sorgine, M.H.F., 2017. Microbiota activates IMD pathway and limits Sindbis infection in Aedes aegypti. Parasit Vectors 10, 103. https://doi.org/10.1186/s13071-017-2040-9

Besson, B., Overheul, G.J., Wolfinger, M.T., Junglen, S., van Rij, R.P., 2024. Pan-flavivirus analysis reveals sfRNA-independent, 3′ UTR-biased siRNA production from an insect-specific flavivirus. Journal of Virology 98, e01215-24. https://doi.org/10.1128/jvi.01215-24

Blair, C.D., Olson, K.E., Bonizzoni, M., 2019. The Widespread Occurrence and Potential Biological Roles of Endogenous Viral Elements in Insect Genomes. Current Issues in Molecular Biology 34, 13–30. https://doi.org/10.21775/cimb.034.013

Blakqori, G., Lowen, A.C., Elliott, R.M., 2012. The small genome segment of Bunyamwera orthobunyavirus harbours a single transcription-termination signal. J Gen Virol 93, 1449–1455. https://doi.org/10.1099/vir.0.042390-0

Bolling, B.G., Weaver, S.C., Tesh, R.B., Vasilakis, N., 2015. Insect-Specific Virus Discovery: Significance for the Arbovirus Community. Viruses 7, 4911–4928. https://doi.org/10.3390/v7092851

Bouloy, M., Weber, F., 2010. Molecular Biology of Rift Valley Fever Virus. Open Virol J 4, 8–14. https://doi.org/10.2174/1874357901004010008

Brackney, D.E., Correa, M.A., Cozens, D.W., 2020. The impact of autophagy on arbovirus infection of mosquito cells. PLoS Negl Trop Dis 14, e0007754. https://doi.org/10.1371/journal.pntd.0007754

Brackney, D.E., Scott, J.C., Sagawa, F., Woodward, J.E., Miller, N.A., Schilkey, F.D., Mudge, J., Wilusz, J., Olson, K.E., Blair, C.D., Ebel, G.D., 2010. C6/36 Aedes albopictus cells have a dysfunctional antiviral RNA interference response. PLoS Negl Trop Dis 4, e856. https://doi.org/10.1371/journal.pntd.0000856

Brady, O.J., Hay, S.I., 2020. The Global Expansion of Dengue: How Aedes aegypti Mosquitoes Enabled the First Pandemic Arbovirus. Annual Review of Entomology 65, 191–208. https://doi.org/10.1146/annurev-ento-011019-024918

Breving, K., Esquela-Kerscher, A., 2010. The complexities of microRNA regulation: mirandering around the rules. Int J Biochem Cell Biol 42, 1316–1329. https://doi.org/10.1016/j.biocel.2009.09.016

Bridgen, A., Weber, F., Fazakerley, J.K., Elliott, R.M., 2001. Bunyamwera bunyavirus nonstructural protein NSs is a nonessential gene product that contributes to viral pathogenesis. Proc Natl Acad Sci U S A 98, 664–669. https://doi.org/10.1073/pnas.98.2.664

Brinton, M.A., Basu, M., 2015. Functions of the 3′ and 5′ genome RNA regions of members of the genus *Flavivirus*. Virus Research, Special Issue: Functions of the ends of positive strand RNA virus genomes 206, 108–119. https://doi.org/10.1016/j.virusres.2015.02.006

Brown, J.E., Evans, B.R., Zheng, W., Obas, V., Barrera-Martinez, L., Egizi, A., Zhao, H., Caccone, A., Powell, J.R., 2014. Human impacts have shaped historical and recent evolution in Aedes aegypti, the dengue and yellow fever mosquito. Evolution 68, 514–525. https://doi.org/10.1111/evo.12281

Buchholz, U.J., Finke, S., Conzelmann, K.K., 1999. Generation of bovine respiratory syncytial virus (BRSV) from cDNA: BRSV NS2 is not essential for virus replication in tissue culture, and the human RSV leader region acts as a functional BRSV genome promoter. J Virol 73, 251–259. https://doi.org/10.1128/JVI.73.1.251-259.1999

Buhler, C., Winkler, V., Runge-Ranzinger, S., Boyce, R., Horstick, O., 2019. Environmental methods for dengue vector control – A systematic review and meta-analysis. PLOS Neglected Tropical Diseases 13, e0007420. https://doi.org/10.1371/journal.pntd.0007420

Campbell, C.L., Keene, K.M., Brackney, D.E., Olson, K.E., Blair, C.D., Wilusz, J., Foy, B.D., 2008. Aedes aegypti uses RNA interference in defense against Sindbis virus infection. BMC Microbiol 8, 47. https://doi.org/10.1186/1471-2180-8-47

Carpenter, A., Clem, R.J., 2023. Factors Affecting Arbovirus Midgut Escape in Mosquitoes. Pathogens 12, 220. https://doi.org/10.3390/pathogens12020220

Carvalho, F.D., Moreira, L.A., 2017. Why is Aedes aegypti Linnaeus so Successful as a Species? Neotrop Entomol 46, 243–255. https://doi.org/10.1007/s13744-017-0520-4

Chary, S., Carreira, P.E., Nicholas, S., McNamara, K.B., Cockburn, I.A., Nordström, K., Jones, T.M., Gloag, R., Ashe, A., Hugo, L.E., Hayashi, R., 2025. Conserved but mechanistically diverse piRNA defence against gypsy LTR retrotransposons in insect ovaries. https://doi.org/10.1101/2025.09.05.674496

Chauhan, M., Martinak, P.E., Hollenberg, B.M., Goodman, A.G., 2025. Drosophila melanogaster Toll-9 elicits antiviral immunity against Drosophila C virus. Journal of Virology 99, e02214-24. https://doi.org/10.1128/jvi.02214-24

Chaves-Carballo, E., 2005. Carlos Finlay and Yellow Fever: Triumph over Adversity. Mil Med 170, 881–885. https://doi.org/10.7205/MILMED.170.10.881

Chen, X.-G., Jiang, Xuanting, Gu, J., Xu, M., Wu, Y., Deng, Y., Zhang, C., Bonizzoni, M., Dermauw, W., Vontas, J., Armbruster, P., Huang, X., Yang, Y., Zhang, H., He, W., Peng, H., Liu, Y., Wu, K., Chen, J., Lirakis, M., Topalis, P., Van Leeuwen, T., Hall, A.B., Jiang, Xiaofang, Thorpe, C., Mueller, R.L., Sun, C., Waterhouse, R.M., Yan, G., Tu, Z.J., Fang, X., James, A.A., 2015. Genome sequence of the Asian Tiger mosquito, Aedes albopictus, reveals insights into its biology, genetics, and evolution. Proc Natl Acad Sci U S A 112, E5907-5915. https://doi.org/10.1073/pnas.1516410112

Ciechanowska, K., Szczepanska, A., Szpotkowski, K., Wojcik, K., Urbanowicz, A., Kurzynska-Kokorniak, A., 2024. The human Dicer helicase domain is capable of ATP hydrolysis and single-stranded nucleic acid binding. BMC Biol 22, 287. https://doi.org/10.1186/s12915-024-02082-x

Contu, L., Balistreri, G., Domanski, M., Uldry, A.-C., Mühlemann, O., 2021. Characterisation of the Semliki Forest Virus-host cell interactome reveals the viral capsid protein as an inhibitor of nonsense-mediated mRNA decay. PLOS Pathogens 17, e1009603. https://doi.org/10.1371/journal.ppat.1009603

Cook, S., Bennett, S.N., Holmes, E.C., De Chesse, R., Moureau, G., de Lamballerie, X., 2006. Isolation of a new strain of the flavivirus cell fusing agent virus in a natural mosquito population from Puerto Rico. J Gen Virol 87, 735–748. https://doi.org/10.1099/vir.0.81475-0

Couderc, E., Crist, A.B., Daron, J., Varet, H., van Hout, F.A.H., Miesen, P., Palatini, U., Dabo, S., Vial, T., Lambrechts, L., Merkling, S.H., 2025. Aedes aegypti VLG-1 challenges the assumed antiviral nature of Vago genes. BMC Biol 23, 223. https://doi.org/10.1186/s12915-025-02325-5

Crava, C.M., Varghese, F.S., Pischedda, E., Halbach, R., Palatini, U., Marconcini, M., Gasmi, L., Redmond, S., Afrane, Y., Ayala, D., Paupy, C., Carballar-Lejarazu, R., Miesen, P., van Rij, R.P., Bonizzoni, M., 2021. Population genomics in the arboviral vector Aedes aegypti reveals the genomic architecture and evolution of endogenous viral elements. Mol Ecol 30, 1594–1611. https://doi.org/10.1111/mec.15798

Crochu, S., Cook, S., Attoui, H., Charrel, R.N., De Chesse, R., Belhouchet, M., Lemasson, J.-J., de Micco, P., de Lamballerie, X., 2004. Sequences of flavivirus-related RNA viruses persist in DNA form integrated in the genome of Aedes spp. mosquitoes. J Gen Virol 85, 1971–1980. https://doi.org/10.1099/vir.0.79850-0

Crooks, G.E., Hon, G., Chandonia, J.-M., Brenner, S.E., 2004. WebLogo: A Sequence Logo Generator. Genome Research 14, 1188–1190. https://doi.org/10.1101/gr.849004

da Costa, C.F., da Silva, A.V., do Nascimento, V.A., de Souza, V.C., da Silva Monteiro, D.C., Terrazas, W.C.M., Passos, R.A. dos, Nascimento, S., Lima, J.B.P., Naveca, F.G., 2018. Evidence of vertical transmission of Zika virus in field-collected eggs of Aedes aegypti in the Brazilian Amazon. PLOS Neglected Tropical Diseases 12, e0006594. https://doi.org/10.1371/journal.pntd.0006594

da Costa, C.F., Dos Passos, R.A., Lima, J.B.P., Roque, R.A., de Souza Sampaio, V., Campolina, T.B., Secundino, N.F.C., Pimenta, P.F.P., 2017. Transovarial transmission of DENV in Aedes aegypti in the Amazon basin: a local model of xenomonitoring. Parasit Vectors 10, 249. https://doi.org/10.1186/s13071-017-2194-5

Daubney, R., Hudson, J.R., 1931. Enzootic Hepatitis or Rift Valley Fever. An Un-described Virus Disease of Sheep, Cattle and Man from East Africa. Journal of Pathology and Bacteriology 545–79.

Dick, G.W.A., Kitchen, S.F., Haddow, A.J., 1952. Zika Virus (I). Isolations and serological specificity. Transactions of the Royal Society of Tropical Medicine and Hygiene 46, 509–520. https://doi.org/10.1016/0035-9203(52)90042-4

Dietrich, I., Jansen, S., Fall, G., Lorenzen, S., Rudolf, M., Huber, K., Heitmann, A., Schicht, S., Ndiaye, E.H., Watson, M., Castelli, I., Brennan, B., Elliott, R.M., Diallo, M., Sall, A.A., Failloux, A.-B.,

Schnettler, E., Kohl, A., Becker, S.C., 2017a. RNA Interference Restricts Rift Valley Fever Virus in Multiple Insect Systems. mSphere 2, e00090-17. https://doi.org/10.1128/mSphere.00090-17

Dietrich, I., Shi, X., McFarlane, M., Watson, M., Blomström, A.-L., Skelton, J.K., Kohl, A., Elliott, R.M., Schnettler, E., 2017b. The Antiviral RNAi Response in Vector and Non-vector Cells against Orthobunyaviruses. PLOS Neglected Tropical Diseases 11, e0005272. https://doi.org/10.1371/journal.pntd.0005272

Donald, C.L., Kohl, A., Schnettler, E., 2012. New Insights into Control of Arbovirus Replication and Spread by Insect RNA Interference Pathways. Insects 3, 511–531. https://doi.org/10.3390/insects3020511

Donaldson, M.K., Zanders, L.A., Jose, J., 2025. Functional Roles and Host Interactions of Orthoflavivirus Non-Structural Proteins During Replication. Pathogens 14, 184. https://doi.org/10.3390/pathogens14020184

Duc, C., Yoth, M., Jensen, S., Mouniée, N., Bergman, C.M., Vaury, C., Brasset, E., 2019. Trapping a somatic endogenous retrovirus into a germline piRNA cluster immunizes the germline against further invasion. Genome Biology 20, 127. https://doi.org/10.1186/s13059-019-1736-x

Dummunee, K., Parry, R.H., Redecke, L., Varjak, M., Brennan, B., Kohl, A., McFarlane, M., 2025. The catalytic tetrad of *Aedes aegypti* argonaute 2 is critical for the antiviral activity of the exogenous siRNA pathway. Journal of Biological Chemistry 301, 108332. https://doi.org/10.1016/j.jbc.2025.108332

Dutuze, M.F., Nzayirambaho, M., Mores, C.N., Christofferson, R.C., 2018. A Review of Bunyamwera, Batai, and Ngari Viruses: Understudied Orthobunyaviruses With Potential One Health Implications. Front. Vet. Sci. 5. https://doi.org/10.3389/fvets.2018.00069

Elbashir, S.M., Lendeckel, W., Tuschl, T., 2001. RNA interference is mediated by 21- and 22-nucleotide RNAs. Genes Dev 15, 188–200. https://doi.org/10.1101/gad.862301

Elmer, K., Helfer, S., Mirkovic-Hösle, M., Förstemann, K., 2014. Analysis of Endo-siRNAs in Drosophila, in: Werner, A. (Ed.), Animal Endo-SiRNAs: Methods and Protocols. Springer, New York, NY, pp. 33–49. https://doi.org/10.1007/978-1-4939-0931-5_4

Evans, A.B., Winkler, C.W., Peterson, K.E., 2021. Orthobunyaviruses (*Peribunyaviridae*), in: Bamford, D.H., Zuckerman, M. (Eds.), Encyclopedia of Virology (Fourth Edition). Academic Press, Oxford, pp. 654–665. https://doi.org/10.1016/B978-0-12-809633-8.21542-2

Evans, B.R., Kotsakiozi, P., Costa-da-Silva, A.L., Ioshino, R.S., Garziera, L., Pedrosa, M.C., Malavasi, A., Virginio, J.F., Capurro, M.L., Powell, J.R., 2019. Transgenic Aedes aegypti Mosquitoes Transfer Genes into a Natural Population. Sci Rep 9, 13047. https://doi.org/10.1038/s41598-019-49660-6

Farnesi, L.C., Martins, A.J., Valle, D., Rezende, G.L., 2009. Embryonic development of Aedes aegypti (Diptera: Culicidae): influence of different constant temperatures. Mem. Inst. Oswaldo Cruz 104, 124–126. https://doi.org/https://doi.org/10.1590/S0074-02762009000100020

Faull, K.J., Williams, C.R., 2015. Intraspecific variation in desiccation survival time of Aedes aegypti (L.) mosquito eggs of Australian origin. J Vector Ecol 40, 292–300. https://doi.org/10.1111/jvec.12167

Fernández-Sanlés, A., Ríos-Marco, P., Romero-López, C., Berzal-Herranz, A., 2017. Functional Information Stored in the Conserved Structural RNA Domains of Flavivirus Genomes. Front. Microbiol. 8. https://doi.org/10.3389/fmicb.2017.00546

Ferreira-de-Lima, V.H., Andrade, P. dos S., Thomazelli, L.M., Marrelli, M.T., Urbinatti, P.R., Almeida, R.M.M. de S., Lima-Camara, T.N., 2020. Silent circulation of dengue virus in Aedes albopictus (Diptera: Culicidae) resulting from natural vertical transmission. Sci Rep 10, 3855. https://doi.org/10.1038/s41598-020-60870-1

Ferreira-de-Lima, V.H., Lima-Camara, T.N., 2018. Natural vertical transmission of dengue virus in Aedes aegypti and Aedes albopictus: a systematic review. Parasites Vectors 11, 77. https://doi.org/10.1186/s13071-018-2643-9

Flores, H.A., O'Neill, S.L., 2018. Controlling vector-borne disease by releasing modified mosquitoes. Nat Rev Microbiol 16, 508–518. https://doi.org/10.1038/s41579-018-0025-0
Frangeul, L., Blanc, H., Saleh, M.-C., Suzuki, Y., 2020. Differential Small RNA Responses against Co-Infecting Insect-Specific Viruses in Aedes albopictus Mosquitoes. Viruses 12, 468. https://doi.org/10.3390/v12040468
Franz, A.W.E., Kantor, A.M., Passarelli, A.L., Clem, R.J., 2015. Tissue Barriers to Arbovirus Infection in Mosquitoes. Viruses 7, 3741–3767. https://doi.org/10.3390/v7072795
Fredericks, A.C., Russell, T.A., Wallace, L.E., Davidson, A.D., Fernandez-Sesma, A., Maringer, K., 2019. Aedes aegypti (Aag2)-derived clonal mosquito cell lines reveal the effects of pre-existing persistent infection with the insect-specific bunyavirus Phasi Charoen-like virus on arbovirus replication. PLoS Negl Trop Dis 13, e0007346. https://doi.org/10.1371/journal.pntd.0007346
Gardela, J., Yautibug, K., Talavera, S., Vidal, E., Sossah, C.C., Pagès, N., Busquets, N., 2024. Tissue distribution and transmission of Rift Valley fever phlebovirus in European Culex pipiens and Aedes albopictus mosquitoes following intrathoracic inoculation. J Gen Virol 105, 002025. https://doi.org/10.1099/jgv.0.002025
Gestuveo, R.J., Parry, R., Dickson, L.B., Lequime, S., Sreenu, V.B., Arnold, M.J., Khromykh, A.A., Schnettler, E., Lambrechts, L., Varjak, M., Kohl, A., 2022. Mutational analysis of Aedes aegypti Dicer 2 provides insights into the biogenesis of antiviral exogenous small interfering RNAs. PLoS Pathog 18, e1010202. https://doi.org/10.1371/journal.ppat.1010202
Giorgi, C., Accardi, L., Nicoletti, L., Gro, M.C., Takehara, K., Hilditch, C., Morikawa, S., Bishop, D.H.L., 1991. Sequences and coding strategies of the S RNAs of Toscana and Rift Valley fever viruses compared to those of Punta Toro, Sicilian sandfly fever, and Uukuniemi viruses. Virology 180, 738–753. https://doi.org/10.1016/0042-6822(91)90087-R
Gleghorn, M.L., Maquat, L.E., 2014. "Black sheep" that don't leave the double-stranded RNA-binding domain fold. Trends Biochem Sci 39, 328–340. https://doi.org/10.1016/j.tibs.2014.05.003
Gloria-Soria, A., Ayala, D., Bheecarry, A., Calderon-Arguedas, O., Chadee, D.D., Chiappero, M., Coetzee, M., Elahee, K.B., Fernandez-Salas, I., Kamal, H.A., Kamgang, B., Khater, E.I.M., Kramer, L.D., Kramer, V., Lopez-Solis, A., Lutomiah, J., Martins, A., Micieli, M.V., Paupy, C., Ponlawat, A., Rahola, N., Rasheed, S.B., Richardson, J.B., Saleh, A.A., Sanchez-Casas, R.M., Seixas, G., Sousa, C.A., Tabachnick, W.J., Troyo, A., Powell, J.R., 2016. Global genetic diversity of Aedes aegypti. Mol Ecol 25, 5377–5395. https://doi.org/10.1111/mec.13866
Goic, B., Stapleford, K.A., Frangeul, L., Doucet, A.J., Gausson, V., Blanc, H., Schemmel-Jofre, N., Cristofari, G., Lambrechts, L., Vignuzzi, M., Saleh, M.-C., 2016. Virus-derived DNA drives mosquito vector tolerance to arboviral infection. Nat Commun 7, 12410. https://doi.org/10.1038/ncomms12410
Goic, B., Vodovar, N., Mondotte, J.A., Monot, C., Frangeul, L., Blanc, H., Gausson, V., Vera-Otarola, J., Cristofari, G., Saleh, M.-C., 2013. RNA-mediated interference and reverse transcription control the persistence of RNA viruses in the insect model Drosophila. Nat Immunol 14, 396–403. https://doi.org/10.1038/ni.2542
Gothe, S., Jagtap, S., Böhmer, P., Reuter, M., Frank, S., Sreenu, V.B., Bell-Sakyi, L., Merits, A., Altinli, M., Schnettler, E., 2026. Characterization of Culex pipiens cell lines: virus infection and RNAi response. Parasites Vectors 19, 94. https://doi.org/10.1186/s13071-026-07248-w
Gunawardane, L.S., Saito, K., Nishida, K.M., Miyoshi, K., Kawamura, Y., Nagami, T., Siomi, H., Siomi, M.C., 2007. A slicer-mediated mechanism for repeat-associated siRNA 5' end formation in Drosophila. Science 315, 1587–1590. https://doi.org/10.1126/science.1140494
Hansen, S.R., Aderounmu, A.M., Donelick, H.M., Bass, B.L., 2019. Dicer's Helicase Domain: A Meeting Place for Regulatory Proteins. Cold Spring Harb Symp Quant Biol 84, 185–193. https://doi.org/10.1101/sqb.2019.84.039750
Hierholzer, J.C., Killington, R.A., 1996. Virus isolation and quantitation. Virology Methods Manual 25–46. https://doi.org/10.1016/B978-012465330-6/50003-8
Hilton, L., Moganeradj, K., Zhang, G., Chen, Y.-H., Randall, R.E., McCauley, J.W., Goodbourn, S., 2006. The NPro Product of Bovine Viral Diarrhea Virus Inhibits DNA Binding by Interferon

Regulatory Factor 3 and Targets It for Proteasomal Degradation. Journal of Virology 80, 11723–11732. https://doi.org/10.1128/jvi.01145-06
Horstick, O., Boyce, R., Runge-Ranzinger, S., 2017. Dengue Vector Control: Assessing what works? The Southeast Asian journal of tropical medicine and public health.
Horwich, M.D., Li, C., Matranga, C., Vagin, V., Farley, G., Wang, P., Zamore, P.D., 2007. The Drosophila RNA Methyltransferase, DmHen1, Modifies Germline piRNAs and Single-Stranded siRNAs in RISC. Current Biology 17, 1265–1272. https://doi.org/10.1016/j.cub.2007.06.030
Huang, Y.-J.S., Higgs, S., Vanlandingham, D.L., 2019. Emergence and re-emergence of mosquito-borne arboviruses. Current Opinion in Virology, Emerging viruses: intraspecies transmission • Viral Immunology 34, 104–109. https://doi.org/10.1016/j.coviro.2019.01.001
Ikegami, T., Won, S., Peters, C.J., Makino, S., 2007. Characterization of Rift Valley Fever Virus Transcriptional Terminations. Journal of Virology 81, 8421–8438. https://doi.org/10.1128/jvi.02641-06
Jänkänpää, H.J., Frenkel, M., Zulfugarov, I., Reichelt, M., Krieger-Liszkay, A., Mishra, Y., Gershenzon, J., Moen, J., Lee, C.-H., Jansson, S., 2013. Non-Photochemical Quenching Capacity in Arabidopsis thaliana Affects Herbivore Behaviour. PLOS ONE 8, e53232. https://doi.org/10.1371/journal.pone.0053232
Ji, L., Chen, X., 2012. Regulation of small RNA stability: methylation and beyond. Cell Res 22, 624–636. https://doi.org/10.1038/cr.2012.36
Ji, X., 2008. The mechanism of RNase III action: how dicer dices. Curr Top Microbiol Immunol 320, 99–116. https://doi.org/10.1007/978-3-540-75157-1_5
Johnson, R.M., Stopard, I.J., Byrne, H.M., Armstrong, P.M., Brackney, D.E., Lambert, B., 2024. Investigating the dose-dependency of the midgut escape barrier using a mechanistic model of within-mosquito dengue virus population dynamics. PLoS Pathog 20, e1011975. https://doi.org/10.1371/journal.ppat.1011975
Kandasamy, S.K., Fukunaga, R., 2016. Phosphate-binding pocket in Dicer-2 PAZ domain for high-fidelity siRNA production. Proceedings of the National Academy of Sciences 113, 14031–14036. https://doi.org/10.1073/pnas.1612393113
Kärber, G., 1931. Beitrag zur kollektiven Behandlung pharmakologischer Reihenversuche. Archiv f. experiment. Pathol. u. Pharmakol 162, 480–483. https://doi.org/10.1007/BF01863914
Keene, K.M., Foy, B.D., Sanchez-Vargas, I., Beaty, B.J., Blair, C.D., Olson, K.E., 2004. RNA interference acts as a natural antiviral response to O'nyong-nyong virus (Alphavirus; Togaviridae) infection of Anopheles gambiae. Proc Natl Acad Sci U S A 101, 17240–17245. https://doi.org/10.1073/pnas.0406983101
Kim, K.W., Lee, B., Eom, S., Shin, D., Park, C., Kim, S., Yi, H., 2023. Universal primers for rift valley fever virus whole-genome sequencing. Sci Rep 13, 18688. https://doi.org/10.1038/s41598-023-45848-z
Kokernot, R.H., Smithburn, K.C., Meillon, B. de, Paterson, H.E., 1958. Isolation of Bunyamwera Virus from a Naturally Infected Human Being and Further Isolations from Aedes (Banksinella) Circumluteolus Theo. https://doi.org/10.4269/ajtmh.1958.7.579
Kreher, F., Tamietti, C., Gommet, C., Guillemot, L., Ermonval, M., Failloux, A.-B., Panthier, J.-J., Bouloy, M., Flamand, M., 2014. The Rift Valley fever accessory proteins NSm and P78/NSm-GN are distinct determinants of virus propagation in vertebrate and invertebrate hosts. Emerg Microbes Infect 3, e71. https://doi.org/10.1038/emi.2014.71
Krueger, F., James, F., Ewels, P., Afyounian, E., Weinstein, M., Schuster-Boeckler, B., Hulselmans, G., sclamons, 2023. FelixKrueger/TrimGalore: v0.6.10 - add default decompression path. https://doi.org/10.5281/zenodo.7598955
Kumar, A., Srivastava, P., Sirisena, P., Dubey, S.K., Kumar, R., Shrinet, J., Sunil, S., 2018. Mosquito Innate Immunity. Insects 9, 95. https://doi.org/10.3390/insects9030095
Kuno, G., Chang, G.-J.J., 2005. Biological Transmission of Arboviruses: Reexamination of and New Insights into Components, Mechanisms, and Unique Traits as Well as Their Evolutionary

Trends. Clinical Microbiology Reviews 18, 608–637. https://doi.org/10.1128/cmr.18.4.608-637.2005
Kwaśnik, M., Rożek, W., Rola, J., 2021. Rift Valley Fever – a Growing Threat To Humans and Animals. J Vet Res 65, 7–14. https://doi.org/10.2478/jvetres-2021-0009
Langmead, B., Salzberg, S.L., 2012. Fast gapped-read alignment with Bowtie 2. Nat Methods 9, 357–359. https://doi.org/10.1038/nmeth.1923
Léger, P., Lara, E., Jagla, B., Sismeiro, O., Mansuroglu, Z., Coppée, J.Y., Bonnefoy, E., Bouloy, M., 2013. Dicer-2- and Piwi-mediated RNA interference in Rift Valley fever virus-infected mosquito cells. J Virol 87, 1631–1648. https://doi.org/10.1128/JVI.02795-12
Lequime, S., Paul, R.E., Lambrechts, L., 2016. Determinants of Arbovirus Vertical Transmission in Mosquitoes. PLoS Pathog 12, e1005548. https://doi.org/10.1371/journal.ppat.1005548
Lewis, S.H., Quarles, K.A., Yang, Y., Tanguy, M., Frézal, L., Smith, S.A., Sharma, P.P., Cordaux, R., Gilbert, C., Giraud, I., Collins, D.H., Zamore, P.D., Miska, E.A., Sarkies, P., Jiggins, F.M., 2018. Pan-arthropod analysis reveals somatic piRNAs as an ancestral defence against transposable elements. Nat Ecol Evol 2, 174–181. https://doi.org/10.1038/s41559-017-0403-4
Li, M., Zhou, Y., Cheng, J., Wang, Y., Lan, C., Shen, Y., 2024. Response of the mosquito immune system and symbiotic bacteria to pathogen infection. Parasit Vectors 17, 69. https://doi.org/10.1186/s13071-024-06161-4
Liu, S., Han, Y., Li, W.-X., Ding, S.-W., 2023. Infection Defects of RNA and DNA Viruses Induced by Antiviral RNA Interference. Microbiology and Molecular Biology Reviews 87, e00035-22. https://doi.org/10.1128/mmbr.00035-22
Liu, W., Sun, F.-J., Tong, Y.-G., Zhang, S.-Q., Cao, W.-C., 2016. Rift Valley fever virus imported into China from Angola. The Lancet Infectious Diseases 16, 1226. https://doi.org/10.1016/S1473-3099(16)30401-7
Lucas, K.J., Myles, K.M., Raikhel, A.S., 2013. Small RNAs: a new frontier in mosquito biology. Trends Parasitol 29, 295–303. https://doi.org/10.1016/j.pt.2013.04.003
Lutomiah, J.J.L., Mwandawiro, C., Magambo, J., Sang, R.C., 2007. Infection and vertical transmission of Kamiti river virus in laboratory bred Aedes aegypti mosquitoes. J Insect Sci 7, 1–7. https://doi.org/10.1673/031.007.5501
Ma, J.-B., Ye, K., Patel, D.J., 2004. Structural basis for overhang-specific small interfering RNA recognition by the PAZ domain. Nature 429, 318–322. https://doi.org/10.1038/nature02519
MacRae, I.J., Zhou, K., Li, F., Repic, A., Brooks, A.N., Cande, W.Z., Adams, P.D., Doudna, J.A., 2006. Structural Basis for Double-Stranded RNA Processing by Dicer. Science 311, 195–198. https://doi.org/10.1126/science.1121638
Marconcini, M., Pischedda, E., Houé, V., Palatini, U., Lozada-Chávez, N., Sogliani, D., Failloux, A.-B., Bonizzoni, M., 2021. Profile of Small RNAs, vDNA Forms and Viral Integrations in Late Chikungunya Virus Infection of Aedes albopictus Mosquitoes. Viruses 13, 553. https://doi.org/10.3390/v13040553
Mbaoma, O.C., Thomas, S.M., Beierkuhnlein, C., 2025. Significance of vertical transmission of arboviruses in mosquito-borne disease epidemiology. Parasit Vectors 18, 137. https://doi.org/10.1186/s13071-025-06761-8
McFarlane, M., Arias-Goeta, C., Martin, E., O'Hara, Z., Lulla, A., Mousson, L., Rainey, S.M., Misbah, S., Schnettler, E., Donald, C.L., Merits, A., Kohl, A., Failloux, A.-B., 2014. Characterization of Aedes aegypti Innate-Immune Pathways that Limit Chikungunya Virus Replication. PLOS Neglected Tropical Diseases 8, e2994. https://doi.org/10.1371/journal.pntd.0002994
Merkling, S.H., Crist, A.B., Henrion-Lacritick, A., Frangeul, L., Couderc, E., Gausson, V., Blanc, H., Bergman, A., Baidaliuk, A., Romoli, O., Saleh, M.-C., Lambrechts, L., 2023. Multifaceted contributions of Dicer2 to arbovirus transmission by Aedes aegypti. Cell Reports 42. https://doi.org/10.1016/j.celrep.2023.112977
Miesen, P., Girardi, E., van Rij, R.P., 2015. Distinct sets of PIWI proteins produce arbovirus and transposon-derived piRNAs in Aedes aegypti mosquito cells. Nucleic Acids Res 43, 6545–6556. https://doi.org/10.1093/nar/gkv590

Miesen, P., Ivens, A., Buck, A.H., van Rij, R.P., 2016a. Small RNA Profiling in Dengue Virus 2-Infected Aedes Mosquito Cells Reveals Viral piRNAs and Novel Host miRNAs. PLoS Negl Trop Dis 10, e0004452. https://doi.org/10.1371/journal.pntd.0004452

Miesen, P., Joosten, J., Rij, R.P. van, 2016b. PIWIs Go Viral: Arbovirus-Derived piRNAs in Vector Mosquitoes. PLOS Pathogens 12, e1006017. https://doi.org/10.1371/journal.ppat.1006017

Mondotte, J.A., Gausson, V., Frangeul, L., Suzuki, Y., Vazeille, M., Mongelli, V., Blanc, H., Failloux, A.-B., Saleh, M.-C., 2020. Evidence For Long-Lasting Transgenerational Antiviral Immunity in Insects. Cell Rep 33, 108506. https://doi.org/10.1016/j.celrep.2020.108506

Morazzani, E.M., Wiley, M.R., Murreddu, M.G., Adelman, Z.N., Myles, K.M., 2012. Production of Virus-Derived Ping-Pong-Dependent piRNA-like Small RNAs in the Mosquito Soma. PLOS Pathogens 8, e1002470. https://doi.org/10.1371/journal.ppat.1002470

Moreira, L.A., Iturbe-Ormaetxe, I., Jeffery, J.A., Lu, G., Pyke, A.T., Hedges, L.M., Rocha, B.C., Hall-Mendelin, S., Day, A., Riegler, M., Hugo, L.E., Johnson, K.N., Kay, B.H., McGraw, E.A., van den Hurk, A.F., Ryan, P.A., O'Neill, S.L., 2009. A Wolbachia symbiont in Aedes aegypti limits infection with dengue, Chikungunya, and Plasmodium. Cell 139, 1268–1278. https://doi.org/10.1016/j.cell.2009.11.042

Mueller, C.G., Cao-Lormeau, V.-M., 2018. Chapter 8 - Insect-Borne Viruses and Host Skin Interface, in: Boulanger, N. (Ed.), Skin and Arthropod Vectors. Academic Press, pp. 275–292. https://doi.org/10.1016/B978-0-12-811436-0.00008-3

Mutso, M., Saul, S., Rausalu, K., Susova, O., Žusinaite, E., Mahalingam, S., Merits, A., 2017. Reverse genetic system, genetically stable reporter viruses and packaged subgenomic replicon based on a Brazilian Zika virus isolate. J Gen Virol 98, 2712–2724. https://doi.org/10.1099/jgv.0.000938

Myles, K.M., Wiley, M.R., Morazzani, E.M., Adelman, Z.N., 2008. Alphavirus-derived small RNAs modulate pathogenesis in disease vector mosquitoes. Proc Natl Acad Sci U S A 105, 19938–19943. https://doi.org/10.1073/pnas.0803408105

Nag, D.K., Brecher, M., Kramer, L.D., 2016. DNA forms of arboviral RNA genomes are generated following infection in mosquito cell cultures. Virology 498, 164–171. https://doi.org/10.1016/j.virol.2016.08.022

Nag, D.K., Kramer, L.D., 2017. Patchy DNA forms of the Zika virus RNA genome are generated following infection in mosquito cell cultures and in mosquitoes. J Gen Virol 98, 2731–2737. https://doi.org/10.1099/jgv.0.000945

Nanyingi, M.O., Munyua, P., Kiama, S.G., Muchemi, G.M., Thumbi, S.M., Bitek, A.O., Bett, B., Muriithi, R.M., Njenga, M.K., 2015. A systematic review of Rift Valley Fever epidemiology 1931-2014. Infect Ecol Epidemiol 5, 28024. https://doi.org/10.3402/iee.v5.28024

Ng, W.C., Soto-Acosta, R., Bradrick, S.S., Garcia-Blanco, M.A., Ooi, E.E., 2017. The 5′ and 3′ Untranslated Regions of the Flaviviral Genome. Viruses 9, 137. https://doi.org/10.3390/v9060137

O'Brien, J., Hayder, H., Zayed, Y., Peng, C., 2018. Overview of MicroRNA Biogenesis, Mechanisms of Actions, and Circulation. Front Endocrinol (Lausanne) 9, 402. https://doi.org/10.3389/fendo.2018.00402

Öhlund, P., Lundén, H., Blomström, A.-L., 2019. Insect-specific virus evolution and potential effects on vector competence. Virus Genes 55, 127–137. https://doi.org/10.1007/s11262-018-01629-9

Okamura, K., Ishizuka, A., Siomi, H., Siomi, M.C., 2004. Distinct roles for Argonaute proteins in small RNA-directed RNA cleavage pathways. Genes Dev 18, 1655–1666. https://doi.org/10.1101/gad.1210204

Olschewski, S., Cusack, S., Rosenthal, M., 2020. The Cap-Snatching Mechanism of Bunyaviruses. Trends in Microbiology 28, 293–303. https://doi.org/10.1016/j.tim.2019.12.006

Olson, K.E., Bonizzoni, M., 2017. Nonretroviral integrated RNA viruses in arthropod vectors: an occasional event or something more? Current Opinion in Insect Science 22, 45–53. https://doi.org/10.1016/j.cois.2017.05.010

Osborne, J.C., Elliott, R.M., 2000. RNA binding properties of bunyamwera virus nucleocapsid protein and selective binding to an element in the 5' terminus of the negative-sense S segment. J Virol 74, 9946–9952. https://doi.org/10.1128/jvi.74.21.9946-9952.2000

Palatini, U., Masri, R.A., Cosme, L.V., Koren, S., Thibaud-Nissen, F., Biedler, J.K., Krsticevic, F., Johnston, J.S., Halbach, R., Crawford, J.E., Antoshechkin, I., Failloux, A.-B., Pischedda, E., Marconcini, M., Ghurye, J., Rhie, A., Sharma, A., Karagodin, D.A., Jenrette, J., Gamez, S., Miesen, P., Masterson, P., Caccone, A., Sharakhova, M.V., Tu, Z., Papathanos, P.A., Van Rij, R.P., Akbari, O.S., Powell, J., Phillippy, A.M., Bonizzoni, M., 2020. Improved reference genome of the arboviral vector Aedes albopictus. Genome Biology 21, 215. https://doi.org/10.1186/s13059-020-02141-w

Palatini, U., Miesen, P., Carballar-Lejarazu, R., Ometto, L., Rizzo, E., Tu, Z., van Rij, R.P., Bonizzoni, M., 2017. Comparative genomics shows that viral integrations are abundant and express piRNAs in the arboviral vectors Aedes aegypti and Aedes albopictus. BMC Genomics 18, 512. https://doi.org/10.1186/s12864-017-3903-3

Palmer, W.H., Varghese, F.S., van Rij, R.P., 2018. Natural Variation in Resistance to Virus Infection in Dipteran Insects. Viruses 10, 118. https://doi.org/10.3390/v10030118

Paradkar, P.N., Trinidad, L., Voysey, R., Duchemin, J.-B., Walker, P.J., 2012. Secreted Vago restricts West Nile virus infection in Culex mosquito cells by activating the Jak-STAT pathway. Proceedings of the National Academy of Sciences 109, 18915–18920. https://doi.org/10.1073/pnas.1205231109

Paupy, C., Delatte, H., Bagny, L., Corbel, V., Fontenille, D., 2009. *Aedes albopictus*, an arbovirus vector: From the darkness to the light. Microbes and Infection, Forum on Chikungunya 11, 1177–1185. https://doi.org/10.1016/j.micinf.2009.05.005

Pepin, M., Bouloy, M., Bird, B.H., Kemp, A., Paweska, J., 2010. Rift Valley fever virus (Bunyaviridae: Phlebovirus): an update on pathogenesis, molecular epidemiology, vectors, diagnostics and prevention. Vet. Res. 41, 61. https://doi.org/10.1051/vetres/2010033

Pierson, T.C., Diamond, M.S., 2020. The continued threat of emerging flaviviruses. Nat Microbiol 5, 796–812. https://doi.org/10.1038/s41564-020-0714-0

Poirier, E.Z., Goic, B., Tomé-Poderti, L., Frangeul, L., Boussier, J., Gausson, V., Blanc, H., Vallet, T., Loyd, H., Levi, L.I., Lanciano, S., Baron, C., Merkling, S.H., Lambrechts, L., Mirouze, M., Carpenter, S., Vignuzzi, M., Saleh, M.-C., 2018. Dicer-2-Dependent Generation of Viral DNA from Defective Genomes of RNA Viruses Modulates Antiviral Immunity in Insects. Cell Host & Microbe 23, 353-365.e8. https://doi.org/10.1016/j.chom.2018.02.001

Powell, J.R., Tabachnick, W.J., 2013. History of domestication and spread of Aedes aegypti--a review. Mem Inst Oswaldo Cruz 108 Suppl 1, 11–17. https://doi.org/10.1590/0074-0276130395

Quinlan, A.R., Hall, I.M., 2010. BEDTools: a flexible suite of utilities for comparing genomic features. Bioinformatics 26, 841–842. https://doi.org/10.1093/bioinformatics/btq033

Rabe, I.B., Hills, S.L., Haussig, J.M., Walker, A.T., dos Santos, T., San Martin, J.L., Gutierrez, G., Mendez-Rico, J., Rodriguez, J.C., Elizondo-Lopez, D., Gonzalez-Escobar, G., Chanda, E., Al Eryani, S.M., Kodama, C., Yajima, A., Kakkar, M., Kato, M., Wijesinghe, P.R., Samaraweera, S., Brindle, H., Tissera, H., Kelley, J., Lackritz, E., Rojas, D.P., 2025. A Review of the Recent Epidemiology of Zika Virus Infection. Am J Trop Med Hyg 112, 1026–1035. https://doi.org/10.4269/ajtmh.24-0420

Ramos-Lorente, S., Romero-López, C., Berzal-Herranz, A., 2021. Information Encoded by the Flavivirus Genomes beyond the Nucleotide Sequence. International Journal of Molecular Sciences 22, 3738. https://doi.org/10.3390/ijms22073738

Reffsin, S., Miller, J., Ayyanathan, K., Dunagin, M.C., Heyman, Y., Jain, N., Schultz, D.C., Cherry, S., Raj, A., 2026. Single-cell susceptibility to viral infection is driven by variable cell states. Cell 189, 179-195.e21. https://doi.org/10.1016/j.cell.2025.10.021

Rice, C.M., Levis, R., Strauss, J.H., Huang, H.V., 1987. Production of infectious RNA transcripts from Sindbis virus cDNA clones: mapping of lethal mutations, rescue of a temperature-sensitive

marker, and in vitro mutagenesis to generate defined mutants. Journal of Virology 61, 3809–3819. https://doi.org/10.1128/jvi.61.12.3809-3819.1987
Rodriguez-Andres, J., Axford, J., Hoffmann, A., Fazakerley, J., 2023. Mosquito transgenerational antiviral immunity is mediated by vertical transfer of virus DNA sequences and RNAi. iScience 27, 108598. https://doi.org/10.1016/j.isci.2023.108598
Rogers, K., 2025. Aedes | Description, Life Cycle, & Disease Transmission | Britannica [WWW Document]. URL https://www.britannica.com/animal/Aedes (accessed 9.27.25).
Roussel, A., Lescar, J., Vaney, M.-C., Wengler, Gisela, Wengler, Gerd, Rey, F.A., 2006. Structure and Interactions at the Viral Surface of the Envelope Protein E1 of Semliki Forest Virus. Structure 14, 75–86. https://doi.org/10.1016/j.str.2005.09.014
Rozen-Gagnon, K., Gu, M., Luna, J.M., Luo, J.-D., Yi, S., Novack, S., Jacobson, E., Wang, W., Paul, M.R., Scheel, T.K.H., Carroll, T., Rice, C.M., 2021. Argonaute-CLIP delineates versatile, functional RNAi networks in *Aedes aegypti*, a major vector of human viruses. Cell Host & Microbe 29, 834-848.e13. https://doi.org/10.1016/j.chom.2021.03.004
Rückert, C., Ebel, G.D., 2018. How Do Virus–Mosquito Interactions Lead to Viral Emergence? Trends in Parasitology 34, 310–321. https://doi.org/10.1016/j.pt.2017.12.004
Rückert, C., Prasad, A.N., Garcia-Luna, S.M., Robison, A., Grubaugh, N.D., Weger-Lucarelli, J., Ebel, G.D., 2019a. Small RNA responses of CuIex mosquitoes and cell lines during acute and persistent virus infection. Insect Biochem Mol Biol 109, 13–23. https://doi.org/10.1016/j.ibmb.2019.04.008
Rückert, C., Prasad, A.N., Garcia-Luna, S.M., Robison, A., Grubaugh, N.D., Weger-Lucarelli, J., Ebel, G.D., 2019b. Small RNA responses of CuIex mosquitoes and cell lines during acute and persistent virus infection. Insect Biochem Mol Biol 109, 13–23. https://doi.org/10.1016/j.ibmb.2019.04.008
Saito, K., Sakaguchi, Y., Suzuki, Takeo, Suzuki, Tsutomu, Siomi, H., Siomi, M.C., 2007. Pimet, the Drosophila homolog of HEN1, mediates 2′-O-methylation of Piwi- interacting RNAs at their 3′ ends. Genes Dev. 21, 1603–1608. https://doi.org/10.1101/gad.1563607
Saldaña, M.A., Etebari, K., Hart, C.E., Widen, S.G., Wood, T.G., Thangamani, S., Asgari, S., Hughes, G.L., 2017. Zika virus alters the microRNA expression profile and elicits an RNAi response in Aedes aegypti mosquitoes. PLoS Negl Trop Dis 11, e0005760. https://doi.org/10.1371/journal.pntd.0005760
Salimi, H., Cain, M.D., Klein, R.S., 2016. Encephalitic Arboviruses: Emergence, Clinical Presentation, and Neuropathogenesis. Neurotherapeutics 13, 514–534. https://doi.org/10.1007/s13311-016-0443-5
Samuel, G.H., Pohlenz, T., Dong, Y., Coskun, N., Adelman, Z.N., Dimopoulos, G., Myles, K.M., 2023. RNA interference is essential to modulating the pathogenesis of mosquito-borne viruses in the yellow fever mosquito Aedes aegypti. Proceedings of the National Academy of Sciences 120, e2213701120. https://doi.org/10.1073/pnas.2213701120
Sanchez-Vargas, I., Olson, K.E., Black, W.C., 2021. The Genetic Basis for Salivary Gland Barriers to Arboviral Transmission. Insects 12, 73. https://doi.org/10.3390/insects12010073
Sánchez-Vargas, I., Scott, J.C., Poole-Smith, B.K., Franz, A.W.E., Barbosa-Solomieu, V., Wilusz, J., Olson, K.E., Blair, C.D., 2009. Dengue Virus Type 2 Infections of Aedes aegypti Are Modulated by the Mosquito's RNA Interference Pathway. PLOS Pathogens 5, e1000299. https://doi.org/10.1371/journal.ppat.1000299
Scherer, C., 2021. Identifying the diverse functionalities and characteristics of the RNAi response against arthropod-borne viruses in mosquitoes. University Hamburg.
Scherer, C., Knowles, J., Sreenu, V.B., Fredericks, A.C., Fuss, J., Maringer, K., Fernandez-Sesma, A., Merits, A., Varjak, M., Kohl, A., Schnettler, E., 2021. An Aedes aegypti-Derived Ago2 Knockout Cell Line to Investigate Arbovirus Infections. Viruses 13, 1066. https://doi.org/10.3390/v13061066
Schnettler, E., Donald, C.L., Human, S., Watson, M., Siu, R.W.C., McFarlane, M., Fazakerley, J.K., Kohl, A., Fragkoudis, R., 2013. Knockdown of piRNA pathway proteins results in enhanced Semliki

Forest virus production in mosquito cells. J Gen Virol 94, 1680–1689. https://doi.org/10.1099/vir.0.053850-0
Schnettler, E., Sreenu, V.B., Mottram, T., McFarlane, M., 2016. Wolbachia restricts insect-specific flavivirus infection in Aedes aegypti cells. J Gen Virol 97, 3024–3029. https://doi.org/10.1099/jgv.0.000617
Schultz, M.J., Frydman, H.M., Connor, J.H., 2018. Dual Insect specific virus infection limits Arbovirus replication in Aedes mosquito cells. Virology 518, 406–413. https://doi.org/10.1016/j.virol.2018.03.022
Schuster, S., Overheul, G.J., Bauer, L., van Kuppeveld, F.J.M., van Rij, R.P., 2019. No evidence for viral small RNA production and antiviral function of Argonaute 2 in human cells. Sci Rep 9, 13752. https://doi.org/10.1038/s41598-019-50287-w
Shalamova, L., Barth, P., Pickin, M.J., Kouti, K., Ott, B., Humpert, K., Janssen, S., Lorenzo, G., Brun, A., Goesmann, A., Hain, T., Hartmann, R.K., Rossbach, O., Weber, F., 2024. Nucleocapsids of the Rift Valley fever virus ambisense S segment contain an exposed RNA element in the center that overlaps with the intergenic region. Nat Commun 15, 7602. https://doi.org/10.1038/s41467-024-52058-2
Shocket, M.S., Verwillow, A.B., Numazu, M.G., Slamani, H., Cohen, J.M., El Moustaid, F., Rohr, J., Johnson, L.R., Mordecai, E.A., 2020. Transmission of West Nile and five other temperate mosquito-borne viruses peaks at temperatures between 23°C and 26°C. Elife 9, e58511. https://doi.org/10.7554/eLife.58511
Sinha, N.K., Iwasa, J., Shen, P.S., Bass, B.L., 2018. Dicer uses distinct modules for recognizing dsRNA termini. Science 359, 329–334. https://doi.org/10.1126/science.aaq0921
Sinha, N.K., Trettin, K.D., Aruscavage, P.J., Bass, B.L., 2015a. Drosophila Dicer-2 Cleavage Is Mediated by Helicase- and dsRNA Termini-Dependent States that Are Modulated by Loquacious-PD. Molecular Cell 58, 406–417. https://doi.org/10.1016/j.molcel.2015.03.012
Sinha, N.K., Trettin, K.D., Aruscavage, P.J., Bass, B.L., 2015b. Drosophila Dicer-2 Cleavage Is Mediated by Helicase- and dsRNA Termini-Dependent States that Are Modulated by Loquacious-PD. Molecular Cell 58, 406–417. https://doi.org/10.1016/j.molcel.2015.03.012
Siu, R.W.C., Fragkoudis, R., Simmonds, P., Donald, C.L., Chase-Topping, M.E., Barry, G., Attarzadeh-Yazdi, G., Rodriguez-Andres, J., Nash, A.A., Merits, A., Fazakerley, J.K., Kohl, A., 2011. Antiviral RNA Interference Responses Induced by Semliki Forest Virus Infection of Mosquito Cells: Characterization, Origin, and Frequency-Dependent Functions of Virus-Derived Small Interfering RNAs. Journal of Virology 85, 2907–2917. https://doi.org/10.1128/jvi.02052-10
Smithburn, K.C., Haddow, A., 1944. Semliki Forest Virus. I. Isolation and Pathogenic Properties. Journal of Immunology.
Stollar, V., Thomas, V.L., 1975. An agent in the Aedes aegypti cell line (Peleg) which causes fusion of Aedes albopictus cells. Virology 64, 367–377. https://doi.org/10.1016/0042-6822(75)90113-0
Stoye, J.P., 2012. Studies of endogenous retroviruses reveal a continuing evolutionary saga | Nature Reviews Microbiology. Nature Reviews Microbiology 395–406.
Strauss, J.H., Strauss, E.G., 1994. The alphaviruses: gene expression, replication, and evolution. Microbiological Reviews 58, 491–562. https://doi.org/10.1128/mr.58.3.491-562.1994
Suzuki, Y., Baidaliuk, A., Miesen, P., Frangeul, L., Crist, A.B., Merkling, S.H., Fontaine, A., Lequime, S., Moltini-Conclois, I., Blanc, H., van Rij, R.P., Lambrechts, L., Saleh, M.-C., 2020. Non-retroviral Endogenous Viral Element Limits Cognate Virus Replication in Aedes aegypti Ovaries. Curr Biol 30, 3495-3506.e6. https://doi.org/10.1016/j.cub.2020.06.057
Suzuki, Y., Frangeul, L., Dickson, L.B., Blanc, H., Verdier, Y., Vinh, J., Lambrechts, L., Saleh, M.-C., 2017. Uncovering the Repertoire of Endogenous Flaviviral Elements in Aedes Mosquito Genomes. Journal of Virology 91, 10.1128/jvi.00571-17. https://doi.org/10.1128/jvi.00571-17
Takeshita, D., Zenno, S., Lee, W.C., Nagata, K., Saigo, K., Tanokura, M., 2007. Homodimeric structure and double-stranded RNA cleavage activity of the C-terminal RNase III domain of human dicer. J Mol Biol 374, 106–120. https://doi.org/10.1016/j.jmb.2007.08.069

Tassetto, M., Kunitomi, M., Whitfield, Z.J., Dolan, P.T., Sánchez-Vargas, I., Garcia-Knight, M., Ribiero, I., Chen, T., Olson, K.E., Andino, R., 2019. Control of RNA viruses in mosquito cells through the acquisition of vDNA and endogenous viral elements. eLife 8, e41244. https://doi.org/10.7554/eLife.41244

ter Horst, A.M., Nigg, J.C., Dekker, F.M., Falk, B.W., 2019. Endogenous Viral Elements Are Widespread in Arthropod Genomes and Commonly Give Rise to PIWI-Interacting RNAs. Journal of Virology 93, 10.1128/jvi.02124-18. https://doi.org/10.1128/jvi.02124-18

Terasaki, K., Kalveram, B., Johnson, K.N., Juelich, T., Smith, J.K., Zhang, L., Freiberg, A.N., Makino, S., 2021. Rift Valley fever virus 78kDa envelope protein attenuates virus replication in macrophage-derived cell lines and viral virulence in mice. PLOS Neglected Tropical Diseases 15, e0009785. https://doi.org/10.1371/journal.pntd.0009785

Turell, M.J., Rossi, C.A., 1991. Potential for Mosquito Transmission of Attenuated Strains of Rift Valley Fever Virus. The American Journal of Tropical Medicine and Hygiene 44, 278–282. https://doi.org/10.4269/ajtmh.1991.44.278

Varela, M., Schnettler, E., Caporale, M., Murgia, C., Barry, G., McFarlane, M., McGregor, E., Piras, I.M., Shaw, A., Lamm, C., Janowicz, A., Beer, M., Glass, M., Herder, V., Hahn, K., Baumgärtner, W., Kohl, A., Palmarini, M., 2013. Schmallenberg Virus Pathogenesis, Tropism and Interaction with the Innate Immune System of the Host. PLOS Pathogens 9, e1003133. https://doi.org/10.1371/journal.ppat.1003133

Varjak, M., Dietrich, I., Sreenu, V.B., Till, B.E., Merits, A., Kohl, A., Schnettler, E., 2018a. Spindle-E Acts Antivirally Against Alphaviruses in Mosquito Cells. Viruses 10, 88. https://doi.org/10.3390/v10020088

Varjak, M., Donald, C.L., Mottram, T.J., Sreenu, V.B., Merits, A., Maringer, K., Schnettler, E., Kohl, A., 2017a. Characterization of the Zika virus induced small RNA response in Aedes aegypti cells. PLOS Neglected Tropical Diseases 11, e0006010. https://doi.org/10.1371/journal.pntd.0006010

Varjak, M., Leggewie, M., Schnettler, E., 2018b. The antiviral piRNA response in mosquitoes? Journal of General Virology 99, 1551–1562. https://doi.org/10.1099/jgv.0.001157

Varjak, M., Maringer, K., Watson, M., Sreenu, V.B., Fredericks, A.C., Pondeville, E., Donald, C.L., Sterk, J., Kean, J., Vazeille, M., Failloux, A.-B., Kohl, A., Schnettler, E., 2017b. Aedes aegypti Piwi4 Is a Noncanonical PIWI Protein Involved in Antiviral Responses. mSphere 2, e00144-17. https://doi.org/10.1128/mSphere.00144-17

Vasilakis, N., Tesh, R.B., 2015. Insect-specific viruses and their potential impact on arbovirus transmission. Current Opinion in Virology, SI: 15 Virus–vector interactions•Viral immunology 15, 69–74. https://doi.org/10.1016/j.coviro.2015.08.007

Vega-Rúa, A., Schmitt, C., Bonne, I., Krijnse Locker, J., Failloux, A.-B., 2015. Chikungunya Virus Replication in Salivary Glands of the Mosquito Aedes albopictus. Viruses 7, 5902–5907. https://doi.org/10.3390/v7112917

Vodovar, N., Bronkhorst, A.W., van Cleef, K.W.R., Miesen, P., Blanc, H., van Rij, R.P., Saleh, M.-C., 2012. Arbovirus-derived piRNAs exhibit a ping-pong signature in mosquito cells. PLoS One 7, e30861. https://doi.org/10.1371/journal.pone.0030861

Weaver, S.C., Charlier, C., Vasilakis, N., Lecuit, M., 2018. Zika, Chikungunya, and Other Emerging Vector-Borne Viral Diseases. Annual Review of Medicine 69, 395–408. https://doi.org/10.1146/annurev-med-050715-105122

Weaver, S.C., Reisen, W.K., 2010. Present and future arboviral threats. Antiviral Research 85, 328–345. https://doi.org/10.1016/j.antiviral.2009.10.008

Werren, J.H., 1997. Biology of Wolbachia. Annu Rev Entomol 42, 587–609. https://doi.org/10.1146/annurev.ento.42.1.587

Whitfield, Z.J., Dolan, P.T., Kunitomi, M., Tassetto, M., Seetin, M.G., Oh, S., Heiner, C., Paxinos, E., Andino, R., 2017. The Diversity, Structure, and Function of Heritable Adaptive Immunity Sequences in the Aedes aegypti Genome. Curr Biol 27, 3511-3519.e7. https://doi.org/10.1016/j.cub.2017.09.067

Wostenberg, C., Lary, J.W., Sahu, D., Acevedo, R., Quarles, K.A., Cole, J.L., Showalter, S.A., 2012. The Role of Human Dicer-dsRBD in Processing Small Regulatory RNAs. PLOS ONE 7, e51829. https://doi.org/10.1371/journal.pone.0051829

Xia, H., Zhang, C., Guo, Z., Chen, L., Chen, K., 2025. The JAK-STAT pathway in invertebrates: An emerging battleground for host–virus warfare. Insect Sci. https://doi.org/10.1111/1744-7917.70109

Yang, Z., Vilkaitis, G., Yu, B., Klim, 2007. Approaches for Studying MicroRNA and Small Interfering RNA Methylation In Vitro and In Vivo. Methods in Enzymology 427, 139–154. https://doi.org/10.1016/S0076-6879(07)27008-9

Yen, P.-S., Failloux, A.-B., 2020. A Review: Wolbachia-Based Population Replacement for Mosquito Control Shares Common Points with Genetically Modified Control Approaches. Pathogens 9, 404. https://doi.org/10.3390/pathogens9050404

Zaid, A., Burt, F.J., Liu, X., Poo, Y.S., Zandi, K., Suhrbier, A., Weaver, S.C., Texeira, M.M., Mahalingam, S., 2021. Arthritogenic alphaviruses: epidemiological and clinical perspective on emerging arboviruses. The Lancet Infectious Diseases 21, e123–e133. https://doi.org/10.1016/S1473-3099(20)30491-6

Zhang, G., Asad, S., Khromykh, A.A., Asgari, S., 2017. Cell fusing agent virus and dengue virus mutually interact in Aedes aegypti cell lines. Sci Rep 7, 6935. https://doi.org/10.1038/s41598-017-07279-5

Zhang, Y., Ba, J., Luan, J., Qi, Z., Liu, B., 2025. Orthoflavivirus infection and the mTOR signaling pathway. Front. Microbiol. 16. https://doi.org/10.3389/fmicb.2025.1565350

Acknowledgements

Who would have thought I'd one day sit here and write the last words of my dissertation? Not me. Especially not without the help of a lot of exceptional people around me.

First of all, I want to thank Prof. Dr. Esther Schnettler for not just giving me the opportunity to do my PhD in her lab, but also for helping me and my fellow PhD students every step of the way. No matter the amount of questions and confusion, you were always there to listen, to help, to give advice and share a story or two. Your guidance and spirit help every person in that lab, and it especially helped to ground me and keep the vision going.

The same way I want to thank my fellow students: Philipp, Sarah, Swati, Svea and Alessia. Without you guys the last three years would have been indefinitely harder. No matter if it was pure banter or if we locked in to help each other with experiments or data analysis. I will miss our chats and the sometimes chaotic but always fun atmosphere both in the lab and the basement office, our little Slytherin dungeon room. These thanks also extent to Dr. Mine Altinli, Marlis, and last but not least, Bernhard. The support you supplied was indispensable for both me and this thesis.

I also want to give a big thank you to Dr. Susann Dornbusch. We were brought together by the pure circumstance of work for our respective dissertations and the paper we penned together, but it quickly developed into a friendship I do not want to miss. Thank you for countless hours spent on both zoom for work and the phone for private conversations. Thank you for helping me realize I was good at what I am doing, for always being there when I needed to vent or ask a question that none of my friends would be able to answer. Thank you for being a friend when I needed one.

Also thank you to my co-supervisors, Dr. Beatriz Escudero-Pérez and Dr. Tobias Spielmann for your advice and support. Special thanks to Beatriz for not just being a supervisor, but also a friend, who has shared her home and her city with me. I will never forget the amazing week we had in Barcelona thanks to you.

Another person that derserves a big thank you: Marta. Thank you for being the best friend I could have ever wished for. Thank you for your unconditional support, the long nights and boozy days, the always amazing food and the laughter we share. You are a big part of what makes my life good, and I would never want to miss that. I can't wait to continue seeing the world with you.

I could never finish writing the acknowledgements without mentioning my mother. My biggest supporter, my number one fan and coolest mother ever. Despite the difficulties we had to face through both our lifes, you never faltered in your determination to give me the best chance I could have at life. I am forever grateful to have you, and without you, I wouldn't be here – not just because you gave me life, but because I would have never managed to get this far without your love and support. Thank you for being you.

(Extremely) honourable mentions of people I want to thank for being in my life: Julia, the best roommate; Toni and Lily, my Hamburg gaming companions; Felix and Fin, my Glasgow gaming companions; Natscha and Matti, and Tine and Emil, the sweet boys and their amazing mothers; Doro, the best deep-talk friend; and of course: Eddie and Morty, my lovely cats.

Chapter 8: Supplementary data

Publication 1

Supplementary data is available online.

Publication 3

Supplementary data is available online.

Publication 4

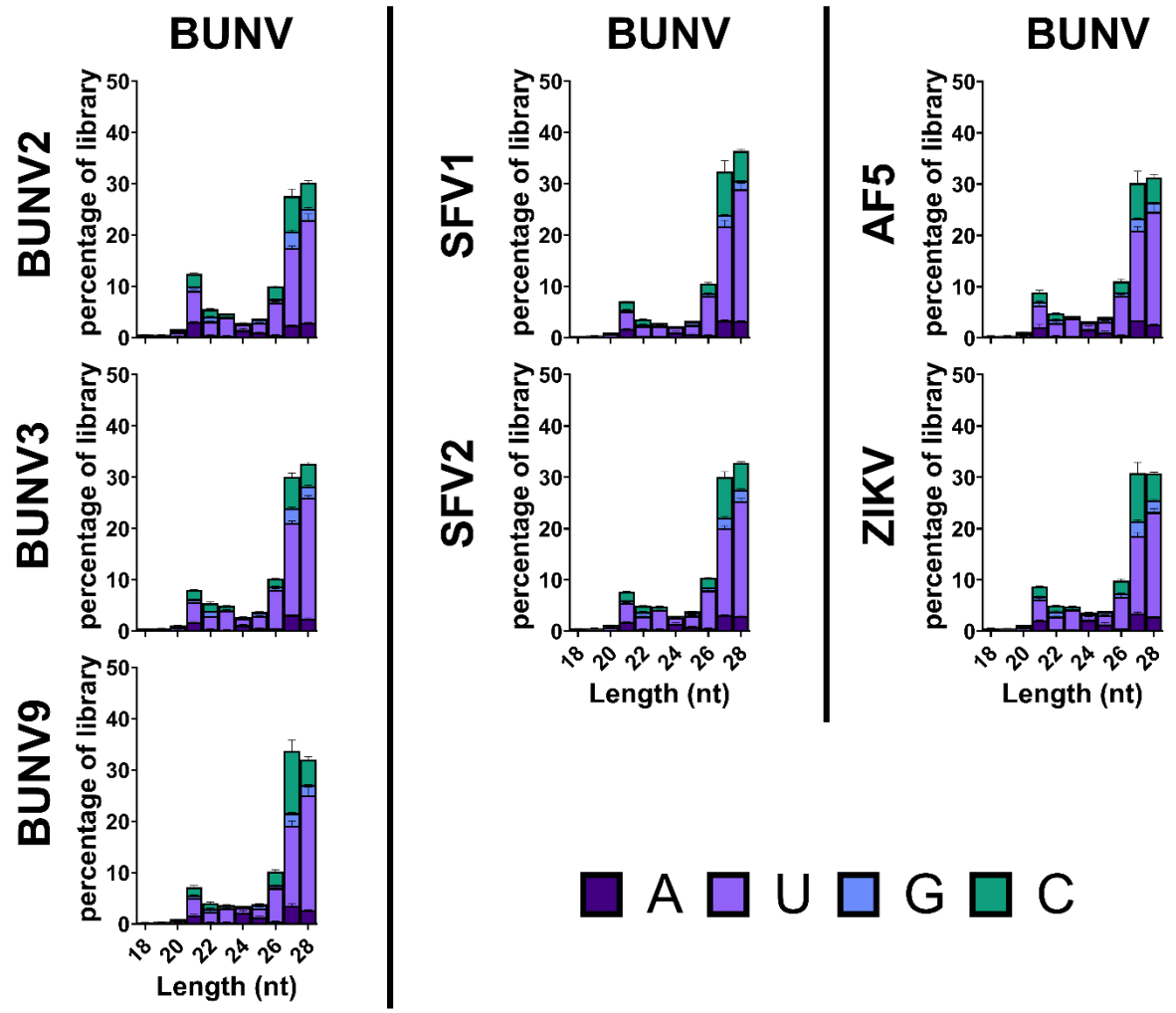


Fig. S1: Size distribution and first base bias of raw BUNV-Nluc infected small RNA data libraries. After production of BUNV, SFV and ZIKV primed AF5 cells, the cells were infected with BUNV-Nluc alongside naïve AF5 cells, as control, before total RNA extraction and small RNA sequencing. Graphs are averaged from three independent biological repeats with error bars indicating ± SD. The colours indicate first nucleotide prevalence (Adenine – dark purple, Uracil – light purple, Guanine – blue, Cytosine – green).

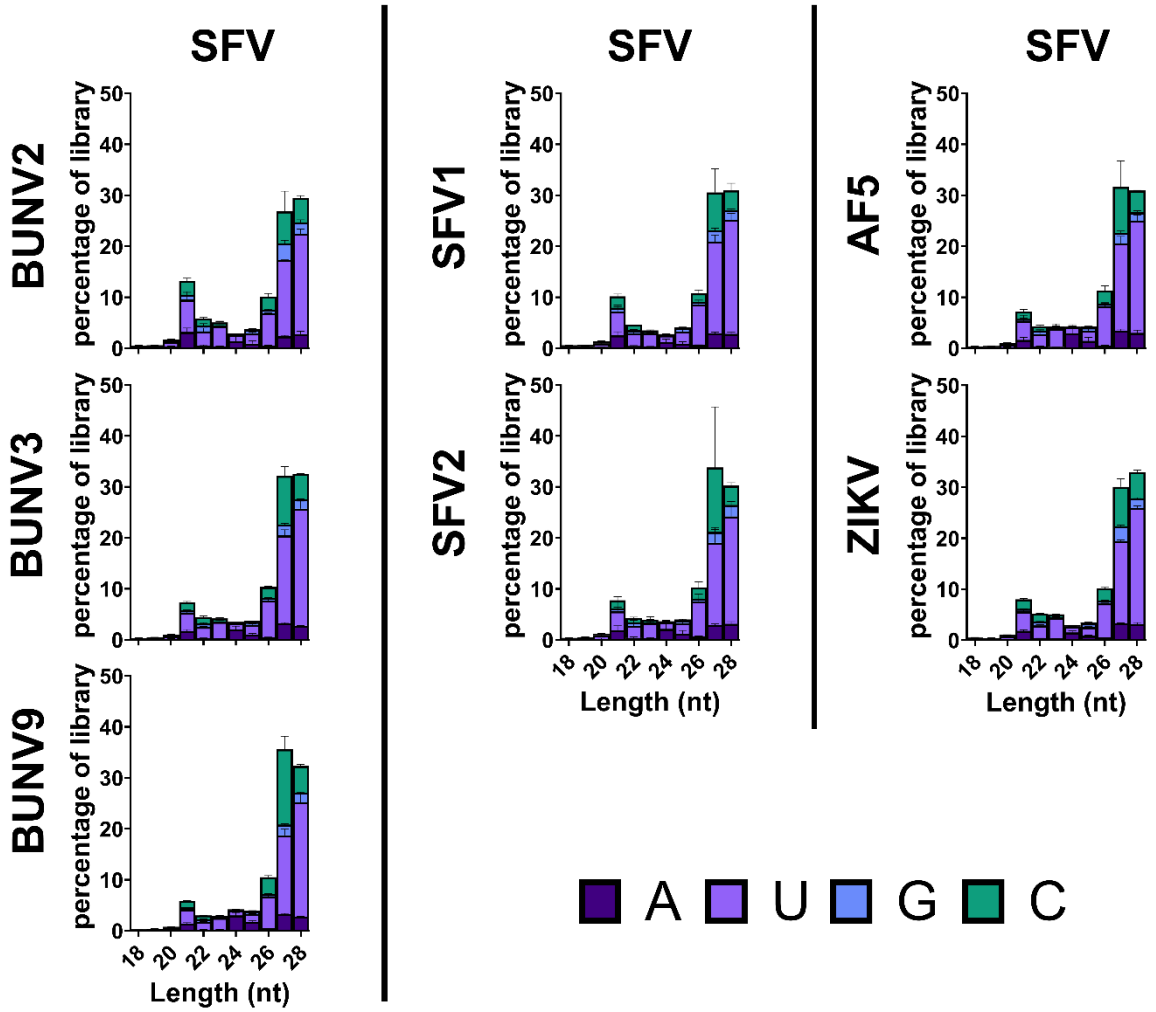


Fig. S2: Size distribution and first base bias of raw SFV-Nluc infected small RNA data libraries. BUNV, SFV and ZIKV primed AF5 cells were infected with SFV-Nluc alongside naïve AF5 cells, as control, before total RNA extraction and small RNA sequencing. Graphs are averaged from three independent biological repeats with error bars indicating ± SD. (Adenine – dark purple, Uracil – light purple, Guanine – blue, Cytosine – green).

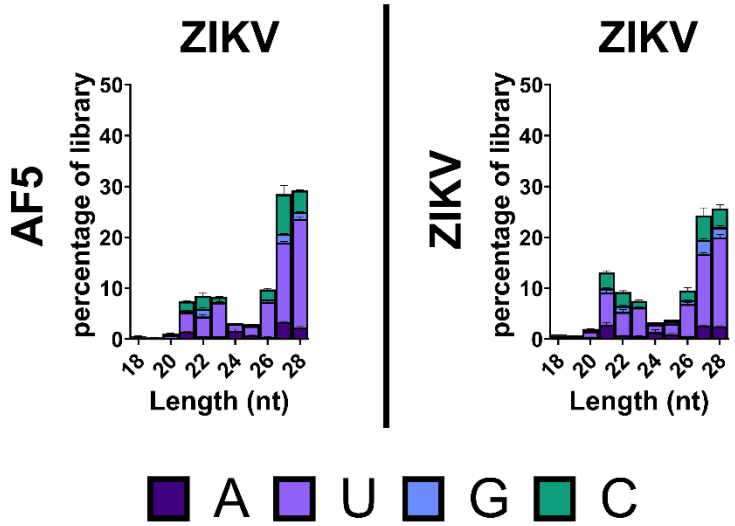


Fig. S3: Size distribution and first base bias of raw ZIKV-Nluc infected small RNA data libraries. ZIKV primed AF5 cells were infected with ZIKV-Nluc alongside naïve AF5 cells, as control, before total RNA extraction and small RNA sequencing. Graphs are averaged from three independent biological repeats with error bars indicating ± SD. (Adenine – dark purple, Uracil – light purple, Guanine – blue, Cytosine – green).

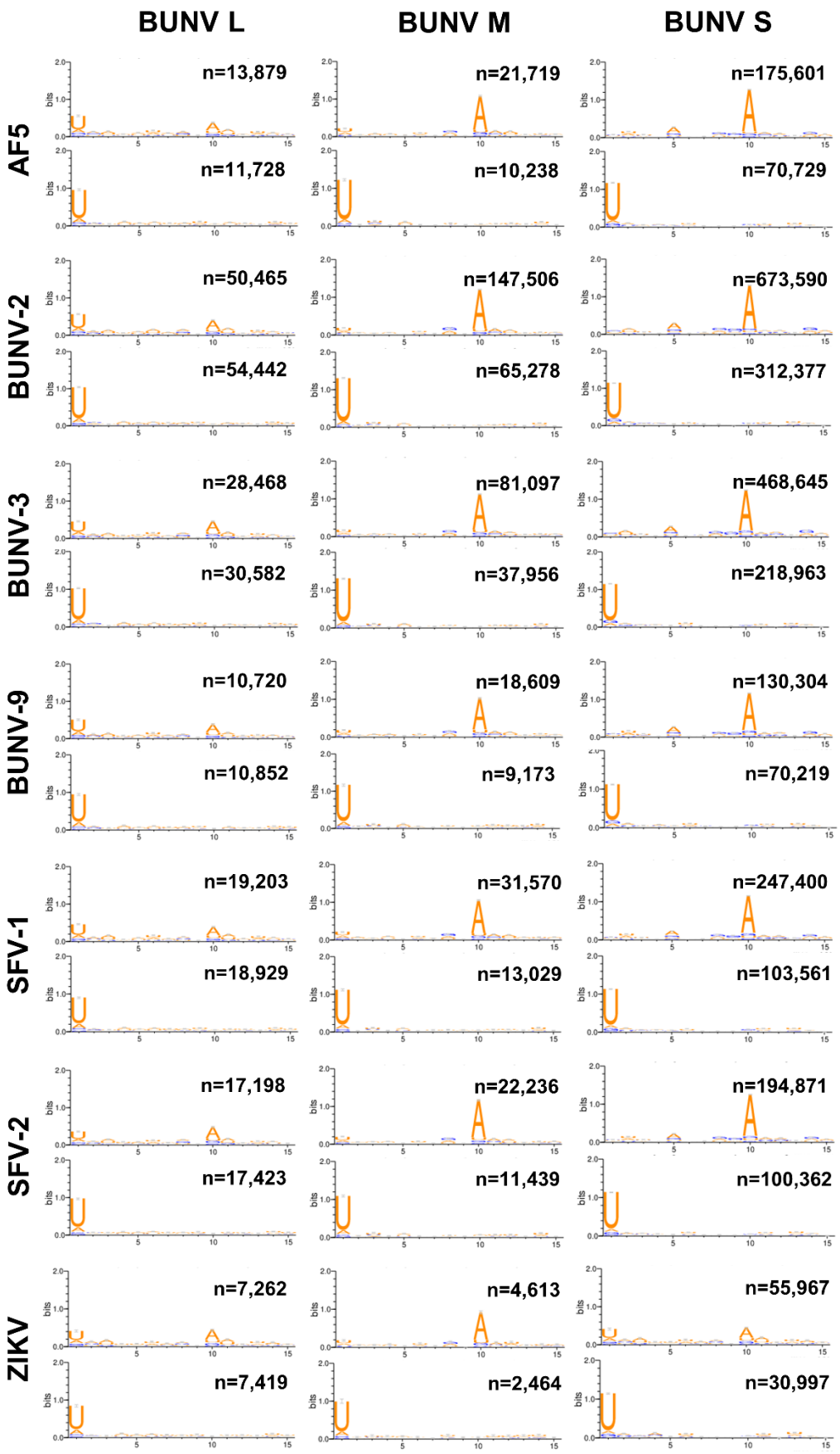

BUNV L
BUNV M
BUNV S
AF5
n=13,879
n=21,719
n=175,601
n=11,728
n=10,238
n=70,729
BUNV-2
n=50,465
n=147,506
n=673,590
n=54,442
n=65,278
n=312,377
BUNV-3
n=28,468
n=81,097
n=468,645
n=30,582
n=37,956
n=218,963
BUNV-9
n=10,720
n=18,609
n=130,304
n=10,852
n=9,173
n=70,219
SFV-1
n=19,203
n=31,570
n=247,400
n=18,929
n=13,029
n=103,561
SFV-2
n=17,198
n=22,236
n=194,871
n=17,423
n=11,439
n=100,362
ZIKV
n=7,262
n=4,613
n=55,967
n=7,419
n=2,464
n=30,997

Fig. S4: BUNV-specific piRNAs in BUNV-Nluc infected primed cells and naïve AF5 control. After production of BUNV, SFV and ZIKV primed AF5 cells, the cells were infected with BUNV-Nluc alongside naïve AF5 cells, as control, before total RNA extraction and small RNA sequencing. Sequence logos for the L- (Large, left side), M- (Medium, middle) and S-segment (Small, right side) of BUNV with 25-28 nt reads trimmed down to first 15 nt. Graphs present base frequencies at each position of reads mapping to BUNV antigenome (top) and genome (bottom). Height of each symbol corresponding to RNA bases (A - Adenine, U - Uracil, G - Guanine, C - Cytosine) represents the relative frequency of the corresponding nucleotide, while the combined height of the stacks at a given position indicates conservation presented as bits. Number of reads across three independent biological repeats are shown in top right of each figure. Error bars indicate ~95% credible interval.

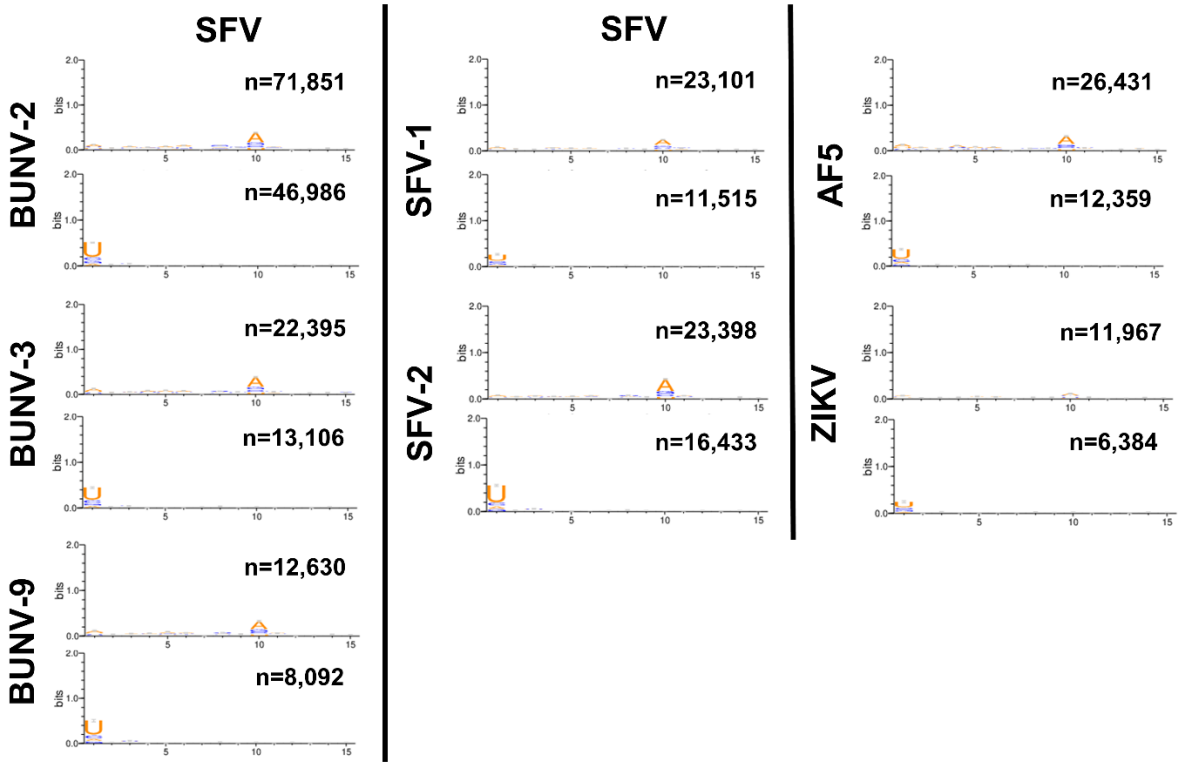


Fig. S5: SFV-specific piRNAs in SFV-Nluc infected primed cells and naïve AF5 control. BUNV, SFV and ZIKV primed AF5 cells were infected with SFV-Nluc alongside naïve AF5 cells, as control, before total RNA extraction and small RNA sequencing. Sequence logos for SFV-Nluc infected samples with 25-28 nt reads trimmed down to first 15 nt. Graphs present base frequencies at each position of reads mapping to SFV genome (top) and antigenome (bottom). Height of each symbol corresponding to RNA bases (A - Adenine, U - Uracil, G - Guanine, C - Cytosine) represents the relative frequency of the corresponding nucleotide, while the combined height of the stacks at a given position indicates conservation presented as bits. Number of reads across three independent biological repeats are shown in top right of each figure. Error bars indicate ~95% credible interval.

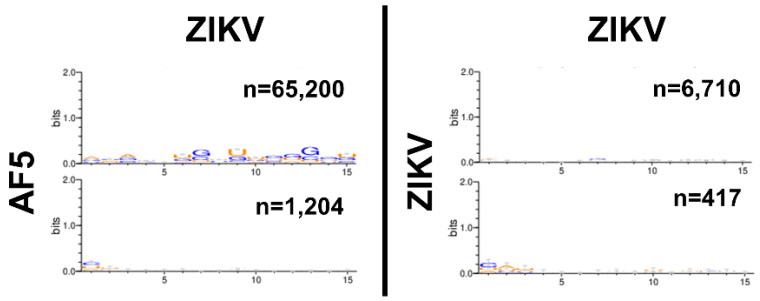


Fig. S6: ZIKV-specific piRNAs in SFV-Nluc infected primed cells and naïve AF5 control. ZIKV primed AF5 cells were infected with ZIKV-Nluc alongside naïve AF5 cells, as control, before total RNA extraction and small RNA sequencing. Sequence logos for ZIKV-Nluc infected samples with 25-28 nt reads trimmed down to first 15 nt. Graphs present base frequencies at each position of reads mapping to ZIKV genome (top) and antigenome (bottom). Height of each symbol corresponding to RNA bases (A - Adenine, U - Uracil, G - Guanine, C - Cytosine) represents the relative frequency of the corresponding nucleotide, while the combined height of the stacks at a given position indicates conservation presented as bits. Number of reads across three independent biological repeats are shown in top right of each figure. Error bars indicate ~95% credible interval.

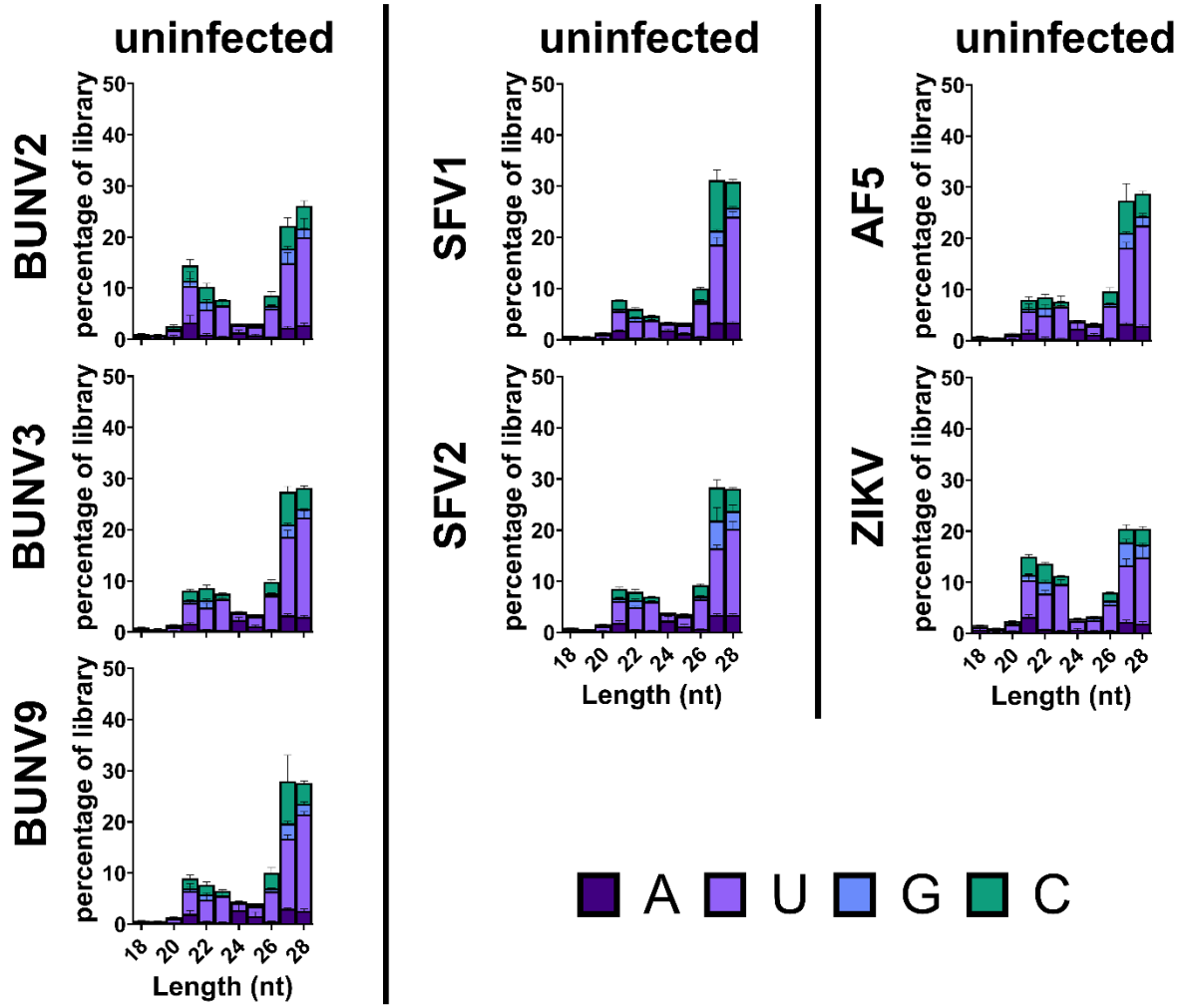


Fig. S7: Size distribution and first base bias of raw uninfected small RNA data libraries. Uninfected BUNV, SFV and ZIKV primed AF5 cells and naïve AF5 cells for control were used for total RNA extraction and small RNA sequencing. Graphs are averaged from three independent biological repeats with error bars indicating ± SD. (Adenine – dark purple, Uracil – light purple, Guanine – blue, Cytosine – green).

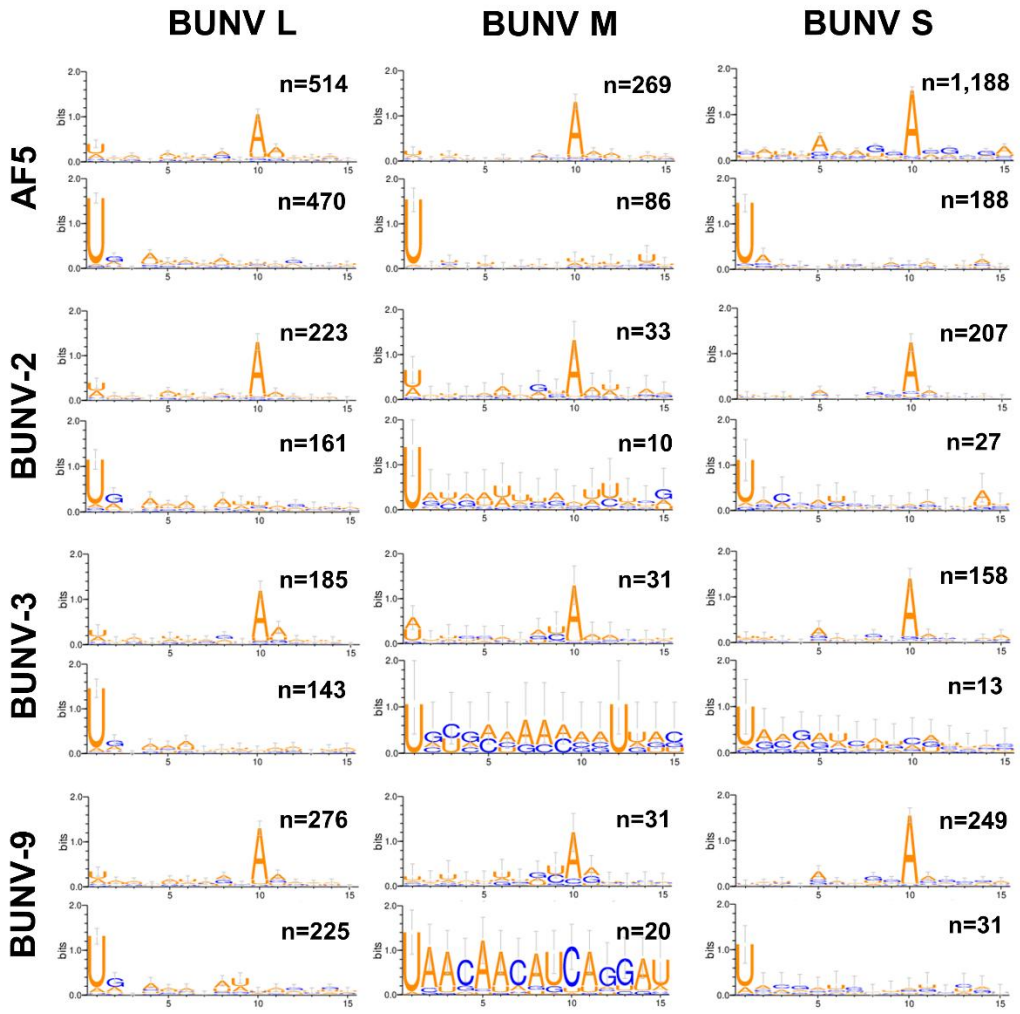


Fig. S8: BUNV-specific piRNAs in uninfected, BUNV-Nluc primed cells and naïve AF5 control. Uninfected BUNV primed AF5 cells and naïve AF5 cells for control were used for total RNA extraction and small RNA sequencing. Sequence logos for the L- (Large, left side), M- (Medium, middle) and S-segment (Small, right side) of BUNV with 25-28 nt reads trimmed down to first 15 nt. Graphs present base frequencies at each position of reads mapping to BUNV antigenome (top) and genome (bottom). Height of each symbol corresponding to RNA bases (A - Adenine, U - Uracil, G - Guanine, C - Cytosine) represents the relative frequency of the corresponding nucleotide, while the combined height of the stacks at a given position indicates conservation presented as bits. Number of reads across three independent biological repeats are shown in top right of each figure. Error bars indicate ~95% credible interval.

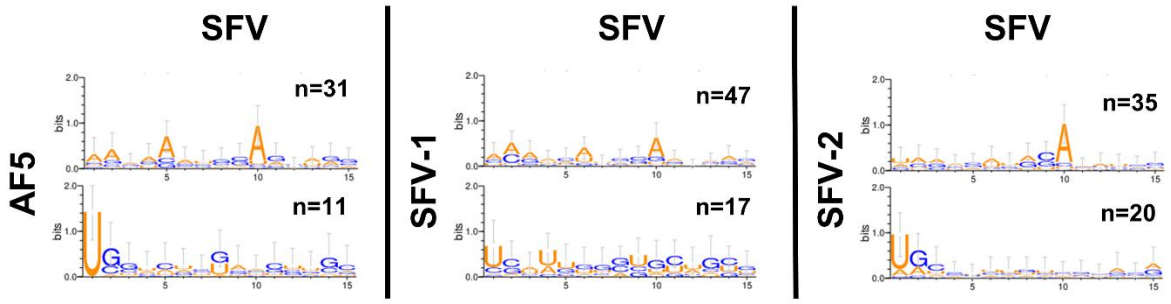


Fig. S9: SFV-specific piRNAs in uninfected, SFV-Nluc primed cells and naïve AF5 control. Uninfected SFV primed AF5 cells and naïve AF5 cells for control were used for total RNA extraction and small RNA sequencing. Sequence logos for SFV-Nluc infected samples with 25-28 nt reads trimmed down to first 15 nt. Graphs present base frequencies at each position of reads mapping to SFV genome (top) and antigenome (bottom). Height of each symbol corresponding to RNA bases (A - Adenine, U - Uracil, G - Guanine, C - Cytosine) represents the relative frequency of the corresponding nucleotide, while the combined height of the stacks at a given position indicates conservation presented as bits. Number of reads across three independent biological repeats are shown in top right of each figure. Error bars indicate ~95% credible interval.

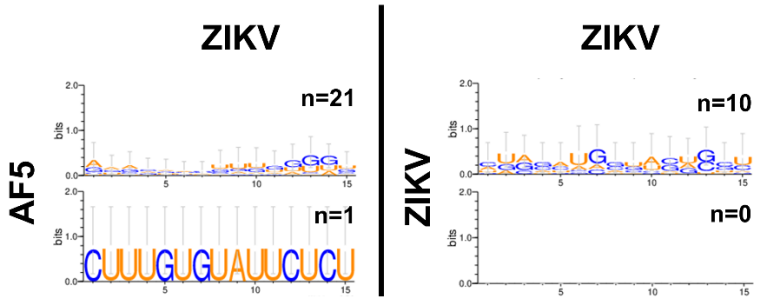


Fig. S10: ZIKV-specific piRNAs in uninfected, ZIKV-Nluc primed cells and naïve AF5 control. Uninfected ZIKV primed AF5 cells and naïve AF5 cells for control were used for total RNA extraction and small RNA sequencing. Sequence logos for ZIKV-Nluc infected samples with 25-28 nt reads trimmed down to first 15 nt. Graphs present base frequencies at each position of reads mapping to ZIKV genome (top) and antigenome (bottom). Height of each symbol corresponding to RNA bases (A - Adenine, U - Uracil, G - Guanine, C - Cytosine) represents the relative frequency of the corresponding nucleotide, while the combined height of the stacks at a given position indicates conservation presented as bits. Number of reads across three independent biological repeats are shown in top right of each figure. Error bars indicate ~95% credible interval.

Table S1. Primer sequences.

Usage	Description	Sequence (5' - 3')	References
PCR (vDNA detection)	BUNV-S 3 FW	AGATGCTGAAAGTCAGTGAACC	
	BUNV-S 3 RV	CCAACCTAAGCTAGAGACAAC	
	SFV_C_FW	ATGACCTTGAGTGTGCCCAG	
	SFV_C_RV	CGACTACCCTCCCCTTGTTG	
	MP12-M3-FW	GGTGCTTAAGTGCCTGAAGA	
	MP12-M3-RV	CCAGACAGTCTACACTTGGTG	
dsRNA production	SFV-T7 FW	GTAATACGACTCACTATAGGGG AACGGCGTATTGGATTGG	(Scherer, 2021)
	SFV-T7 RV	GTAATACGACTCACTATAGGGC TTCCGTTCACAACTATCCTCTG	
	BUNV-S T7 FW	GTAATACGACTCACTATAGGGC TAACTTTAAGCGTGTCCACACC	(Scherer, 2021)
	BUNV-S T7 RV	GTAATACGACTCACTATAGGGG GTAAGACCATCGTCAGGAAC	
	BUNV-L T7 FW	GTAATACGACTCACTATAGGGG GACCCTATACTTTATCCAGC	(Scherer, 2021)
	BUNV-L T7 RV	GTAATACGACTCACTATAGGGC AGTCTCCGTCTAGTAACTTC	
	ZIKV-T7-FW-1	TAATACGACTCACTATAGGGAG ACGTTAGTGGACAGAGGCTG	
	ZIKV-T7-RV-1	TAATACGACTCACTATAGGGAG AAAGTCAAGGCCTGTCCTCG	
	ZIKV-T7-FW-2	TAATACGACTCACTATAGGGAG GAGAGAGTCATTCTGGCTGG	
	ZIKV-T7-RV-2	TAATACGACTCACTATAGGGAG ATGCAACCTGATAGGCCAGC	
CFAV check	CFAV-FW	TTGACGACATATTGAAGAGATAC	
	CFAV-RV	GCCAAGGATACAGTCCAAAAC	
qRT-PCR	Aae-S7 FW	CCAGGCTATCCTGGAGTTG	
	Aae-S7 RV	GACGTGCTTGCCGGAGAAC	
	BUNV M FW	GGGGAAGATACAGGCAATGA	(Scherer, 2021)
	BUNV M RP	CCCACACACAGTCAGTAACAACA	
	SFV-nsP3-FW	GCAAGAGGCAAACGAACAGA	(Rodriguez-Andres et al., 2023)
	SFV-nsP3-RV	GGGAAAAGATGAGCAAACCA	
	TAHV S qPCR FW	GGTGGGACAATGGAGCAGAA	
	TAHV S qPCR RV	CGCTGCCTCAATGCTTTCTT	
	SINV-qPCR-nsp2 FW	CTACAACCTGGCTTTCGGGT	(Gothe et al., 2026)
	SINV-qPCR-nsp2 RV	TAGGACTTCACCACGAGGGT	
	ONNV-qFW-2	CTGAGGCTGAAGGGGATAGG	(Jagtap et al., 2025)
	ONNV-qRV-2	AAAGGGATGGCTACACTGCT	

Table S2. P-values of the antiviral activity analysis of BUNV-Nluc primed cells against BUNV-Nluc using luciferase reporter assay according to Student's t test.

BUNV-Nluc primed, BUNV-Nluc infected (Fig. 10A)						
	BUNV-2 (CFAV +)	BUNV-3 (CFAV -)	BUNV-3 (CFAV +)	BUNV-9 (CFAV -)	BUNV-9 (CFAV +)	control (CFAV +)
BUNV-2 (CFAV +)		0.6604	0.0045	0.0042	0.2451	0.0424
BUNV-3 (CFAV -)	0.6604		0.0930	0.2806	0.3467	0.5807
BUNV-3 (CFAV +)	0.0045	0.0930		0.0008	0.0448	0.0074
BUNV-9 (CFAV -)	0.0042	0.2806	0.0008		0.0153	0.0442
BUNV-9 (CFAV +)	0.2451	0.3467	0.0448	0.0153		0.0500
control (CFAV +)	0.0424	0.5807	0.0074	0.0442	0.0500	

Table S3. P-values of the antiviral activity analysis of SFV-Nluc primed cells against SFV-Nluc using luciferase reporter assay according to Student's t test.

SFV-Nluc primed, SFV-Nluc infected (Fig. 10B)				
	SFV-1 (CFAV +)	SFV-2 (CFAV -)	SFV-2 (CFAV +)	control (CFAV +)
SFV-1 (CFAV +)		0.0171	0.0217	0.4433
SFV-2 (CFAV -)	0.0171		0.2219	0.0156
SFV-2 (CFAV +)	0.0217	0.2219		0.0011
control (CFAV +)	0.4433	0.0156	0.0011	

Table S4. P-values of the antiviral activity analysis of ZIKV-Nluc primed cells against ZIKV-Nluc using luciferase reporter assay according to Student's t test.

ZIKV-Nluc primed, ZIKV-Nluc infected (Fig. 10C)		
	ZIKV (CFAV +)	control (CFAV +)
ZIKV (CFAV +)		0.9499
control (CFAV +)	0.9499	

Table S5. P-values of the antiviral activity analysis of BUNV-Nluc primed cells against SFV-Nluc using luciferase reporter assay according to Student's t test.

BUNV-Nluc primed, SFV-Nluc infected (Fig. 10D)						
	BUNV-2 (CFAV +)	BUNV-3 (CFAV -)	BUNV-3 (CFAV +)	BUNV-9 (CFAV -)	BUNV-9 (CFAV +)	control (CFAV +)
BUNV-2 (CFAV +)		0.0261	0.0003	0.0073	<0.0001	<0.0001
BUNV-3 (CFAV -)	0.0261		0.0084	0.0010	0.7415	0.0006
BUNV-3 (CFAV +)	0.0003	0.0084		0.0020	0.0010	<0.0001
BUNV-9 (CFAV -)	0.0073	0.0010	0.0020		0.0043	0.0158
BUNV-9 (CFAV +)	<0.0001	0.7415	0.0010	0.0043		<0.0001
control (CFAV +)	<0.0001	0.0006	<0.0001	0.0158	<0.0001	

Table S6. P-values of the antiviral activity analysis of SFV-Nluc primed cells against BUNV-Nluc using luciferase reporter assay according to Student's t test.

SFV-Nluc primed, BUNV-Nluc infected (Fig. 10E)				
	SFV-1 (CFAV +)	SFV-2 (CFAV -)	SFV-2 (CFAV +)	control (CFAV +)
SFV-1 (CFAV +)		0.1840	0.6897	0.1312
SFV-2 (CFAV -)	0.1840		0.2132	0.4236
SFV-2 (CFAV +)	0.6897	0.2132		0.1237
control (CFAV +)	0.1312	0.4236	0.1237	

Table S7. P-values of the antiviral activity analysis of ZIKV-Nluc primed cells against BUNV-Nluc using luciferase reporter assay according to Student's t test.

ZIKV-Nluc primed, BUNV-Nluc infected (Fig. 10F)		
	ZIKV (CFAV +)	control (CFAV +)
ZIKV (CFAV +)		0.0017
control (CFAV +)	0.0017	

Table S8. Sequencing and library statistics for small RNA (18-28 nt) from BUNV-Nluc infected samples mapped to BUNV.

Sample	Total read count	Reads mapped to L-segment (%)	Reads mapped to M-segment (%)	Reads mapped to S-segment (%)	Total mapped reads (%)
AF5_BUNV_1	54,990,961	10,203 (0.02)	9,398 (0.02)	64,188 (0.12)	83,789 (0.15)
AF5_BUNV_2	92,371,880	22,103 (0.02)	22,448 (0.02)	154,057 (0.17)	198,608 (0.22)
AF5_BUNV_3	72,520,315	14,605 (0.02)	14,011 (0.02)	102,715 (0.14)	131,331 (0.18)
BUNV2_BUNV_1	67,495,223	65,738 (0.10)	79,738 (0.12)	397,013 (0.59)	542,489 (0.80)
BUNV2_BUNV_2	92,227,484	79,265 (0.09)	113,073 (0.12)	523,824 (0.57)	716,162 (0.78)
BUNV2_BUNV_3	74,658,641	72,732 (0.10)	96,192 (0.13)	439,373 (0.59)	608,297 (0.81)
BUNV3_BUNV_1	37,015,249	27,181 (0.07)	40,337 (0.11)	225,047 (0.61)	292,565 (0.79)
BUNV3_BUNV_2	56,902,985	37,808 (0.07)	58,580 (0.10)	313,924 (0.55)	410,312 (0.72)
BUNV3_BUNV_3	68,753,498	41,097 (0.06)	64,836 (0.09)	330,364 (0.48)	436,297 (0.63)
BUNV9_BUNV_1	41,195,979	12,678 (0.03)	12,053 (0.03)	77,328 (0.19)	102,059 (0.25)
BUNV9_BUNV_2	73,864,724	16,940 (0.02)	15,758 (0.02)	99,512 (0.13)	132,210 (0.18)
BUNV9_BUNV_3	78,871,599	12,780 (0.02)	12,855 (0.02)	82,978 (0.11)	108,613 (0.14)
SFV1_BUNV_1	101,604,819	25,858 (0.03)	23,031 (0.02)	172,917 (0.17)	221,806 (0.22)
SFV1_BUNV_2	131,260,326	29,678 (0.02)	26,388 (0.02)	184,933 (0.14)	240,999 (0.18)
SFV1_BUNV_3	73,129,559	15,371 (0.02)	13.708 (0.02)	102,158 (0.14)	131,237 (0.18)
SFV2_BUNV_1	77,904,275	54,473 (0.07)	41,483 (0.05)	312,034 (0.40)	407,990 (0.52)
SFV2_BUNV_2	40,969,773	4768 (0.01)	2248 (0.01)	18,857 (0.05)	25,873 (0.06)
SFV2_BUNV_3	63,216,974	9240 (0.01)	4906 (0.01)	35,925 (0.06)	50,071 (0.08)
ZIKV_BUNV_1	67,527,428	13,261 (0.02)	4545 (0.01)	42,422 (0.06)	60,228 (0.09)
ZIKV_BUNV_2	54,122,339	12,939 (0.02)	5116 (0.01)	45,691 (0.08)	63,746 (0.12)
ZIKV_BUNV_3	50,113,342	9513 (0.02)	3116 (0.01)	32,462 (0.06)	45,091 (0.09)

Table S9. Sequencing and library statistics for small RNA (18-28 nt) from SFV-Nluc infected samples mapped to SFV.

Sample	Total read count	Reads mapped to SFV (%)
AF5_SFV_1	64,979,147	220.419 (0.34)
AF5_SFV_2	70,389,182	196,905 (0.28)
AF5_SFV_3	82,532,828	151,332 (0.18)
BUNV2_SFV_1	83,852,718	707,675 (0.84)
BUNV2_SFV_2	57,421,665	612,580 (1.07)
BUNV2_SFV_3	81,467,666	494,860 (0.61)
BUNV3_SFV_1	90,695,268	131,860 (0.15)
BUNV3_SFV_2	39,344,749	69,235 (0.18)
BUNV3_SFV_3	49,491,662	302,776 (0.61)
BUNV9_SFV_1	92,083,223	119321 (0.13)
BUNV9_SFV_2	61,662,273	63,656 (0.10)
BUNV9_SFV_3	52,725,145	75,239 (0.14)
SFV1_SFV_1	40,447,398	110,815 (0.27)
SFV1_SFV_2	66,901,646	359,604 (0.54)
SFV1_SFV_3	71,832,130	230,406 (0.32)
SFV2_SFV_1	45,243,859	166,437 (0.37)
SFV2_SFV_2	66,833,908	269,369 (0.40)
SFV2_SFV_3	66,976,111	121,810 (0.18)
ZIKV_SFV_1	79,019,970	148,018 (0.19)
ZIKV_SFV_2	39,179,349	70,940 (0.18)
ZIKV_SFV_3	57,370,754	113,566 (0.20)

Table S10. Sequencing and library statistics for small RNA (18-28 nt) from ZIKV-Nluc infected samples mapped to ZIKV.

Sample	Total read count	Reads mapped to ZIKV (%)
AF5_ZIKV_1	86,904,092	54,010 (0.06)
AF5_ZIKV_2	107,990,504	64,382 (0.06)
AF5_ZIKV_3	92,049,756	44,916 (0.05)
ZIKV_ZIKV_1	104,868,877	12,133 (0.01)
ZIKV_ZIKV_2	70,171,626	12,263 (0.02)
ZIKV_ZIKV_3	109,791,828	11,841 (0.01)

Table S11. Sequencing and library statistics for small RNA (18-28 nt) from uninfected samples mapped to BUNV.

Sample	Total read count	Reads mapped to L-segment (%)	Reads mapped to M-segment (%)	Reads mapped to S-segment (%)	Total mapped reads (%)
AF5_uninfected_1	69,082,221	230 (0.0)	95 (0.0)	317 (0.0)	642 (0.0)
AF5_uninfected_2	86,761,677	399 (0.0)	153 (0.0)	598 (0.0)	1150 (0.0)
AF5_uninfected_3	77,954,008	460 (0.0)	193 (0.0)	604 (0.0)	1257 (0.0)
BUNV2_uninfected_1	47,419,907	169 (0.0)	16 (0.0)	107 (0.0)	292 (0.0)
BUNV2_uninfected_2	55,823,631	175 (0.0)	21 (0.0)	93 (0.0)	289 (0.0)
BUNV2_uninfected_3	51,272,514	154 (0.0)	26 (0.0)	115 (0.0)	295 (0.0)
BUNV3_uninfected_1	41,465,689	143 (0.0)	15 (0.0)	72 (0.0)	230 (0.0)
BUNV3_uninfected_2	59,618,033	140 (0.0)	15 (0.0)	92 (0.0)	247 (0.0)
BUNV3_uninfected_3	37,207,976	124 (0.0)	14 (0.0)	73 (0.0)	211 (0.0)
BUNV9_uninfected_1	45,176,788	185 (0.0)	18 (0.0)	123 (0.0)	326 (0.0)
BUNV9_uninfected_2	64,990,682	211 (0.0)	25 (0.0)	129 (0.0)	365 (0.0)
BUNV9_uninfected_3	60,135,913	198 (0.0)	19 (0.0)	122 (0.0	339 (0.0)

Table S12. Sequencing and library statistics for small RNA (18-28 nt) from uninfected samples mapped to SFV.

Sample	Total read count	Reads mapped to SFV (%)
AF5_uninfected_1	69,082,221	99 (0.0)
AF5_uninfected_2	86,761,677	136 (0.0)
AF5_uninfected_3	77,954,008	160 (0.0)
SFV1_uninfected_1	71,740,661	1174 (0.0)
SFV1_uninfected_2	84,938,597	915 (0.0)
SFV1_uninfected_3	56,557,530	423 (0.0)
SFV2_uninfected_1	73,678,575	91 (0.0)
SFV2_uninfected_2	69,236,614	94 (0.0)
SFV2_uninfected_3	65,938,269	99 (0.0)

Table S13. Sequencing and library statistics for small RNA (18-28 nt) from uninfected samples mapped to ZIKV.

Sample	Total read count	Reads mapped to ZIKV (%)
AF5_uninfected_1	69,082,221	26 (0.0)
AF5_uninfected_2	86,761,677	78 (0.0)
AF5_uninfected_3	77,954,008	45 (0.0)
ZIKV_uninfected_1	40,919,305	13 (0.0)
ZIKV_uninfected_2	32,058,677	3 (0.0)
ZIKV_uninfected_3	42,322,903	62 (0.0)

Table S14. P-values of the antiviral activity analysis of BUNV-Nluc primed cells against BUNV-Nluc using qPCR and RNA from small RNA sequencing according to Student's t test.

BUNV-Nluc primed, BUNV-Nluc infected (Fig. 11A)				
	BUNV-2 (CFAV +)	BUNV-3 (CFAV -)	BUNV-9 (CFAV -)	control (CFAV +)
BUNV-2 (CFAV +)		0.3013	0.4909	0.7229
BUNV-3 (CFAV -)	0.3013		0.0576	0.2343
BUNV-9 (CFAV -)	0.4909	0.0576		0.0469
control (CFAV +)	0.7229	0.2343	0.0469	

Table S15. P-values of the antiviral activity analysis of SFV-Nluc primed cells against SFV-Nluc using qPCR and RNA from small RNA sequencing according to Student's t test.

SFV-Nluc primed, SFV-Nluc infected (Fig. 11B)			
	SFV-1 (CFAV +)	SFV-2 (CFAV -)	control (CFAV +)
SFV-1 (CFAV +)		0.0572	0.0786
SFV-2 (CFAV -)	0.0572		0.0769
control (CFAV +)	0.0786	0.0769	

Table S16. P-values of the antiviral activity analysis of BUNV-Nluc primed cells against SFV-Nluc using qPCR and RNA from small RNA sequencing according to Student's t test.

BUNV-Nluc primed, SFV-Nluc infected (Fig. 11C)				
	BUNV-2 (CFAV +)	BUNV-3 (CFAV -)	BUNV-9 (CFAV -)	control (CFAV +)
BUNV-2 (CFAV +)		0.6667	0.0253	0.0758
BUNV-3 (CFAV -)	0.6667		0.0477	0.0759
BUNV-9 (CFAV -)	0.0253	0.0477		0.0768
control (CFAV +)	0.0758	0.0759	0.0768	

Table S17. P-values of the antiviral activity analysis of SFV-Nluc primed cells against BUNV-Nluc using qPCR and RNA from small RNA sequencing according to Student's t test.

SFV-Nluc primed, BUNV-Nluc infected (Fig. 11D)			
	SFV-1 (CFAV +)	SFV-2 (CFAV -)	control (CFAV +)
SFV-1 (CFAV +)		0.6673	0.0857
SFV-2 (CFAV -)	0.6673		0.8066
control (CFAV +)	0.0857	0.8066	

Table S18. P-values of the antiviral activity analysis of ZIKV-Nluc primed cells against BUNV-Nluc using qPCR and RNA from small RNA sequencing according to Student's t test.

ZIKV-Nluc primed, BUNV-Nluc infected (Fig. 11E)		
	ZIKV (CFAV +)	control (CFAV +)
ZIKV (CFAV +)		0.1957
control (CFAV +)	0.1957	

Table S19. P-values of the antiviral activity analysis of ZIKV-Nluc primed cells against SFV-Nluc using qPCR and RNA from small RNA sequencing according to Student's t test.

ZIKV-Nluc primed, SFV-Nluc infected (Fig. 11F)		
	ZIKV (CFAV +)	control (CFAV +)
ZIKV (CFAV +)		0.0170
control (CFAV +)	0.0170	

Table S20. P-values of the antiviral activity analysis of BUNV-Nluc primed cells against BUNV-Nluc using qPCR according to Student's t test.

BUNV-Nluc primed, BUNV-Nluc infected (Fig. 12A)				
	BUNV-2 (CFAV +)	BUNV-3 (CFAV -)	BUNV-9 (CFAV -)	control (CFAV +)
BUNV-2 (CFAV +)		0.3813	0.0796	0.3487
BUNV-3 (CFAV -)	0.3813		0.4160	0.5662
BUNV-9 (CFAV -)	0.0796	0.4160		0.1122
control (CFAV +)	0.3487	0.5662	0.1122	

Table S21. P-values of the antiviral activity analysis of BUNV-Nluc primed cells against TAHV using qPCR according to Student's t test.

BUNV-Nluc primed, TAHV infected (Fig. 12B)				
	BUNV-2 (CFAV +)	BUNV-3 (CFAV -)	BUNV-9 (CFAV -)	control (CFAV +)
BUNV-2 (CFAV +)		0.0043	0.2829	0.0571
BUNV-3 (CFAV -)	0.0043		0.0369	0.0338
BUNV-9 (CFAV -)	0.2829	0.0369		0.0628
control (CFAV +)	0.0571	0.0338	0.0628	

Table S22. P-values of the antiviral activity analysis of BUNV-Nluc primed cells against SFV-Nluc using qPCR according to Student's t test.

BUNV-Nluc primed, SFV-Nluc infected (Fig. 12C)				
	BUNV-2 (CFAV +)	BUNV-3 (CFAV -)	BUNV-9 (CFAV -)	control (CFAV +)
BUNV-2 (CFAV +)		0.0743	0.0708	0.0683
BUNV-3 (CFAV -)	0.0743		0.6853	0.8682
BUNV-9 (CFAV -)	0.0708	0.6853		0.8382
control (CFAV +)	0.0683	0.8682	0.8382	

Table S23. P-values of the antiviral activity analysis of BUNV-Nluc primed cells against SINV using qPCR according to Student's t test.

BUNV-Nluc primed, SINV infected (Fig. 12D)				
	BUNV-2 (CFAV +)	BUNV-3 (CFAV -)	BUNV-9 (CFAV -)	control (CFAV +)
BUNV-2 (CFAV +)		0.0713	0.0806	0.1169
BUNV-3 (CFAV -)	0.0713		0.0102	0.0619
BUNV-9 (CFAV -)	0.0806	0.0102		0.0997
control (CFAV +)	0.1169	0.0619	0.0997	

Table S24. P-values of the antiviral activity analysis of BUNV-Nluc primed cells against ONNV using qPCR according to Student's t test.

BUNV-Nluc primed, ONNV infected (Fig. 12E)				
	BUNV-2 (CFAV +)	BUNV-3 (CFAV -)	BUNV-9 (CFAV -)	control (CFAV +)
BUNV-2 (CFAV +)		0.0251	0.5507	0.1768
BUNV-3 (CFAV -)	0.0251		0.0400	0.0090
BUNV-9 (CFAV -)	0.5507	0.0400		0.0977
control (CFAV +)	0.1768	0.0090	0.0977	

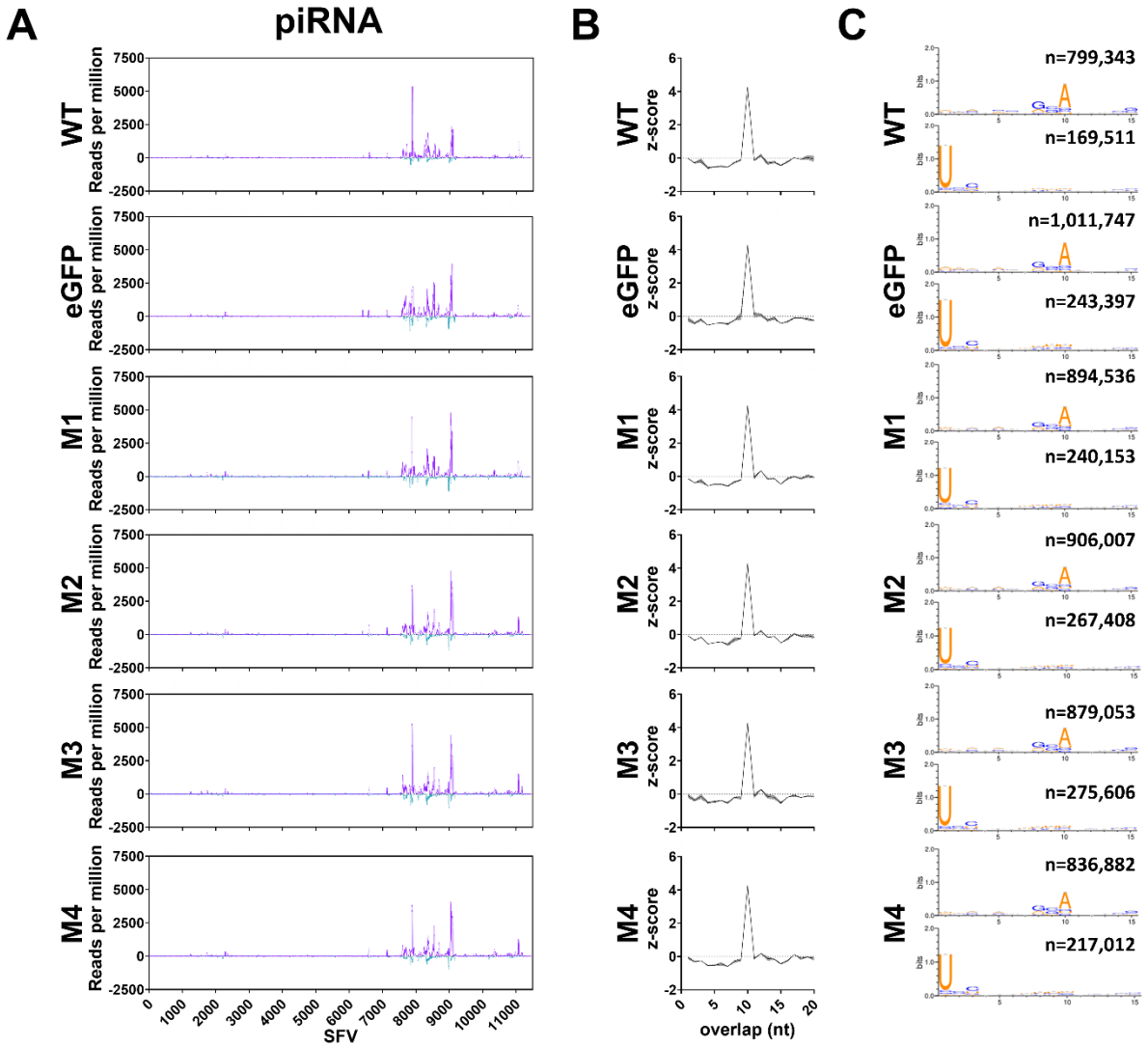


Fig. S11: Analysis of vpiRNAs after SFV infection in Dcr2 PAZ mutant transfected *Ae. aegypti* Dcr2 KO cells (Publication 1). AF319 cells were transfected with expression plasmids encoding myc-tagged WT Dcr2 or Dcr2 PAZ domain mutants M1–M4 or eGFP (negative control). These cells were infected with SFV (MOI = 1) 24 hpt for 48h. Total RNA was extracted and sent for small RNA sequencing. **(A)** 24-30 nt piRNAs of WT or PAZ mutant Dcr2 with eGFP for control, mapped to the SFV genome (purple) and antigenome (blue). Results are presented in reads per million from two independent experiments. **(B)** Overlapping pairs probability z-scores of 24-30 nt SFV-derived piRNAs. Grey region indicates range of the two independent experiments. **(C)** Sequence logos with 24-30 nt reads trimmed down to first 15 nt. Graphs present base frequencies at each position of reads mapping to SFV genome (top) and antigenome (bottom). Height of each symbol corresponding to RNA bases (A = adenine, U = uracil, G = guanine, C = cytosine) represents the relative frequency of the corresponding nucleotide, while the combined height of the stacks at a given position indicates conservation presented as bits. Number of reads across two independent biological repeats are shown in top right of each figure. Error bars indicate ~95% credible interval.

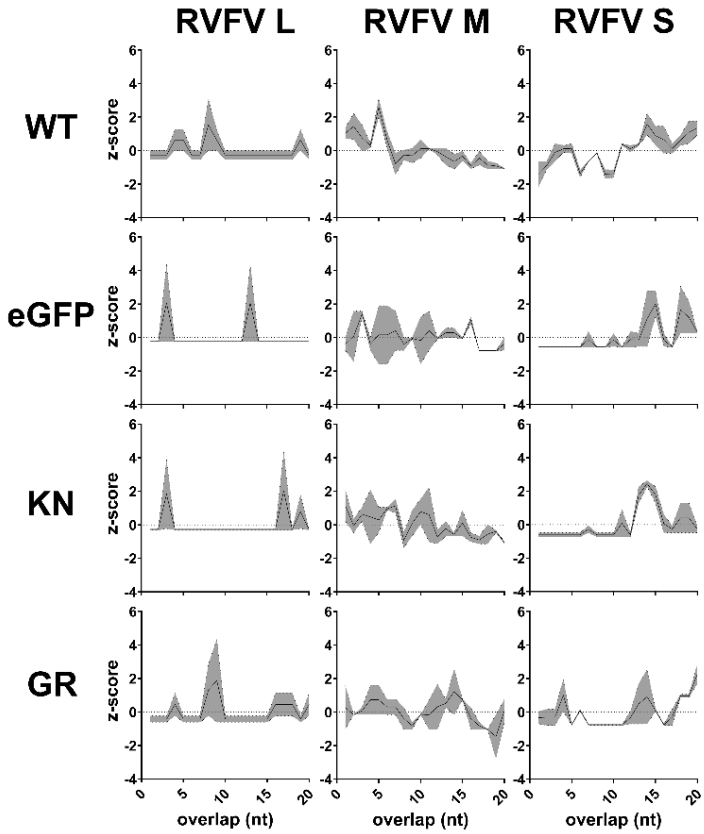


Fig. S12: Overlapping pairs probability of 21 nt sRNAs of Dcr2 WT and helicase mutants in *Ae. aegypti* Dcr2 KO cells (Publication 3). Small RNA sequencing of AF319 cells transiently expressing WT Dcr2, Dcr2 KN or Dcr2 GR helicase mutations with eGFP transfected cells as control, infected with RVFV (MOI 1). RNA isolation was performed 48 hpi. z-scores of 21 nt SFV-derived sRNAs with grey region indicating range of the two independent experiments.

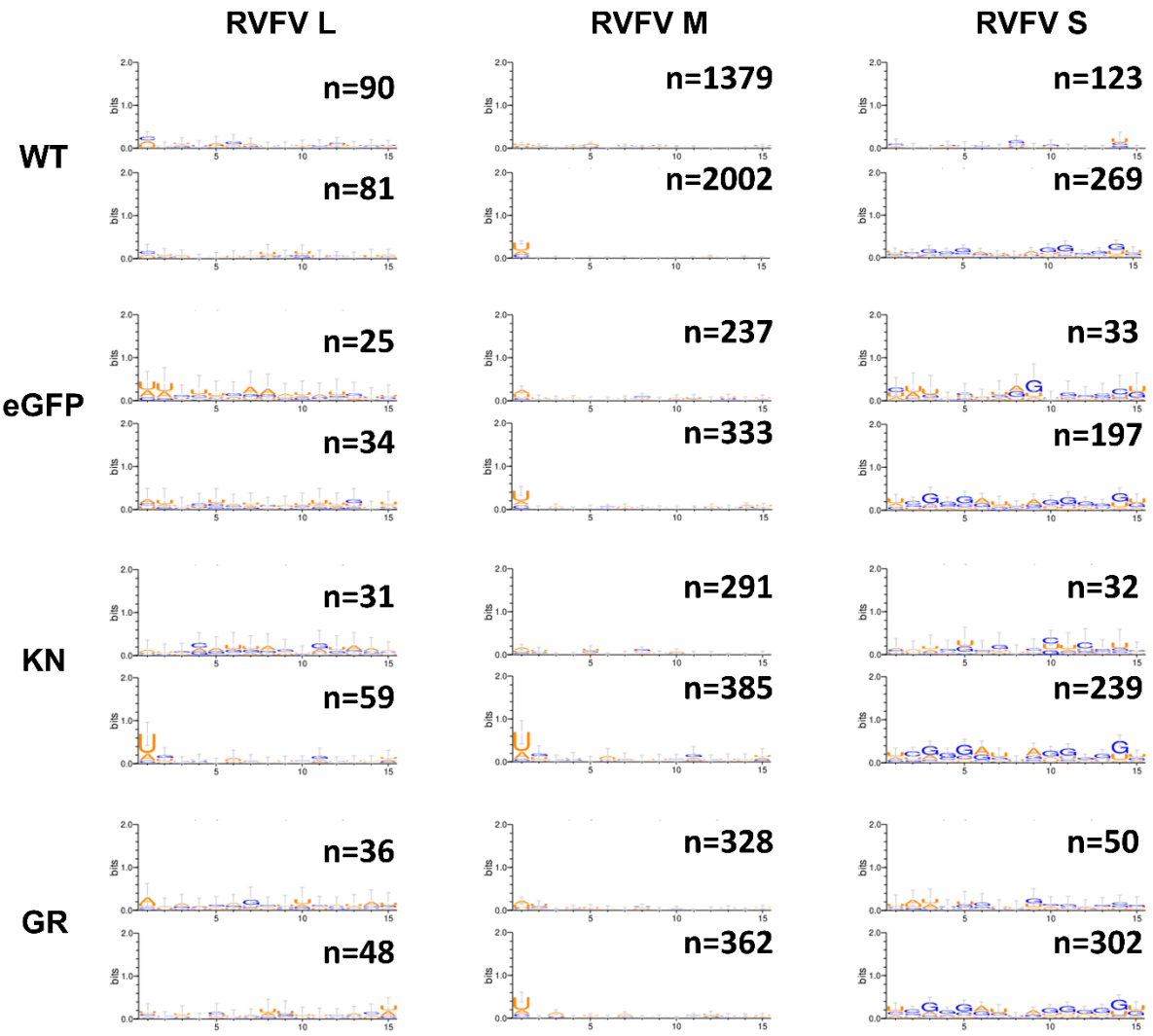


Fig. S13: 21 nt sRNAs produced by helicase mutants to not exhibit U_1/A_{10} bias after RVFV infection (Publication 3). Sequence logos of the RVFV L- (Large, left side), M- (Medium, middle) and S-segment (Small, right side) with 21 nt reads trimmed down to first 15 nt. Graphs present base frequencies at each position of reads mapping to RVFV antigenome (top) and genome (bottom). Height of each symbol corresponding to RNA bases (A = adenine, U = uracil, G = guanine, C = cytosine) represents the relative frequency of the corresponding nucleotide, while the combined height of the stacks at a given position indicates conservation presented as bits. Number of reads across two independent biological repeats are shown in top right of each figure. Error bars indicate ~95% credible interval.

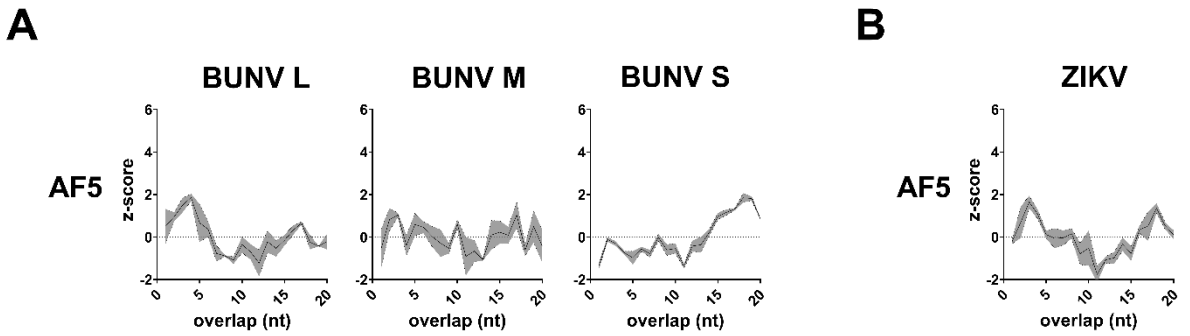


Fig. S14: Overlapping pairs probability of 21 nt sRNAs in AF5 cells after BUNV or ZIKV infection (Publication 4). Small RNA sequencing of AF5 cells infected with **(A)** BUNV-Nluc (MOI 1) or **(B)** ZIKV-Nluc (MOI 1). RNA isolation was performed 48 hpi or 96 hpi, respectively. z-scores of 21 nt BUNV- or ZIKV-derived sRNAs with grey region indicating range of three independent experiments.

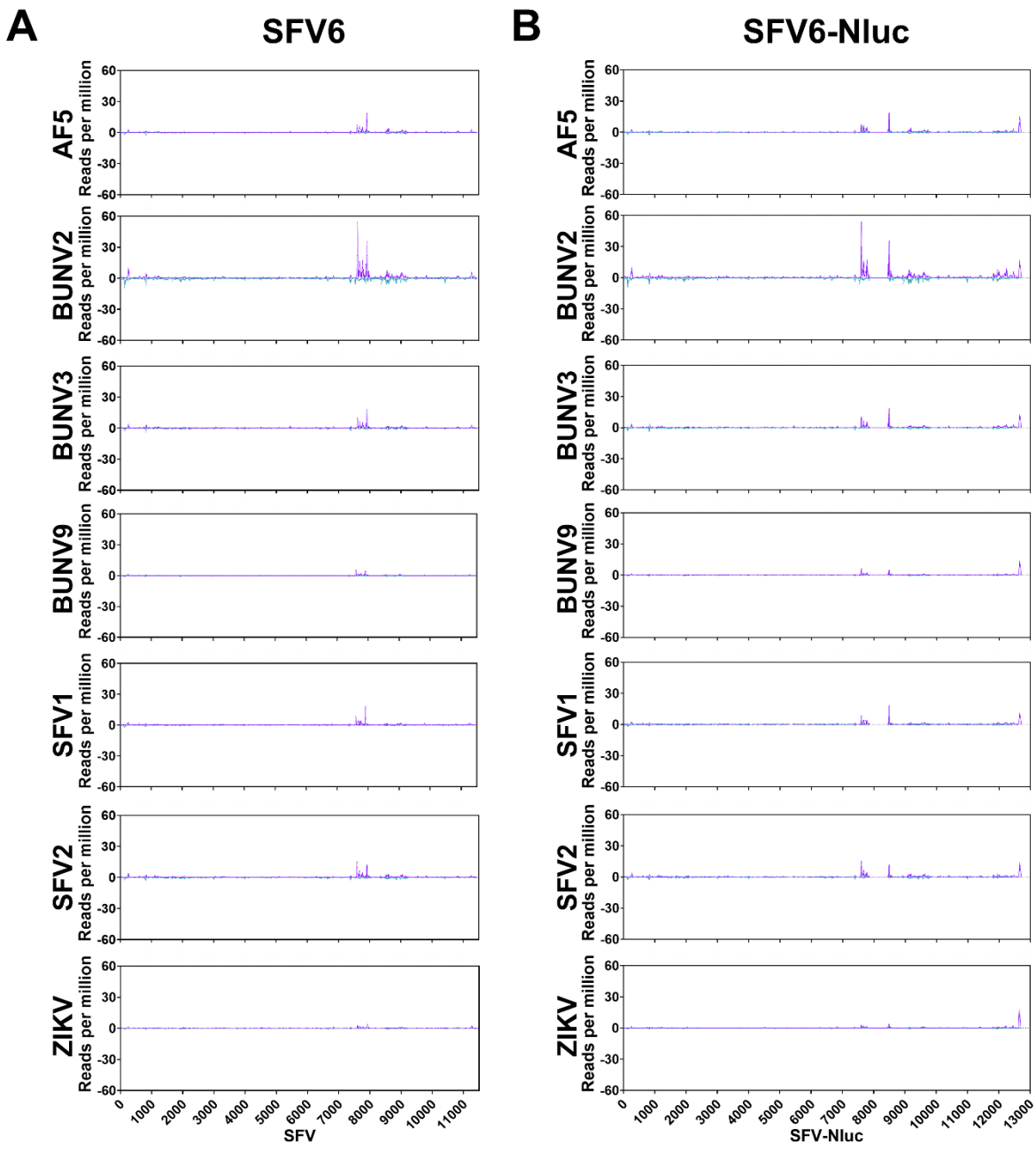


Fig. S15: Subgenomic promotor induces SFV-derived vpiRNA production (Publication 4). 25-28 nt vpiRNAs of SFV-Nluc infected primed cells mapped against **(A)** SFV (SFV6; GenBank ID: KT009012.1) and **(B)** SFV-Nluc. BUNV, ZIKV and SFV primed cells were infected with SFV-Nluc with naïve AF5 cells as control before RNA extraction at 48hpi and subsequent small RNA sequencing. Purple indicates genome mapping and blue indicates antigenomic mapping. Results are presented in reads per million from three independent experiments.